JAERI-M
90-160

ANNUAL REPORT OF THE NAKA FUSION RESEARCH ESTABLISHMENT

FOR THE PERIOD OF APRIL 1 1989 TO MARCH 31 1990

September 1990

Naka Fusion Research Establishment

日本原子力研究所
Japan Atomic Energy Research Institute

JAERI-Mレポートは，日本原子力研究所が不定期に公刊している研究報告書です。
入手の問合わせは，日本原子力研究所技術情報部情報資料課（〒319-11茨城県那珂郡東海村）あて，お申しこしください。なお，このほかに財団法人原子力弘済会資料センター（〒319-11茨城県那珂郡東海村日本原子力研究所内）で複写による実費領布をおこなっております。

JAERI-M reports are issued irregularly.
Inquiries about availability of the reports should be addressed to Information Division Department of Technical Information, Japan Atomic Energy Research Institute, Tokai-mura, Naka-gun, Ibaraki-ken 319-11, Japan.

編集兼発行　日本原子力研究所
印　　刷　いばらき印刷㈱

JAERI-M 90-160

Annual Report of the Naka Fusion Research Establishment for the period of April 1 1989 to March 31 1990

Naka Fusion Research Establishment
Japan Atomic Energy Research Institute
Naka-machi, Naka-gun, Ibaraki-ken

(Received August 24, 1990)

Research and development activities of the Naka Fusion Research Establishment for the period of April 1989 to March 1990 are reported. The experiment on JT-60 was continued to October 1989. In the pellet injection experiment, plasma energy confinement was improved and the maximum fusion product $n_e(0)\tau_E T_i(0)$ reached 1.2×10^{20} m^{-3} s keV. The portion of the bootstrap current was up to 80% of the total plasma current in the high poloidal beta discharge. The fabrication of the new vacuum vessel and poloidal field coils for the JT-60 machine upgrade(JT-60U) have been made. The experiment to improve the confinement on JFT-2M was conducted. The ergodic magnetic limiter coils were installed and the study of their effect on an H-mode began. Quasi-steady-state H-mode discharge(10 sec at maximum) was achieved and a new high-beta regime with the improved Troyon coefficient have been explored in DIII-D. As for theoretical and computational studies, thermal instabilities of an edge plasma, plasma performance determined by the MHD instabilities and burning plasma problems were continued to be investigated. A new type of a vacuum pump--the ceramic turbo-viscous pump--has been developed. The pumping speed and presure attained so far are 280 l/min and 7×10^{-6} Torr, respectively. In the high heat flux technology, small-scale divertor samples are manufactured by means of brazing carbon fiber reinforced carbon composite to copper heat sinks. The thermal cycle tests show they endure against a heat flux up to 10 MW/m^2. As for the development of plasma heating technology, the 50 keV-10A negative hydrogen beam was able to be extracted by means of seeding cesium in the ion plasma generator. 1.4 MW-10sec RF was generated from an improved electron gun in the modified 2GHz-range klystron for JT-60. In the superconducting magnet development, a Nb_3Sn coil with an inner diameter of 1.0 m for the Demo Poloidal Coil Program was successfully magnetized up to 7 T in 1 sec. For the development of tritium processing technology, the gram-level tritium experiments were performed successfully and safely. Conceptual design of the International Thermonuclear Experimental Reactor(ITER) is now proceeding under the auspices of the IAEA. Significant contribution was continued by JAERI participants to support the ITER activities. Design study of the Fusion Experimental Reactor(FER) concept has been also conducted and the related technology R&D has been developed.

Keywords: Fusion Research, JT-60, JFT-2M, FER, ITER, Doublet III-D, NBI, RF, Theory, Vacuum, H-mode, Superconducting, Tritium Processing, Current Drive, Annual Report

JAERI－M 90－160

那珂研究所年報（平成元年度）

（1989年4月1日～1990年3月31日）

日本原子力研究所
那珂研究所

（1990年８月２４日受理）

那珂研究所１９８９年度研究開発成果が報告されている。JT-60に於ける下側ダイバータ実験は、1989年10月まで行われた。ペレット入射実験では、プラズマのエネルギー閉じ込め時間が改善され、最大核融合出力積$n_e\tau_E T_i$は$1.2\times10^{20}m^{-3}$skeVに達した。高ベータ実験に於いては、総プラズマ電流の80%がブートストラップ電流という放電が得られた。JT-60の大電流化改造（JT-60U）では、新しい真空容器とポロイダル磁場コイルが組立られている。JFT-2Mでは、閉じ込め特性を改善する実験が進められ、特にエルゴディック・リミタ・コイルが設置され、Ｈモードへの影響を調べる実験が開始された。ダブレットⅢＤの実験では、準定常的なＨモードが最長で10秒間持続するに至った。また、改良トロヨン係数を持つ新たな高ベータ実験も実施された。理論計算の分野では、周辺プラズマの熱不安定性、MHD不安定性で決まるプラズマ性能評価、燃焼プラズマの問題などの検討が進められた。新しいタイプの真空ポンプ（セラミック・ターボ・荒引排気ポンプ）が開発され、到達真空度7×10^{-6}Torr、排気速度毎分280リッターの性能が今まで確認された。高熱負荷技術では、銅にＣ／Ｃコンポジット材を半田付けしたダイバータ板材に熱サイクル負荷試験を実施し、10MW/m²まで異常がないことが確認された。プラズマ加熱技術開発では、セシウムをイオン源のプラズマ生成部に添加することで、50keV-10Aの負水素イオンビームが引き出された。また、改良された２GHz帯のクライストロンの電子銃から1.4MWのRF波を10秒間発生させることに成功した。超電導技術開発では、実証ポロイダル磁場コイル試験用の内径1mのNb_3Snコイルを1秒間で7テスラまで励磁することに成功した。トリチウム処理技術では、グラム・レベルのトリチウム実験を安全に遂行することに成功した。国際熱核融合実験炉（ITER）の概念設計がIAEAのもとで行われ、原研からの参加者の貢献により検討作業が順調に進められている。原研の次期核融合装置（FER）の設計検討やR&Dも進められた。

那珂研究所：〒311-01 茨城県那珂郡那珂町大字向山801-1

Contents

目　　次

I. PLASMA THEORY AND COMPUTATION

1. Introduction

During the period from April 1, 1989 to March 31, 1990, emphases of theoretical and computational works were put on (1) studies of various problems relating with confinement and heating of a tokamak plasma, (2) analyses of MHD equilibria and stabilities, especially, in relation to design studies of next generation tokamaks, (3) analyses of the burning plasma physics in a tokamak, and (4) development of numerical codes and a plasma simulator.

As for the confinement and heating studies thermal equilibrium and edge plasma stability were analyzed to clarify the marfe and the experimentally obtained density limit. An empirical scaling law of the energy confinement time was derived from experimental data of various tokamaks. Concerning the rf heating analyses modification of the internal kink mode by ICRF wave and ECRH processes were investigated. Parasitic wave excitation of a free electron laser was also studied.

Major efforts of the MHD studies were focused on the database assessment for ITER on the ideal and resistive MHD stabilities, and the plasma motion during the flat top operation and the disruption process. A radiative thermal instabilities were studied taking account of the MHD activity near the plasma center. The MHD stability of a tokamak plasma which obeys the neoclassical Ohm's law was analyzed.

As for the burning plasma physics a general consideration on the burn control of the finite Q reactor, analyses of passive burn control by the toroidal field ripple and the control by the ICRF waves were carried out. Helium ash exhaust in the ITER plasma was also studied.

Physics codes developed in this period were added to the TRITON-II system. Development and improvement of the supporting codes in the TRITON-II system were also continued. In order to facilitate establishment of necessary database for the next generation tokamaks conceptual design analysis and model development of a plasma simulator METIS based on the parallel processing computer technology were carried out. Annex IX on the US-JAERI Data Link of the US-Japan Cooperation Program was concluded and operation of the Data Link was successfully started.

2. Analyses of Confinement and Heating Processes

2.1 Thermal equilibrium and stability of tokamak edge plasma[2.1-1]

In a plasma with parameters near the Hugill limit marfe is often observed, which is believed as a kind of thermal instabilities. Parallel electron thermal conductivity cannot prevent poloidally asymmetric perturbation ($m\neq0,n=0$) in a high density and low electron temperature plasma, and consequently the marfe structure is formed. Thermal equilibrium of scrape-off layer was studied by assuming a simple point model and stability for poloidally asymmetric perturbation was analyzed. The condition for existence of the thermal equilibrium at the edge plasma is similar to the Hugill limit. To examine thermal stability and its saturated states, one dimensional model with parallel electron thermal conduction is employed. The time dependence of electron temperature was solved under the condition with constant n_eT_e along a magnetic field line. Small temperature

I. PLASMA THEORY AND COMPUTATION

1. Introduction

During the period from April 1, 1989 to March 31, 1990, emphases of theoretical and computational works were put on (1) studies of various problems relating with confinement and heating of a tokamak plasma, (2) analyses of MHD equilibria and stabilities, especially, in relation to design studies of next generation tokamaks, (3) analyses of the burning plasma physics in a tokamak, and (4) development of numerical codes and a plasma simulator.

As for the confinement and heating studies thermal equilibrium and edge plasma stability were analyzed to clarify the marfe and the experimentally obtained density limit. An empirical scaling law of the energy confinement time was derived from experimental data of various tokamaks. Concerning the rf heating analyses modification of the internal kink mode by ICRF wave and ECRH processes were investigated. Parasitic wave excitation of a free electron laser was also studied.

Major efforts of the MHD studies were focused on the database assessment for ITER on the ideal and resistive MHD stabilities, and the plasma motion during the flat top operation and the disruption process. A radiative thermal instabilities were studied taking account of the MHD activity near the plasma center. The MHD stability of a tokamak plasma which obeys the neoclassical Ohm's law was analyzed.

As for the burning plasma physics a general consideration on the burn control of the finite Q reactor, analyses of passive burn control by the toroidal field ripple and the control by the ICRF waves were carried out. Helium ash exhaust in the ITER plasma was also studied.

Physics codes developed in this period were added to the TRITON-II system. Development and improvement of the supporting codes in the TRITON-II system were also continued. In order to facilitate establishment of necessary database for the next generation tokamaks conceptual design analysis and model development of a plasma simulator METIS based on the parallel processing computer technology were carried out. Annex IX on the US-JAERI Data Link of the US-Japan Cooperation Program was concluded and operation of the Data Link was successfully started.

2. Analyses of Confinement and Heating Processes

2.1 Thermal equilibrium and stability of tokamak edge plasma[2.1-1]

In a plasma with parameters near the Hugill limit marfe is often observed, which is believed as a kind of thermal instabilities. Parallel electron thermal conductivity cannot prevent poloidally asymmetric perturbation ($m\neq0,n=0$) in a high density and low electron temperature plasma, and consequently the marfe structure is formed. Thermal equilibrium of scrape-off layer was studied by assuming a simple point model and stability for poloidally asymmetric perturbation was analyzed. The condition for existence of the thermal equilibrium at the edge plasma is similar to the Hugill limit. To examine thermal stability and its saturated states, one dimensional model with parallel electron thermal conduction is employed. The time dependence of electron temperature was solved under the condition with constant n_eT_e along a magnetic field line. Small temperature

perturbation with poloidal asymmetry (m=1) is given initially. In low density region, temperature perturbation is smoothed out by the effect of parallel electron thermal conductivity. Near the equilibrium density limits, the temperature perturbation increases and radiation loss is enhanced. As an example, we analyzed an OH(ohmic heating) plasma of JT-60 (R=3m, a=1m, $B_t \leq 4.0$). In Fig.I.2.1-1, region of appearance of marfe in the Hugill diagram is shown by closed triangles and stable symmetric equilibria are shown by open circles.

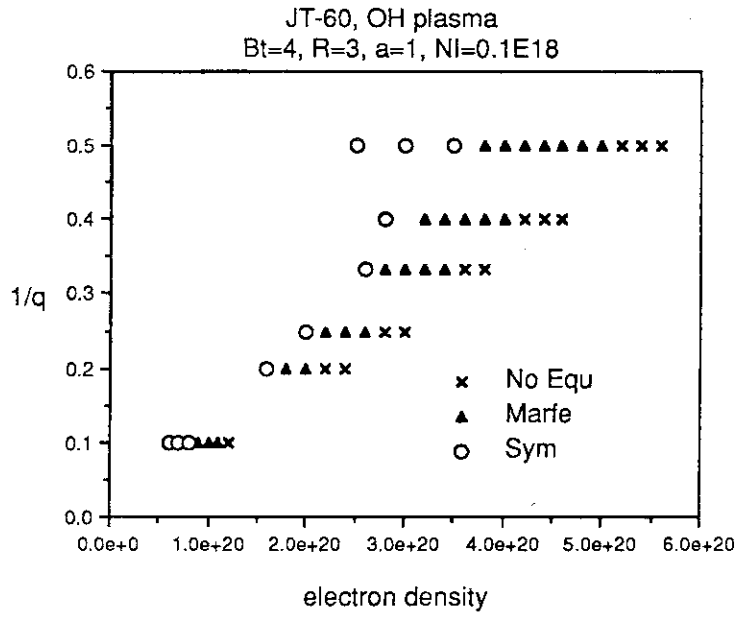

Fig.I.2.1-1 Density limit and marfe. Closed triangles show points where marfe is formed. Open circles show points where symmetric equilibrium is established.

References

[2.1-1] T. Tuda, "Thermal equilibrium and stability of Tokamak edge plasma," ITER-IL-PH-12- 0-J-2 (1990).

2.2 Scaling of L-mode energy confinement

Two types of scaling laws for the L-mode energy confinement time were proposed [2.2-1];

(1) Simple scaling $\tau_E^{sim} = 0.008\ (I_p R/a)\ (M_i V/P)^{0.5}$,

(2) Offset-linear scaling $W_{OH} = 0.016\ M_i^{0.5}\ I_p^{1.25}\ B_t^{0.45}\ R^{1.92}\ a^{-0.38}$,

$\tau_{inc} = 0.025\ M_i^{0.5}\ I_p^{0.6}\ k\ R^{0.5}\ a^{0.5}$.

The multiformity of τ_E scaling laws is attributed to the lack of independent variation of parameters in the ITER L-mode database where a certain combination of several parameters has always almost the same value as $f_s = 0.3Ra^{0.75}k^{0.5} \approx 1$. Therefore, the energy confinement time τ_E is always predicted with an uncertainty of contains uncertainty of $f_s^{\alpha_s}$ as $\tau_E = \tau_{E,ITER89} \times f_s^{\alpha_s}$, where $\tau_{E,ITER89}$ is the basic scaling expression newly proposed at the ITER confinement workshop [2.2-2]. In the JT-60 plasmas with the lower X-point, the values of f_s are about 1.4. The data from these plasmas suggest that the dependence of τ_E on f_s is very weak as $0 \leq \alpha_s \leq 0.2$ [2.2-3].

References

[2.2-1] T. Takizuka, "Scaling of L-mode energy confinement," ITER-IL-PH-4-9-J-2 (1989).
[2.2-2] Compiled by T. Takizuka, V. Mukhovatov, "Summary Report: ITER Confinement Workshop (July 31, August 11, 1989, Garching) ITER-TN-PH-9-2 (1990).
[2.2-3] T. Takizuka, O. Naito, and JT-60 Team, "Global confinement data from JT-60 with lower X-point configuration," ITER-IL-PH-4-0-J-2 (1990).

2.3 Effect of energetic trapped particle generated by ICRF wave on internal kink mode

Effect of energetic trapped particles on an MHD mode was investigated in a case of an ICRF wave heating. The spatial profile of the ion distribution function during the 2nd harmonic heating was calculated by using the bounce averaged Fokker-Planck code for a low field side resonance (LFSR) case and a high field side resonance(HFSR) one. The linear dispersion relation of the internal kink mode with the kinetic correction[2.3-1] of the ICRF wave was numerically solved and a critical power for the fishbone instability was evaluated. It was also found that the growth rate of the fishbone mode for the HFSR case was by about one-order smaller than that of the LFSR one for the same absorption powers, although the effect on the MHD branch was small.

References

[2.3-1] L. Chen, et al., Phys. Rev. Lett. **52** (1984) 1122.

2.4 ECRH of tokamak plasma by finite band-width free electron laser

Free electron laser(FEL) with 1-10GW power level was proposed as one of efficient heating methods of a tokamak plasma. The heating is characterized by the nonlinear electron orbit due to the relativistic frequency detuning and the adiabatic breakdown of the electron phase[2.4-1]. Here, the effect of a multi-wave injection with different frequencies (i.e. a primary wave and side-bands) on the plasma heating was investigated for a fixed radiation power. It was found that the multi-wave injection randomizes the electron phase for the nonlinear orbit and pumps up some electrons into a higher energy state through the orbit overlapping. Consequently, the heating efficiency is increased up to 2-3 times in comparison with that of the single wave case.

References

[2.4-1] W.M. Nevins, et al., Phys. Rev. Lett. **59** (1987) 60.

2.5 Parasitic wave excitation by multi-mode coupling in Raman regime free electron laser[2.5-1]

Analysis of a parasitic wave excitation in the free electron laser is important to determine the quality of an output radiation signal. The mechanisms of the parasitic wave excitation in a high current Raman regime were investigated by use of a 1-dimensional multi-mode FEL amplification code. It was found that a multi-mode coupling among side-band waves and a primary one plays an important role in the parasitic wave excitation in addition to a side-band instability. Such a multi-mode coupling process is observed in both the linear amplification stage and the nonlinear trapping one, and modulates the output signal to a level comparable with that attained only by the side-band instability.

References

[2.5-1] Y. Kishimoto, et al., 1989 Internat'l Conf. on Plasma Physics, New Delhi, Vol.II, 465 (1989).

3. MHD Equilibrium and Stability Analyses

3.1 MHD stability analysis of tokamak plasmas obeying neoclassical Ohm's law

The stability of equilibria with current profiles consistent with the neoclassical ohm's law were studied for localized ideal MHD (ballooning and Mercier) modes. For the ITER reference parameters bootstrap currents are small and reduction of the conductivity is mainly due to the neoclassical effect. The resultant equilibria have low q_0 (safety factor at the magnetic axis) less than unity and can be sustained stably for the localized modes because of the strong magnetic shear caused by the reduction of the conductivity. Troyon's factor of g = 2.5 was obtained for reasonable temperature profiles. The corresponding temperature at the center is $T_0 \approx 16$keV for Ip=22MA and $T_0 \geq 20$keV for Ip=15MA. The stability of the global modes are under investigation.

3.2 Profile effects on ideal MHD beta limit in ITER

The ideal MHD beta limit was analyzed for the ITER-like plasma with a double null-points divertor configuration. A magnetic surface containing more than 99% of all the poloidal magnetic flux inside the separatrix was defined as the plasma surface and the parameters of ITER physics phase were used for the analysis as R=5.8m, a=2.2m, κ_{null}~2.2, δ_{null}~0.5. The ballooning modes have been found to be the most unstable ones for $n \leq 5$ and $n=\infty$ (n:toroidal mode number) for the peaked pressure profiles. As the squared growth rates oscillate with respect to the toroidal mode number n, the most unstable n is sensitive to q_0. In a divertor configuration of an elongated plasma, the magnetic shear is weak near the plasma center and is very strong near the edge. This shear profile causes an internal-mode-like structure. For q_0=1.1, the beta limits are larger for smaller internal inductance l_i. This is due to weak shear near the plasma center for large l_i when the central current density (or q_0) is fixed. The structure of global modes shows a strong mode coupling between low-m and high-m components (m:poloidal mode number). The low-m components become large for a peaked pressure profile and large l_i, which indicates that the most unstable toroidal mode number is sensitive to q_0. The ballooning limit for $l_i \geq 0.8$ is considerably reduced due to a weak shear near the plasma center. However, small reduction of the pressure gradient may enhance the limit to some extent.

3.3 Snake and sawtooth oscillations

In a plasma, $m \neq 0$ radiative thermal instabilities are stabilized by parallel electron heat conduction except for the vicinity of a rational surface. In a very high density and low temperature (T_e<2KeV) case as in pellet injection experiments, the radiative thermal instabilities occur near q=1 surface and a snake phenomenon is observed. We studied this phenomenon by solving the reduced set of the nonlinear resistive MHD equations coupled with an electron temperature transport equation. The time evolution of electron temperature contours are shown in Fig.I.3.3-1. The radially extended valley of the electron temperature distribution made by a pellet injected from left to the plasma center at time t=0, becomes flat in a few steps along the magnetic field lines except for those on the q=1 rational surface by the parallel heat conduction and the snake structure

appears. This snake structure survives for a long time even after complete magnetic field reconnection by the sawtooth collapse, although within the framework of the present resistive MHD model it moves to the plasma center.

3.4 Axisymmetric tokamak simulation by using the TSC code

Time-evolutional characteristics of a free boundary axisymmetric tokamak plasma were investigated by using the tokamak simulation code (TSC)developed at Princeton Plasma Physics Laboratory. In the code, a plasma is modeled with a hybrid method composed of the two-dimensional part governing the behavior of the MHD quantities and one-dimensional part governing the surface averaged adiabatic invariants. Equations are solved by taking into account of the effects of the external circuits and the eddy current in nearby conductors. In the design study of the divertor of ITER, the TSC code was applied to the analysis of double to single null transition and to the simulation of displacement of highly elongated tokamak after the thermal quench of the major disruption.

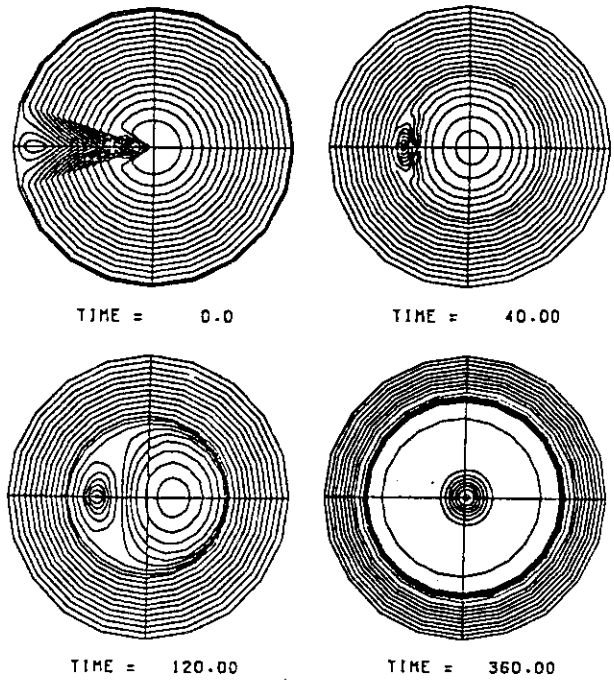

Fig.I.3.3-1
Time evolution of temperature contour during sawtooth collapse. The temperature perturbation, initially given by pellet injection (t=0), because snake structure at q=1(t=40) and survives after complete reconnection(t=360).

3.5 MHD modes of a resistive toroidal plasma

The magnetohydrodynamic (MHD) spectrum of a toroidal resistive plasma was analyzed numerically using the linearized MHD equations, by assuming the classical resistivity. Two codes, RESTOR and SPECTOR, were developed under the Australia-Japan collaboration program. RESTOR is designed to find the most unstable mode on the basis of a fully implicit time-stepping procedure. SPECTOR uses inverse iteration to find the full spectrum including the stable branches. The stable and unstable eigenfrequencies were found by solving the reduced set of the resistive MHD equations. The numerical formulation is due to a flux coordinate system and Fourier expansion in the poloidal and toroidal directions. From the computational results it was concluded that RESTOR can be applicable to the study of weakly unstable modes. The stable parts of the spectrum, obtained by using SPECTOR, show that stable eigenfrequencies lie on characteristic lines in the complex frequency plane. These are almost independent of the resistivity for high magnetic Reynolds number plasmas.

4. Analyses of Burning Plasma in Tokamak

4.1 Burn control in the finite Q reactor [4.1-1]

It is necessary to establish the method of burn control in a controlled thermonuclear fusion reactor to settle the operation point at an equilibrium state and to stabilize the thermal instability. The thermal instability was studied on the basis of a simple point model. The global energy confinement time τ_E is assumed to degrade with the total heating power P_t as $\tau_E \propto P_t^{-\mu}$ and the particle density is assumed unchanged. Figure I.4.1-1 shows the critical temperature T_C, above which a burning plasma is thermally stable without feedback control, for the fusion power multiplication factor Q being high enough.

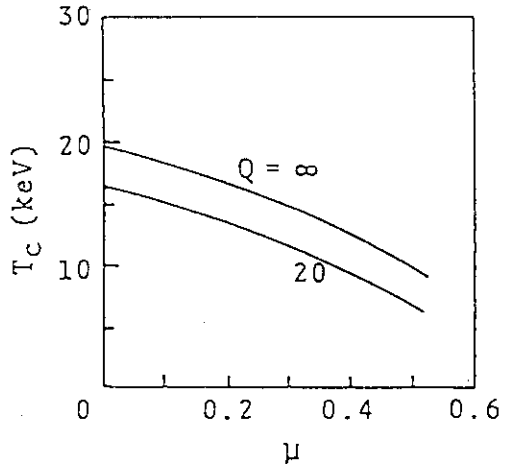

Fig.I.4.1-1
Critical temperature T_C (density weighted average one) as function of μ ($\tau_E \propto P_t^{-\mu}$). Burning plasma is thermally stable in the region $T > T_C$.

In order to reduce the current drive power, it is desirable to operate a steady-state tokamak reactor at the reasonably high temperature, 15keV < T < 25keV, which can be higher than T_C even for $\mu \approx 0$. A feedback control system of additional heating power Pwas proposed to settle the operation point in an equilibrium state;

$$P(t) = P(t-\Delta\tau) - G\{ T(t) - T(t-\Delta\tau) \} + G_I^2 \int_{t-\Delta\tau}^{t} \{ T_O(t') - T(t') \} dt'$$

where T_O is the objective operating temperature and $\Delta\tau$ is chosen to be smaller than τ_E. This system is also effective for stabilizing the thermal instability.

References

[4.1-1] T. Takizuka, et al., "Japanese Contribution on Burn Control," ITER-IL-PH-1-0-J-2 (1990).

4.2 Passive burn control of tokamak plasma by toroidal field ripple [4.2-1]

The feasibility of a passive control, a control method to use the ripple-degraded alpha particle confinement with a free expansion of the major radius, has been confirmed by using a 1.5D transport code. In the transport code, a scaling of ripple loss of alpha particles derived from the results of an orbit-following Monte-Carlo code is used. For the passive burn control, more than 5.0% of major radius margin is necessary and the resulting ripple induced power loss of alpha particles exceeds 20%. Passive burn control in combination with a feedback control of field ripple, a hybrid control, shows a very high performance of burn temperature control. In the hybrid burn control, the necessary major radius margin and the controlled field ripple are only 2~3% and $\delta_C \leq 1\%$, respectively. The resulting total power loss of alpha particles is less than 15%.

References

[4.2-1] K. Tani, M. Azumi, T. Takizuka, "Passive burn control of tokamak plasma by toroidal field ripple," to be published in Fusion Technol..

4.3 Burn control by ICRF waves

We have investigated the additional heating for burn control by use of higher harmonic ICRF waves in a plasma sustained by the deuteron-beam-driven current. Parameters are as follows. $\langle T \rangle \sim 20$ keV, $\langle n_e \rangle \sim 0.7\times10^{20}$ m^{-3}, $B_{to}=4.85$ T, $P_{NB}\sim100$ MW, and $P_{IC}\sim20$ MW. The effect of magnetically trapped particles on the tail formation has been taken into account. The RF power is absorbed mainly by the trapped particles. The increment of the perpendicular pressure of ICRF heated deuterons is about 10% for both the second and the third harmonic heating. The beam-driven current is hardly affected by the ICRF heating. Then, the additional RF heating does not have a negative influence on NBCD. The heating power is variable without change in the beam-driven current. In the linear analysis, $R_\alpha \equiv P_{IC,\alpha}/P_{IC}\sim0.5$ for the third harmonic wave. As the perpendicular tail is formed by the RF wave, the wave couples further with this tail, and the RF power absorbed by deuterons with the tail becomes larger than the linear absorption power. The RF power partition between deuterons and alphas for the third harmonic heating becomes almost the same as that for the second harmonic heating ($R_\alpha\sim0.2$). Thus, the difference between the second and the third harmonic waves in the additional heating for burn control is expected to be slight.

4.4 Helium ash exhaust in ITER [4.4-1]

Helium ash exhaust in ITER for high edge density operation ($n_s \approx 5\times10^{19}$m^{-3}) was studied by using UEDA code, a 2-dimensional fluid code for analysis of divertor plasma. The DT fuel is highly recycled and the cold divertor plasma is realized, $n_d > 10^{21}$m^{-3} and $T_d < 5$eV, while He ash is in the low-recycling state because of the small ionization rate at low T_d. The efficiency of ash exhaust was found to be comparable to or better than that of fuel exhaust, even when the ash exhaust efficiency is reduced by the existence of the thermal force on He.

References

[4.4-1] T. Takizuka, "Helium ash exhaust on ITER," Proc. ITER Specialists' Working Session on Validation and Development of Edge Plasma Models, July 17-21, 1989, Garching.

5. TRITON System

5.1 Parallel algorithm of the resistive MHD code AEOLUS for model plasma simulator ProtoMETIS

Nonlinear resistive MHD code (AEOLUS) employs the reduced set of resistive MHD equations, which is Fourier expanded about poloidal and toroidal directions and uses finite difference method for radial direction. The calculation schemes are divided into two main parts: one is linear implicit calculation and the other is nonlinear convolution calculation, which can be done at each radial grid point independently. So the parallel processing can be introduced to this convolution calculations easily. For implicit calculation, a linear simultaneous equation must be solved. In the axisymmetric toroidal plasma, the matrix consists of N_n block diagonal submatrices corresponding to different toroidal mode number, n. Each submatrix is a M×M block tridiagonal matrix, where M is the number of poloidal modes. The number of the tridiagonal blocks is N_r, which is number of radial grid points. For this implicit calculation, the matrix elements for each

4.3 Burn control by ICRF waves

We have investigated the additional heating for burn control by use of higher harmonic ICRF waves in a plasma sustained by the deuteron-beam-driven current. Parameters are as follows. $\langle T \rangle \sim 20$ keV, $\langle n_e \rangle \sim 0.7\times10^{20}$ m^{-3}, $B_{to}=4.85$ T, $P_{NB}\sim100$ MW, and $P_{IC}\sim20$ MW. The effect of magnetically trapped particles on the tail formation has been taken into account. The RF power is absorbed mainly by the trapped particles. The increment of the perpendicular pressure of ICRF heated deuterons is about 10% for both the second and the third harmonic heating. The beam-driven current is hardly affected by the ICRF heating. Then, the additional RF heating does not have a negative influence on NBCD. The heating power is variable without change in the beam-driven current. In the linear analysis, $R_\alpha \equiv P_{IC,\alpha}/P_{IC}\sim0.5$ for the third harmonic wave. As the perpendicular tail is formed by the RF wave, the wave couples further with this tail, and the RF power absorbed by deuterons with the tail becomes larger than the linear absorption power. The RF power partition between deuterons and alphas for the third harmonic heating becomes almost the same as that for the second harmonic heating ($R_\alpha\sim0.2$). Thus, the difference between the second and the third harmonic waves in the additional heating for burn control is expected to be slight.

4.4 Helium ash exhaust in ITER [4.4-1]

Helium ash exhaust in ITER for high edge density operation ($n_s \approx 5\times10^{19}$m^{-3}) was studied by using UEDA code, a 2-dimensional fluid code for analysis of divertor plasma. The DT fuel is highly recycled and the cold divertor plasma is realized, $n_d > 10^{21}$m^{-3} and $T_d < 5$eV, while He ash is in the low-recycling state because of the small ionization rate at low T_d. The efficiency of ash exhaust was found to be comparable to or better than that of fuel exhaust, even when the ash exhaust efficiency is reduced by the existence of the thermal force on He.

References

[4.4-1] T. Takizuka, "Helium ash exhaust on ITER," Proc. ITER Specialists' Working Session on Validation and Development of Edge Plasma Models, July 17-21, 1989, Garching.

5. TRITON System

5.1 Parallel algorithm of the resistive MHD code AEOLUS for model plasma simulator ProtoMETIS

Nonlinear resistive MHD code (AEOLUS) employs the reduced set of resistive MHD equations, which is Fourier expanded about poloidal and toroidal directions and uses finite difference method for radial direction. The calculation schemes are divided into two main parts: one is linear implicit calculation and the other is nonlinear convolution calculation, which can be done at each radial grid point independently. So the parallel processing can be introduced to this convolution calculations easily. For implicit calculation, a linear simultaneous equation must be solved. In the axisymmetric toroidal plasma, the matrix consists of N_n block diagonal submatrices corresponding to different toroidal mode number, n. Each submatrix is a M×M block tridiagonal matrix, where M is the number of poloidal modes. The number of the tridiagonal blocks is N_r, which is number of radial grid points. For this implicit calculation, the matrix elements for each

radial grid are stored in the memory of each processor element, and the forward and backward substitutions are calculated by transferring the result to the neighboring processor element. For this algorithm, a synchronization with neighboring processor elements is required.

5.2 Adaptation of the TSC code to the JAERI computing system

Princeton TSC code, which is useful for the control analyses of axisymmetric tokamak plasma, was adapted for use in JAERI computing system under the US-Japan collaboration program. The original code was incorporated with the integrative graphic subroutine package ARGUS-V4 to obtain a great number of sorted graphic data. The new TSC version, which has many new capabilities involving impurity transport, RFP-dynamos, current drive, etc., was introduced into JAERI in the late 1989.

5.3 Up-down asymmetric version of the ERATO code

A new version of ERATO code, ERATOAS, which does not assume up-down symmetry of equilibria was developed. A mapping module (ERATO-1, ERATO-2V), matrix construction module (ERATO-3) and eigenvalue solver(ERATO-4) were adapted for up-down asymmetric equilibria. Three kinds of flux surface coordinates are available in the code, i.e., straight field line, equi-arc length and quasi-cylindrical coordinates. The matrices produced by the hybrid finite element discretization of the ideal MHD energy principle are complex matrices, i.e., a general Hermitian matrix for the potential energy and a complex positive definite matrix for the kinetic energy.. The generalized eigenvalue problem is solved by inverse iteration method for sparse matrices used in the up-down symmetric version of ERATO code (ERATOJ). The present version of ERATOAS code supports the free boundary condition with a conducting wall as well as the fixed boundary condition. The ERATOAS code was tested for analytic equilibria with up-down symmetry. The eigenvalues and eigenfunctions agreed with those computed by the symmetric version of ERATOJ code.

5.4 Improvement of graphic module in the GAEA system

The interactive graphic module in the GAEA system was improved by adding several new commands, LIST/BROWSE and OVERLAY. The LIST/BROWSE commands provide functions for listing and looking at interactively mass data stored in the GAEA system. The OVERLAY command supports displaying graphs on a same frame.

6. Others

6.1 Plasma simulator

In order to satisfy the requirement to produce enormous theoretical data sets necessary for the design studies of the next generation tokamaks, conceptual design work of a plasma simulator METIS dedicated for the calculations of the alpha-particle loss analysis and the nonlinear MHD simulation was continued from the last fiscal year on. In this fiscal year a model plasma simulator ProtoMETIS was developed on the basis of the above conceptual design. ProtoMETIS is a 1/10 to

radial grid are stored in the memory of each processor element, and the forward and backward substitutions are calculated by transferring the result to the neighboring processor element. For this algorithm, a synchronization with neighboring processor elements is required.

5.2 Adaptation of the TSC code to the JAERI computing system

Princeton TSC code, which is useful for the control analyses of axisymmetric tokamak plasma, was adapted for use in JAERI computing system under the US-Japan collaboration program. The original code was incorporated with the integrative graphic subroutine package ARGUS-V4 to obtain a great number of sorted graphic data. The new TSC version, which has many new capabilities involving impurity transport, RFP-dynamos, current drive, etc., was introduced into JAERI in the late 1989.

5.3 Up-down asymmetric version of the ERATO code

A new version of ERATO code, ERATOAS, which does not assume up-down symmetry of equilibria was developed. A mapping module (ERATO-1, ERATO-2V), matrix construction module (ERATO-3) and eigenvalue solver(ERATO-4) were adapted for up-down asymmetric equilibria. Three kinds of flux,surface coordinates are available in the code, i.e., straight field line, equi-arc length and quasi-cylindrical coordinates. The matrices produced by the hybrid finite element discretization of the ideal MHD energy principle are complex matrices, i.e., a general Hermitian matrix for the potential energy and a complex positive definite matrix for the kinetic energy.. The generalized eigenvalue problem is solved by inverse iteration method for sparse matrices used in the up-down symmetric version of ERATO code (ERATOJ). The present version of ERATOAS code supports the free boundary condition with a conducting wall as well as the fixed boundary condition. The ERATOAS code was tested for analytic equilibria with up-down symmetry. The eigenvalues and eigenfunctions agreed with those computed by the symmetric version of ERATOJ code.

5.4 Improvement of graphic module in the GAEA system

The interactive graphic module in the GAEA system was improved by adding several new commands, LIST/BROWSE and OVERLAY. The LIST/BROWSE commands provide functions for listing and looking at interactively mass data stored in the GAEA system. The OVERLAY command supports displaying graphs on a same frame.

6. Others

6.1 Plasma simulator

In order to satisfy the requirement to produce enormous theoretical data sets necessary for the design studies of the next generation tokamaks, conceptual design work of a plasma simulator METIS dedicated for the calculations of the alpha-particle loss analysis and the nonlinear MHD simulation was continued from the last fiscal year on. In this fiscal year a model plasma simulator ProtoMETIS was developed on the basis of the above conceptual design. ProtoMETIS is a 1/10 to

1/20 scaled model of METIS and is composed of 20 processor elements made of MC68020 and floating point accelerator WTL1167, and also each with 8MB local memory. Effective processing speed comparable with that of a large scale scalar computer FACOM M380 has been attained for the above problems in this model plasma simulator ProtoMETIS, which encourages development of the plasma simulator METIS for intensive data production.

6.2 Data link

The US-JAERI data link was operated in a tentative manner as in the previous year throughout almost all the period covered by this annual report. And in the last quarter of this fiscal year annex IX(data link) of the implementing arrangement between the USDOE and JAERI was concluded. In the JAERI side of the data link system a VAX 8350 computer is connected to terminals and CAD system via ethernet LAN, and to other VAX computers via PSI(Packet Switching Interface). The VAX 8350 computer is connected to the FACOM M780 host computer via INTERLINK system. This system was effectively used for the information exchange for the ITER joint work as well as the activity of the US-Japan fusion cooperation program.

II. JFT-2M PROGRAM

1. Toroidal Confinement Experiments

1.1 Introduction

The main progress in JFT-2M program is summarized. For 1989, ergodic magnetic limiter was introduced and initial experiments have begun to study its effects on H-modes. A system for divertor bias experiments has also been completed and will be put into operation in 1990 to study its effects on the plasma confinement. Several new diagnostic systems have been constructed in order to improve the diagnostics ability of JFT-2M.

1.2 Confinement studies

1.2.1 Toroidal and poloidal rotation in an H-mode

It is well known that the confinement improvement in the H-mode is due to the formation of the transport barrier near the plasma edge and the so-called pedestal in temperature and density profiles contributes to enhance the plasma stored energy. However, the mechanism of a transition from L-mode to H-mode is not yet understood well and now intensively investigated, both experimentally and theoretically. Possible mechanisms explaining the L/H transition have been proposed and the radial electric field takes an important role near the plasma edge [1.2-1]. This electric field can be evaluated from the momentum balance equation, $E_r = (1/en_i)(dP_i/dr) - (B_pV_t - B_tV_p)$, here P_i and n_i are ion pressure and density, B_t and B_p are toroidal and poloidal magnetic field , and V_t and V_p are toroidal and poloidal rotation velocity.

Temporal evolution of the toroidal and poloidal rotation of plasmas has been deduced from charge-exchange recombination spectroscopy (CXRS) of carbon and the radial electric field has been estimated [1.2-2]. Results are shown in Fig.II.1.2-1~2. After the L/H transition at 750 ms, ion temperature near the edge increases quickly (<16 ms), on the other hand the central ion temperature increases slowly with about 50 ms. In a steady state the ion temperature profile has a pedestal with 200 eV, which is similar to the electron temperature profile. The toroidal rotation velocity has also a pedestal shape with about 20 km/sec at the edge, but its time evolution is very slow in comparison with the temperature change. The change of toroidal rotation direction depends on the direction of the momentum input (co-injection or counter-injection).

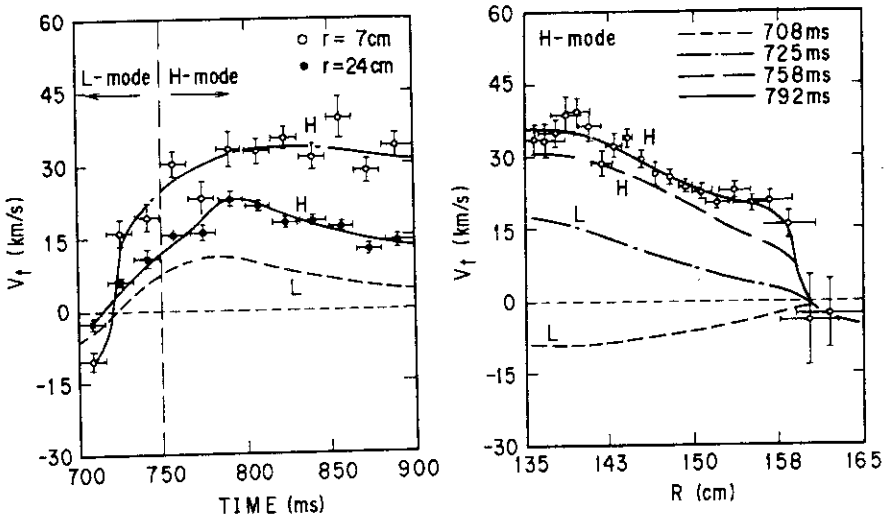

Fig.II.1.2-1 Time evolution of the toroidal rotation profile in the L-mode and the H-mode.

These changes of toroidal rotation may come from reduced neutral particles which bring away momentum in the edge region. The poloidal rotation velocity is obtained only at the plasma edge with using the intrinsic radiation of CVI line. The time evolution of the poloidal rotation velocity is very fast just at the plasma edge, but slow inside. The profile of poloidal rotation has a clear negative drop at the edge (electron diamagnetic direction), and the direction of the change does not depend on the direction of momentum input and plasma current. These features suggest the poloidal rotation has close correlation with the L/H transition. The radial electric field estimated from measurements shows more negative values near the edge than that in the L-mode, and reaches about 200 V/cm. It is to be noted that the grad E_r is negative in the inside region where the temperature gradient is sustained, but it is positive just at the separatrix and it seems to correspond to the sharp density gradient.

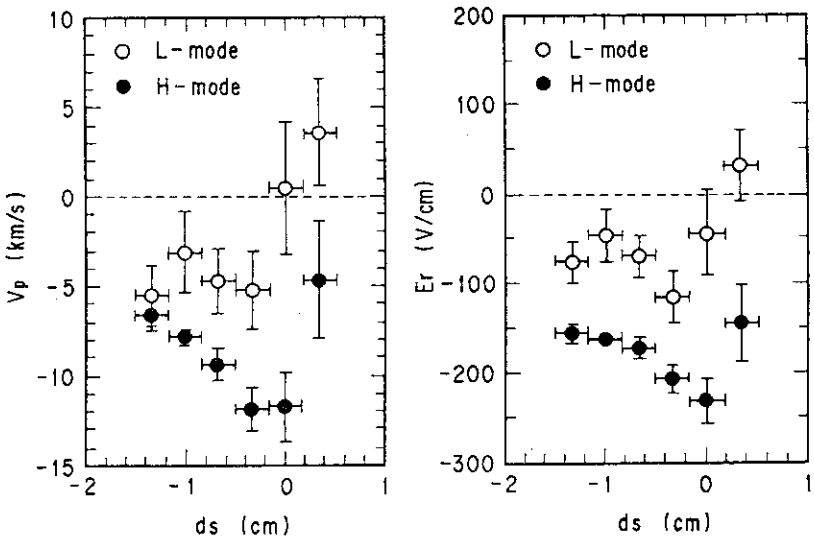

Fig.II.1.2-2 Poloidal rotation profiles and the estimated radial electric field profiles in the L-mode and the H-mode.

In order to determine the more accurate profile of the radial electric field, we are preparing a diagnostic neutral beam for the poloidal rotation measurement, a visible bremsstrahlung radiation detector array for Z_{eff} measurement and TV Thomson scattering system with 81 channels. They will be available in 1990.

1.2.2 Steady state H-mode with ergodic magnetic layer (EML)

The effects of the ergodic magnetic limiter (generated by a localized EML coil system) on the H-mode plasma in single-null open divertor configurations have been investigated. It is observed that the steady state H-mode of NB-heated divertor plasmas is realized by application of EML fields.[1.2-3]

The resonant helical fields are produced by two local coil sets installed outside the vacuum vessel (Fig. II.1.2-3(a)). Selection of high m/low m and even n/odd n modes can be done by the change of coil current directions. The magnetic field structures were studied by the Fourier analysis and the field line tracing. The poloidal mode spectrum is broad due to the locality of EML coils and has its peak at m=5 and 11 near the plasma surface (r=30 cm) for low m and high m cases, respectively (Fig.II.1.2-3(b)). From the island width calculations, it is found that many high-m small islands are involved in the ergodized region in "high m" operation mode, while a

few, low-m large islands are dominant in "low m" operation mode, in which the overlapping of islands reaches q=2 surface at relatively small current (2 kA). The maximum current of the EML coil is 5 kA (40 kAT). The transport coefficient χ_e (= $D_m v_{th.elec.}$, where $D_m = < \delta r^2/2\ell > \sim 9 \times 10^{-7}$ m is the stochastic magnetic diffusivity, $v_{th.elec.}$ is the electron thermal velocity and δr is the radial displacement after traveling a distance ℓ along a magnetic field line) is about 3 ~ 5 m^2/s for high m/odd n case.

For the divertor H-mode cases (I_p = 225 kA, B_t = 1.27 T (counter clockwise (CCW))) with NB-heating, the increases of plasma densities, impurity contents and radiation losses are suppressed by EML (high m/odd n, 3.9 kA) and the steady state H-mode can be realized with D_α burst (Fig.II.1.2-4). The edge electron density is suppressed at the lower level and goes to the steady state point without the transition to L-mode. And also the relaxation of the edge electron temperature gradient (from 90 eV/cm to 68 eV/cm), measured by the electron cyclotron emission, is observed. The dependence of stored energy on electron densities for EML-on case is almost the same with EML-off case (for the higher NB-power case, the improvement of

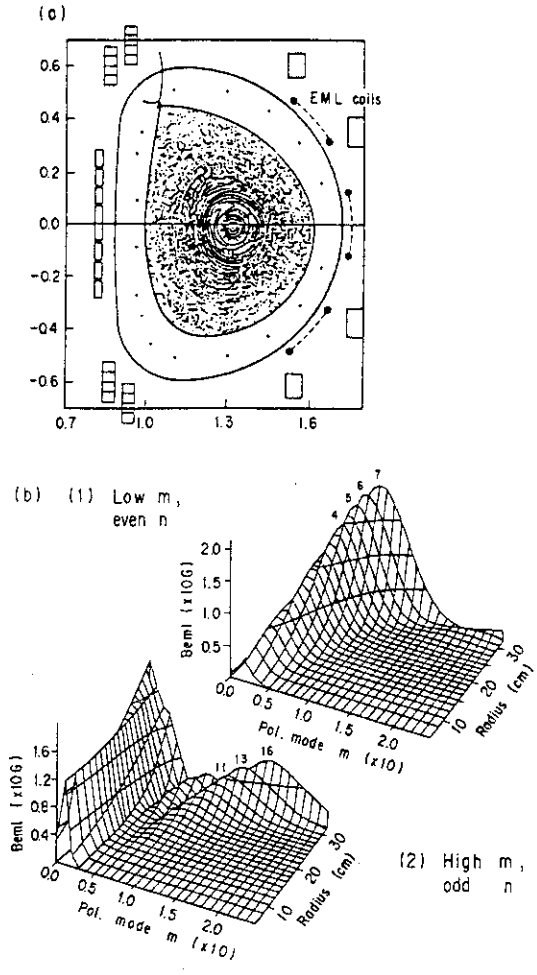

Fig.II.1.2-3 (a) The poloidal position of EML coils and magnetic field puncture plot (High m/even n, 4.9 kA; Divertor, q_{fit} = 3.6). (b) Fourier spectrum profiles of EML field: (1)Low m/odd n, (2)high m/even n. cases (high m/odd n; divertor).

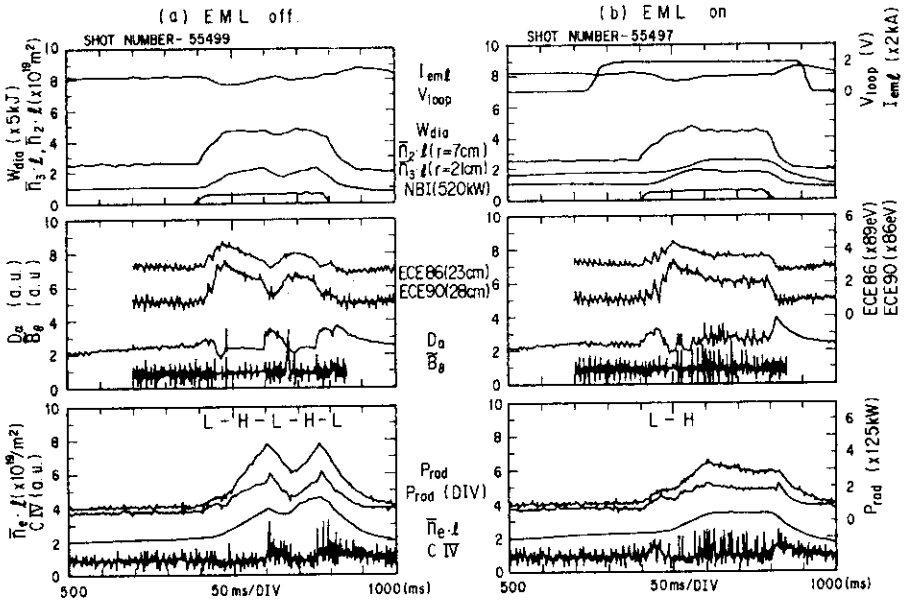

Fig.II.1.2-4
Steady state H-mode by EML, time evolution of (a) EML off and (b) EML on cases (high m/odd n, Div).

the stored energy is observed). The profile of the main plasma density and temperature are also almost the same for both cases with the same mean density. However, the profile of the toroidal rotation measured by the charge exchange recombination spectroscopy is shifted by an amount of about 10 ~ 15 km/s to the electron drift direction, which corresponds to the direction of L-mode case, holding the edge pedestals of ion temperature and toroidal rotation. The asymmetry of the particle flux (deduced from the Langmuir probe measurements) to inner (ion side) and outer (electron side) divertor plates during the H-mode [1.2-4] is decreased at higher electron densities due to the application of EML fields, but is not changed at lower electron densities.

1.2.3 Improved L-mode

An improved L-mode, IL-mode, is observed in JFT-2M.[1.2-5] It is characterized by the peaked profiles of the electron temperature, electron density and radiation loss power. Further investigations have been continued.

The profiles of the temperature and the toroidal rotation velocity in the IL-mode have been obtained by the CXRS. These profiles in the IL-mode are also more peaked in the core region than those in the H-mode as shown in Fig.II.1.2-5. This observation seems to indicate that core confinements of the ion energy and the toroidal momentum are improved in the IL-mode compared with those in the H-mode, in which the confinement is improved at the periphery. Further investigations are continued. Impurity transport (Titanium) is also investigated as described in sub-section 1.5.1, and impurity transport is also improved in the core region in the IL-mode. Sawtooth activity is always reduced in the IL-mode, however, it is not well understood so far that a critical radius in which the confinement is improved corresponds to q=1 surface in the H-phase or another magnetic surface, and it is now under investigations.

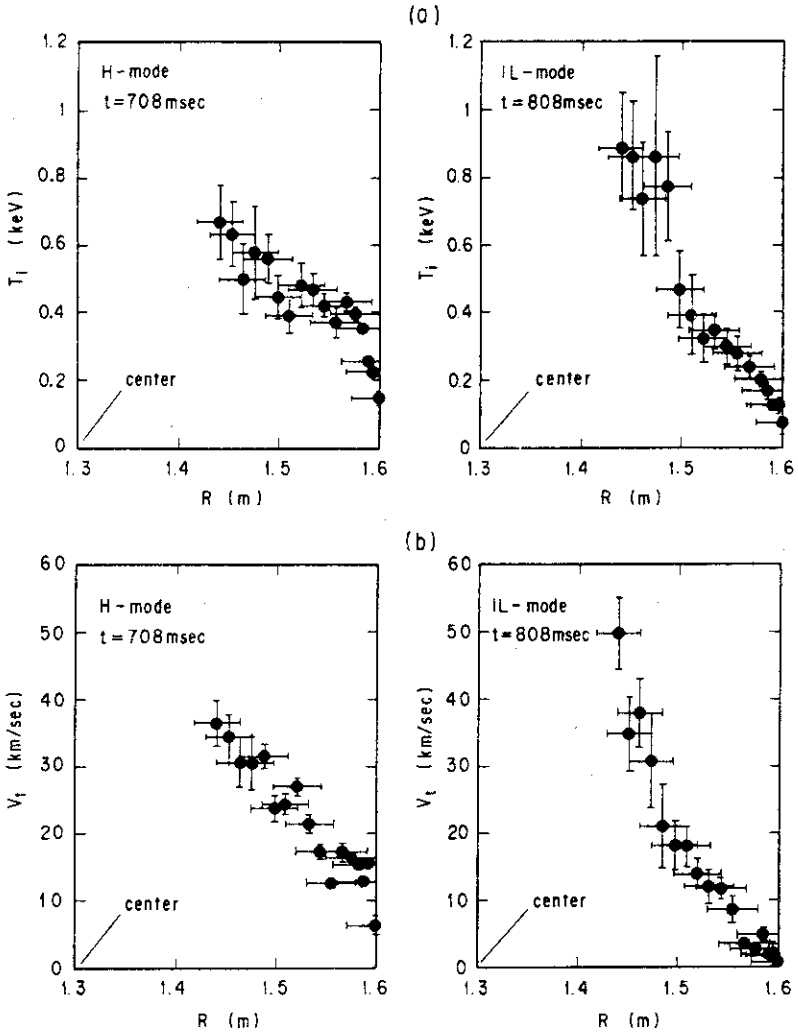

Fig.II.1.2-5 Ion temperature and toroidal rotation profiles in IL-mode and H-mode determined from CXRS of CVI. (a) Ion temperature profiles, (b) Toroidal rotation velocity profiles.

References
[1.2-1] S.-I. Itoh and K. Itoh, Phys. Rev. Lett. **60** (1988) 2276 , K.C. Shaing and E.C.Crume.Jr, Phys. Rev. Lett. **63** (1989) 2369.
[1.2-2] K. Ida, S. Hidekuma, Y. Miura, et al., "Electric Field Profile of H-mode Plasma in JFT-2M Tokamak" , submitted to Phys. Rev. Lett.
[1.2-3] T. Shoji et al., Japan/U.S. Workshop on Edge Plasma Modification in Fusion Plasmas, Nagoya (Jan. 16-18, 1990); 17th EPS Conf., Amsterdam, (1990) paper H30.
[1.2-4] I. Nakazawa et al., in Proc. 16th EPS Conf., Venice, Part III (1989) 887.
[1.2-5] M.Mori, N.Suzuki, Y.Uesugi, et.al., Nucl. Fusion, **28**, No.10 (1988) 1892.

1.3 Current drive experiments

1.3.1 Current drive by fast wave

The coupling and absorption characteristics of the fast wave excited by a phased four-loop antenna array have been investigated in JFT-2M [1.3-1,2]. The frequency of the fast waves is 200 MHz, which corresponds to approximately the tenth harmonic of the ion cyclotron frequency of hydrogen.

The loading resistance depends strongly on the antenna phasing. It decreases with Nz since the width of the evanescent layer increases with N_z. The loading resistance increases with the density up to $2x10^{19}m^{-3}$, but beyond that it starts to decrease with density, because of the steeping of the density gradient.

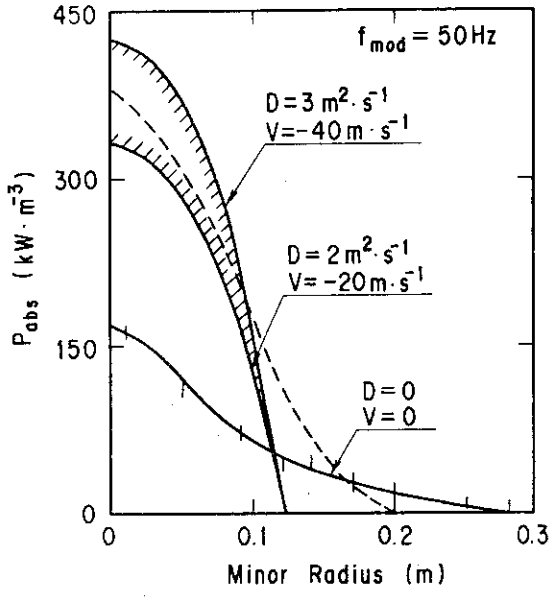

Fig.II.1.3-1 Power deposition profiles at P_{FW}=600 kW with the electron thermal diffusion coefficient, D, and the convection velocity, V, as parameters. The normalized deposition profile calculated from single-pass absorption is shown by the dashed line, $n_e=2X10^{19}m^{-3}$, I_p=230 kA, B_t=1.3 T and Δf=p.

The absorption efficiency of the excited fast wave is improved with increasing the plasma density and temperature, and with decreasing the phase velocity of the fast wave. The results are consistent with the theoretical predictions obtained from ray-tracing calculations. The power deposition profile is obtained through synchronous detection of the electron cyclotron emission modulated by a periodic heat source. In this modulation experiment with a limiter plasma on JFT-2M, the electron thermal diffusivity is 2-3 m^2/s and the convection velocity is 20-40 m/s at n_e = $2X10^{19}m^{-3}$ and I_p=230 kA. The resultant power deposition profile has a peak at the plasma center and agrees well with that calculated with the ray-tracing code (Fig.II.1.3-1). The absorption efficiency calculated from the power deposition profile is 0.3-0.4 at $n_e = 2x10^{19}$ m^{-3} and T_{e0}=0.7 keV, which agrees roughly with that estimated from the initial rise of the plasma stored energy. The electron heating efficiency estimated from the absorption efficiency is $(4-5)x10^{19}$ eVm^{-3}/kW and the incremental confinement time is 8-10 ms in the H-mode phases, which is slightly longer than that in L-mode plasmas heated by NB and/or ICRH in JFT-2M.

1.3.2 Current drive by electron cyclotron wave

Current drive by electron cyclotron wave heating with frequency of 60 GHz has been examined on the JFT-2M tokamak in the automatic voltage regulation (AVR) mode operation in which OH primary voltage is set at constant. The wave for the second harmonic X-mode is injected at the angle of ~ 12 degrees with respect to the toroidal magnetic field. When electron cyclotron wave heating (ECH) power of 180 kW was applied on the way of the decay of the plasma current, appreciable sustainment of the plasma current of ~ 30 kA was observed, even accompanying large negative loop voltage. This result suggested that the current drive by ECH occurs. The averaged electron density is ~ $2\times10^{18}m^{-3}$ and the toroidal magnetic field is B_t=1.07 T. The electron cyclotron emission and soft X-ray energy analysis indicated the generation of the energetic electrons by ECH. Therefore, the effect of the decrease of the symmetric resistivity may not be ruled out.

The dependence of the time derivative of the plasma current, dIp/dt, and the loop voltage, V_L, on the toroidal magnetic field is shown in Fig.II.1.3-2. This does not seem to be explained by the decrease of the plasma resistivity due to the bulk electron heating. To make it clear that the ECH drives the plasma current directly, the detailed analysis on the experiments is required.

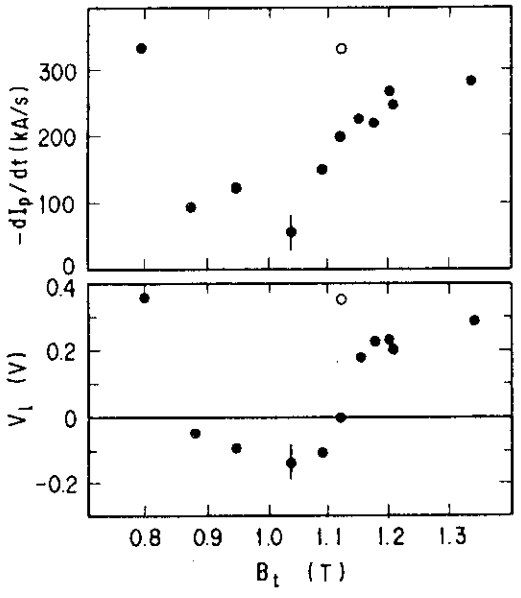

Fig.II.1.3-2 Bt dependence of the dI_p/dt and Vl. P_{ECH} = 180 kW and n_e ~ $2\times10^{18}m^{-3}$.

References
[1.3-1] Y.Uesugi, et al., Nucl. Fusion **30** (1990) 297.
[1.3-2] Y.Uesugi, et al., Nucl. Fusion **30** (1990) 831.

1.4 Particle control (for confinement improvement and long pulse operation)

1.4.1 Plasma fueling by pellet injection

The improvement of the confinement by pellets is observed when the particles are fueled effectively around the center. In this case, the pellet ablation cloud radius is estimated by the H_α/D_α detector array. Figure II.1.4-1 shows a schematic picture of the evaluation procedure. The two things are assumed in this estimation. One is that a pellet moves on the mid plane and the poloidal cross-section of an ablation cloud is circular (radius; r_c). The other is that the intensity of the emissions from the pellet ablation cloud does not change during its passage through the width of the spatial resolution of the H_α/D_α

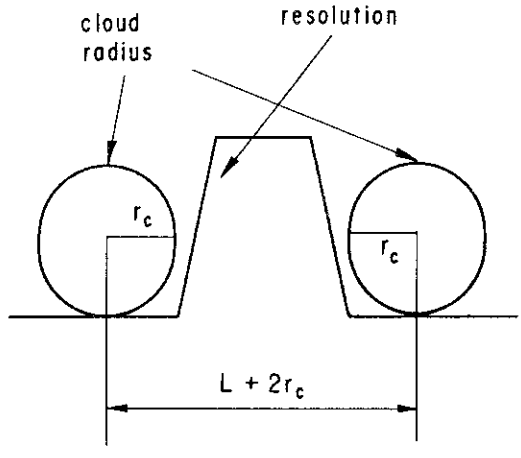

Fig.II.1.4-1 Schematic picture of the evolution procedure.

detector array (about 19mm). The detecting time(t) of a diode is given as $t=(2r_c+L)/V_P$, where L is the resolution at the mid plane and V_P is the speed of a pellet. Figure II.1.4-2 shows the evaluated ablation cloud radius. The cloud radius is about 12 mm. It is about 10 times of the frozen pellet size. The cloud radius does not change much in the plasma, and H_α/D_α-line intensity abruptly decreases and the pellet completely sublimates near the plasma center in this case.

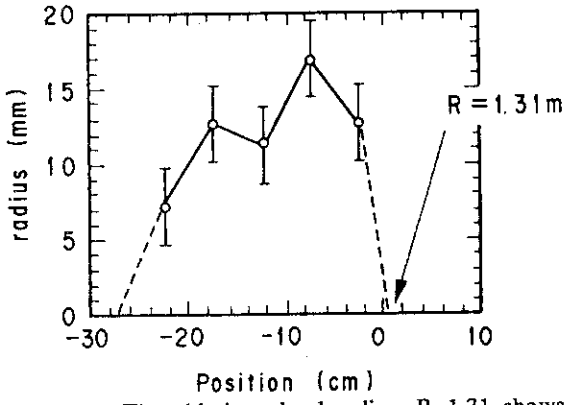

Fig.II.1.4-2 The ablation cloud radius. R=1.31 shows the plasma center and -30 means outside from the center.

1.4.2 Particle balance study with a pump limiter

Particle balance in JFT-2M is studied with a pump limiter by analyzing density decay time after the termination of gas-puffing of a D-shaped limiter discharge.[1.4-1] The particle balances with and without the pump limiter are compared. The plasma is shifted toward inboard limiter in order to create enough clearance between the outer limiter and the plasma edge, because such a geometry is compatible to enhanced confinement discharges. The pump limiter is located on the top of torus. The clearance between the pump limiter head and the plasma edge is 1 cm. The particle recycling is, therefore, dominant at the inboard limiter. The line-averaged plasma density is adjusted to the same value (4.6×10^{13} cm^{-3}) in both cases, with and without the pump limiter, at t=800 ms at where, without the pump limiter, the strong neutral buildup in the plasma periphery takes place.

For the particle balance analysis, the following model is adopted (details are in ref.[1.4-1]).

$$\frac{dN}{dt} = \eta Q_{puff} - \frac{N}{\tau_p} + (1-p)R_r\frac{N}{\tau_p} \qquad (1)$$

$$= \eta Q_{puff} - \frac{N}{\tau_p^G}, \qquad (1)'$$

where

$$\frac{1}{\tau_p^G} = \frac{1 - R_r p}{\tau_p} + \frac{R_r}{\tau_p} = \frac{1}{\tau_p^*} + \frac{1}{\tau_p'} \qquad (2)$$

and

$$\tau_p^* = \frac{\tau_p}{1 - R_r}, \quad \tau_p' = \frac{\tau_p}{pR_r}. \qquad (3)$$

Here N is the total particle number inside the confined region, η is the fueling efficiency for gas-puff feed rate Q_{puff}, τ_p is the particle confinement time, p is a usual exhaust efficiency defined as Γ_{PL}/Γ where Γ_{PL} is the particle flux removed by the pump limiter ($\Gamma_{PL}=pN/\tau_p$) and Γ is the total outflux from the confined region ($\Gamma=N/\tau_p$), R_r is the overall recycling coefficient. Experimentally obtained values are N (1.2×10^{20}), Q_{puff} (3.9×10^{20}/s for the case without the pump limiter and 3.5×10^{20}/s with the pump limiter), τ_p^G (the density decay time with pump limiter:

0.85 s) and τ_p^* (without the pump limiter: 0.97 s). The total loss flux, $\Gamma_{PL} + \Gamma^*$, becomes N/τ_p^G in Eq.(1)' where Γ^* is the remainder which is not pumped and not recycled back to the confined region [$\Gamma^*=(1-p)N/\tau_p^*$]. Then Eq.(1) can be rewritten in a simple form as:

$$\frac{dN}{dt} = \Gamma_0 - \Gamma^* - \Gamma_{PL} \qquad (4)$$

where $\Gamma_0 = \eta Q_{puff}$.

A figure of merit for the pump limiter is defined here as $M = \Gamma_{PL}/(\Gamma_{PL}+\Gamma^*)$ unlikely to p, since Γ^*, comparable to $(1-\eta)Q_{puff}$, can contribute to increase peripheral gas pressure. By using the density decay times τ_p and τ_p^*, the values Γ_{PL}, Γ^* and M become insensitive to the estimation of τ_p if $\tau_p \ll \tau_p^*$ and $p \ll 1$, and it is possible to estimate these values experimentally without knowing exact value of τ_p.

From above equations, R_r, p, M, Γ^* and Γ_{PL} are derived as 0.98, 2.9×10^{-3}, 0.12, 1.2×10^{20}/s and 1.8×10^{19}/s respectively assuming that τ_p is 20 ms and the changes in N/τ_p and η are negligibly small at the time just before and after the change in Q_{puff}. The fueling efficiency is obtained as η=0.66 with the pump limiter or η=0.51 without the pump limiter. Resultant particle balance is illustrated in Fig.II.1.4-3 with the unit of particle flux in Torrℓ/s.

In conclusion, particle balance is clarified on JFT-2M limiter discharges and following results are obtained. Experiments show that the pump limiter prevents the formation of strong neutral buildup at the plasma edge. With shorter density decay time and lower gas feed rate for the same density at around t=800 ms, the pump limiter improves the fueling efficiency by about 30% compared with the other case which is in the neutral buildup regime. The pump limiter removes 12% of the effective loss flux (N/τ_p^G) with the effective pumping speed S_{eff} of 8×10^2 ℓ/s and the pressure of 5×10^{-4} Torr in the expansion chamber. The value of Γ_{PL} agrees well with the product of S_{eff} and the pressure in the expansion chamber (2.6×10^{19}/s). Without using the pump limiter, effective pumping speed of 4.5×10^5 ℓ/s would be necessary to pump out this amount with the measured peripheral pressure of 5×10^{-7} Torr. Higher edge temperature (or

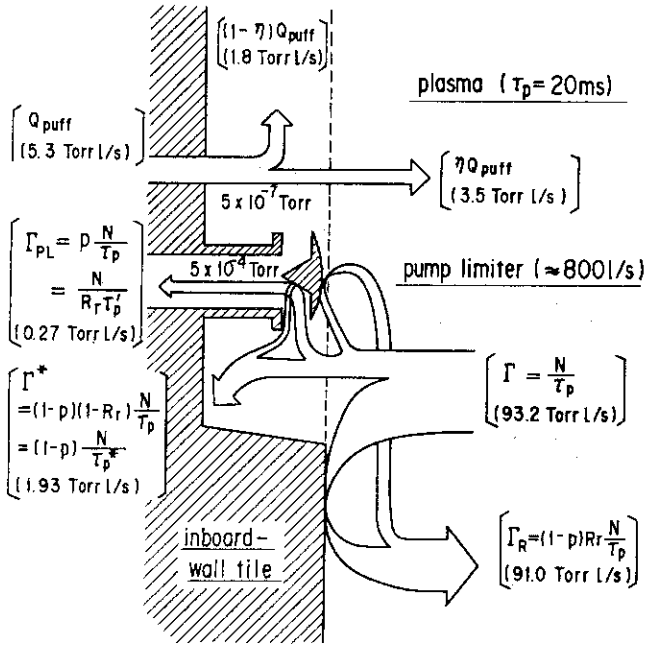

Fig.II.1.4-3 The chart of overall particle balance of the JFT-2M limiter discharge with a pump limiter.

less edge cooling) with the pump limiter results in the improvements in the fueling efficiency and the limits of both the confinement and density.

References

[1.4-1] S. Sengoku et al., presented at the 8th Int. Conf. on "Plasma Surface Interactions in Fusion Devices", Juelich, May, 1988, J. Nucl. Mater., **162** (1989) 667-673.

1.5 Diagnostics

1.5.1 Impurity transport in the improved confinement mode in JFT-2M

Impurity behaviors during the H- and the improved L-mode (IL-mode) [1.5-1] were studied by using the grazing-incident monochromator (3-60nm) and the MIST impurity transport code[1.5-2]. Time evolutions of TiXX line emissions indicated clear sawtooth activity during the H-mode and no activity during the IL-mode. The titanium ion density profile was relatively flat during the H-mode, while it became more centrally peaked during the IL-mode. By using MIST code, the titanium ion transport was analyzed. Measured electron temperature and density profiles were used and the corona equilibrium was assumed to calculate line emissions. Transport coefficients (the diffusion coefficient (D) and the convective velocity (v_{in})) near the plasma center were determined to fit the measured Ti^{19+} ion density profile on the time evolution of the TiXX line emission. The obtained transport coefficients were that $D/D_{NC}<3$ and $v_{in}/v_{NC}<3$ in the IL-mode and $D/D_{NC}>10$ and $v_{in}/v_{NC}<3$ in the H-mode. Here, D_{NC} and v_{NC} are the transport coefficients calculated from the neoclassical theory [1.5-3]. By using these transport coefficients, the titanium ion concentration (n_{Ti}/n_e) near the plasma center and the radiation power loss of the titanium ion (P_{Rad}^{Ti}) near the plasma center (r<a/5, a: minor radius) were estimated during the H- and the IL-mode. Obtained results were that $n_{Ti}/n_e \approx 0.3\%$ and $P_{Rad}^{Ti} \approx 20\%$ of the total input power in the IL-mode and $n_{Ti}/n_e \approx 0.1\%$ and $P_{Rad}^{Ti} \approx 2\%$ in the H-mode. These results were qualitatively agreed with the radiation loss profiles measured by the bolometer array.

References

[1.5-1] M.Mori, et al.; Nucl. Fusion **28** (1988) 433.
[1.5-2] R.A.Hulse; Nucl. Technology/Fusion **3** (1983) 259.
[1.5-3] P.H.Rutherford, et al.; "Impurity Transport in Tokamaks", Princeton Plasma Physics Laboratory Report PPPL-1297 (1976).

1.5.2 Change of low energy neutral spectra at L/H and H/L transition

The low energy neutral particle flux emitted from the JFT-2M tokamak is measured by Time-Of-Flight (TOF) method. The particle energy is deduced from the difference of the flight time, such that the particle mass (hydrogen or deuterium) is not discriminated. This complicates the evaluation of the particle energy in the case of a hydrogen neutral beam heated deuterium plasma. Therefore, a pure hydrogen or a pure deuterium plasma is the best target to discuss about a change of an energy spectrum at L/H and H/L transition. Figure II.1.5-1(a) shows the energy spectra during the L-phase and just after the H-transition. Comparing these two spectra, the number of neutral particles whose energy is less than 400eV is decreased by the H-transition but those greater than 500eV does not change. The flux at 200eV in the H-phase is 2 times smaller than that in the L-phase. As a result a flat part of the energy spectrum can be seen in the energy

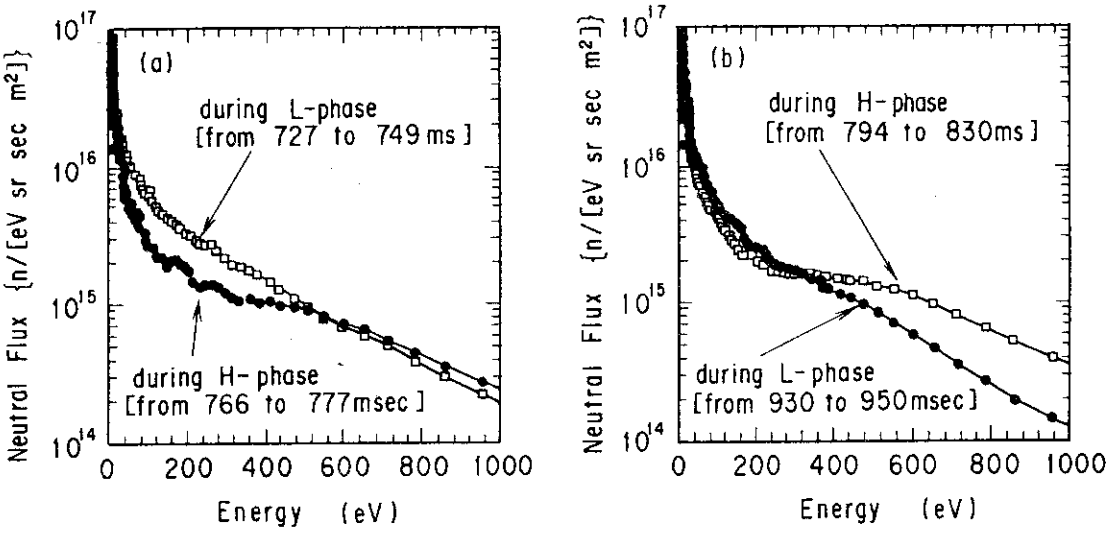

Fig.II.1.5-1 (a) Energy spectrum at the L-phase and just after the L/H transition, (b) Energy spectrum at the H-phase and after the H/L transition.

range from 300eV to 500eV. The slopes of the low energy (E<200eV) and the high energy (600eV<E<1000eV) part do not change much, but the reduction of the low energy flux and the invariance of the high energy flux lead to the fast change of the average energy. The fast change of the average energy is comparable to that of the edge electron temperature obtained from the electron cyclotron emission (ECE) measurements. The change of the neutral flux is also fast and there is a good correlation with the H_α/D_α signal at the divertor. Figure II.1.5-1 (b) shows the energy spectra during the H-phase and after the H/L-transition. Comparing the spectra of the H-phase in Fig. II.1.5-1 (a) and II.1.5-1 (b), the total flux increases but the shape of the spectra does not change much. The same remark is also applicable the spectra of the L-phase. The change of the energy spectrum at the H/L transition is the reverse change at the L/H transition.

1.5.3 TV Thomson scattering system

A cooperative program of Thomson scattering system for the JFT-2M tokamak has started between Princeton University Plasma Physics Laboratory (PPPL) and Japan Atomic Energy Research Institute (JAERI). This program is planned for two years from Dec. 1989 to Dec. 1991. The purpose of this program is the development of a TV Thomson scattering system for the JFT-2M tokamak and its installation as shown in Fig.II.1.5-2. The image obtained from the CCD gives a high spatial resolution.

This system is composed of six subsystems. PPPL will develop the optical subsystem and a part of the detector subsystem and JAERI will develop the remainder of the detector subsystem, the controller and data acquisition subsystem, the software subsystem and will construct the vacuum component subsystem and the laser oscillator subsystem.

The laser beam is incident horizontally on the beam dump which is composed of a carbon block. The effective length of measurement through plasma is 70 cm and measurements will be made at 81 points along the laser beam. It gives a 8.6 mm spatial resolution. The range of electron

temperature and density measurements will be 50 eV - 8 keV and (0.1 - 0.3)x10^{13} - 4x10^{14} cm^{-3}, respectively. The characteristics of this system are as follows; The horizontal plasma shift is measured with high spatial resolution, in contrast to the present 13 points vertical measuring system. The spatial resolution is better than any other Thomson scattering system.

The schedule of installation will be in January 1991 and the first data will become in April-May 1991 after some tests and the calibration.

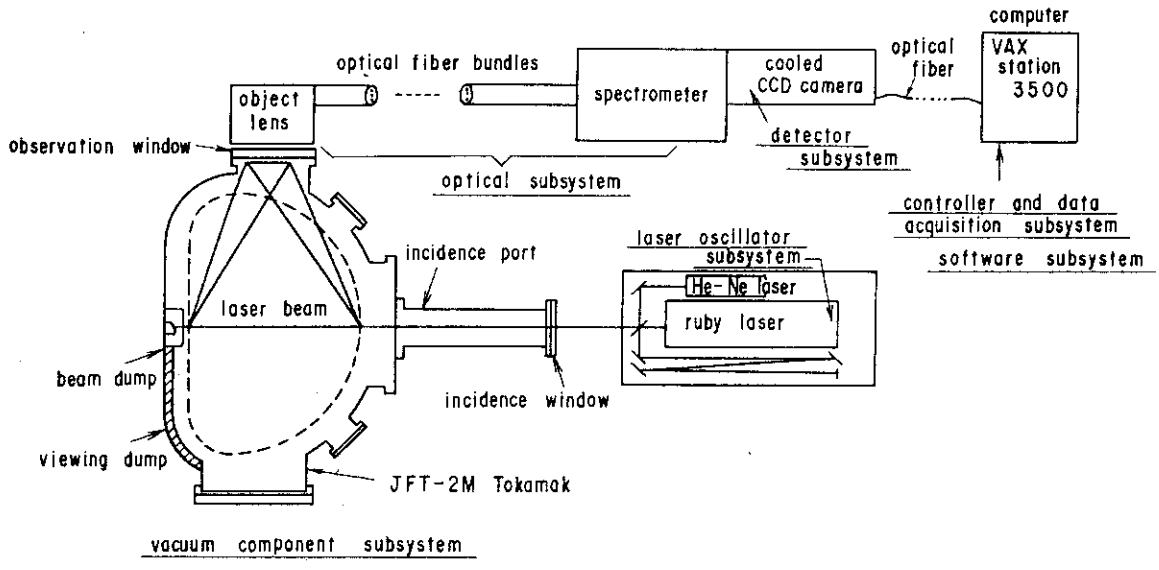

Fig.II.1.5-2 Sketch of TV Thomson scattering system in the JFT-2M tokamak under co-operative program.

1.5.4 Charge exchange recombination spectroscopy (CXRS) system

A space- and wavelength-resolving visible spectrometer has been installed in the JFT-2M tokamak to measure the profiles of ion temperatures poloidal/toroidal rotation velocities with CVI 5292Å (n=8-7) charge-exchange recombination line as shown in Fig.II.1.5-3.

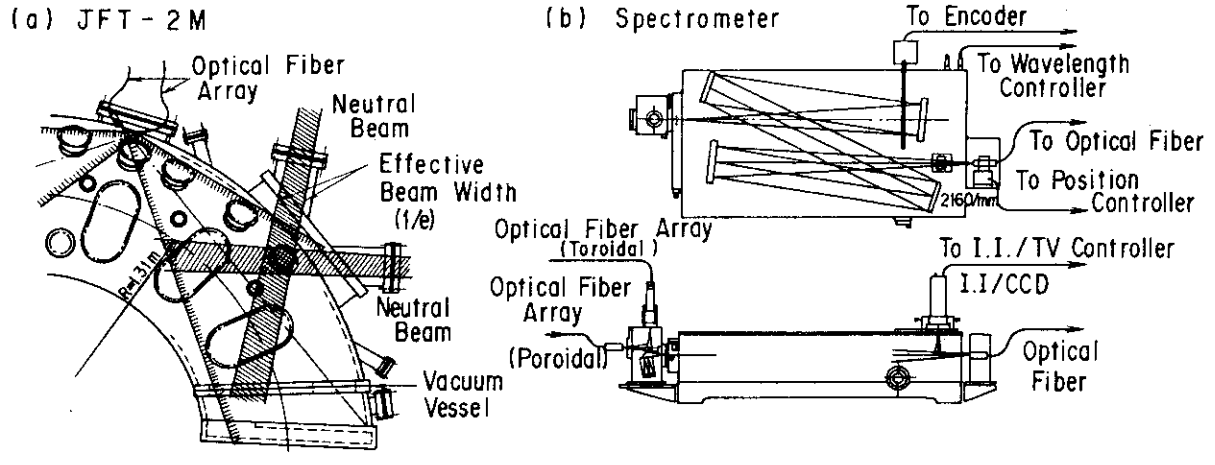

Fig.II.1.5-3 (a) Arrangement of the optical fiber arrays of the CXRS system and the neutral-beam lines, (b) spectrometer, optical fiber arrays and detectors of the CXRS system.

Two sets of 34-=channel toroidal optical fiber arrays, one viewing a fast neutral beam and the other viewing off the neutral-beam line toroidally in the opposite direction to subtract background and to determine a zero-velocity wavelength, are arranged on the entrance slit of the spectrometer. Another two sets of 22-channel poloidal arrays are also arranged on the same entrance slit. The optical fiber (100-m-core and 125-m-diam) viewing the cold plasma near the periphery are arranged with two lines (effective slit width is 200m), while the optical fibers viewing the hot plasma core are arranged with four lines (effective slit width is 400m) to collect more light from the plasma center where the beam attenuation is sever.

These optical fibers are led into the entrance slit of 1m Czerny-Turner spectrometer with 2160-grooves/mm. At the exit focal plane the light from each fiber gives the spectrum from one spatial position. The light from all fibers is focused, in both direction parallel and perpendicular to the slit, onto a gated image intensifier coupled with a CCD TV camera with 1:1 image fiber. The output of the CCD is a standard TV composite video signal and it is digitized with 6810 digitizer (12-bit accuracy 5-MHz sampling and 1024-kword memory). The data is transferred to the workstation VAX 3200. This workstation has 8MB of memory, 157MB magnetic disk and two drive of 5" optical disk (300 MB for each side).

This CXRS system has the spatial resolution of 1cm for the toroidal arrays and 4mm for the poloidal arrays, this resolution is precise enough to study the thermal barrier and poloidal rotation shear near the plasma periphery in H-mode plasma. The time resolution is limited to only 60Hz.

1.5.5 Diagnostic beam

A new diagnostic beam system for a CXRS measurement is now under construction in order to improve a signal to noise ratio (S/N). Designed performances of the diagnostic beam are shown in Table II.1.5-1. The value of the beam energy, 40keV, is determined in order that a sufficient intensity of a carbon line emission can be obtained. The perpendicular injection is also more suitable than the tangential injection for reduction of beam attenuation because of its shorter path length. Further improvement of S/N ratio can be achieved with chopping the beam. Since the charge-exchange recombination line emission is detected through a top port as shown in Fig.II.1.5-4, the beam has vertically elongated cross-section in order to get higher intensity.

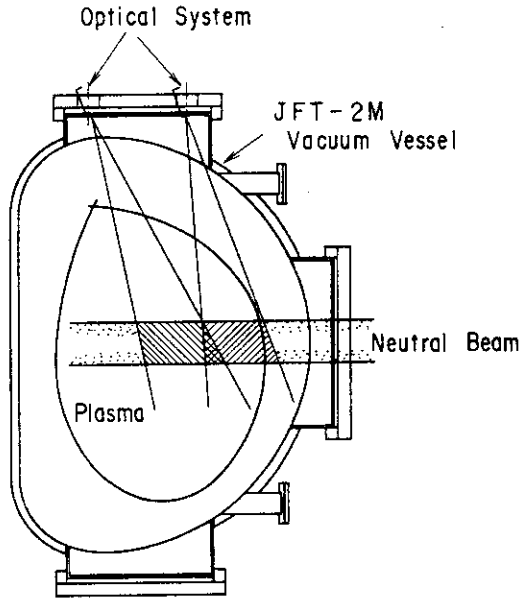

Fig.II.1.5-4 Cross-sectional view of a CXRS system with a new diagnostic beam.

Table II.1.5-1 Expected performance of Diagnostic Beam

Beam Energy	40 keV
Beam Current	2.5 A (neutral beam) /5 A (ion beam current)
Beam Species	Hydrogen Atom
Pulse Width	0.5 sec
Capability of Power Supply	2 sec
Beam Cross-Section	11 cm (vertical) x ~5 cm (horizontal)
Injection Angle	Horizontal and near Perpendicular Injection
Beam Chopping	Possible

2. Operation and Maintenance

2.1 Introduction

Facility Operation and Engineering Division has been engaged in operation and maintenance of JFT-2M, neutral beam injection (NBI) system, RF heating devices [fast wave current drive system (FW) and electron cyclotron heating (ECH) system] and flywheel motor-generator (MG), and also in development of auxiliary equipments and instruments. In this fiscal year, all devices have been operated smoothly on schedule, and the careful maintenance has been performed daily and periodically.

2.2 Operation and maintenance

In this fiscal year, regular inspection of a bearing of the motor-generator (MG) has been performed. The old space-heater of MG was replaced by a new one. In the JFT-2M machine, a power supply for divertor coils (Q-coils) was up-graded from 10 kA to 14 kA. Two local coil sets, EML coils, which produce the ergodic magnetic layer near the plasma surface, were installed outside the vacuum vessel, and also a divertor biasing equipment for a particle control and the neutral beam system for plasma production and diagnostics were set up. The copper filaments of an ion source on the neutral beam heating system were replaced to molybdenum ones to stabilize beam collimation. The ECH system was improved from 0.1 sec operation at 0.4 MW to 0.5 sec . New antennae for a current drive by fast wave were mounted inside the vacuum vessel, coupling and turning tests will be

Table II.2.2-1 Operation of MG, JFT-2M, NBI, ECH and FW

	(Fiscal Year)	1988	1989 APR-JUN	1989 JUL-SEP	1989 OCT-DEC	1990 JAN-MAR	Total
MG	MG(#1) (hours) MG(#2) (hours)	1206 1204	165 164	375 374	189 189	139 139	868 866
JET-2M	Total days of operation (days)	147	19	48	26	19	112
	Number of times of discharge (shots)	8919	1072	2668	1311	851	5902
	Baking (times)	4	1	0	1	0	2
	Discharge Cleaning (hours)	187	24	40	11	100	175
	Pellet injection (days)	28	5	12	5	0	22
NBI	Total days of operation (days)	85	13	42	22	8	85
	Flashing injection conditioning (shots)	A: 43817 B: 37564	8192 4080	18652 23162	12533 10249	4393 4036	A: 43770 B: 41527
FW	Total days of operation (days)	94	14	19	4	20	57
	Power injection (hours)	652	84	171	34	171	460
ECH	Total days of operation (days)	37	5	11	1	8	25
	Times of power injection (times)	31262	80625	6284	27	7839	94775

Table II.1.5-1 Expected performance of Diagnostic Beam

Beam Energy	40 keV
Beam Current	2.5 A (neutral beam) /5 A (ion beam current)
Beam Species	Hydrogen Atom
Pulse Width	0.5 sec
Capability of Power Supply	2 sec
Beam Cross-Section	11 cm (vertical) x ~ 5 cm (horizontal)
Injection Angle	Horizontal and near Perpendicular Injection
Beam Chopping	Possible

2. Operation and Maintenance

2.1 Introduction

Facility Operation and Engineering Division has been engaged in operation and maintenance of JFT-2M, neutral beam injection (NBI) system, RF heating devices [fast wave current drive system (FW) and electron cyclotron heating (ECH) system] and flywheel motor-generator (MG), and also in development of auxiliary equipments and instruments. In this fiscal year, all devices have been operated smoothly on schedule, and the careful maintenance has been performed daily and periodically.

2.2 Operation and maintenance

In this fiscal year, regular inspection of a bearing of the motor-generator (MG) has been performed. The old space-heater of MG was replaced by a new one. In the JFT-2M machine, a power supply for divertor coils (Q-coils) was up-graded from 10 kA to 14 kA. Two local coil sets, EML coils, which produce the ergodic magnetic layer near the plasma surface, were installed outside the vacuum vessel, and also a divertor biasing equipment for a particle control and the neutral beam system for plasma production and diagnostics were set up. The copper filaments of an ion source on the neutral beam heating system were replaced to molybdenum ones to stabilize beam collimation. The ECH system was improved from 0.1 sec operation at 0.4 MW to 0.5 sec . New antennae for a current drive by fast wave were mounted inside the vacuum vessel, coupling and turning tests will be

Table II.2.2-1 Operation of MG, JFT-2M, NBI, ECH and FW

	(Fiscal Year)	1988	1989 APR-JUN	1989 JUL-SEP	1989 OCT-DEC	1990 JAN-MAR	Total
MG	MG(#1) (hours)	1206	165	375	189	139	868
	MG(#2) (hours)	1204	164	374	189	139	866
JET-2M	Total days of operation (days)	147	19	48	26	19	112
	Number of times of discharge (shots)	8919	1072	2668	1311	851	5902
	Baking (times)	4	1	0	1	0	2
	Discharge Cleaning (hours)	187	24	40	11	100	175
	Pellet injection (days)	28	5	12	5	0	22
NBI	Total days of operation (days)	85	13	42	22	8	85
	Flashing injection conditioning (shots)	A: 43817 B: 37564	8192 4080	18652 23162	12533 10249	4393 4036	A: 43770 B: 41527
FW	Total days of operation (days)	94	14	19	4	20	57
	Power injection (hours)	652	84	171	34	171	460
ECH	Total days of operation (days)	37	5	11	1	8	25
	Times of power injection (times)	31262	80625	6284	27	7839	94775

completed in the next fiscal year.

A summary of the operation of the MG, JFT-2M, NBI, ECH and FW are shown in Table II.2.2-1.

2.3 Development of equipments and instruments

2.3.1 Pellet injection system

A multi-pellet injector, extruder type, has been developed since 1988, which is based on the design developed at ORNL as shown in Fig.II.2.3-1. The apparatus serves both to solidify hydrogen-isotope gas and to force-feed it to a gun section, the punch-type chambering mechanism/gun-barrel combination unit. The frozen hydrogen inventory in the extruder is about 1.96 cm^3 as determined the inside diameter of the brass sleeve (0.5 cm in diameter) and the useful piston travel (10 cm). An extrusion nozzle dimension at an entrance to the gun section is 1.6 mm x 3.2 mm (rectangular-type cross-section). A pellet size is 1.5 mm in diameter and 1.6 mm in length. The chambering mechanism and a fast-opening magnetic valve can be operated at a repetition rate of 10 Hz or more without a solid hydrogen-isotope. A cooling-down time of the cryogenic extruder is within 90 min. with a liquid helium consumption rate of 15 ℓ/h. The three coolers are cooled down to about 5 °K, enough to freeze hydrogen-isotope gas. Extruding performance tests have done to study the formation of solid hydrogen-isotope. Good quality of solid-hydrogen filaments is formed and extruded under condition in Table II.2.3-1. The hydrogen filament is extruded at a speed of about 24-32 mm/s, 4 times of the piston speed. In delivering tests of pellets, repetition rate obtained is 5 Hz to date.

Fig.II.2.3-1 Multi pellet injector (extruder type).

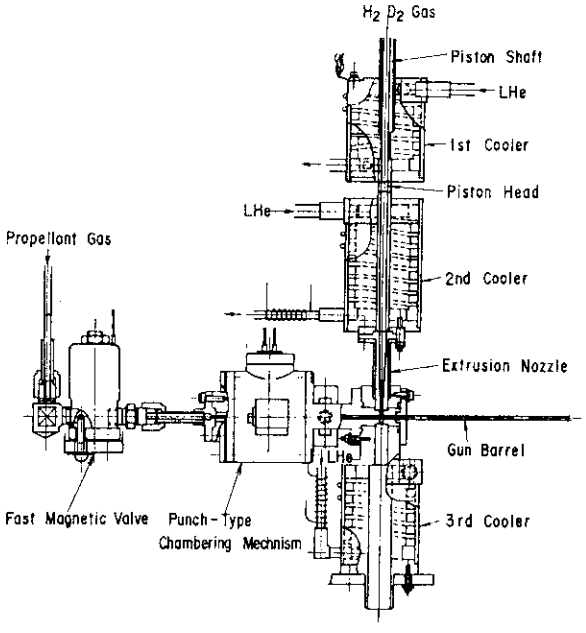

Table II.2.3-1 Conditions of freezing temperatures of the hydrogen gas and of the extruding of the solid hydrogen.

Parameter	Condition
Temperatures 1st Cooler 2nd Cooler 3rd Cooler	 14～18°K 10～11°K 10～11°K
Condensation Pressure	750～900 Torr
Condensation Time	1～2 min.
Piston Speed	6～8 mm/s

2.3.2 Time-of-flight (TOF) neutral particle diagnostic apparatus

The TOF diagnostic apparatus is installed on the top of the JFT-2M vacuum vessel as shown in Fig.II.2.3-2. The system consists of the chopper, the flight tube, the detector and a turbo molecular pump. The chopper consists of a rotating cylinder with slits driven by a TMP (Ohsaka Vacuum TG360M) and a fixed stator slit. The cylinder does not intersect TMP blades, such that the TMP works as a pump as well as a chopper. The cylinder is made of aluminum alloy

and there are 9 pairs of slit on it. One slit of each pair is narrow (0.15mmW x 6.0mmH) and the other is wide (3.0mmW x 6.0mmH). The wide slit is required such that no particles coming through the chopper slit are cut off during flight through the cylinder [2.3-1]. The size of stator slit is 0.15mmW x 6.0mmH. The vacuum condition is well as shown in Fig.II.2.3-2. There are two windows 40 degrees away from the neutral path to monitor the particle gating. A He-Ne laser and an avalanche photo diode (APD) detector on an x, y, z and rotation stage are set in front of the window. Then the trigger timing of this monitor can be changed by changing the position of a slit between He-Ne laser and APD. The calculated energy resolution depends on the particle energy and is less than 20% at 1000eV/amu for 1.5m flight length. Since the cylinder, which has 9 pairs of slit, rotates at a speed of 36000rpm, the neutrals are chopped in bunches every 185μsec. This 185μsec is the minimum time resolution of this system.

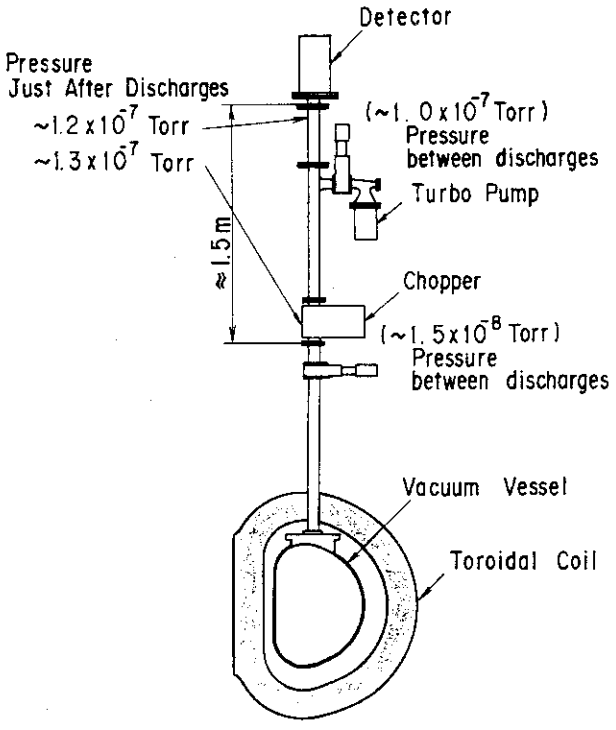

Fig.II.2.3-2 The installation of TOF system on JFT-2M. The vacuum condition at chopper and at the detector is also shown.

The detector (Hamamatsu R943EMT) is a secondary electron multiplier with Be-Cu plate. The detector is magnetically shielded by a 1cm iron and magnetic shield case (Hamamatsu E989-26). The Be-Cu plate has an efficiency to detect electrons, ions, photons and neutrals. In the tokamak environment, the unwanted charged particles are automatically deflected by the stray magnetic fields. But the unwanted intense photons cannot be rejected from the neutral outflux. We use a switch-off technique of R943EMT to distinguish intense photons from the neutral outflux. The gate assembly (Hamamatsu C1392-03MOD) controls the switching of R943EMT by applying an inverse voltage at 2nd and 4th dynodes. The duration of this switch-off depends on the TTL pulse width. The negative emission coefficient of Be-Cu plate by neutral atoms (η) is a very important parameter to evaluate the energy spectrum. The value of η was carefully calibrated by Verbeek[2.3-2]. We use the value of η reported by Verbeek by a fitting curve. The gain of the electron multiplier is also important to evaluate an absolute neutral flux. The gain calibration depending on a negative HV is performed by Hamamatsu K.K. using an electron beam. The electron multiplier output (current) is converted to a voltage by a preamplifier (2.05×10^3 V/A) and is digitized by a CAMAC transient recorder controlled by a personal computer system.

References

[2.3-1] Y.Miura, F.Okano and Y.Matsuzaki, "Low energy Neutral Particle Energy Analyzer by Time of Flight Method", JAERI-M 89-018 (1989) (in Japanese).
[2.3-2] H.Verbeek and W.Eckstein, IPP Report IPP9/45 December 1983.

III. COOPERATIVE PROGRAM ON TOKAMAK EXPERIMENT

1. DIII-D (Doublet III) Experiment

Recent new device capabilities have enabled new tokamak operation regimes to be entered. Completion of a neutron radiation shield around the DIII-D tokamak allowed deuterium neutral beam operations with improved confinement and increased injection power of 20 MW. A number of diagnostics improvements have occurred this past year including a UCLA microwave scattering system for turbulence studies, a new dual channel UV spectrometer and an X-ray spectrometer from the Soviet Union. The accomplishments of the DIII-D program over the last year have been substantial and are summarized as follows.

A record plasma beta of 9.3 % was achieved with a double-null divertor operation and values of 8 % beta were sustained for 0.9 sec. These values are well beyond that needed for IT-ER and now high beta H-mode plasmas with 5.2% (total stored energies of 3.6 MJ) have been realized at full 2.1 T toroidal field. A new discharge regime with normalized beta ($\beta t/(I/aB)$) as high as 5 has been explored(Fig.III.1-1). These discharges are calculated to be near the theoretical stability limit. Further increased understanding of the dependence of the beta limit on profiles offers the possibility that with direct control of current and pressure profiles steady-state operation at even larger values of normalized beta may be possible.

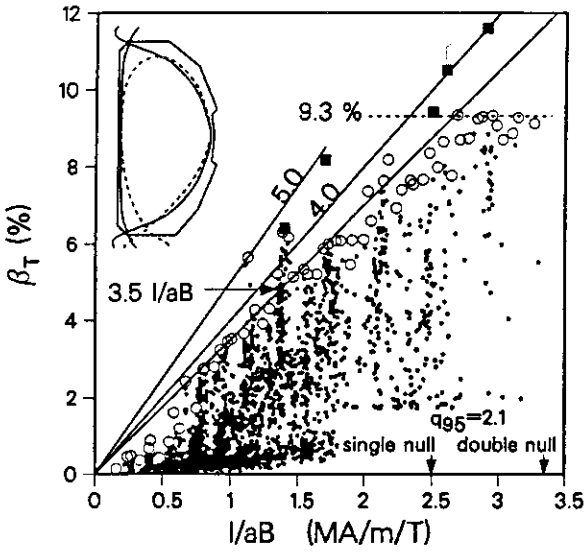

Fig.III.1-1 Volume average toroidal beta of DIII-D discharges vs. normalized current. The open circles highlight the highest beta discharges at each I/aB. The squares are the calculated theoretical beta limit [1-1].

Helium-glow conditioning of the vacuum vessel walls, field error compensation and deuterium operation have produced tripled ion temperature to 17 keV reaching levels required for ignition. In this hot-ion H-mode, local transport analysis indicated that the ion thermal diffusivity is close to the neo-classical value and the heat loss is dominated by electrons. In addition, the energy confinement times of deuterium H-mode plasmas as high as 0.34 sec have been achieved. These significant values in DIII-D are indicated as an increased fusion

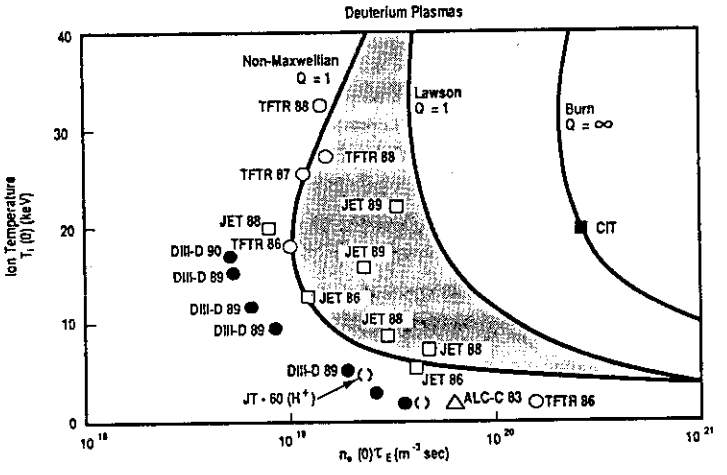

Fig.III.1-2 High temperature and high confinement DIII-D plasmas are shown in the Lawson diagram indicating $n\tau T$ of $10^{20}m^{-3}$sec keV.

ignition parameter $n\tau T$ to $10^{20}m^{-3}$ sec keV in Fig.III.1-2. A coordinated H-mode size scaling study was carried out with DIII-D and JET. By adjusting the frequency and amplitude of ELMs, a 10-second-long pulse of H-mode discharge free from deuteron density dilution and radiation collapse (slowly decaying Zeff) was demonstrated to be possible.

An array of ten inside launch waveguide systems for ECH heating were successfully operated with power levels up to 1.8 MW at 60 GHz, resulting in important physics data such as efficient heating for electrons, H-mode, ELM suppression, sawtooth suppression, preionization (breakdown with electric field as low as 0.15 V/m) and also rf driven current of 50-100 kA level. One MW ion Bernstein wave ICH experiments were carried out and indicated coupling limited to the edge without central heating.

As to the H-mode physics study, a sudden increase in the edge poloidal flow (or equivalently inward directed radial electric field of about 30kV/m) has been observed based on spectroscopic determination of plasma rotation and correlated with the L to H-mode transition. A decrease in associated plasma fluctuations was measured with microwave reflectometry and FIR scattering. These new measurements are being compared to H-mode theories. A drastic drop of fluctuation level associated with L to H transition is shown in Fig.III.1-3.

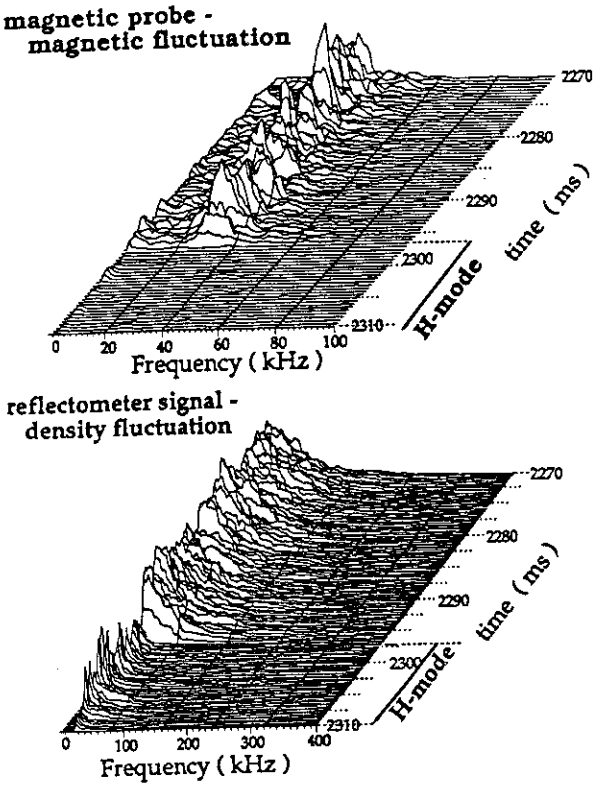

Fig.III.1-3 Edge magnetic and density fluctuations drop drastically at L to H transition. Microwave reflectometer measurements are by UCLA[1-2].

During the Japanese fiscal year 1989 a total of six individual scientists from JAERI contributed to the productivity and progress of the joint research program in the fields of coordinating the fluctuation studies and to an active participation in the U.S. Transport Task Force, ECH experiments and TORAY code calculations, the poloidal field measurement by motional Stark effect, the density fluctuation studies with the diagnostics improvement for the evaluation of the suppression depth of edge fluctuations, and the high beta study. Papers concerning the plasma shaping control for divertor equilibria [1-3], ELM activities with the ballooning stability analysis in highly shaped H-mode discharges[1-4] and edge magnetic fluctuations in L-mode plasmas[1-5] have been prepared for publication in journals.

In 1989 construction work on an Advanced Divertor Program(a combination of divertor baffle/biasable divertor plate structure), 2 MW 110 GHz system utilizing 0.5 MW gyrotrons, an antenna for fast wave current drive, and new diagnostics were initiated. During the next year the D

III-D program will emphasize transport studies at high beta both with detailed experiments as well as with fluctuation diagnostics. Beta studies will investigate higher elongation and triangularity in double-null divertor operation. Heating and current drive will be explored with 2 MW ECH, 2 MW ICRF and 20 MW neutral beams.

Continued discussions between the US and JAERI resulted in a plan for a joint multi-megawatt high power ECH program at the 16th Steering Committee meeting at Naka site. The basic idea is as follows: Through the vigorous support of the USDOE, 0.5 MW level gyrotrons are now available and MW-level gyrotrons operating at 110 GHz with CW capability will soon be available. A US-Japan ECH collaboration has been proposed to capitalize on the availability of this new higher power ECH source. Subject to the availability of funds, a system with five MW-level gyrotrons will be fabricated and then used for approximately one year of commissioning and experiments on DIII-D, for the first time in the world with this power level. Following its use on DIII-D, the equipment will be transferred to Japan for installation and conduct of high power ECH experiments on the JT-60U tokamak. Two working groups to investigate the implementation of this program were established.

References

[1.-1] J.R.Ferron,et al.,Phys. of Fluids **B2**(1990)1280
[1.-2] K.H.Burrell,et al.,ibid.1405
[1.-3] S.Kinoshita,et al.,GA-A19584(1989)
[1.-4] T.Ozeki,et al.,GA-A19495(1989)
[1.-5] Y.Neyatani,et al.,GA-A19698(1989).

2. Microwave Tokamak Experiment

2.1 Present status of MTX experiment

The Microwave Tokamak eXperiment (MTX) is a project to heat a plasma using extremely intense microwave pulse from a Free Electron Laser (FEL) at Laurence Livermore National Laboratory (LLNL) in U.S.A. Collaboration between JAERI and LLNL under Annex VI to the Japan-US Implementing Arrangement began in May 1988.

MTX tokamak started operation and a target plasma for FEL microwave injection had been established in the last year. The first FEL microwave pulse was injected into the plasma for this year. During the run period ending the 10th of November, microwave pulses up to 150 MW at 140 GHz were generated and transmitted on the quasi-optical system to the tokamak. Transmission measurements were carried out showing no evidence of nonlinear effect at this power level.

2.2 Contribution of JAERI

2.2.1 Diagnostics in JFY88

1) Soft X-ray system has been installed on MTX and after a process debugging and characterization of the electronics, data has been taken with 100 ns time response, which is the expected design value. Examples of data are shown in Fig.III.2.2-1.
2) Neutron Diagnostic System has been installed on MTX and finished a debugged and characterization of the electronics. preliminary data have been obtained during this year because of a few deuterium discharges.

3) Microwave Diagnostic Box and associated equipment are installed in the microwave transmission line at the entrance to the tokamak and have been used extensively in the FEL experiments. Many 140GHz microwave diagnostics mainly made by LLNL are installed in this box.

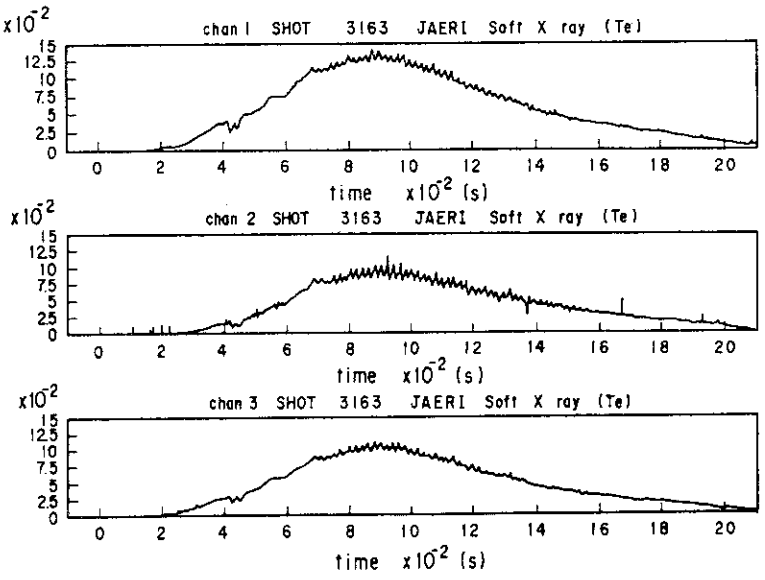

Fig.III.2.2-1 Soft X-ray signals from MTX tokamak. Currently 3 energy channels are testing time response of detectors (photon flux).

Neutral diagnostic system has been calibrated by neutron source installed inside tokamak vacuum chamber and has also been checked with electron temperature of high density MTX tokamak discharge. The system has been operated routinely. Soft X-ray system installed on MTX in JFY88 has also been operated routinely.

2.2.2 Diagnostics in JFY89

The following diagnostics were sent to LLNL in March 1990:

1) Soft X-ray Camera, which is an upgrade of the soft X-ray system, consists of 2x10 sensor channel (with one backup sensor) and additional 6 channel digitizer system. The 2x10 sensor channels were made with the largest sensitive area possible for the MTX port size.
2) Second Harmonic Electron Cyclotron Emission Monitor (ECE) looks from the inside wall of the tokamak to observe a heated electron. LLNL made and installed the antenna and interface to the tokamak. This system has 2 frequency band for observation at near the center where microwaves are absorbed and near the edge where some nonlinear parasitic absorption may occur. Each band is separated into 2 channels at intermediate frequency to extend a spatial resolution.
3) Three microwave mirrors are used at the quasi optical transmission line to change focusing of the microwave beam.
4) Microwave dummy load system for intermediate power was made to measure a calorie of energy from the FEL microwave pulse. The sensitivity is several tens of joule minimum and up to several hundred watt with continuous input. This will be used for gyrotron testing at first.

2.2.3 Diagnostics in JFY90

In JFY90, JAERI will provide : (1) Microwave Electric Field Diagnostic System and (2) Reflectometer for density fluctuation measurement.

The former, so-called Laser Assisted Particle Probe Spectroscopy (LAPPS), will be made with collaboration of several participants: JAERI, Hiroshima University, University of California at Davis, and LLNL. We have had many work shops on this item this year. Although the measurement appears difficult for a variety of technical and physical reasons, calculations indicate that it should be possible. A part of neutral beam injector was already made in JFY89.

IV. JT-60 PROGRAM

1. Overview

During the past year, the JT-60 tokamak research program has made significant advances and contributions in many areas. An important feature of this work has been the combination of achievement in advancing the operation parameters of tokamaks toward the reactor regime and development of a better understanding of the physics mechanisms underlying tokamak behavior, especially in the areas of confinement, divertor function and current drive. There were two major additions to the operation area during 1989 that have had a significant impact on expanding the performance capability of the tokamak: i) a four-barrel pneumatic pellet injector with speed of 2.3 km/s and sizes of 3 mm and 4 mm, and ii) a new multijunction-type lower hybrid launcher with sharp power spectra of $\Delta N_{||} \sim 0.5$ and high directivity. These additions have allowed us extensive capabilities in plasma density and current profile control and it has allowed the confinement program to be extended into more relevant regimes of higher center peaked plasma pressure, and more clear profile control in the production of high energy electron current. Associated with these additional equipments, research effort has been the work on 1) improvements in plasma confinement with profile control and 2) steady state operation study. Experiments have been carried out in the wide range of parameters: $0.5\times10^{19}\ m^{-3} < \bar{n}_e < 1.8\times10^{20}\ m^{-3}$, 0.3 MA < Ip < 3.1 MA, $B_T < 4.8$ T, $P_{NB} < 23$ MW, $P_{LH} < 7$ MW and $P_{IC} < 2.5$MW. Both limiter and lower X-point divertor configurations were employed. The operating gas was hydrogen and, in some cases, helium.

Improvements in confinement were demonstrated with pellet injection, LH current drive, high-Ti mode operation or ICRF. Peaked density profiles of $n_e(0)/\langle n_e \rangle < 4.5$ were produced with successive three or four pellets injection. The sawtooth period was prolonged up to 1 sec by the pellet injection. Both density and pressure profiles were peaked inside the q=1 surface. The electron density and the total pressure at the plasma center reached $3\times10^{20}\ m^{-3}$ and 2 atms, respectively. The energy confinement time was improved by 30-40 % relative to gas fuelled discharges for NB heating of 5-15 MW. The achieved $n_e(0)\tau_E Ti(0)$ is $1.2\times10^{20}\ m^{-3}$skeV at Ip=3.1MA, which is twice that of gas fuelled discharges. A clear correlation was found between the improved stored energy inside the q=1 surface and the peakedness of density profile. The maximum value of the local pressure gradient inside q=1 surface and the onset condition of the fast crash are consistent with ideal MHD ballooning and low-n kink stability analysis.

The control and understanding of sawtooth stabilization with LH current drive has been extensively investigated with the new LH launcher. A broad high energy electron current profile was obtained with high $N_{||}$ injection. On the other hand, low $N_{||}$ injection was effective for suppression of sawtooth activities. Low-$N_{||}$ LH current driven discharges with high power NB heating showed centrally peaked high energy electron current and ion temperature profiles during the sawtooth free periods of up to 1.8 sec. The appearance of sawtooth at a finite minor radius at the switch-off of LH , and the existence of m=1 oscillation in some marginally stabilized discharge suggest that q(0) may be less than or equal to unity during sawtooth suppression period. From the correlation between the sawtooth stabilization period and the intensity of high energy electrons

near the plasma center, it is expected that the existence of high energy electrons or local current profile modification may be possible keys to the sawtooth suppression mechanism.

The extension of the operation regime of LH current drive has greatly benefited the confinement program. The H-mode was achieved in limiter discharges with LH current drive for the first time. Simultaneous application of RF powers at two different frequencies such as 1.74 + 2.23 GHz or 1.74 + 2.0 GHz appeared to be effective in the attainment of the H-mode. The threshold lower hybrid power was as low as ohmic heating power with hydrogen plasmas. Nearly steady-state ELM-free H-mode with durations up to 3.3 sec was established without significant impurity accumulation.

The extension of JT-60's NB perpendicular injection into high field (B_T=4.5T) and low plasma current has successfully yielded high-Ti and high-βp discharge regime . The discharge was realized with ~20MW NB injection into low density(~$0.5\times10^{19}m^{-3}$) lower X-point discharges. For the Ip regime of 0.5-0.7 MA (q_{eff}=8-13), the discharge showed no sawtooth activity. This resulted in an improved confinement, a peaked density profile of $n_e(0)\sim6\times10^{19}m^{-3}$ and high Ti(0) of 12keV. In these discharge a clear correlation was found between the peakedness of ion temperature and electron density profiles.

Effective acceleration of high energy ions was observed in the H-minority He plasma by the combined heating of NB and ICRF with second to fourth harmonics of hydrogen cyclotron frequency. Giant sawteeth with a maximum period of 410 ms were observed. The energy confinement time was improved by a factor of 1.2 during the giant sawtooth period.

The main experimental issues for the steady-state operation research were non-inductive current drive and particle and heat control with divertor . LH current drive experiments were carried out for a wide range of $N_{||}$(1.0-3.4). The current drive efficiency η_{CD} was proportional to the product of $1/N_{||}^2$ and accessible power fraction, i.e. spectrum dependence of η_{CD} showed a good agreement with Fisch's theory. The maximum η_{CD} of $3.4\times10^{19}m^{-2}A/W$ has been achieved with LH injection of 2-4.5MW for lower X-point discharges with $\bar{n}_e$ up to $3.0\times10^{19}m^{-3}$ and Ip=1-1.75 MA. The achieved value is well approaching $5\times10^{19}m^{-2}A/W$, which is the efficiency necessary for the ITER steady-state operation.

The neoclassical bootstrap current was confirmed in the wide range of βp. The ratio of bootstrap current to the total current increased in proportion to βp and reached 80 % at $\beta p\sim3.2$. The existence of the bootstrap current was also demonstrated by keeping the primary OH current constant and measuring the decay time of the total current. The result is encouraging for the design of high-Q(20-30) steady-state tokamak reactor.

One of the major problems in the next-step device is the exhaust of fusion produced α-particles. To simulate the α-particle production in D-T plasmas, 30keV helium NB was injected into NB heated lower X-point discharges, which produced centrally peaked birth profile of α-particles. Both the H_2 and helium pressure in the divertor region increased in proportion to $\bar{n}_e^3$. The helium pressure reached 0.02 Pa (10% of H_2 pressure) at $\bar{n}_e=5\times10^{19}m^{-3}$, in which α-particle density is 10% of the main proton density. A simple extension of the present result is promising

for the helium exhaust in future device; pump speed of several tens m^3/s will be sufficient for 1000MW fusion power reactor operating at $\bar{n}_e=1x10^{20}m^{-3}$.

Another major problem of present and next-step device is the divertor plate heat flux, in which a solution is expected to produce strong remote radiative cooling in the divertor region. The capability of remote radiative cooling has been extensively investigated with high power NB injection of ~20MW in lower X-point discharge. Over a threshold main plasma density and safety factor, strong remote radiative cooling of up to 50 % of the total input power was observed in JT-60. Under this situation, discharges with 23MW NB injection showed no carbon burst during whole injection period of 4 sec. Measurement of Hα and carbon lines and heat flux density revealed that the divertor plasmas are dense and cold (n_{ediv}~$2.4x10^{20}m^{-3}$,T_{ediv}~26eV), and the remote radiative cooling is a mixture of carbon and hydrogen radiation.

2. Operation

2.1 Summary

The operation schedule of JT-60 in FY 1989 is shown in Fig. IV.2.1-1. In April, we conducted 2-cycle operations. The inspections were also carried out to finally confirm the integrity of the cooling pipe of toroidal field coil. In May, we had the maintenance of JT-60 facilities for about a month. In this shutdown period, the damaged carbon tiles were replaced by new ones. The operation restarted in June and continued to October. In this period, 9-cycle operations were conducted. After the advanced experiment, the modification for JT-60 upgrade has been performed and will continue to March in 1991. In September and October, we regularly obtained high plasma current of 3.1MA at toroidal magnetic field of 4.8T.

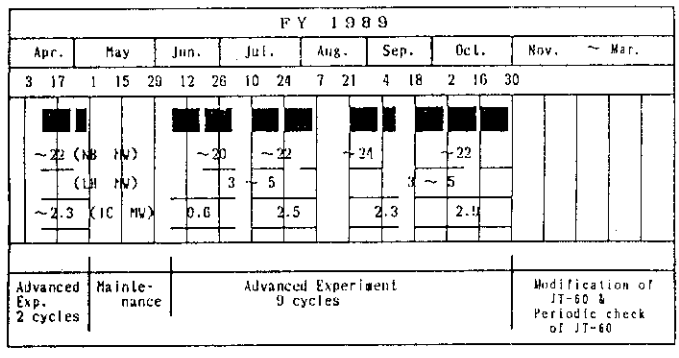

Fig.IV.2.1-1 Operation schedule in FY 1989

The operation from FY 1985 to FY 1989 is summarized in Table IV.2.1-1. The average number of shots per day by fiscal year is shown in Fig.IV.2.1-2. The average number of shots has increased steadily year by year. The reasons for the result of the increase are

Table IV.2.1-1 Summary of the JT-60 operation results

Item ＼ FY	1985	1986	1987	1988	1989	Total
Operation days	58.5	118	81.5	133.5	92	483.5
Scheduled days for Plasma	38	102.5	66.5	105.5	87.5	400
Plasma Pulses						
Total	451	1885	1611	2744	2299	8990
OH	439	778	782	642	365	3006
NB		446	504	709	563	2222
RF		334	144	803	756	2037
NB+RF		267	121	532	584	1504
Sequence Stop	12	60	60	56	31	221
Average Number of Shots/Day	11.9	18.4	24.2	26.0	26.3	22.5
Number of Troubles	215	344	164	146	62	931
Ave. Number of Troubles/Day	3.7	2.9	2.0	1.1	0.7	1.9
Hours of TDC	141.6	140.6	37.7	98.6	77.9	496.4
Pulses of TDC (X 1000)	336	383	126	391	349	1,585
Commissioning Shots	89	70	120	181	24	484

for the helium exhaust in future device; pump speed of several tens m^3/s will be sufficient for 1000MW fusion power reactor operating at $\bar{n}_e=1x10^{20}m^{-3}$.

Another major problem of present and next-step device is the divertor plate heat flux, in which a solution is expected to produce strong remote radiative cooling in the divertor region. The capability of remote radiative cooling has been extensively investigated with high power NB injection of ~20MW in lower X-point discharge. Over a threshold main plasma density and safety factor, strong remote radiative cooling of up to 50 % of the total input power was observed in JT-60. Under this situation, discharges with 23MW NB injection showed no carbon burst during whole injection period of 4 sec. Measurement of Hα and carbon lines and heat flux density revealed that the divertor plasmas are dense and cold (n_{ediv}~$2.4x10^{20}m^{-3}$,T_{ediv}~26eV), and the remote radiative cooling is a mixture of carbon and hydrogen radiation.

2. Operation

2.1 Summary

The operation schedule of JT-60 in FY 1989 is shown in Fig. IV.2.1-1. In April, we conducted 2-cycle operations. The inspections were also carried out to finally confirm the integrity of the cooling pipe of toroidal field coil. In May, we had the maintenance of JT-60 facilities for about a month. In this shutdown period, the damaged carbon tiles were replaced by new ones. The operation restarted in June and continued to October. In this period, 9-cycle operations were conducted. After the advanced experiment, the modification for JT-60 upgrade has been performed and will continue to March in 1991. In September and October, we regularly obtained high plasma current of 3.1MA at toroidal magnetic field of 4.8T.

The operation from FY 1985 to FY 1989 is summarized in Table IV.2.1-1. The average number of shots per day by fiscal year is shown in Fig.IV.2.1-2. The average number of shots has increased steadily year by year. The reasons for the result of the increase are

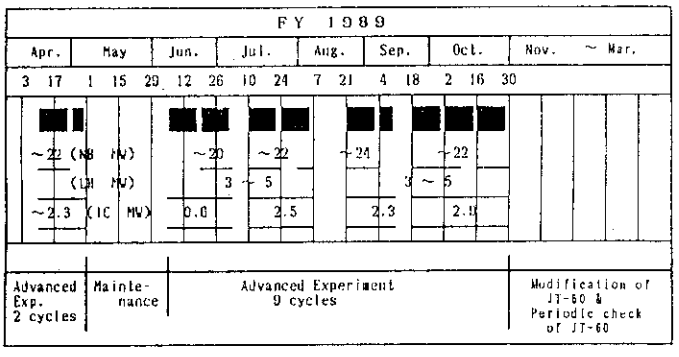

Fig.IV.2.1-1 Operation schedule in FY 1989

Table IV.2.1-1 Summary of the JT-60 operation results

Item \ FY	1985	1986	1987	1988	1989	Total
Operation days	58.5	118	81.5	133.5	92	483.5
Scheduled days for Plasma	38	102.5	66.5	105.5	87.5	400
Plasma Pulses						
Total	451	1885	1611	2744	2299	8990
OH	439	778	782	642	365	3006
NB		446	504	709	563	2222
RF		334	144	803	756	2037
NB+RF		267	121	532	584	1504
Sequence Stop	12	60	60	56	31	221
Average Number of Shots/Day	11.9	18.4	24.2	26.0	26.3	22.5
Number of Troubles	215	344	164	146	62	931
Ave. Number of Troubles/Day	3.7	2.9	2.0	1.1	0.7	1.9
Hours of TDC	141.6	140.6	37.7	98.6	77.9	496.4
Pulses of TDC (X 1000)	336	383	126	391	349	1,585
Commissioning Shots	89	70	120	181	24	484

as follows. First, the operation time increased by one hour to 8:00-22:45 in FY 1986. Secondly, daily checking time required for startup and shutdown decreased according to operational experience. Thirdly, troubles and time for its repair are greatly reduced by improvement of the electrical insulation check system, development of the leak test system. As shown in Fig.IV.2.1-3, the average number of troubles per day decreased from 5.1 in FY 1986 to 2.0 in FY 1989. The down time by troubles per day decreased from 174 minutes in FY 1986 to 76 minutes in FY 1989, too. In FY 1989, we carried out 2,299 shots of experimental discharge. The total number of shots for the past five years amounts to 8,990.

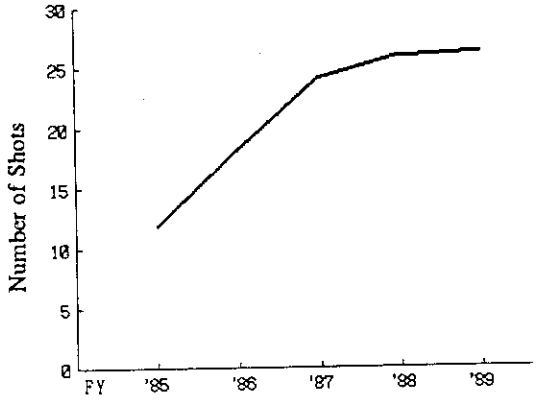

Fig.IV.2.1-2 Average number of shots per day by fiscal year

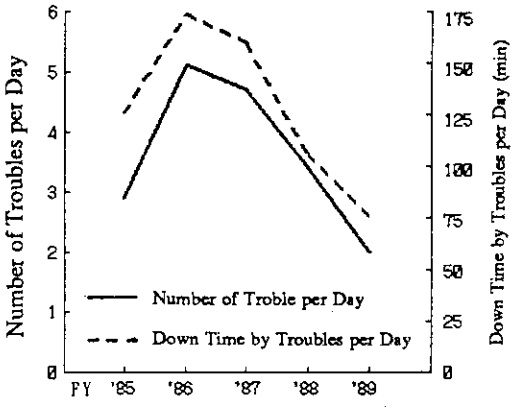

Fig.IV.2.1-3 A summary of trouble analysis

2.2 Tokamak

2.2.1 Operation and maintenance

After the operation period(Jan.-Apr. 1989), we replaced the damaged first wall tiles including those of the divertor armors, went through the official inspection on the high pressure gas devices such as the liquid nitrogen supplier of the pumping system and the solid fuel supplier of the pellet injector, replaced several number of the all-metal gate valves which suffered with vacuum leak at their respective membrane, and installed the in-situ coating devices with running tests for titanium evaporation to the carbon wall that was to be performed in the following operation period starting in June.

The pellet injector, after modification, was operated successfully recording the pellet speed of 2.3 km/s, which contributed greatly to attain a recording value of the fusion integration $n\tau T$.

Titanium coating to the carbon wall was performed with two in situ coating devices applying a filament assembly respectively containing 40 g titanium in the cases that the vacuum vessel was in baking and not in baking. It contributed to develop the experimental space. The operation period ended on 27th October 1989. Putting safety measures on the devices and instruments for their long time stop, the construction work for modifying JT-60 for higher plasma current operation started.

During the concerning operation period, we came across several events which required days of machine stop for countermeasures. The major events can be stated as follows.

(1) Drop out of sliding supporter for anti-quake rod

In July 1989, the grounding circuit for the vacuum vessel was found in disorder. It was found that a sliding support for one of the ten antiquake supports of the vacuum vessel dropped out causing short circuit between the vacuum vessel and the support structure for the poloidal coils. It came from the fact that a key restricting move of the sliding support rose up from its standard position due to repeated vibration of the vacuum vessel. The dropped out sliding support was partly machined, and installed in its own position modifying the stop key not to rise up again.

(2) Vacuum leak at the bellows of a large diameter port

In October 1989, during experimental operation with baking, a vacuum leak (12 Pam^3/s) took place at the bellows of a large diameter port for pumping system. Lowering the temperature of the vacuum vessel and filling it up with nitrogen gas, the bellows was taken up. A metal blind plate was welded to the rest of the port. Inspecting the inner surface of the bellows, a piece of carbon with evaporated titanium (5mm x 5mm x 2 mm) was found, and beside that was a pin hole of 1 mm diameter likely melted by the hot piece.

2.2.2 Outgassing mechanism after current decaying phase in disruptive and normal discharges[2.2-1]

The outgassing from the first wall made of graphite has been investigated with a newly developed pressure gauge. This gauge can measure the pressure near hydrogen plasmas in a fast response time (<10 ms). Large amounts of gases are abruptly released in two stages during a disruption of the plasma. The first gas-release occurs at the same time as the soft x-ray crash. This is ascribed to the heat flux due to the loss of the plasma thermal energy (thermal quench). The second appears during the current decay phase. This is caused by the heat flux due to the loss of the plasma magnetic energy. The disruption of a 1 MA plasma outgases a surface area of ~10 m^2. The typical disruption releases 30-80 Pam^3 of gases in ~30 ms. Then three quarters of them return to the wall. Nevertheless, the evacuated gas quantity after a typical disruption is almost equal to or greater than the input. On the other hand, the evacuated quantity after a normal discharge is less than the input. The outgassing occurs after the end of the plasma with quiet current decay. It holds for ~30 s with rates decreasing gradually from 1-2 to 0.1-0.2 Pam^3/s. The hydrogen atoms probably diffuse from the bulk of the graphite after ions and charge-exchange fast neutrals from the plasma impinge into the wall during the decay of the plasma current. The activation energy of the bulk diffusion is estimated to be less than 1.5 eV.

References

[2.2-1] N. Ogiwara and M. Maeno, to be published in J. Vac. Sci. Technol Sep/Oct (1990).

2.3 Control system

In this operation period from April to October in 1989, no big modifications were performed in the JT-60 central control system ZENKEI [2.3-1], and then it functioned very stably. The number of the troubles occurred in ZENKEI amazingly decreased to only 16, which corresponds to about 9 % of the total number of the troubles in JT-60. Most of the troubles were due to hardware troubles in the interfaces of CAMAC and GPIB. Software trouble was extremely decreased in the quality control activities performed in the software development. The total time to restore was about 8 hrs., which corresponds to about one third of that occurred in the previous year.

References

[2.3-1] I. Kondo, et al., Fusion Engineering and Design **5** (1987) 69.

2.4 Power supply system

The JT-60 power supply system[2.4-1] consists of the toroidal field power supply system (TFPS), the poloidal field power supply system (PFPS) and the motor generator for the plasma heating system (H-MG). Each system has one motor generator (MG) as an energy storage device. In FY 1989 the TFPS's MG, the PFPS's MG and the H-MG were operated for 1158.4, 1164.4 and 1275.8 hours, respectively. These MGs have been operated for about five years since their completion, so they were overhauled in turn from November 1989. The overhauls of the PFPS's MG and the H-MG were finished in FY 1989.

In the operation of this fiscal year, 23 troubles occurred in the TFPS. Most of the troubles were caused by mismovement of the devices to detect the system malfunction. The troubles occurred in the PFPS amounts to 92, most of which were due to overcurrent or overvoltage which were induced by plasma disruptions. The H-MG had no troubles in this period.

The auxiliary system, which consists of the secondary cooling system, the power distribution system and the emergency power supply system, has been operated smoothly in FY 1989.

References

[2.4-1] R. Shimada, et al., Fusion Engineering and Design **5** (1987) 47.

2.5 Neutral beam injection system

JT-60 neutral beam injection system (JT-60 NBI) is originally designed to inject 20 MW neutral hydrogen beams at energy of 75 - 100 keV with 14 units. From the requirement of increasing the injection power at the moderate beam energy of around 70 keV, the ion sources were modified to increase the extraction current by adjusting the gap lengths of the acceleration grids [2.5-1]. The JT-60 NBI was operated with modified ion sources in 1989. Fig.IV.2.5-1 shows the troubles in 1989. Half of them were the troubles of the control system.The number of the troubles decreased compared to that of the initial operations, which was 259 in 1986. However, there are not big difference for the past three years.

In order to simulate the behavior of helium ash in a D-T fusion reactor, the helium beam injection into a hydrogen plasma heated by the hydrogen beam injection was required. One unit out of the 14 units was modified for the helium beam injection.

Since the mass weight of the helium ion is four times heavier than the hydrogen ion, two times larger reflecting magnetic field is required to maintain the same orbits of helium ions as those of hydrogen ions.

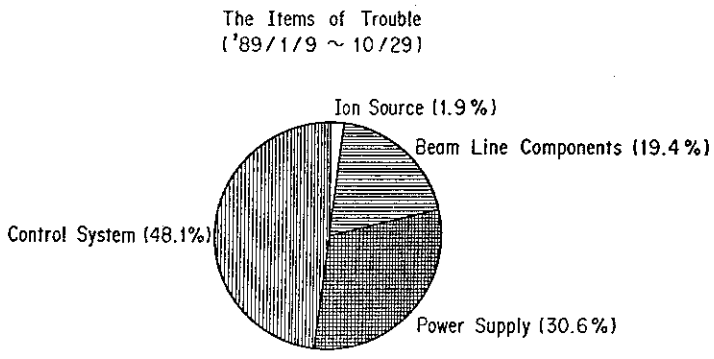

The Items of NBI trouble	The number of troubles
Control system	52
Cooling (Water) System	0
Power Supply	33
Cryogenic System	0
Beam Line Components	21
Auxiliary Vacuum System	0
Ion Source	2
Total	108

Fig.IV.2.5-1 Troubles of JT-60 NBI operation in 1989

The maximum acceleration voltage with helium beam is limited to around 35 kV due to the current capacity of the reflecting magnet power supply. To increase the injection power, a single stage acceleration system was used. It can be achieved easily by changing the connections of the power supply and the ion sources. After the beam extraction test on a proto type unit, the helium beam injection into JT-60 was performed using a unit. The other 13 units injected hydrogen beams to generate a reactor-grade plasma.The helium beams of around 31.5 kV, 40 A were extracted from the two ion sources. The maximum pulse length was 3 sec [2.5-1].

Since a cryopump system of JT-60 NBI cannot pump out helium gas, a special gas pumping system is necessary in the long pulse injection of helium beam. The cryopump was modified to a cryo-sorption pump [2.5-2] by adding SF_6 gas feeder tubes. SF_6 gas was condensed on the surface of the cryopanels at 4K ahead of pumping the helium gas. The condensed surface layer of SF_6 gas has capability of helium gas pumping at a liquid helium temperature. Prior to helium gas pumping operation, the SF_6 gas of about 40000 Pa.m^3 was fed onto the large size pump (1 m in width x 4m in height, roughly) and about 6000 Pa.m^3 onto the small size pump (0.6 m x 1m, roughly). The total pumping speed with six panels (total pumping area : 15 m^2)of the cryo-sorption pump is about 800 m^3/s for helium gas at the pressure of the order of 10^{-3} Pa. The cryo-soption pump was operated well with long pulse helium beam injection up to 3 sec, and any problem was not found [2.5-3].

References

[2.5-1] Kuriyama M., et al., Proc. of 13th Symp. on Fusion Engineering, Knoxville (1989) p.996.
[2.5-2] Shibanuma K., et al., J. of Vacuum Soc. of Japan, 31-5 (1988) p.311 (in Japanese).
[2.5-3] Kikuchi K., et al., JAERI-M 90-056.

2.6 Radio frequency heating system

The radio frequency heating system in the JT-60 is composed of three units of Lower Hybrid Range of Frequencies (LHRF) heating system with 2 GHz band 24 MW output power and one unit of Ion Cyclotron Ranges of Frequencies (ICRF) heating system with 120 MHz band 6 MW output power [2.6-1]. In this period, multi-MW rf power was injected and basic rf experiments were successfully performed, such an improvement of confinement by using two-frequency LHRF waves injection [2.6-2], and an efficient minority heating in ICRF. [2.63]

The operation of klystron in the LHRF have reached about 3300 hours in NEC LD4444 and 5000 hours in Toshiba E-3778 since the initiation of operation. Though the klystron can operate for one or two weeks, we must perform spot knocking after the operation to recover the deterioration of withstand voltage. However, there have been several klystrons that could not recover the withstand voltage. We performed to repair the electron guns of the klystron in that case. The improvement points are in the followings.

1) Cathode material is changed from oxide coating into metal coating, which reduces barium detachment from a cathode.

2) Gap between a body and an anode and that between an anode and a cathode are enlarged, which reduces electric field intensity.

3) The configuration of a corona ring is changed so as to reduce electric field concentration.

4) The cathode ceramic makes a taper type with difference in level, which reduces the electric field intensity and increases distance along the surface, and can reduce the effect of the discharge due to detached impurity.

These configuration is shown in Fig.IV.2.6-1 compared with the former electron gun. The improvement of the electron gun brought the successful recovery of withstand voltage to reduce the crowbar operation to continue satisfactory klystron operation, which were shown in Fig.IV.2.6-2. The smallness of the number of crowbar operation means the stable operation in klystrons.

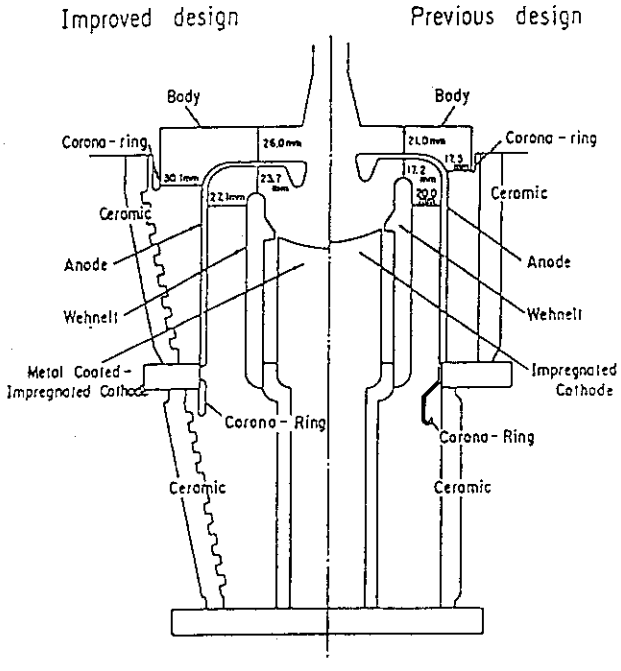

Fig.IV.2.6-1 Improvement of electron gun in the klystron compared with former design

In this period, the DC break in LHRF system made arcing at a certain frequency. The design change of choke structure in the DC break was made to avoid arcing.

Operation of the ICRF heating system was performed in this period without serious problem. The test of the phase-shifter is performed. The contacting part in an inner conductor was changed from a finger type into a multi-lam band type. This improvement brought reliable

operation of 10000 cycles and the driving length of 1000 m at 120 MHz with 2 kg/cm^2 pressurized condition. Since guard limiters made of molybdenum with thin carbon coating was damaged during operation, the material of the guard limiter was replaced by carbon tiles. Some of troubles of stub-tuner and some discharge in an inner conductor of coaxial cable occurred during operation, however, the quick restoration was made for continuous rf operation.

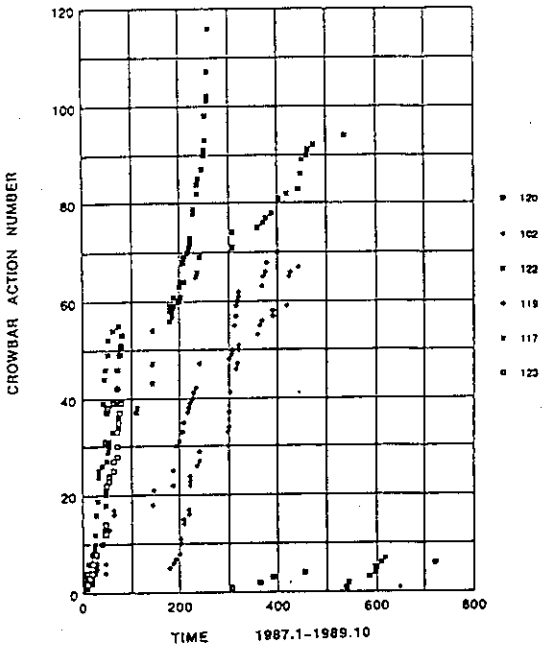

Fig.IV.2.6-2 Reduction of crowbar circuit operation after the improvement of electron gun.

References

[2.6-1] K. Uehara et al., to be published in Fusion Eng. Design

[2.6-2] S.Tsuji et al., Phys. Rev. Lett. 64, 1023(1990)

[2.6-3] T.Fujii et al.,Fusion Eng. Design 12, 139(1990)

2.7 Diagnostic system

In the phase of JT-60 shut-down (May 1989), some diagnostic systems were improved. In the H_α monitor systems, the H_α line could be monitored in all discharges by inserting filter in order to reject the carbon lines, and the long pulses(75msx3) in the active beam system could be injected. In the phase, the millimeter wave plasma radar, the grating polychromator and the Zeeman polarimeter were newly installed. These three new systems are described in section IV.3.7.3. The JT-60 diagnostic system and status at the end of October 1989 are summarized in Table IV.2.7-1.

Table IV.2.7-1 Status of the JT-60 diagnostics systems

Diagnostic System	Subsystem	Specification etc.	Status Oct. 1989
A-1 Electron Density Measuring System	a. Sub-mm Wave Interferometer	CO_2 pumped CH_3OH LASER, 2 chords $\Delta n_e = 1\times10^{17}$ m^{-3}	Operational
	b. 2-mm Wave Interferometer	1 cord, $\Delta n_e = 1\times10^{16}$ m^{-3}	Operational
	Millimeter Wave Plasma Radar System	$\tilde{n}_e$, n_e (r) $6\times10^{18} < n_e < 3\times10^{19}$ m^{-3}	Operational
A-2 Electron Temperature Measuring System	a. Fourier Transform Spectrometer	Fourier Spectrometer real time FFT, Δt = 10-30ms	Operational
	Grating Polychromator Diagnostic System	20 channels. $\Delta t \geq 20$ μs $\lambda/\lambda \sim 130$	Operational
	c. Multipulse Laser Scattering Apparatus	Multipulse, 2 Lasers ($\Delta t \geq 2$ ms) 8 points for minor radius	Operational
A-3 Ion Temperature Measuring System	a. Neutral Particle Energy Analyser Array	45° Deflection Electro-Static Energy Analyser, E=0.1-110keV, 1 viewing chord E⁄B Type Mass Energy Analyser (H,D,He) E=1-300keV, 1 viewing chord	Operational
	b. Neutral Particle Mass Energy Analyser	E⁄B Type Mass Energy Analyzer (H,D,He) E=0.1-110keV, 1 viewing chord	Operational

Table IV.2.7-1 Status of the JT-60 diagnostics systems (continued)

Diagnostic System	Subsystem	Specification etc.	Status Oct. 1989
A-3 Ion Temperature Measuring System	c. Active Beam Scattering Apparatus	H^0_e Beam (200keV, 3.5A, Multi-Pulse), E/B Type Mass Energy Analyzer, θ=5.3°	Operational
	d. Neutron Detector	NE 213 Liquid Scintillation Neutron Spectrometer, E=1.5-4MeV	Operational
	Tangential CX Neutral Particle Analyzer	E/B Type Mass Energy Analyser (H,D,He) E=1-500keV, 1 viewing chord	Operational
A-4 Impurity Measuring System	a. Light Impurity Spectrometer	Flat-Field Grazing Incidence Spectrometer λ=5-1300Å, 4 viewing chords	Operational
	b. Light Impurity Spectrometer (Doppler)	Normal Incidence Vacuum Spectrometer λ=600-9000Å,	Operational
	c. Heavy Impurity Spectrometer (Doppler)	2.5m Johann Type Crystal Spectrometer, Ti-Kα, Ni-Kα, Kr-Kα	Operational
	d. Spectrometer for Divertor	Flat-Field Grazing Incidence Spectrometer λ=5-1300Å, 1 viewing chord	Operational
	e. Visible Monochromator	0.5m Visible Monochromator λ=2000-7000Å,	Operational
	f. Grazing Incidence Monochromator	3m Grazing Incidence Monochromator λ=10-1300Å,	Operational
	Charge Exchange Recombination Spectroscopy	Fiber Optics and 0.5m Visible Spectrometer 8 viewing chords for Heating Beam	Operational
	Visible Spectrometer for Divertor	Fiber Optics and 0.5m Visible Spectrometer λ=4000-7000Å,	Operational
	Visible Monochromator for Z_{eff}	Fiber Optics and 0.25m Visible Spectrometer, λ=5232Å	Operational
	Zeeman Polarimeter	Polarizer and 1.2m Visible Monochromator, (Plasma Current Distribution Measurement)	Operational
A-5 Radiation Flux Measuring System	a. High Speed Counting PHA	Ge(1) X-ray Spectrometer E=3-110keV, 1 viewing chord	Operational
	b. Hα Monitor	Filter and Photo Diode, 7 viewing chords for Main Plasma and 1 for Divertor	Operational
	b'. Pellet Ablation Monitor	Hα Filter and Multi-channel Photo Diode 7 for Position and 1 for Total	Operational
	c. PIN Diode Arrays	PIN, 62 viewing chords for Main Plasma	Operational
	d. Bolometer Arrays	Au Bolometer, 31 viewing chords for Main Plasma and 1 for Divertor	Operational
	e. HX Monitor	NaI(Tl), 4 viewing chords	Operational
A-6 Peripheral Plasma & Wall Surface Measuring System	a. Infrared TV	CdHgTe Detector, Temperature Distribution of Divertor Plates, T=400-1200°C	Operational
	b. Visible TV	CCD Camera with Hα Filter	Operational
	c. Electro Magnetic Probes	15 Channel $\tilde{n}_e$ Probes and a B_N Probe with 25kHz Sampling Rate and a Fast $\tilde{n}_e$ Probe with 200kHz Sampling Rate	Operational
	d. Spectrometer for Periphery	2 Visible Spectrometers and Rotary Mirror λ=2000-7000Å,	Operational
A-7 Data Processing System	CAMAC, Inter-Shot Processor, Real Time Processor, Timing System, Console Desk, Transient Mega Data Strage		Operational
A-8 Diagnostic Support System	Vacuum System, Vacuum Control System, Power Supply Compressed Air Supply, Water Supply, Support Structure		Operational

3. Experimental Result

3.1 Pellet injection experiments

3.1.1 Experimental set-up and pellet ablation

Pellet injector is the pneumatic gan type with each two hydrogen cylindrical ice pellets of 3.0mm diameter x 3.0mm length and 4.0mm diameter x 4.0mm length. Pellets are injected with an angle of 47 degree from the midplane as shown in Fig.IV.3.1-1. The flight line of pellet is off-axis with ~10cm separation from the magnetic axis in a limiter plasma configuration. Setup of diagnostics are presented in Fig.IV.3.1-1. Ablation profile of the pellet is monitored by 10ch detector array of Hα emission. Line integrated density is measured by 2 chords of FIR submilimeter interferometer, the nearest point of that line to the plasma center is ~0.5m. Soft X-ray emission profile is measured by 30 channel pin diode array.

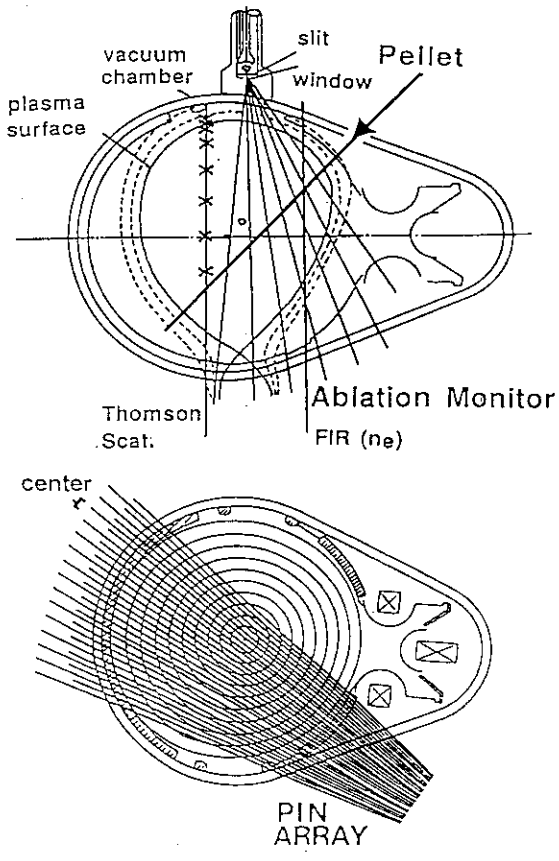

Fig.IV.3.1-1 Diagnostics.

The ablation profiles of a pellet injected OH and low power NB heated(<~5MW) plasma are investigated by using Milora's neutral gas shield model[3.1-1] with self-limiting ablation model proposed by Houlberg et al[3.1-2]. Good agreement is obtained between the measured profiles and the predictions of the neutral gas shield model in the case of shallow pellet injection outside the q=1 radius. However, ablation profile of a pellet with deep penetration inside the q=1 radius at low q plasma (q(a)=~2.2) is hard to be explained by neutral gas shielding model. Low magnetic shear inside the q=1 radius of ~0.4 m seems to be the possible reason of deeper penetration than the model prediction.

To increase supply of particles in the plasma core directly, 4 pellets injection in a short time period of ~50 ms is optimized with low power NB heating of ~5MW. Then high density peaking factor of $n_e(0)/\langle n_e\rangle_V$=~3.0 is obtained in 3.1MA limter plasmas as presented in Fig.IV.3.1-2($n_e(0)$;central electron density, $\langle n_e\rangle_V$; the volume averaged electron density). The total radiation loss is low level (~20% of absorbed power) and no

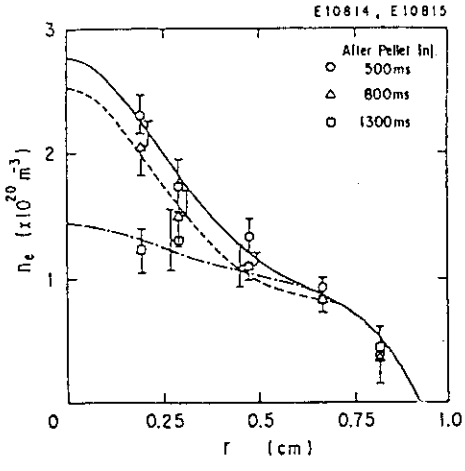

Fig.IV.3.1-2 Density profile after the pellet injection.

peaked profile of radiation is observed, that suggests the accumulation of impurity is not severe in spite of peaked density profile.

Density peaking factor defined at 400~500 ms after the pellet injection increases with deeper penetration depth (pd) of the last injected pellet measured by the Hα emission profile as presented in Fig.IV.3.1-3(a). Pd>0.0 means that a pellet penetrates beyond the nearest point to the plasma center. The density peaking factor of ~3.0 is obtained with pd of ~0.5m. Penetration depth of last pellet is almost proportional to the particle number supplied in the plasma core. Because the last small pellet penetrates deeper with lower electron temperature, that suggests former two large pellets and one small pellet ablated near the plasma center and decreases the electron temperature. The start time of the full reconnected sawtooth after the last pellet injection is presented in Fig.IV.3.1-3(b). A long time period of the sawtooth-free phase is obtained only at pd=0.3~0.6m. This suggests that the large supply of particles inside the q=1 rational surface has the strong relation with the suppression of the fully reconnected sawtooth.

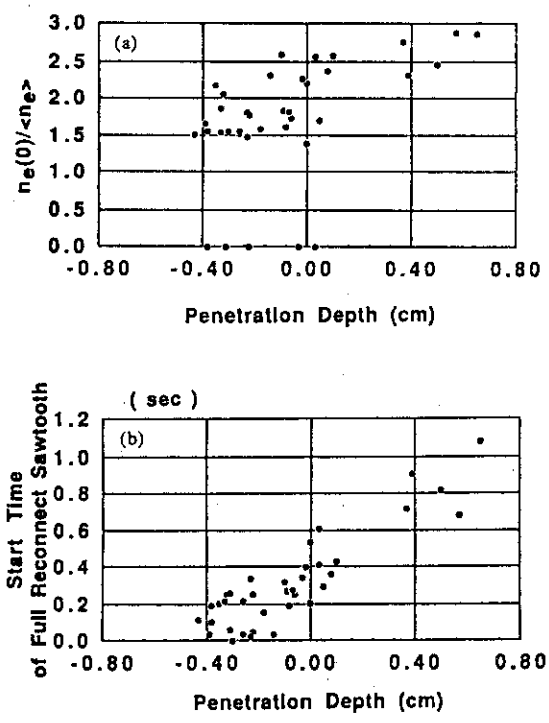

Fig.IV.3.1-3 Dependence of penetration depth on density peaking factor and start time of the full reconnected sawtooth.

3.1.2 Improvement in energy confinement

The stored energy(W^{DIA}) of pellet injected limiter plasmas measured by a diamagnetic loop is presented in Fig.IV.3.1-4 by closed points versus the absorbed heating power(Pabs), and that of gas fuelled plasmas is presented by open points. The plasma current is scanned from 1.5MA to 3.1MA with NB heating power of ≤23MW, ICRF power of ≤3MW. The maximum increase in the stored energy compared with the gas fuelled plasma rises with the plasma current almost linearly. At Ip=2.8 and 3.1MA, the largest improvement in energy confinement of ~30% with the increased stored

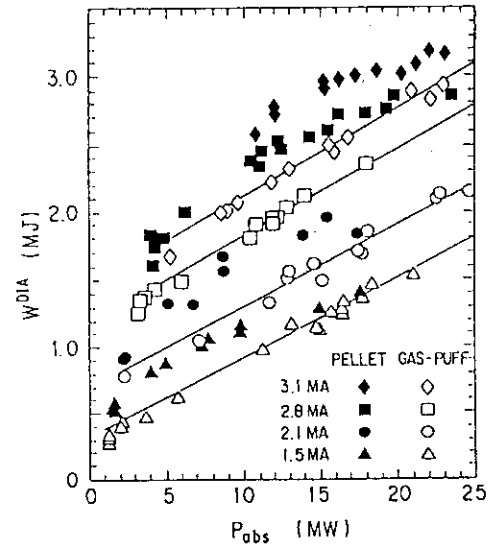

Fig.IV.3.1-4 Stored energy versus absorbed heating power.

energy of ~0.6MJ from the gas fuelled plasmas is obtained at Pabs=10~15MW and the improvement in the energy confinement degrades with the increase in heating power at >15MW.

The energy confinement time is improved with the density peaking factor as presented in Fig.IV.3.1-5 at Ip=2.8MA and 10MW <Pabs <12 MW. The stored energy is clearly improved with the peaked density profile. For the sake of the improvement in the energy confinement and the peaked density profile, the fusion product defined by $n_e(0)\tau_E Ti(0)$ reaches $12x10^{19}m^{-3}seckeV$ with Ti(0)=3.4keV in 3.1MA limiter hydrogen discharges as shown in Fig.IV.3.1-6. Where Ti(0) is measured by Doppler broadening of TiXXI Kα line. On the other hand the maximum value obtained by the gas fuelled plasmas is $6.6x10^{19}m^{-3}seckeV$ in 3.15MA limiter discharge.

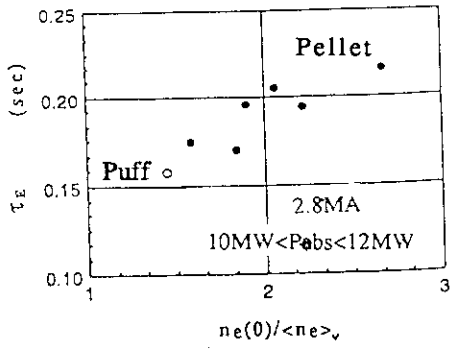

Fig.IV.3.1-5 Energy confinement time versus density peaking factor.

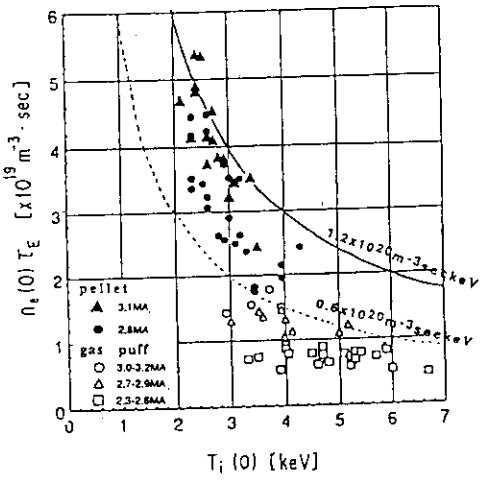

Fig.IV.3.1-6 Lawson diagram.

3.1.3 MHD effect on energy confinement

Suppression of sawtooth activity is observed during the rise of the stored energy, that suggests the stabilization of the sawtooth activity is essential for getting a peaked density profile and improved confinement[3.1-3] . Transport study suggests suppression of the sawtooth activities with improved particle diffusivity inside q=1 rational surface and inward pinch with linear function of minor radius are essential to explain the enhancement in the energy confinement[3.1-4].

β_I (β poloidal defined inside the q=1 rational surface) saturates at high power NB. On the other hand peaked pressure profile inside q=1 rational surface is observed. So the effect of high-n Ballooning instability and low-n internal kink instability is investigated. The current profile is essential in these investigation. Then current profile modification by pellet injection is studied by solving diffusion equation of the poloidal magnetic field with getting consistent loop voltage and plasma internal inductance with experimental results, that suggests q(0) is kept lower than 1.0 owing to the fast recovery of electron temperature after the pellet injection[3.1-5]. Furthermore peaking of soft X-ray emission profile is observed just inside q=1 radius, that is observed before pellet injection. These results suggests q=1 radius exists during the sawtooth suppression.

Analysis of MHD instability with scanning q(0) from 0.9 to 0.98 suggests that ideal ballooning instability limit the maximum pressure gradient and n=1 internal kink instability limits the increase in β_I[3.1-6].

References
[3.1-1]S.L.Milora, ORNL/TM-8616 (1983)
[3.1-2]W.A.Houlberg, et.,al., ORNL/TM-6549 (1979)
[3.1-3]K.Shimizu, et.al.,JAERI-M 90-066 (1990) 20
[3.1-4]Y.Kamada, et.al., Nuclear Fusion 29 (1989) 1785
[3.1-5]R.Yoshino, Nuclear Fusion 29 (1990) 2231
[3.1-6]T.Ozeki, et al., JAERI-M 90-066 (1990) 16

3.2 LHRF experiments

3.2.1 Lower hybrid current drive experiments with multi-junction launcher

Key issues for the development of steady state tokamak reactor are to get high current drive efficiency above $5x10^{19}m^{-2}A/W$ and large current drive product up to 500 $x10^{19}m^{-2}$ MA. Previous experiment of the LHCD in the outer and lower X-point and limiter discharge in JT-60 and other small tokamaks clarified the scaling of the current drive efficiency ($\eta_{CD}=n_eR_pI_{RF}/P_{LH}$) on plasma parameters as $\eta_{CD}\propto<T_e>/(5+Z_{eff})$ [3.2-1]. Improvement of directivity and sharpness of $N_{||}$ spectrum predicts higher current drive efficiency by a factor of 1.3~1.5[3.2-2]. The results of the experiment in JT-60 are shown in Fig.IV.3.2-1, where current drive efficiency η_{CD} VS $<T_e>$ is shown with results of other previous experiments. Progress of the current drive efficiency due to the higher performance of plasma parameters based on the scaling and further development of the efficiency by the introduction of the multi-junction launcher are clearly seen in the figure. The maximum value of $3.4x10^{19}m^{-2}A/W$ is achieved and is almost 2 times higher than the results of other machines.

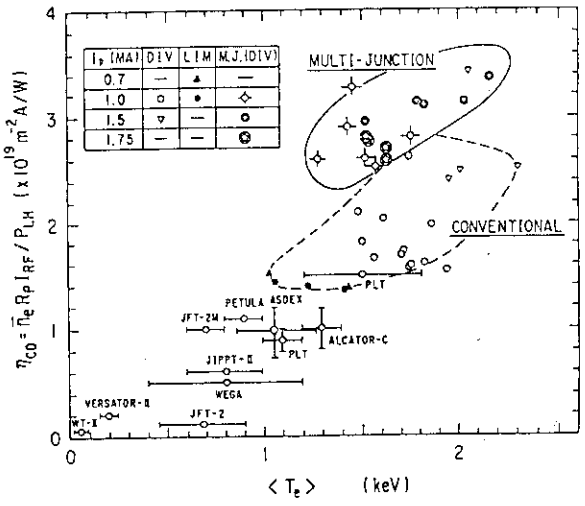

Fig.IV.3.2-1 Dependence of η_{CD} on $<T_e>$ and its comparison between the conventional and multi-junction launchers. Results in other tokamaks are also shown.

Large current drive is another key for the steady state tokamak reactor. The index to measure the quantity of the non-inductive current drive is identified by $CDP \equiv n_e R_p I_{RF}$ which we call " current dive product "(*CDP*). The next generation tokamaks of FER and ITER require the value of ~$500x10^{19}m^{-2}$MA, while the values were ~$1x10^{19}m^{-2}$MA in the maximum in the previous non-inductive current drive experiments in JT-60. The maximum LHCD power of 4.5MW with improved $N_{||}$ spectrum was injected into JT-60 plasma and produced the maximum value of $12.5x10^{19}m^{-2}$MA. The enlargement of the *CDP* by a factor of ~10 compared with those in other LHCD experiments have been achieved.

3.2.2 Suppression of sawtooth and current profile control by LHCD

The effect of LH on sawtooth activity is shown in Fig.IV.3.2-2, where 4.6 MW of NB power is injected into a divertor discharge with q_{eff} = 3.2. In a discharge without LH (E8866),

sawtooth already exists before the NB injection. Whereas in a discharge with LH (E8879), sawtooth is suppressed for 1.7 seconds by 2 MW of LH injection. The sawtooth starts at around 20 % of the minor radius. This result implies that the central safety factor q(0) may be less than or equal to unity during sawtooth suppression by LHCD. During the sawtooth free period, soft X-ray signal and ion temperature have peaked profiles. Therefore it is expected that a confinement in the central portion is improved during sawtooth free phase. If the sawtooth is suppressed by a global current flattening, it is expected that a wave with higher $N_{||}^{peak}$ is more effective in sawtooth suppression. Whereas the experimental results exhibit an opposite tendency; the sawtooth suppression time Δt_{ST} has a maximum around $N_{||}^{peak} \sim 1.3$ which corresponds to the maximum current drive efficiency [3.2-3]. To summarize, the appearance of sawtooth at a finite minor radius and the existence of m = 1 oscillation suggest that q(0) may be less than or equal to unity during sawtooth suppression period. A better suppression efficiency for lower $N_{||}$ also supports that sawtooth suppression mechanism is not likely to be by a global current flattening.

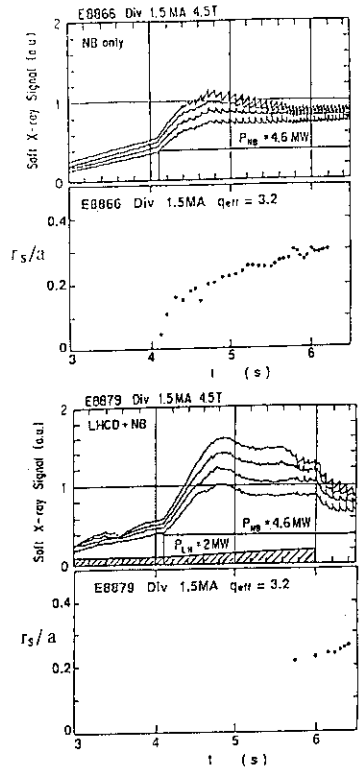

Fig.IV.3.2-2 Typical waveform for sawtooth suppression.

One of applications of a non-inductive current drive is a profile control which modifies the MHD activities in tokamak plasmas. This scheme is very attractive to improve plasma performance, since the profile is actively controlled by it. In a series of LHCD experiments, the injected power spectrum of LH wave was scanned using the newly installed multi-junction launcher [3.2-2] ($N_{||}$ scan experiment). In the $N_{||}$ scan experiment, increasing $N_{||}$ of the injected RF spectrum the central HX intensity decreased and its spatial profile became broader. This indicates that the RF power was absorbed in the more peripheral region with increasing $N_{||}$ and that the current profile became broader with $N_{||}$, which was confirmed by the decreasing of plasma internal inductance l_i with $N_{||}$. The good correlation between the broadening of HX profile and the decreasing of l_i against the $N_{||}$ was observed [3.2-3].

3.2.3 Volt-second saving by LHCD

The volt-second consumption of the Ohmic primary circuit is reduced by lower hybrid (LH) current drive (CD) during the current rise phase. Most of the LH power is consumed in compensating the resistive voltage typically 0.8 V. The resistive voltage is evaluated as the difference between the surface voltage and the inductive voltage. With LH injection, the resistive voltage drops to ~ 0 V while the inductive portion being almost unchanged. Which means that the LH power is consumed mainly for compensating the resistive voltage. Up to 2.5 V·s of flux is

saved by 2 MW × 2.5 s of LH injection which could be projected to several tens of volt-seconds in ITER class reactors [3.2-4].

3.2.4 Lower hybrid electron heating in high plasma current

The efficient electron heating was obtained in relatively low density plasma of n_e= $1.7x10^{19}m^{-3}$ with low power heating, where the electron temperature of 6 keV was measured by Thomson scattering. Electron heating efficiency η_e^{LH}= 2~3 eV $10^{19}m^{-3}$/kW of the LHEH is notably higher than those of NBI heating and close to the ohmic heating. The high performance of the LHEH was not maintained in the higher density and higher power experiments. Stored energy became to saturate. Instead parametric instabilities and fast ions of short life time appeared [3.2-3,5]. The fast hydrogen ion flux and intensity of the parametric instabilities increased at the same time. Dependence of the relative intensity of parametric instabilities on the density with various plasma currents is shown in Fig.IV.3.2-3(a).It is clear that high plasma current reduces the parametric instabilities [3.2-6]. The improvement of the heating performance corresponding to the reduction of parametric instabilities were obtained as seen in Fig.IV.3.2-3(b). It is found that the τ_E^{INC} decreases with density in the same plasma current but it is recovered by the increase in the plasma current. Higher density and higher power cause the parametric instabilities but higher plasma current reduces them. High plasma current reduced parametric instabilities and recovered the heating performance up to P_{abs}~ 10MW and n_e=$7x10^{19}m^{-3}$ with the same 2GHz frequency. High plasma current as well as high frequency of lower hybrid wave extend the electron heating region, which is favorable for future tokamak.

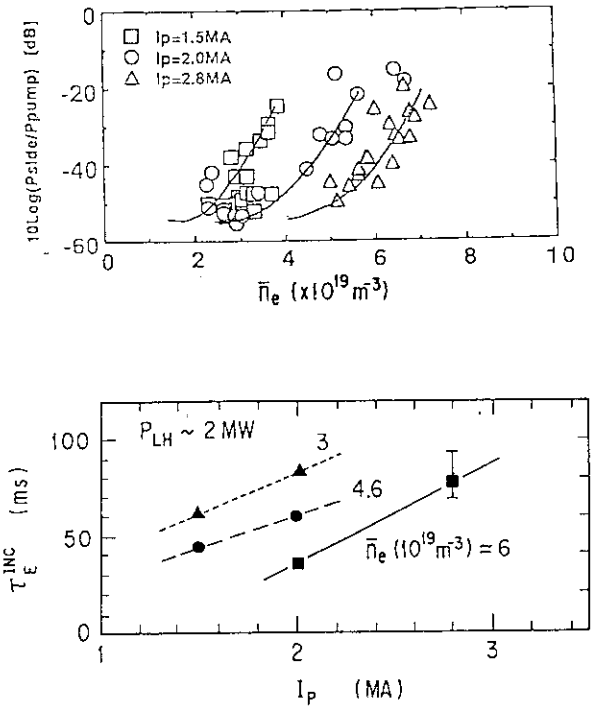

Fig.IV.3.2-3 (a) Intensity of Parametric instabilities in terms of density in cases of various plasma currents. (b) Improvement of the t_E^{INC} as a function of plasma current.

References

[3.2-1] K. Ushigusa, T. Imai, Y. Ikeda, et al., Nuclear Fusion **29** (1989) 1052.
[3.2-2] Y. Ikeda, T. Imai, K. Ushigusa, et al., Nuclear Fusion **29** (1989) 1815.
[3.2-3] JT-60 Team, JAERI-M 90-066.
[3.2-4] O. Naito, K. Ushigusa, Y. Ikeda,. et al., submitted to Nucl. Fusion.
[3.2-5] T. Imai, et al., Phys. Rev. Lett., **43** (1979) 586.
[3.2-6] R. Cesario, P. Ridolfini, Nucl. Fusion **27** (1987)435.

3.3 ICRF experiments

3.3.1 Hydrogen minority second harmonic heating in helium discharges

Effective plasma heating is obtained for the ohmically heated target helium plasmas, $\bar{n}_e$ = 1.3 - 6.6 x 10^{19} m^{-3}, I_P = 1-2.4 MA and q_{eff} = 6.4-2.6 in limiter configuration with H-minority 2 w_{cH} heating, especially with (p, 0) phasing. The giant sawtooth oscillations with a period of ~250 ms in the central electron temperature are observed. The incremental energy confinement time defined as $\tau_E^{inc}=(DW^{DIA}-DW_s(D\bar{n}_e))/(P_{IC}+I_PDV_L)$ can be regarded as the total heating efficiency, where $DW_s(D\bar{n}_e)$ is increment in the ohmic stored energy due to the increase in $\bar{n}_e$ and DV_L the change in one turn loop voltage during the ICRF heating. Figure IV.3.3 - 1 shows the $\bar{n}_e$ dependence of τ_E^{inc} in various heating regimes at I_P = 1.5 MA. Excellent values of τ_E^{inc} ≈ 90 - 120 ms are achieved by H-minority $2\omega_{cH}$ heating with (p,0) phasing, which are approximately constant at $\bar{n}_e$ = 2.5 - 5.6 x 10^{19} m^{-3}. The (p, 0) phasing heating shows larger τ_E^{inc} than the (0,0) phasing one in both H-minority and H-majority heating schemes.

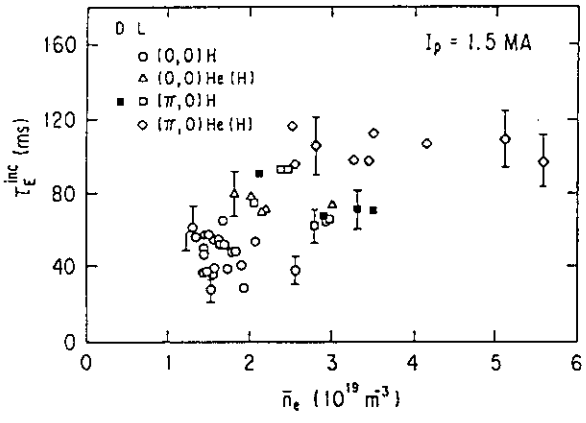

Fig.IV.3.3-1 Dependence of τ_E^{inc} on $\bar{n}_e$ for different heating regimes at I_P = 1.5 MA.

Figure IV.3.3 - 2 shows the I_P dependence of τ_E^{inc} for various heating regimes at I_P=1-2.4MA which corresponds to q_{eff}≈6.4-2.6. The (p,0) phasing data for H-minority 2 ω_{cH} heating increase from 1MA to 1.5MA and are approximately constant at τ_E^{inc}≈90-120 ms from 1.5 MA up to 2.4MA at low and high densities. The degradation of τ_E^{inc} is not clearly observed at q_{eff}<3 (I_P > 2.1MA). Non-Maxwellian ion tails are observed at I_P=1.5, 1.9 MA, indicating that the maximum ion energy reaches 80-130 keV but not observed at I_P=1 MA. Accordingly, the ion tail is one of the causes that bring improvement of τ_E^{inc} at $I_P \geq$ 1.5 MA because the ion tail enhances the power absorption. These weak I_P and $\bar{n}_e$ dependences of τ_E^{inc} for H-minority 2 ω_{cH} heating support Shimomura-Odajima scaling of τ_E^{inc} given by $\tau_E^{inc}(ms)= 85\ k\ a_p^2\ M_{eff}^{1/2}$ [3.3-1] , where k is the ellipticity and M_{eff} the effective ion mass in AMU and a_p the minor radius in m. But the data are larger by a factor of about 1.5 than Shimomura-Odajima scaling if M_{eff}=1. Consequently, helium mass effect is one of the possibilities that improve τ_E^{inc}, which is clearly observed for combined ICRF and NBI heating as described in the next section.

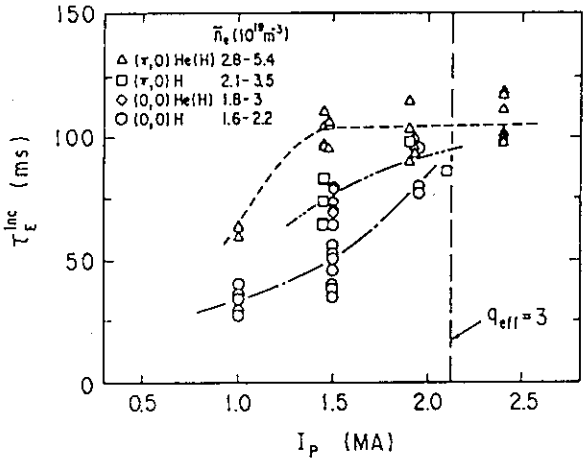

Fig. IV.3.3-2 Ip dependence of τ_E^{inc} for different heating regimes in the range of I_P = 1- 2.4 MA.

3.3.2 Higher harmonic ICRF heating in combination with NBI heating

Third harmonic ICRF heating in combination with NBI (H beam) heating has been carried out with B_T=3T, I_P=0.7-1.4 MA, q_{eff}=7-3.2, $\bar{n}_e$=1.7-4x10^{19}m^{-3}, P_{IC}=1.7-2.3MW, P_{NBI}=2-18 MW in both helium and hydrogen discharges. A typical result for third harmonic heating at I_P=1 MA is shown in Fig.IV.3.3-3. The stored energy increases step by step according to heating power. The central electron temperature T_e^{ECE} increases significantly and giant sawtooth oscillations are observed at the phase of the combination of high power NBI (~10 MW). The sawtooth period reaches 410 ms, which is about 6 times longer than the energy confinement time (~ 70 ms).

Figure IV.3.3-4 shows the plasma stored energy as function of the absorbed power for various third harmonic heating regimes. There is no significant difference between the heating regimes up to ~ 8 MW of the absorbed power. Above that power level, combined third harmonic and NBI heating indicates better energy confinement, especially with helium discharges. The energy confinement time for the combined third harmonic and NBI heating is about 20 % higher than that of NBI heating alone. The giant sawtooth seems to improve the energy confinement since it is observed in this power range as mentioned above.

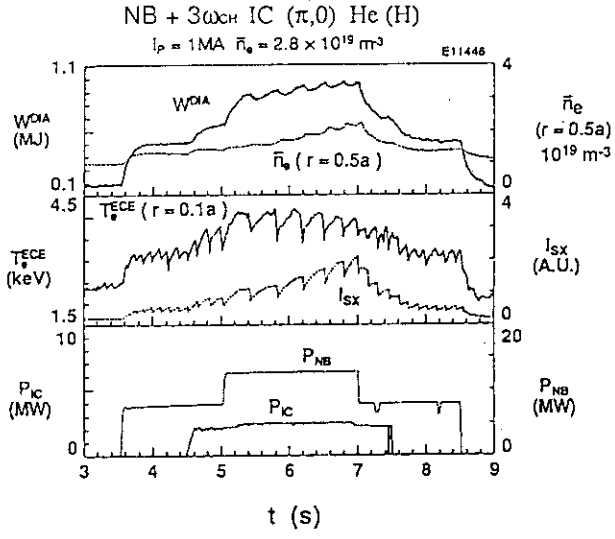

Fig.IV.3.3-3 Typical result for combined third harmonic ICRF and NBI heating

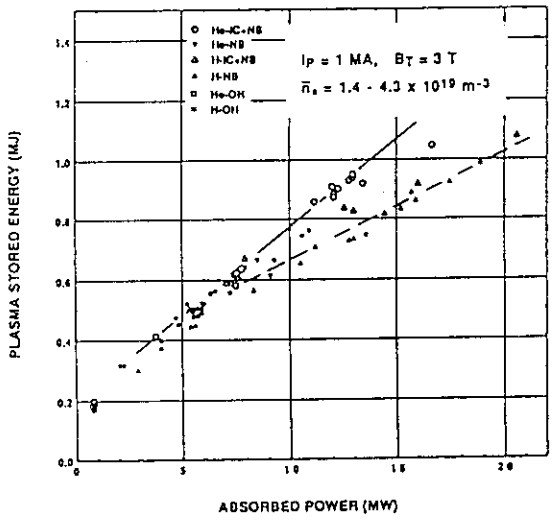

Fig.IV.3.3-4 Plasma stored energy as a function of absorbed power for various third harmonic heating regimes.

Combined second harmonic and NBI heating is examined in helium discharges at high electron densities ($\bar{n}_e$~ 6 x 10^{19} m^{-3}) in order to keep low proton-to-electron concentration ratio even in application of NBI. The stored energy increases with the similar τ_E^{inc} of ~90 ms up to 10MW of the absorbed power for both combined second harmonic and NBI heating and NBI heating alone in these helium discharges. On the other hand, τ_E^{inc} is ~55ms for the hydrogen discharges with NBI heating alone [3.3-2]. Therefore, it is concluded that the enhancement of the incremental energy confinement time in helium-dominant discharge is due to mass effect.

References

[3.3-1] Y. Shimomura, K. Odajima, Comments Plasma Phys. Controlled Fusion **10** (1987) 207.
[3.3-2] O. Naitoh, et al., JAERI-M 89-033 (1989) p.89.

3.4 H-mode and IDC experiments

3.4.1 Divertor H-mode with NBI

The H-mode has been investigated with JT-60 hydrogen and helium discharges with hydrogen beams. In the previous experiments with a null at the outer midplane or bottom side of the discharge, H-mode period was short, the threshold power was higher than 14.5 MW, and improvement in confinement was modest (< 10%) [3.4-1]. We conducted an H-mode investigation with walls and graphite divertor plates gettered with titanium. The amount of titanium flashed each day was 5-10 g, which corresponds to 50-100 monolayers. Titanium gettering reduced the amount of oxygen by a factor of 3 in both ohmic and neutral-beam heated discharges. Particle recycling coefficient, as inferred by the global particle confinement time τ_p^*, was also reduced by a factor of two. However, little change was observed in carbon impurity content. Z_{eff} values were about 2 at relatively low density discharges(line-average density of 2×10^{19} m^{-3}) at modest power levels (10MW). After titanium gettering each day, we did parameter scans of wide ranges to search for the best condition to obtain H-mode transition. A clear L to H transition was observed with 9.5 MW beam power, which is a significant reduction from the previous results without titanium. The toroidal field was 3.3 T, the plasma current was 1 MA, q_{eff} was 3.8, and the line-average density prior to the transition was 2.1×10^{19} m^{-3}. Taking into account the increase in absorbed power due to density increase, we estimate the improvement in energy confinement to be about 30%. However, this transition was also associated with a significant increase in carbon impurity, Zeff increase from 2.0 to 2.6, and radiation power increase up to 70% of input power, which terminated the H-mode phase.

Reproducibility of this kind of a clear LH transition was very poor. The major cause of the difficulty to access H-mode seems to be the working gas. The configuration remains to be a possible candidate. Neutral particles may affect the accessibility to the H-mode if the divertor configuration is too much open to allow the neutral particles to flow back to the main plasma.

3.4.2 Limiter H-mode with LHCD

The H-mode has been observed in limiter discharges at I_p = 1.5 MA and B_t = 4.5 T with lower hybrid current drive (LHCD) on JT-60 [3.4-2]. The discharges exhibited the characteristics of the H mode such as sudden improvements in particle and energy confinements, increase in edge electron temperature, rise in reflection coefficient of RF power, and edge localized modes (ELMs) as shown in Fig.IV.3.4-1. A preliminary measurement by a millimeter-wave-reflectometer revealed reduction in edge density

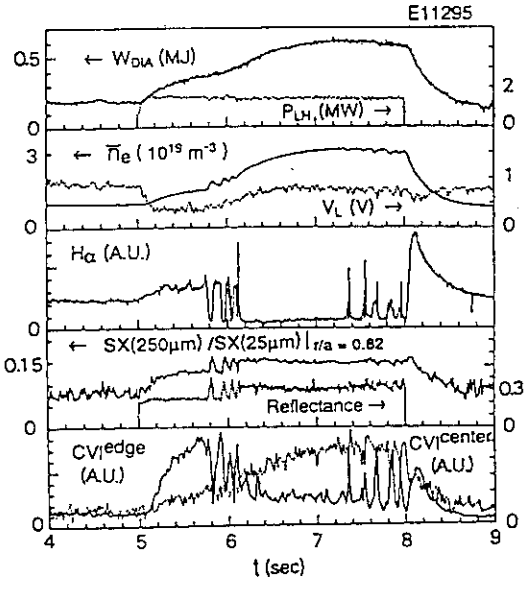

Fig.IV.3.4-1 Time evolution of an H-mode shot with LHCD. The reflection coefficient is from the conventional launcher. The edge CVI signal is along a chord with a tangential radius of r/a~0.9.

fluctuations as well. The lower limit for the H-mode in terms the line averaged electron density was about 2×10^{19} m^{-3}. The threshold LH power for the H-mode transition was about 1.2 MW with hydrogen plasmas. Although simultaneous application of RF powers at two different frequencies such as 1.74 + 2.23 GHz or 1.74 + 2.0 GHz appeared to be effective in the attainment of the H-mode, it is not the critical factor in obtaining the H-mode with LHCD since the total LH power at 2.0 GHz of higher than 2.0 MW produced the H-mode.

By feedback controlling the line averaged electron density to be above a threshold of about 2×10^{19} m^{-3}, we could lengthen the H-mode phase up to 4.6 sec. Nearly steady-state ELM-free H-mode with durations up to 3.3 sec was established. The Z_{eff} value estimated from visible bremsstrahlung emission and the n_e and T_e profiles from Thomson scattering measurements increased slightly from about four during the L phase to around five at the later phase of the H-mode. Spectroscopic measurements indicate that the dominant impurity was carbon and hence the protons were diluted to less than 40 % of electrons. The soft x-ray emission profile became slightly peaked with time, which suggested impurity accumulation at the center. Nevertheless the radiation power measured by bolometer arrays remained about 40 % of the total input power. The carbon contents during the ELM-free phase are not at acceptable levels partly because shielding effects in the limiter configuration are weaker than in divertor configurations. The H-mode with LHCD, however, has not been achieved in the lower X-point configuration contrary to expectation.

The properties of energy confinement are summarized in Fig. IV.3.4-2. The plasma stored energy increases almost linearly with the total input power as shown in Fig. IV.3.4-2 (a). Here we assumed that the injected LH power was completely absorbed by the plasma. The scatter of the data points is mainly due to he variation of the electron density. The energy confinement is enhanced by up to 30 % by the H-mode. The increment in the plasma stored energy, however, is primarily gained by the increase in the electron density as plotted in Fig. IV.3.4-2(b). The L-mode plasmas with LHCD have almost the same electron density dependence as the ohmic stored energy of $W_{OH} \propto n_e^{0.62}$ presumably because the total input power does not greatly exceed the ohmic input. Although the difference is small, the H-mode data points appear to have a little stronger n_e dependence than ohmic. NBI heating was combined to examine the effect of wave-particle interactions. The beam pulse at 1.2 MW broke the H phase as observed in the concurrent rise in the H_α emission and fall in the electron density. Note that the trace of the electron cyclotron emission at $1.5\omega_{ce}$ dropped at the same time. Hard x-ray emission behaved similarly to $I_{ECE}(1.5\omega_{ce}) \times n_e$. During the L phase with NBI, beam

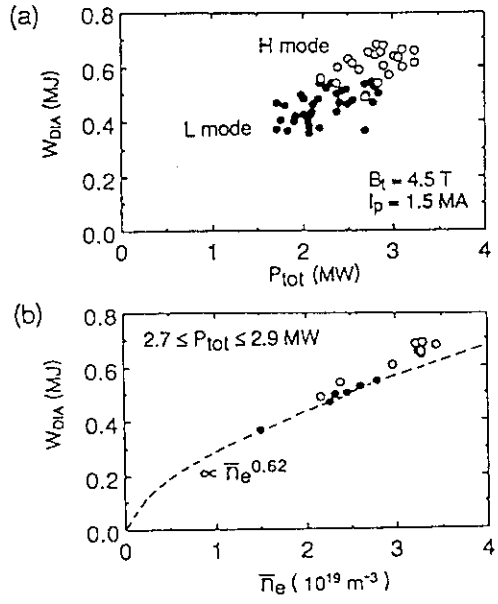

Fig.IV.3.4-2 (a)Plasma stored energy as a function of $P_{tot} = P_{OH} + P_{LH}$. (b)Electron density dependence of plasma stored energy with restricted total power.

acceleration by the LH waves was observed in the neutral flux. These facts suggest that the H-mode could not be sustained when the LH power was absorbed by beam ions. Such ion tails were not observed in the H phase with LH alone. No parametric decay instabilities were observed neither. Non-thermal ECE spectra suggest a favorable effect of fast electrons on the H transition.

3.4.3 IDC regime

The improved divertor confinement(IDC) regime observed in the lower X-point configuration of JT-60 is suitable for steady-state operation with remote radiative cooling in the divertor region up to 10 MW [3.4-3].

We operated JT-60 in four combinations of I_p and B_t polarities to examine the effects of ion grad**B** drift direction on IDC and to check the symmetry of the device. We found that IDC developed only when the ion grad**B** drift was toward the X-point. Reversal of B_t direction changed particle confinement and light impurity behavior significantly as shown in Fig. IV.3.4-3. Reduction in neutral pressure around the main plasma and oxygen impurities was observed when the ion grad**B** drift was toward the X-point and when the heating power exceeded a threshold power of about 9 MW. The carbon impurities buildup near the X-point which enhance divertor radiation and hence reduce heat load on the divertor plates.

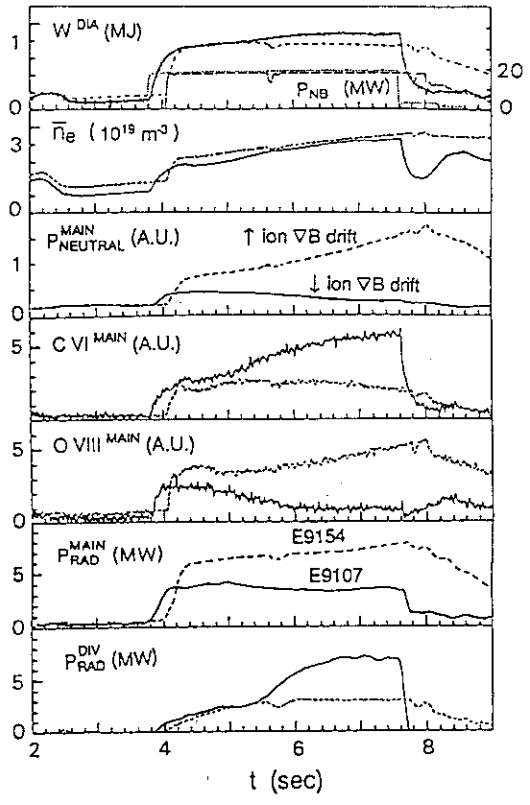

Fig.IV.3.4-3 Comparison of two discharges with nearly identical operational parameters except B_t and I_p polarities.

The energy confinement improvement by up to 20 % is correlated with the improvement in particle confinement. The reduction of oxygen appears to be caused by the improved particle confinement through reduced charge exchange ion flux which hit the first falls. The particle confinement was found not to improve when the ion grad**B** drift was away from the X-point.

References

[3.4-1] H. Nakamura, S. Tsuji, M. Nagami, et al., Nucl. Fusion **30** (1990) 235.
[3.4-2] S. Tsuji, K. Ushigusa, Y. Ikeda, *et al.*, Phys. Rev. Lett. **64** (1990) 1023.
[3.4-3] S. Tsuji, M. Akiba, T. Ando, et al., Plasma Physics and Controlled Nuclear Fusion Research 1988 (Proc. 12th Int. Conf. Nice, 1988), IAEA, Vienna Vol. **1**, p. 265.

3.5 High-poloidal-beta experiments

In tokamak research, improvement of energy confinement and its sustainment in steady state for auxiliary heated plasmas remain the critical issues for a forthcoming tokamak reactor. After changing the divertor geometry to the lower X-point configuration in JT-60, the hot-ion

enhanced confinement regime has been found in 1989 by means of centrally-oriented near-perpendicular neutral beam injection. High-poloidal-beta experiments have been carried out in this regime with high-power long-pulse neutral beam heating with ~21 MW for 3-5 s into divertor hydrogen plasmas with a rather small volume (R~2.9 m, a~0.70 m)[3.5-1]. Results from I_p scan experiments in $0.3 \leq I_p(MA) \leq 1.2$ are summarized in Fig.IV.3.5-1. Confinement properties were most improved in the low-I_p regime around 0.5-0.7 MA at B_t=4.5 T, in which high temperatures of T_i~12 keV and T_e~6 keV were obtained and the L-mode enhancement factor reached τ_E/τ_E^L~1.6 to the Goldston L-mode scaling. High-β_p values around 3 ($\varepsilon\beta_p$~0.8) have been achieved with low collisionality (ν_e^*~0.2) in the range of Z_{eff} ~2-4. These discharges are also close to the stability boundary for high-n ideal ballooning modes.

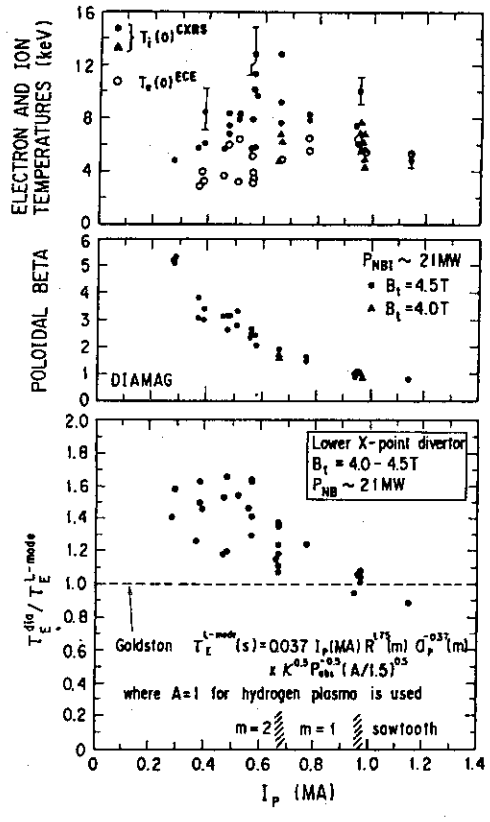

Fig.IV.3.5-1 Results from I_p scan in high β_p experiments

This regime with high q_{cyl} (=4-13) was free from sawtooth oscillations probably because of q(0) above unity increased by large bootstrap currents. Highly peaked $T_i(r)$ and $n_e(r)$ profiles were obtained up to $T_{i0}/\langle T_i\rangle$~4.2 and $n_{e0}/\langle n_e\rangle$~2.7. Peaking parameters of $T_e(r)$ are found to be mostly independent of q_{cyl}, indicating a large divergence from prediction of the q-dependent profile consistency assuming Spitzer resistivity and q(0)=1. As T_i~$2T_e$ at center, the energy balances are characterized by their decoupling for electrons and ions, where the convection losses exceed the conduction losses. The local transport analysis shows that the enhanced confinement results from improvement of ion heat transport in the central region. Profiles of the toroidal rotation velocity, $V_\phi(r)$, measured by charge-exchange-recombination-spectroscopy were also observed to be highly peaked up to ~1×10^5 m/s in the center with high rotational shear in spite of nearly balanced injection. The tendency of peaking commonly observed for the profiles of T_i, n_e and V_ϕ appears to be correlated together with a degree of enhanced confinement.

The discharges are similar to the supershots with tangential beam injection into a deuterium plasma in TFTR[3.5-2]. However, no disruptive β_p limit has been observed up to β_p^{dia}~5 in JT-60 in contrast with the clear limit at β_p^{dia}~2 (or $\varepsilon\beta_p$~0.7) in TFTR. In high-β_p discharges ($\beta_p \geq 2$), continuous m=2/n=1 and m=3/n=1 modes tend to degrade the confinement properties. In lower I_p than ~0.5 MA, the energy confinement is significantly deteriorated with increasing MHD activities, where the plasma pressure anisotropy is strongly enhanced up to $\beta_p^{dia}/\beta_p^{equ}$ ~1.6. A new MHD phenomenon limiting increase of β_p values named as "β_p collapse" has been found to be a large

partial collapse localized possibly at q=3 surface without precursor oscillations just before the crash falling within ~100 μs, as the β_p^{dia} value approaches or exceeds ~3. Improvement of the energy confinement occurring before the β_p collapse is initiated by the transition of dominant MHD instability from m=2 modes to m=3 modes related to the expansion of an enhanced confinement boundary from q=2 to q=3 surface. Also, the V_ϕ increases with a peaked profile up to ~1×10^5 m/s at center in the co-direction accompanied with large negative radial electric fields. The stored energy continues to increase with the ion temperature until the β_p collapse occurs.

In these experiments, a steady-state bootstrap-current discharge up to 80 % of the total plasma current has been demonstrated under the condition of negligibly small beam currents[3]. Considerable efforts have been also devoted to the confirmation of bootstrap currents through comparison between experiment and theory. Comparison of the ratios of resistive loop voltages as a function of β_p^{dia} is shown in Fig.IV.3.5-2, where the only case with neoclassical bootstrap currents agrees with experiments over an extensive range of poloidal beta values, $0.1\leq\beta_p^{dia}\leq3.2$. The characteristic decay time of the plasma current during I_F (field coil currents)-constant experiments also indicates reasonable agreement with the L/R decay time predicted from neoclassical theory. Thus, the bootstrap currents are concluded to be substantial, implying that electrons along the field lines behave classically in spite of these anomalous behavior in the perpendicular direction.

In conclusion, while the β_p collapses sometimes limit the improvement of confinement, the β_p values of ~3 were realized stably, leading to the demonstration of 80 % bootstrap current discharge. The hot-ion enhanced confinement regime carrying a large fraction of intrinsic bootstrap currents obtained in JT-60 will provide a significant impact on a steady-state operation scenario for a future tokamak reactor.

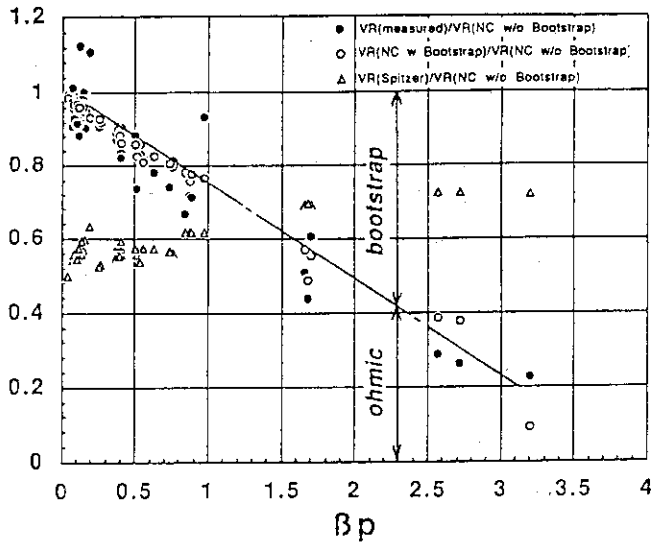

Fig.IV.3.5-2 Resistive loop voltage ratios as a function of β_p

References

[3.5-1] S. Ishida et al., JAERI-M 90-066, p.146.

[3.5-2] J.D.Strachan et al., Phys. Rev. Letter **58**(1987)1004.

[3.5-3] M.Kikuchi et al, Nucl. Fusion **30**(1990) 343.

3.6 Transport analysis

Local heat transport properties have been analyzed in L-mode phase of divertor (single null X-point), and limiter discharges with hydrogen neutral beam heating into hydrogen plasmas, based on sets of consistent experimental data including ion temperature profiles from CXR measurements. We have made parameter scans of the variation of transport characteristics with total input power ($P_{abs}\leq18$ MW) at current ($I_P\leq2.0$ MA).

In a data set for relative lower density $\bar{n}_e \leq 3.0\times10^{19}m^{-3}$ and up to moderate heating power, $P_{abs} \leq 12.0$ MW, energy loss channels of electron and ion are separately determined. FigureIV.3.6-1 shows the power loss fraction at r=2/3a for various loss channels, electron and ion conduction losses, convection and radiation losses. The ion conduction loss increases with the total input power and plays a major role of energy loss mechanisms for limiter, L-mode discharges with 1 MA. Such a property is also observed in diverted, low plasma current discharges (I_p<1.5 MA). On the other hands, the conduction loss of the electron is found to be larger than that of the ion for high current, limiter discharges at relatively low power (I_p=2.0 MA, $P_{abs} \leq 10$ MW) as is shown in Fig. IV.3.6-2.

The electron and ion thermal conductivities (κ_e and κ_i, respectively) are evaluated at r=a/2 of the plasma minor radius for above cases. Figure IV.3.6-3 shows κ_e and κ_i as a function of total input power, P_{abs}, for discharges with I_p=1.0 MA and 2.0 MA. For both 1.0 MA discharges of limiter and divertor, the ion heat conductivity significantly increases in proportion to P_{abs} and is about three times κ_e at P_{abs}~9 MW, whiles κ_e gradually enlarges with input power. On the other hands, the transport process in high current limiter discharges (I_p=2.0 MA) is fairly different from the low current (I_p=1.0 MA) case. κ_e is larger than κ_i at low power level of 4 MW. The enhancement of κ_e corresponds to the increasing electron conduction loss which is caused by an increase in ohmic heating power and a decrease of energy equipartition channel between electrons and ions. However, κ_i tends to increase with total input power and becomes comparable to κ_e at P_{abs}~6 MW, as is neutral beam heating power dominant in total heating power. Therefore, the power degradation of

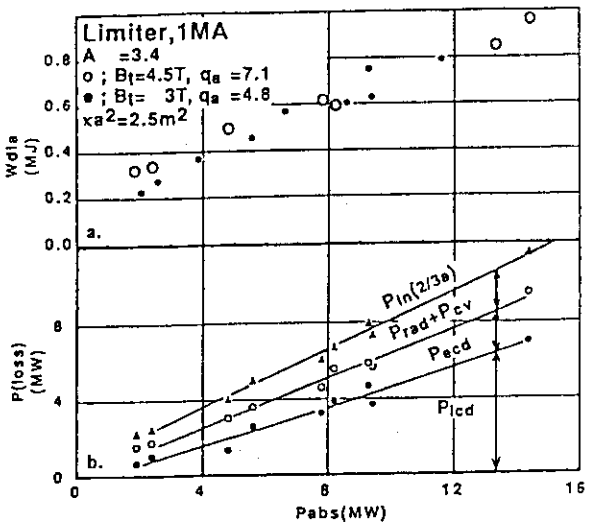

Fig.IV.3.6-1 The energy content adn power losses from various loss channels evaluated at r=2/3a: Pin; absorbed poer, Prad+Pcv; radiation and convection, Pecd ; electron conduction loss, Picd; ion conduction loss

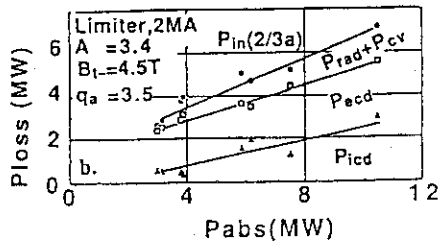

Fig.IV.3.6-2 The power losses for 2 MA, limiter discharges.

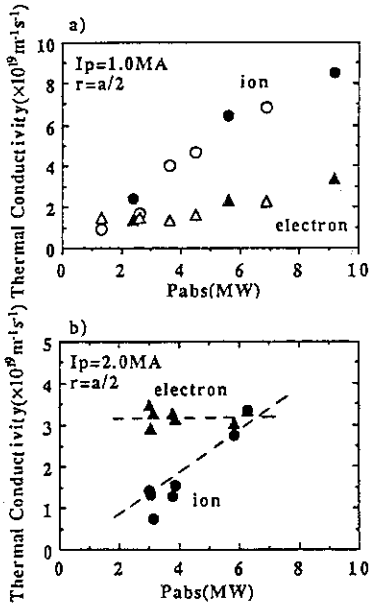

Fig.IV.3.6-3 Poser dependencies of thermal conductivity (r=a/2), in which circles show κ_i and triangles κ_e. Open and closed symbols present divertor and limiter discharges, respectively; a) Ip=1.0 MA ; b) Ip=2.0 MA.

global confinement observed in L-mode plasmas is mainly due to degradation in ion transport.

Ion temperature gradient instability, η_i-mode, is proposed as one of highly probable candidates which are responsible for such degradation in ion transport. The study concentrates on the η_i-mode induced transport. The ion energy balance equation is solved by using ion thermal diffusivity based on the η_i-mode and ion temperature profiles are compared with measured ones, while other plasma parameters such as n_e,n_i,T_e,J_z,Z_{eff},P^e_{NB},P^i_{NB} and P_{rad} are fixed. Three different formula of χ_i model driven by η_i-mode turbulence are employed, i.e., Domingues & Waltz, Lee & Diamond, and Romanelli. (Three different models of χ_i result in little difference in calculated ion temperature profiles.)

The calculated ion temperature profiles show considerably good agreement with experimental data in the wide range of plasma parameters with L-mode characteristics;

I_p=1.0~1.8 MA, P_{abs}=1.3~16.7MW, $\bar{n}_e$=1.2~5.0×$10^{19}$$m^{-3}$ for divertor plasmas and

I_p=2.0~2.7 MA, P_{abs}=3.0~17.4MW, $\bar{n}_e$=1.5~6.5×$10^{19}$$m^{-3}$ for limiter plasmas.

It seems possible to conclude that the ion transport can be satisfactorily modeled by theories based on electrostatic micro-instabilities destabilized by ion temperature gradients. The question is still open, because there are some cases which are difficult to reconcile with this proposed model, especially for limiter discharges of low plasma current and low electron density.

3.7 Topics

3.7.1 Helium ash experiments

To realize quasi-steady state or steady state burning plasma, helium (He) ash produced by DT reaction must be controlled within 5 to 10% of DT density. Moreover,to measure ratio of He to DT in divertor is important for tritium inventory study.Therefore, in JT-60 lower divertor experiments, He ash exhaust characteristics has been studied with ohmic heating and neutral beam (NB)heating of P_{NB}<18MW and Ip<1.5MA.In addition to He gas puffing,He fuelling by helium NB was done to simulate central generation of He ash in DT reaction. Helium enrichment factor defined by $(P_{He}/2P_{H2})^{MAIN}/(\Delta n_e/2n_e)^{DIV}$,where P is divertor neutral pressures of He and H2,Δn_e is increment of electron density and ne is electron density. Divertor neutral pressures of hydrogen(H2) and He were measured by a residual gas mass analyzer. In both cases of He gas and He NB fuelling, divertor neutral pressures of He and H_2 increase in proportion to ne^3. Enrichment factor is 0.3 to 0.6 and increases with ne. Non-linear dependence for the He neutral pressure on ne in NB discharges shows that required pumping speed of He can be reduced by high electron density discharge.He ion density was measured by CXRS methods. He ion density and energy distribution measurements using the two-electron transfer reaction by He probe beam were performed.The deduced He ion density and energy distribution were reasonable.This indicates that the two-electron transfer technique is promising for thermal and epithermal helium detection. Using spatial distribution and temporal behavior of the He ion density, transport analysis is now under investigation.

3.7.2 Disruptions[3.7-1]

From statistical investigation, disruption frequency in JT-60 was found to be less than 20~30% for total discharges in every experimental period. The ratio of disruptions during NB heating with constant power, which is a good criterion of disruption frequency used for designing next step tokamaks, is 7.2% for total NB heating discharges, 1872. The cause of the disruptions was classified. Unavoidable disruptions due to sudden impurity influx (0.6%) and unidentified causes (0.8%) are only 1.4% for total NB heating discharges, and other disruptions are caused due to the miss-operations or dirty plasmas with NB conditioning, which are avoidable.

The characteristics of energy loss channels in disruptions, heat flow, induction of the vessel current and radiation loss, were investigated. The heat loss to divertor plates in the thermal quench phase was measured with an IRTV camera with scanning speed of 51cm/0.4 msec. The followings were found from the measurement for a disruption of 1.7 MA lower X-point ohmic discharge. 1) Sudden temperature rise up to more than 1100°C (saturated) was observed at the inner divertor plates within 0.8 msec. 2) The heat flux caused by disruptions appeared at the different place by about 5 cm outside of the peak of the steady heat flux before disruptions. 3) The in-out asymmetry of the heat flux is considered to be closely related with the magnetic structure of m=2 mode growing before disruptions. The radiation loss measured with bolometer arrays reached about 70-100% of the magnetic energy, which indicates that the radiation is a dominant loss channel of the magnetic energy in the current quench phase. The induced vessel current is 0.3-0.4 MA for 3.1 MA disruption. The energy loss is less than 10 % of the magnetic energy. The generation of runaway electrons is an important phenomenon, but has not been measured yet.

3.7.3 Diagnostic topics

(1) 20-channel grating polychromator diagnostic system

A twenty-channel grating polychromator diagnostic system has been built to measure electron temperature profiles and electron temperature fluctuations in JT-60. The details of the system are described in Ref. [3.7-2]. The schematic diagram of the system is shown in Fig.IV.3.7-1. Figure IV.3.7-2 shows the electron temperature fluctuations at R~3.10m and R~3.16m in pellet experiments with injection of neutral beams and lower hybrid frequency waves. In this figure, a rapid decrease of

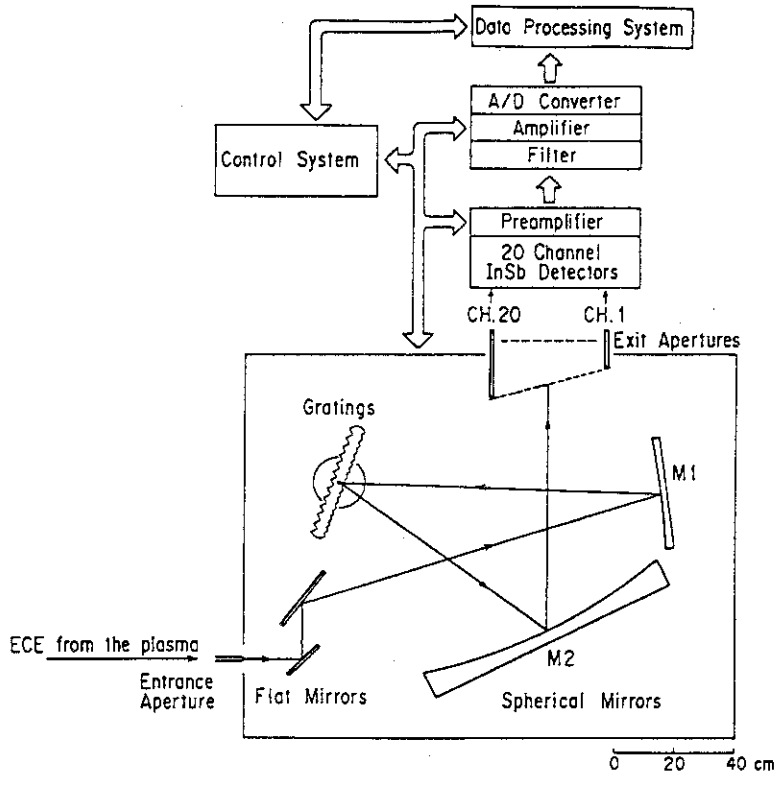

Fig.IV.3.7-1 Schematic of the grating polychromator diagnostic system.

electron temperatures followed by pellet injection is observed along with sawtooth oscillations.

(2) Millimeter-wave plasma radar system

A broadband reflectometric system in O-mode system has been built to measure electron density profiles and electron density fluctuations in JT-60[3.7-3]. The Schematic diagram of the JT-60 reflectometer is shown in Fig.IV.3.7-3. The details of the system are described in ref.[3.7-3]. For the density profiles determination, full Ka-Q band frequencies of BWOs have been swept for the continuous measurement of the group delay of reflected waves. The system also comprises a fixed frequency reflectometer with 24 and 34 GHz Gunn oscillators for the density fluctuation measurements.

(3) Zeeman polarimeter

A current profile measurement system using a He beam has been constructed for the diagnosis in the discharges with the lower hybrid current drive (LHCD) on JT-60. The spectral line of the He beam atoms is split into three components by the normal Zeeman effect. The line with $\Delta M=0$ transition (π-component) is polarized parallel to the magnetic field. The local pitch angle ($\theta=\tan^{-1}(B_p/B_T)$) of the magnetic field lines can be determined by measuring the polarization angle of the π-component.

Figure IV.3.7-4 shows the outline of the current distribution measurement system. In order to recover the difficulty of the low intensity, we have developed. The beam intensity is equivalent to 0.6 A and the maximum energy is 200 keV. A

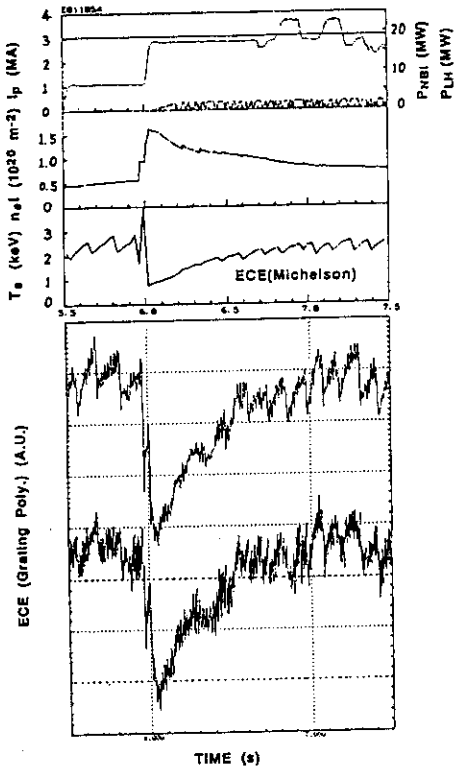

Fig.IV.3.7.-2 Typical temporal evolutions of the ECE signals at R~3.10m and 3.16m.

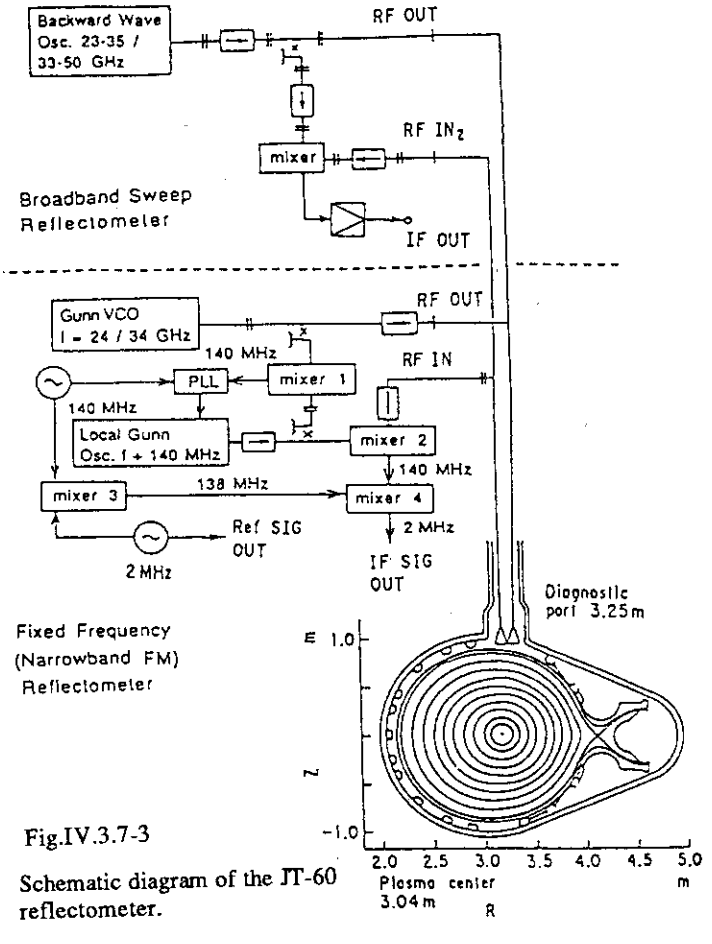

Fig.IV.3.7-3 Schematic diagram of the JT-60 reflectometer.

Wollaston prism splits the incident light (He I 5015 Å) into two beams whose polarization directions are perpendicular each other. The two beams are monochromatized by a Littrow type spectrometer whose wavelength band is 0.1 Å, and detected by a high efficiency avalanche photo diode detector whose detection efficiency is 30-32% at the wavelength. The details of the system are described in ref.[3.7-4]

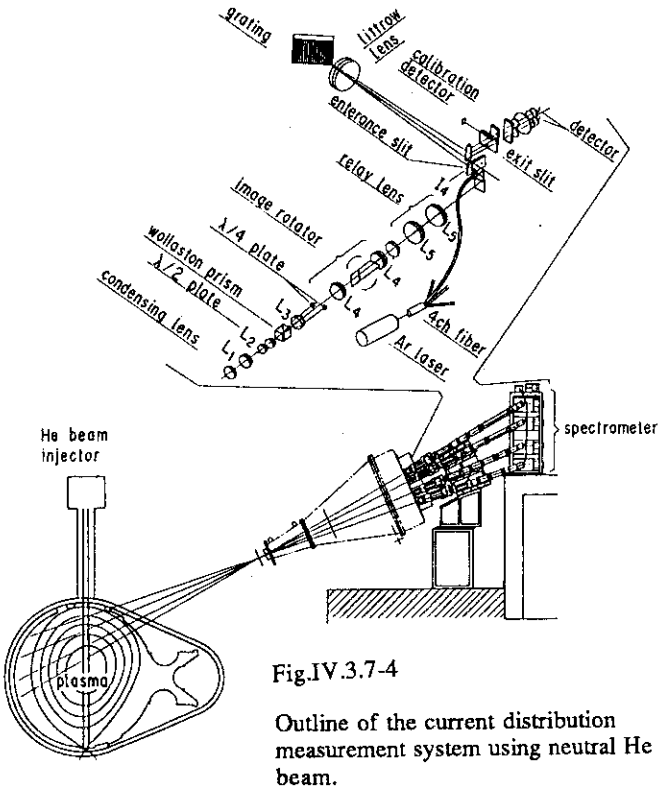

Fig.IV.3.7-4

Outline of the current distribution measurement system using neutral He beam.

References

[3.7-1] JT-60 Team, JAERI-M 90-066, 244-267
[3.7-2] M. Sato, et al. 14th Int. Conf. on Infrared and Millimeter Waves, Wurzburg, Germany, 1989.
[3.7-3] T. Fukuda, T. Matoba, A. Inoue. ibid
[3.7-4] N. Nishino, et al., JAERI-M 90-066

4. JT-60 Upgrade Developments

4.1 Tokamak

4.1.1 Summary of status

In light of recent results which indicate that both energy confinement and beta improve by increasing plasma current, the upgrade of JT-60 device (JT-60U) has been decided in order to double the plasma current [4.1-1,2]. The objectives of this upgrade are to improve plasma performance with minimum modification and to obtain physical and engineering database for the design of next-step tokamak. In the modification, the original poloidal field (PF) coil system and vacuum vessel are exchanged for new ones with large D-shaped cross sections, which allow plasma current of up to 6 MA, plasma volume of up to 100 m^3 and plasma elongation of 1.4 to 1.8 with single null divertor configuration as shown in Fig.IV.4.1-1. The existing toroidal field (TF) coils and their support fixtures will be used after reinforcement. The existing high power heating system and the power supply system will be also used after minor modification. Neutron shields for deuterium operation are being prepared. Table IV.4.11 gives main parameters of JT-60U.

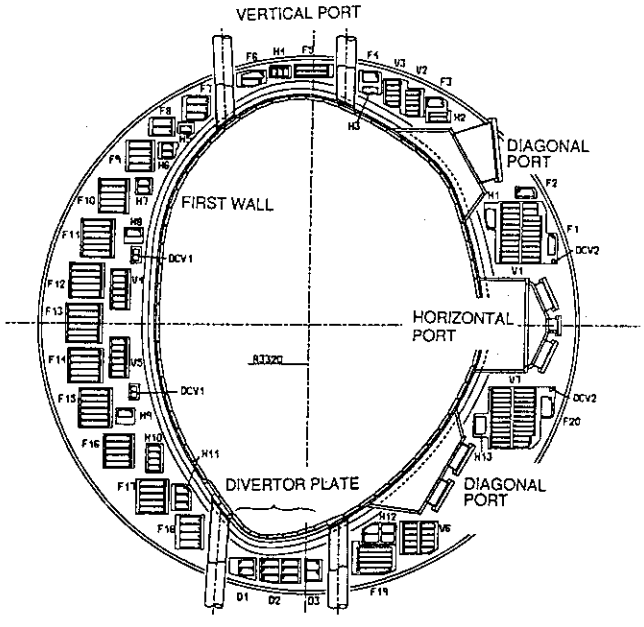

Fig.IV.4.1-1 Arrangement of the poloidal field coils and the vacuum vessel.

The design of JT-60U was initiated in 1987 and the fabrications of new PF coil system and vacuum vessel started at the end of 1988. These fabrications were completed from December 1989 to March 1990. Each equipments was transported to the Naka Site according to its completion.First walls and divertor armors are under fabrication in factories. The experiments of JT-60 was finished at the end of October 1989, followed by the disassembly in three months. JT-60U starts operating in 1991.

Table IV.4.1-1 Main parameters of JT-60U.

Parameters	Divertor	Limiter
Plasma current	6 MA	6.5 MA
Major radius	3.2 - 3.4 m	3.2 - 3.4 m
Minor radius (horizontal)	0.8 - 1.1 m	0.8 - 1.1 m
Minor radius (vertical)	1.5 m	1.5 m
Elongation	1.4 - 1.8	1.4 - 1.8
Plasma volume	< 100 m^3	< 110 m^3
Toroidal field	4.2 T (14.4 T·m)	
Discharge duration	15 s	
Discharge interval	10 ~ 15 min.	
Flux swing	61 V·s	
Neutral beam		
Torus input power	40 MW	
Beam energy	120 kV	
ICRF		
Torus input power	< 5 MW	
Frequency	110 - 130 MHz	
LHCD		
Torus input power	< 10 MW	
Frequency	1.7 - 2.3 GHz	
Pellet injection	< 2.8 km/s, 4 mm ϕ	

4.1.2 Vacuum vessel

The thickness of the vessel including armor tiles must be reduced so that a plasma can be as large as possible within the limited bore of the existing TF coil. On the other hand, the integrated forces in the vertical and horizontal directions due to disruption are about 10 MN and 20 MN, respectively. Therefore, the new vacuum vessel must have sufficient strength against these electromagnetic forces. A thick wall vessel with bellows structure used in the original JT-60 and JET does not satisfy the above requirement. A continuous chamber with so called double-skin structure is adopted to obtain a large vacuum vessel with sufficient strength.

A schematic picture of the vessel structure is shown in Fig.IV.4.1-2. This structure is determined after stress analyses of a multi-arc and a polygonal shape [4.1-3]. Inconel 625 is the material used for the vessel because of its high strength and high electrical resistivity. The double-skin structure consists of 6.1 mm thick inner and outer skins and poloidally-oriented square pipes with 3 mm in thickness. The wall of the outboard midplane ring is a thick plate to maintain its structural strength in spite of its many large port openings. The inboard midplane has a ring flame and the port bases are also made of thick plates. The vacuum vessel is supported by 36 support rods at the inner and outer midplane from the PF coil support structure as

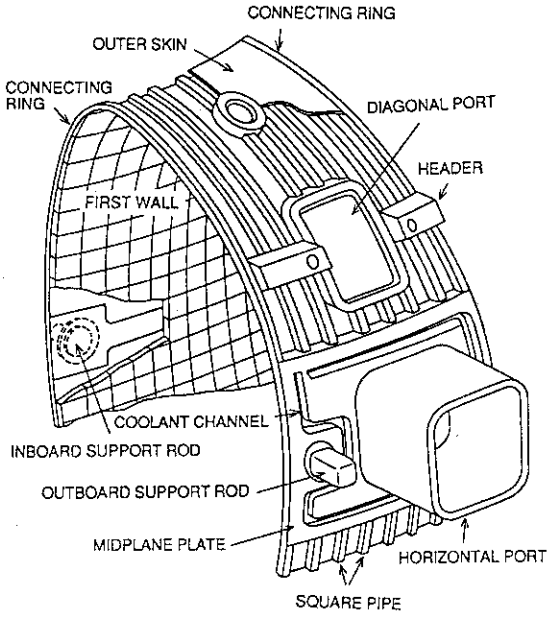

Fig.IV.4.1-2 Schematic diagram of the vacuum vessel.

shown in Fig.IV.4.1-2. This type of support structure was determined after stress analyses of a vessel supported at the midplane and a vessel supported at the bottom. The vacuum vessel is cooled and baked with nitrogen gas circulating through channels between the skins and pipes. The vessel can be baked out up to 300 °C.

It is one of the most important issues to maintain a plasma in an enhanced confinement regime under intense heating. Suppression of impurity influx from divertor plates is important for this purpose. NB input power of JT-60U is 40 MW, which is the largest in the present tokamaks. Thus, a carbon-fiber composite (C/C) with thermal conductivity of up to 300 W/m°C is used for the divertor plates in JT-60U. Water cooling pipes are introduced into the vacuum vessel for the heat removal of the divertor plates so as to suppress thermal stress due to low thermal conduction between the inner and outer skins. The surface of the vacuum vessel except divertor plates are covered with graphite tiles. The inboard tiles are designed to withstand the heat flux of up to 3 MW/m^2 while the heat flux onto the outboard tiles is much smaller. These graphite tiles are inertially cooled and the heat is removed through the cooling channel of the vacuum vessel after each shot.

4.1.3 Poloidal field coil

The PF coil system consists of an ohmic heating coil (F), a vertical field coil (V), a horizontal field coil (H), a divertor coil (D) and a sector coil (DCW) as shown in Fig. 1. The maximum values of coil current are close to those of JT-60 so as to minimize the modification of the power supply. These coils are designed to produce 3 types of divertor configurations to study the dependence of diverted plasma confinement on the aspect ratio, major radius, minor radius and elongation. The V-coil is divided into 4 blocks and the plasma configuration can be selected by the tap change in the coil feeder. In the standard mode, the divertor plasma with elongation of 1.5 and an aspect ratio of 3.4 can be produced. In the elongated mode, the divertor plasma with elongation of 1.76 and an aspect ratio of 3.8 can be produced. Continuous mode permits continuous control of the elongation and the triangularity, but this option requires an additional power supply.

To increase the passive index n_s and to obtain stable discharges with high elongation, conductors of the H-coil are distributed around the vacuum vessel and conductors of V_2, V_3 and V_6 are designed to serve as passive stabilizers in the elongated mode.

Return conductors of the V-coil can be eliminated and the V-coil is designed to have a flux swing capacity of 19 V·s. On the other hand, the capacity of the F-coil is increased up to 42 V·s by increasing its current from 92 kA to 120 kA. The total capacity of 61 V·s is 2.4 times as large as that of the original JT-60 while the total ampere turn increases by 15%.

Conductors of the F-coil are arranged to minimize an axisymmetric stray field inside the vacuum vessel. The design criterion of this axisymmetric stray field in the tokamak at breakdown phase is that the region with $|B_p|<5\times10^{-3}$ T should be wider than 1 m^2. To satisfy this condition, slight excitation of the D-coil is necessary because of lack of the F-coil blocks in the bottom region.

Disruption control, together with particle and impurity control, is crucial to obtain steady-state discharges. Four sets of sector coils named DCW are provided both at the inboard side and at

the outboard side of the vacuum vessel. This DCW coil can produce m = 3/n = 2 small magnetic islands at q=1.5 surface, which may induce "mini-disruption" as shown in JIPP T-IIU. Because of the ergodization of m = 2/n = 1 magnetic islands by this mini-disruption, the temperature profile will be changed and studies of disruption control will be possible as demonstrated in JIPP T-IIU. An attempt will be also made to control particle and impurity concentration during H-mode and to control edge plasma phenomenon such as ELMs.

4.1.4 Miscellaneous remarks

The poloidal field produced by the PF coils and the plasma cause a significant overturning moment on the TF coils. The TF coils are originally designed to withstand this overturning force of 450 tons for 50,000 shots acting on the upper or lower half of the TF coil. With the new PF coil system and the new plasma configuration, a overturning force of up to 600 tons is estimated. Since the primary stress of up to 833 MPa is generated at the coil case in the new operation conditions (Fig.IV.4.1-3(A)), reinforcement is necessary for the TF coils and their support fixtures. To increase the strength, two coils adjacent to each other are welded together at the inboard side of the coil case. The upper support structure is also reinforced to increase the stiffness and to decrease the displacement of the coils. The reinforcement reduces the stress to 470 MPa as shown in Fig.IV.4.1-3(B).

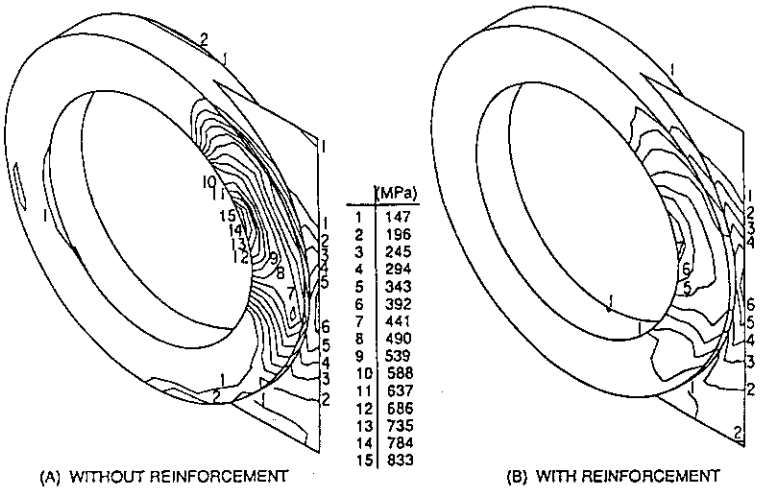

Fig.IV.4.1-3 Primary stress contour on the coil case of the toroidal field coil.

References

[4.1-1] M. Kikuchi, T. Ando, et al., Proc. of 15th Symp. on Fusion Technol., Utrecht, 1988 (Pergamon Press, 1989) Vol. 1, pp. 287.
[4.1-2] H. Horiike, T. Ando, et al., Present Status of JT-60 Upgrade, Proc. 13th Symp. on Fusion Engrg., Knoxville, 1989.
[4.1-3] T. Horie, T. Ando, et al., Stress Analysis of JT-60U Tokamak, ibid.

4.2 Control system

4.2.1 Plasma control

(1) VME multiprocessor system

We have been developing a VME multi-processor system [4.2-1] for plasma position and current control at the JT-60 upgrade. System design of the hardware and software was completed. Parallel processing with three 32-bit RISC microprocessors MC88000 (Motorola Co., USA)

makes it possible to calculate plasma state variables precisely and to execute the sophisticated plasma control fast. As shown in Fig.IV.4.2-1, the VME system is connected to its supervisory minicomputer and the direct digital controllers (DDC's) in the poloidal field coil power supply through CAMAC branch highways. Development of the hardware was also completed. In particular, I/O modules of up-down counters (UDC), analog-to-digital converters (ADC) and a clock pulse generator (CPG) were newly developed. We performed some tests for evaluating the speed of the data transfer among the VME-bus system, the minicomputer and the DDC's [4.2-2]. The VME multiprocessor system, then, promises to execute the feedback control with a cycle time of 250 μsec for the plasma vertical position and with that of 500 μsec for the control of the other parameters. Noise tests of the VME components were also performed. In particular, VME bus extensions with bus repeater / expanders were examined. No bus error was found at the test where impulse noise with peak voltage up to 7 kV was applied to the front panel of the system controller module.

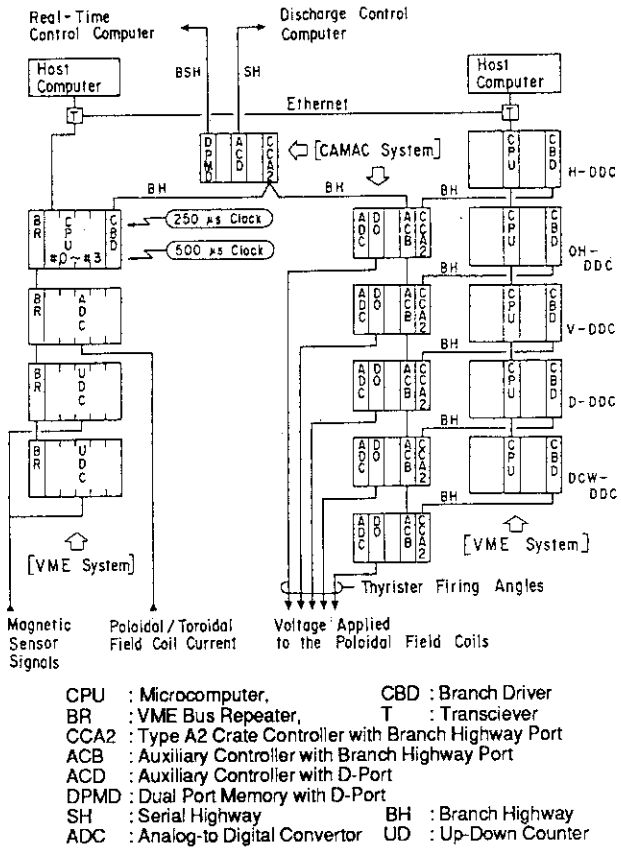

Fig.IV.4.2-1 Configuration of the VME multiprocessor system for plasma position and current control at the JT-60 upgrade

The software installed in the processors are now under development. The system integration test is scheduled July through September, 1990.

(2) Development of a plasma shape identification method

One of the methods to calculate plasma position and shape in real time is that using the expressions derived beforehand by regression analysis using the equilibrium database. We intend to use this method for plasma control at an initial stage of the JT-60U operation, and the actual expressions are now under development.

Besides the above method, we have also developed a new method (the TOLFEX method) [4.2-3] to identify a plasma shape with a Legendre-Fourier expansion of the vacuum poloidal flux function in the toroidal coordinates. The method is based on the analytical solution of the Grad-Shafranov equation in a vacuum region. The center of the toroidal coordinates (R_0,Z_0) and the coefficients of the flux eigenfunctions are determined by "the 2-step least square method" with the observed flux and plasma current values. The shape of the plasma is given by the contour of the constant flux value, which is the minimum value among the flux values at the fixed limiters and an X-point. This method has the following features: (a) Magnetic probes are not used in the

method. (b) It can take eddy currents into consideration. (c) It is robust to the loss of the flux loops and the existence of noise. (d) Application of the method may be limited to plasmas with ellipticity $\kappa \leq 1.7$. Figure IV.4.2-2 shows an example of the shape identified by the TOLFEX method for a divertor plasma with a current of 6 MA. The method can be executed in real time where a table-look-up procedure is applied for calculation. In JT-60U the execution time is estimated to be about 2 msec by parallel processing with three MC88000 processors and a main memory of about 15 Mbytes. Then, at present it is not applicable to the vertical plasma position feedback control where the cycle time of 250 μsec is required, but it is possible to apply the method to real-time visualization of the plasma shape.

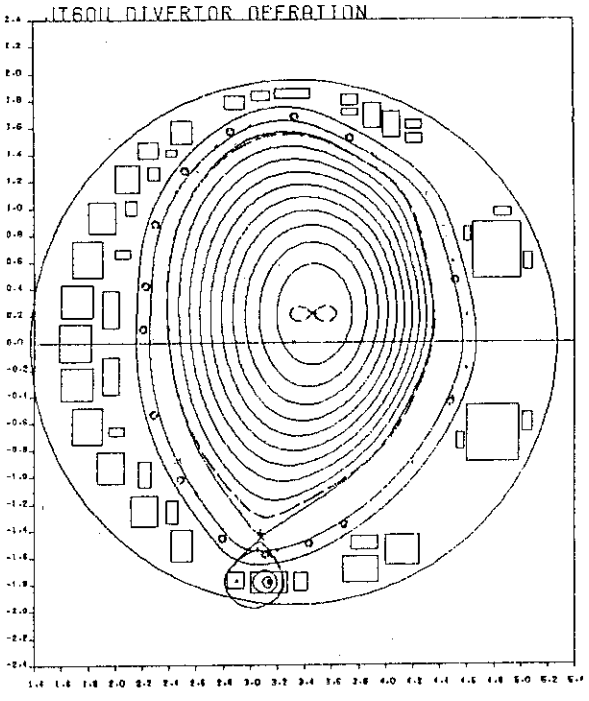

Fig.IV.4.2-2 An example of the identified JT-60U plasma shape by the TOLFEX method(dashed line) in comparison with the output of the equilibrium code(solid line). (A 6MA standard divertor plasma)

4.2.2 Man/machine interface

A new man/machine interface in ZENKEI is now under development on the basis of the five-year operational experience. The development is focused on the following improvements: (1) the function for setting discharge condition parameters, (2) the functions for monitoring the plant status and discharge results and (3) work environments in the JT-60 central control room.

As shown in Fig.IV.4.2-3, the man/machine interface is installed on a network system with 9 workstations. A minicomputer of HIDIC-V90/45 (Hitachi, Ltd.) is also provided as a supervisor of the workstations. This minicomputer is also connected with the present central control computer system through a shared memory and a dedicated computer linkage. One of the workstations is dedicated for a file server of discharge condition parameters. The type of the workstation is Sun-3/470GX-32-P14 (CPU: MC68030, 33 MHz) with a main memory of 32

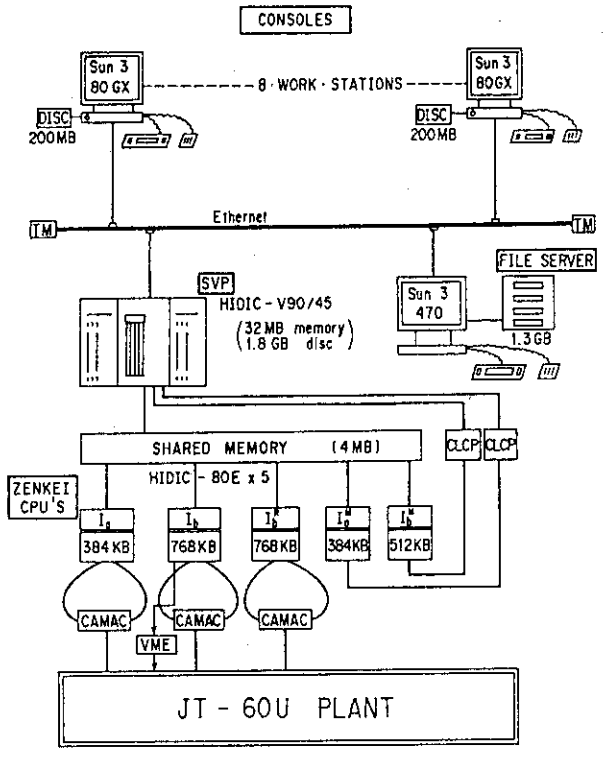

Fig.IV.4.2-3 Configuration of the new man/machine interface system in the JT-60 central control system, ZENKEI.

Mbytes, a floating processor of MC68882 (33 MHz) and a 1.4-Gbyte disk unit. The other workstations are for operation. Their type is Sun-3/80FGX-8 (CPU: MC68030 20 MHz) with a main memory of 8 Mbytes, a floating processor of MC68882 (20 MHz) and a 200-Mbyte disk unit.

The hardware of the system has already been prepared and its software is now under development. We will start a test run of the new man/machine interface system in December, 1990.

References

[4.2-1] T. Kimura, et al., IEEE Trans. on Nuclear Science **35** (1989) 1554.
[4.2-2] Y. Kawamata, et al., JAERI-M 90-005 (1990) (in Japanese).
[4.2-3] K. Kurihara, et al., JAERI-M 90-001 (1990) (in Japanese).

4.3 Power supply system

4.3.1 Remodeling of equipment

Some remodelings have been done in the PFPS. Main modifications are as follows.

(1) Reinforcement of the quadrupole field power supply

The quadrupole field power supply which is used for controlling plasma vertical position in JT-60U has been reinforced. The rated direct current increased from ±25 kA to ±30 kA, and then the convertors are tolerated for 10 ms at the plus current of 90 kA and for 30 ms at the minus current of 70 kA. Moreover, in order to suppress quickly the vertical instabilities of the vertically elongated plasma, the number of firing pulses of thyristors was increased from 12 pulses to 24 pulses and their controllers made from digital computers have been modified to execute the coil current control with very short processing time of 300 μs.

(2) Development of ceramic resistors for snubber circuits

The duration time of the plasma current will be extended to 15 seconds in JT-60U. Then, in the ohmic heating power supply and the vertical field power supply, a new type of resistor for the snubber circuits has been developed and its efficiency was confirmed. The resistor is made of ceramic and has large thermal capacity. As a result of this development, all snubber resistors in the both power supplies will be exchanged for the new ones in FY 1990.

(3) Modification of the ohmic heating power supply

The VCB system is not necessary for plasma breakdown in JT-60U because the minimum breakdown voltage of plasma in JT-60 was only 13 V and the time constant of the new vacuum vessel in JT-60U is longer than that in JT-60. Then, the DC circuit breaker system which had been used for plasma current initiation have been removed from the main circuit in the ohmic heating power supply. Moreover, the power supply was modified to be a bipolar power supply with the rated current of ±120 kA.

In FY 1990, the control system in the PFPS will be reorganized according to these remodelings.

4.3.2 New DDC system

In order to improve handling and efficiency of the PFPS's control system, a new DDC (Direct Digital Control) system is now under development by using a VME system which has a 20 MHz MC68030 32-bit processor. The configuration of the new DDC system is shown in Fig.IV.4.3-1. A VME system is connected with I/O modules housed in a CAMAC crate through a CAMAC branch highway. The system is developed with a workstation "AS 3260" (Toshiba Corp.) on a network system of Ethernet. Softwares in the new system are programmed by the C Language. Its control cycle is 250 μs at minimum. Installation of the hardware had been finished in FY 1988, and R&D's were started in April 1989 with a test system. A prototype of the software was developed. Then, the run speed was examined and it was evaluated that the new system was applicable to the real DDC system. Manufacture of the software for the horizontal field power supply was started in September and its test operation with the dummy coil was done at the end of December. From January 1990, the softwares for the other power supplies are manufacturing on the basis of the results of the test operation.

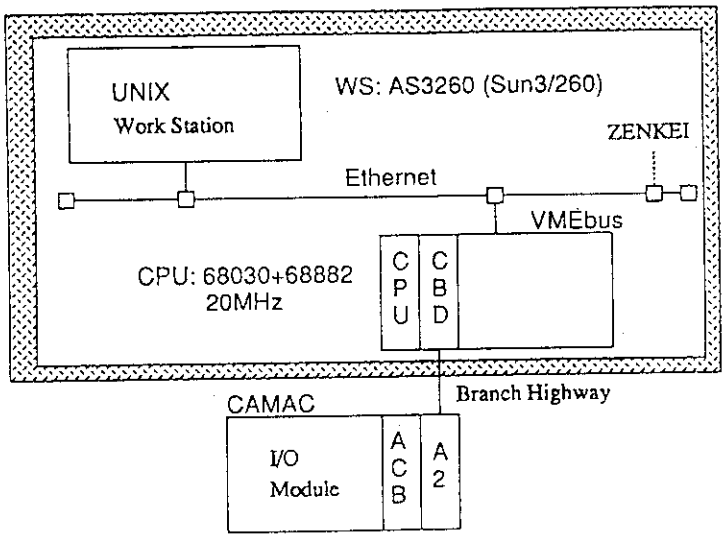

Fig.IV.4.3-1 Configuration of the New DDC system

4.4 Neutral beam injection system

In the JT-60U heating experiments, a higher beam energy is required due to a large plasma minor radius and a deuterium plasma. Design study of the acceleration power supply showed that the acceleration voltage could be increased up to 120 kV with a minor modification. The modification is mainly adding the GTO thyristors for a GTO switch and capacitors for a DC filter. A bending magnet power supply is required to increase the output current. To confirm the performance of the acceleration power supply up to 120 kV, an acceleration power supply among those of the 14 units was modified and tested combined with a ion source for 120 kV. In the ion source, the first acceleration gap and the second one were adjusted from 4 mm to 4.5 mm and from 5 mm to 10 mm, respectively. The outer surfaces of the ceramic insulators were re-shaped to reduce the concentration of electric field. After some tests of the power supply alone up to 120 kV, the beam extraction test was performed. With three-week operation, the beam of 110 kV, 72 A was extracted from two ion sources, while the acceleration voltage reached 117 kV without beam extraction [4.4-1]. The modification of the power supply system of the other 13 units started on November 1989.

In order to operate a deuterium beam up to 120 kV in JT-60 NBI, the magnetic field of the ion bending magnet must be strengthened up to 2.3 kG at the center of the magnet. However, the bending magnet had been designed to produce the magnetic field of 1.5 kG at the center of the magnet for hydrogen beam of 100 keV. In using a higher magnetic field than 1.5 kG, a non-linear relation between the coil current and the magnetic field have to be confirmed, because the ion core begins to be saturated magnetically over 1.5 kG. In addition, an effect of magnetic hysteresis with the periodical beam operation have to be investigated. These magnetic properties were investigated with a one-fourth model of the bending magnet for JT-60 NBI. The non-linearity between the coil current and the magnetic field due to the magnetic saturation was less than around 8 % with the magnetic field of 2.3 kG for the deuterium beam of 120 keV. The magnetic hysteresis was not observed below the magnetic field of 2.3 kG.

The stray magnetic field of the JT-60U is estimated to increase up to 330 G at the center of the NBI tank in a divertor discharge of 6 MA plasma current. Against the stray magnetic field, the magnetic shielding system will not work well due to the magnetic saturation of the magnetic shield material. After the investigation of the various shielding structures, an addition of the third cancelling coil to the present two cancelling coil system was determined. The optimization of the position and the ampere-turn of the coil was carried out with the one-fourth model of the magnetic shielding system for JT-60 NBI. The coil is positioned at the boundary of the neutralizer cell shielding and the ion source one, and the required ampere-turn is about 16.8 kAT.

To reduce the ripple loss and expand the plasma experimental region, tangential injection system was investigated [4.4-2]. Beamline components of the present two units are re-installed in a newly designed beamline box. Fig.IV.4.4-1 shows a cross-sectional view of the tangential injection system. The beamline box is made of stainless steel and the stray magnetic field is shielded actively by the cancelling coil system to reduce the error field at the plasma surface. By the magnetic field analysis, the cancelling coil system was designed to use two large coils and two small coils. The large coils are set around the beamline box, and the small coils are at the intermediate of the upper and lower bending magnets in the beamline box. The required ampere-turns are 82 kAT and 4 kAT, respectively. Four beamline units out of the 14 units are planned to be modified for the tangential injection system.

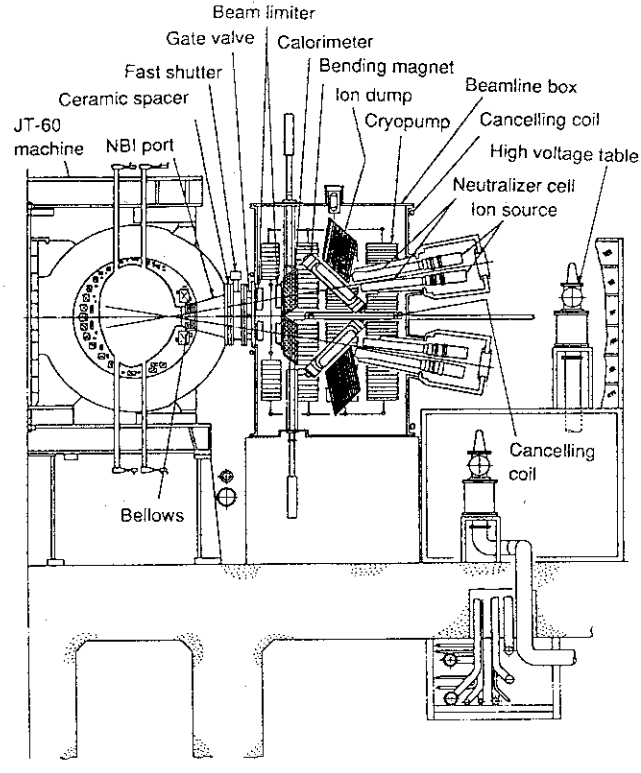

Fig.IV.4.4-1 A cross-sectional view of the tangential injection system for JT-60U.

A negative-ion-based neutral beam injection system is proposed as a current driver in higher density plasmas in JT-60U [4.4.-3]. Fig.IV.4.4-2 shows a ground plane of the negative-ion-based neutral beam injection system. The system will tangentially inject 0.5MeV,10 MW deuterium beams with two beamlines. This program aims at clarifying physics problems related to high energy NBI as follows; (1)To confirm the validity of neutral beam current drive in fusion reactors by demonstrating 2 MA level beam driven current in medium and/or high density plasmas. (2)To clarify the phenomena related to neutral beam current drive such as multi-step ionization processes, plasma rotation and beam driven Alfven instability. (3)To examine heating efficiency for a reactor-grade high density and high temperature plasma by a higher (>> 15 Te) energy NBI. The detailed investigation of the system is being carried out, and it will be completed by the end of 1993.

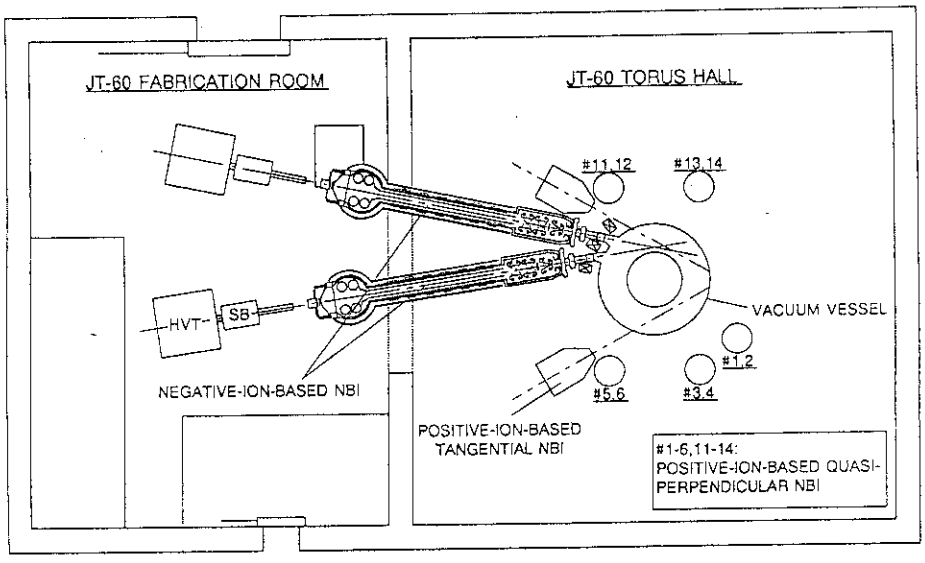

Fig.IV.4.4-2 A ground plane of the negative-ion-based neutral beam injection system for JT-60U.

References

[4.4-1] M.Kuriyama, et al., Proc. of 13th Symp. on Fusion Engineering, Knoxville, (1989) p.996.
[4.4-2] M.Matsuoka, et al., JAERI-M 90-086.
[4.4-3] M.Matsuoka, et al., JAERI-M 89-117.

4.5 Radio-frequency system

4.5.1 LHRF system

According to upgrade plan of JT-60, LHRF heating system was modified to study steady state operation by non-inductive current drive. The energy confinement time is also expected to be improved by increasing a plasma current, which can be supplied by an rf power due to the rf current drive [4.5-1]. Since the multi-junction type launcher had been successfully introduced in the JT-60 LHCD experiments with the high current drive efficiency, we decided to adopt again the multi-junction type launcher on the JT-60U. The JT-60U has two ports for LHRF launch. One is oblique type injection and the other is horizontal type injection. In this period we constructed one of the multi-junction LHRF launchers with oblique type. The feature in JT-60U launcher is mainly that the rf wave spectrum can be controlled by changing frequencies and phase differences between main waveguides. A manufacturing without deformation of waveguides and thin septum are essential to launch a

designed wave spectrum. A diffusion bonding method to produce the waveguides was applied to assure the low cost and to minimize the time required for manufacturing the launcher since whole launcher modules must be bonded at the same time. After 250 C baking, the preconditioning of launcher was performed in a vacuum tank at the JT-60 rf building.

The pierce hole for passing waveguide (W/G) transmission line from the RF amplifier room into the torus hall was reconstructed to prepare experiments using deuterium. In this period, the reconstruction of one unit among three units was performed. The cross section of the pierce hole is reduced from 2500 wide x 200 height to 1050 wide x 850 height to decrease dose of radio activity at the rf amplifier room II.

4.5.2 ICRF system

ICRF heating system for JT-60U provides the power of 9.5 MW with a double launcher. Two antenna were manufactured for JT-60. The cross section of the antenna is changed from 52 cm x 37 cm to 74 cm x 86 cm and the power density is reduced to 1/2 of that of the former JT-60 ICRF antenna. In addition, the antenna is also designed so as to couple with an H-mode plasma, which has a steep density gradient in front of the launcher. The outer radius of feed through is enlarged from 152 to 203/230 and the inner conductor was coated with carbon. The antenna system equips with the ark senser to monitor the rf discharge. The matching unit is composed of a line stretcher and a sub-tuner with wide band to assure theupgrade of withstand voltage. Improvements of the control system such as monitor points, the improvement of the software, the check of rf power and phased monitor and the rearrangement of the protection unit were performed so as to be applicable to two antenna injection. The high power amplifier (HPA) will be changed from Varian 8973 tetrode to Varian X-2274 new tetrode with the output power of 1.5 MW and the total output power will be increased from 6 MW to about 9.5 MW. The antenna of the ICRF launcher for JT-60U is shown in Fig.IV.4.5-1

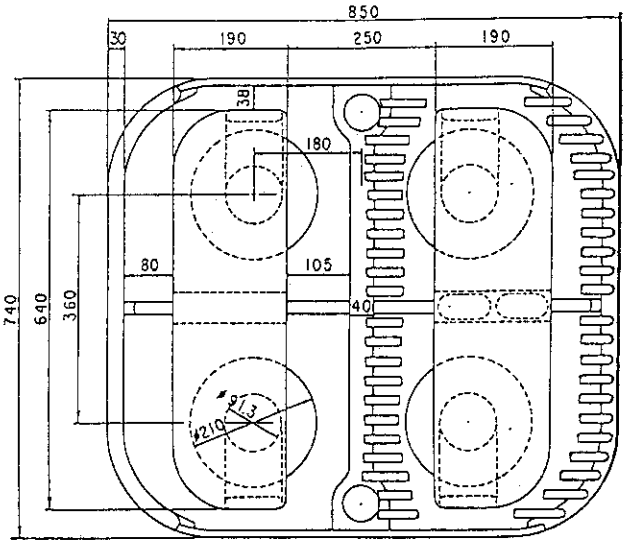

Fig.IV.4.5-1 ICRF antenna for JT-60U, viewing from plasma side.

References

[4.5-1] K.Uehara,O. Naito M.Seki et al., Phys.Rev.Lett 64,757 (1990)

4.6 Diagnostic system

On JT-60 upgrade, diagnostic systems will be improved to measure detailed spatial distributions of plasma parameters (electron temperature, electron density, ion temperature, poloidal field, hard X-ray and so on) and to measure velocity distributions of high energy particles. The diagnostic systems for planning are shown in Table IV.4.6-1.

Table IV.4.6-1 Planning of JT-60U diagnostics

Measured parameter	Diagnostics	Specification (Planning)	Status I: improvement R: rearrangement N: new establishment
Electron density	FIR Interferometer	Spatial 2 chords	I
	CO_2 Interferometer	Spatial 3 chords	N
	Reflectometer	$\Delta r \sim 1 \sim 2$ cm, $\Delta t \leq 1$ ms 8 fixed frequency X/O mode 110-170GHz Broadband X mode	R
Electron temperature profile and Electron density profile	Thomson Scattering	2 Lasers $\Delta t \geq 2$ms spatial ≥ 30 points $\Delta r \geq 8$ mm	I
Electron temperature	ECE (Polychromator)	spatial 20 points, Δt=20 μs	R
	ECE (Fourier transform spectrometer)	spatial 30 points, $\Delta t \sim 20$ ms	R
Electron velocity distribution function	Hard X-ray (vertical)	spatial 8 chords, E=30~600 keV	I
	Hard X-ray (horizontal)	spatial 2 chords, E=30~600 keV	N
	ECE (Fourier transform spectrometer)	spatial 30 points, $\Delta t \sim 20$ ms	R
Ion temperature	charge Exchange Recombination Spectrometer	3 × spatial 20 points Ti $\geq$100 eV	I
	Active Beam Scattering	spatial 1 point, Ti $\geq$1 keV	R
	Heavy Impurity Spectrometer (Doppler)	spatial 1 point, Ti $\geq$1 keV	I
	Light Impurity Spectrometer (Doppler)	spatial 1 point Ti=50~1000 keV	R

Table IV.4.6-1 Planning of JT-60U diagnostics (continued)

Measured parameter	Diagnostic	Specification (Planning)	Status
Ion velocity distribution function	CX (perpendicular)	spatial 1 chords, E=1~110keV	R
		spatial 2 chords, E=1~110keV E=1~300keV	R
	CX (tangential)	spatial 2 chords, E=1~110, 500keV	R
Impurity	X-ray Spectrometer	spatial 1 chord, λ=1~10 Å	R
	Grazing Incidence Spectrometer	spatial 1 chord, λ=5~1300 Å	R
	Grazing Incidence Spectrometer for Divertor	spatial 1 chord, λ=5~1300 Å	R
	Grazing Incidence Monochromator	spatial 1 chord, λ=10~1300 Å	R
	Spectrometer for Periphery	spatial 18 chords, λ=2000~7000Å	R
	Visible Monochromator	spatial 1 chords, λ=2000~7000Å	R
	Visible Spectrometer for Divertor	spatial 38 chords, λ=4000~7000Å	N
	Fiber Optics and Filters, for Z_{eff}	spatial 11 chords, λ=5230 Å	N
	Soft X-ray Pulse Hight Analyzer	spatial 1 chord, E=3~110keV	R
Current density profile	Zeeman Polarimeter	spatial 6 points	R
	Faraday Rotation	spatial 2 chords, Δt≥10ms $\Delta\theta_F \simeq 0.2$ deg.	I
Charged fusion product	Escaping Particle Monitor	spatial 1 point, E=3~10MeV	R
Neutron	Fission chamber	spatial 3 points	N
	2.45/14MeV Neutron detector	spatial 1 chord	R
Radiation loss profile	Bolometer Array(Main)	2 Arrays ×16 chords	I
	Bolometer Array(Divertor)	spatial 1 chords	I
MHD	PIN Diode Arrays	2 Arrays × 32 chords	I
	Electro Magnetic Probes	56 probes	I
Peripheral Plasma	Hα monitor(Poloidal)	spatial 10 chords	I
	Hα monitor(Divertor)	spatial 1 chord	I
	Hα monitor (Outer peripheral)	spatial 2 chords	I
	Hα monitor(Toroidal)	spatial 6 points	N
	Electrostatic probe	2 Arrays ×15 probes	N
Others	IRTV/(Hα TV)	T=400-1200°C	I
	Tangential TV	horizontally 3 cameras	I
	Pellet Monitor	spatial 10 points	I

V. TECHNOLOGY DEVELOPMENT

1. Surface Physics and Vacuum Technology

1.1 Introduction

The primary objective of the surface physics studies is to investigate the interaction between plasma and wall or limiter materials by using low energy ion accelerators. These studies will help us to find out optimum conditions for minimizing impurity production and controlling hydrogen recycling.

One the other hand, vacuum technology is one of the key technologies for the operation and maintenance of current fusion devices. It has also been more and more recognized that not only application of conventional techniques but also development of innovative techniques is required for realization of the next step fusion reactors. The technology area includes wall preparation, pumping system, gauging, leak hunting and in-vessel manipulators.

1.2 Hydrocarbon formation due to interaction of graphite with hydrogen ions

In 1989 fiscal year we carried out the experiment of isotope exchange between hydrogen and deuterium through the formation of mixed hydro- and deutero-methane[1.2-1]. We have continued the measurements to study whether heavier mixed hydrocarbon of $C_xH_yD_z$ molecules is formed when carbon materials are exposed to the simultaneous or successive bombardments of H^+ and D^+ ions. Figure V.1.2-1 shows typical results of the successive bombardments of 6 keV H_3^+ and 6kV D_3^+ ions at 500 °C[1.2-2]. It can be seen that the signal intensities of mass 29(C_2H_3D, C_2HD_2) and mass 31(C_2HD_3) had a maximum, and that those of masses 32(C_2D_4) and 26 (C_2H_2) increased and decreased, respectively, with increasing D fluence. These results indicate that the isotope exchange between hydrogen and deuterium occurs through a channel of C_2 hydrocarbon formation as well as of methane formation in graphite target.

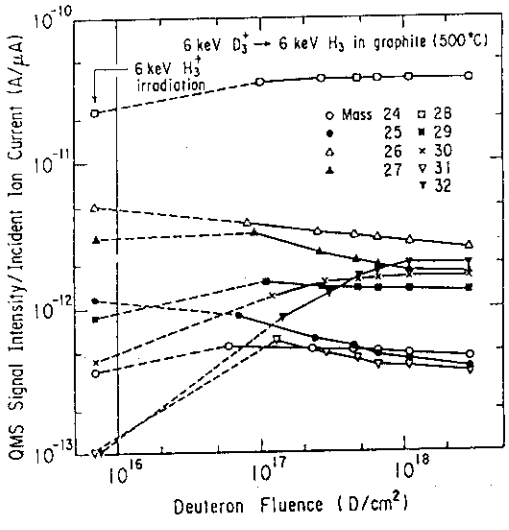

Fig.V.1.2-1 D fluence dependence of measured QMS signal intensities from mass 24 to mass 32 divided by incident ion current after subtracting background intensities from the raw signal intensities. The target of pyrolytic graphite was bombarded with 6 keV H_3^+ up to saturation and subsequently with 6 keV D_3^+ at 500 °C.

References

[1.2-1] Annual Report of the Naka Fusion Research Establishment 1989 JAERI-M 89-100.
[1.2-2] R Yamada, J. Appl. Phys. **67** (1990) 4118.

1.3 Permeation of deuterium implanted into thin copper plate

The permeation rate of deuterium implanted into copper foil was measured as a function of temperature (80-500°C) and implantation flux ((0.2 -1.0)x10^{10} D-atoms/cm^2s). When the backsurface of the sample was argon-bombarded prior to the deuterium implantation, the permeation rate exhibited simple temperature dependence; it increased with increasing temperature above 200°C while it was nearly independent of temperature below 200°C as shown in Fig.V.1.3-1. The dependence of the permeation rate on the implantation flux also changed around 200°C (Fig.V.1.3-1). This transition can be attributed to the change in the transport regime. The recombination coefficient of deuterium on copper surface was evaluated from the permeation flux. The value was several orders of magnitude smaller than the one calculated with the model proposed by Pick and Richards.

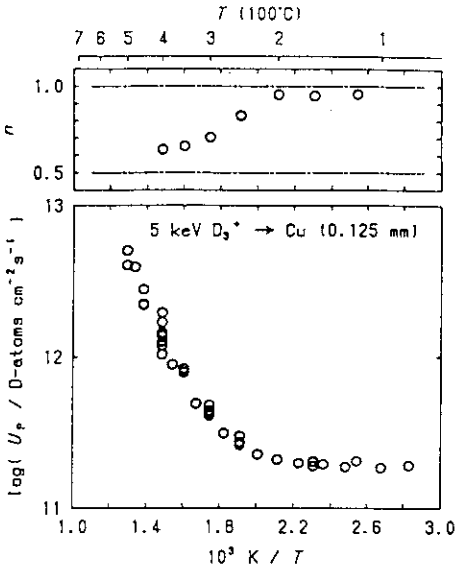

Fig.V.1.3-1

Temperature dependence of the permeation flux U_p and the index n, which indicates that the U_p is proportional to the n-th power of the implantation flux.

1.4 Development of ceramic turbo-viscous pump

In order to establish a torus pumping system for fusion reactors involving ITER, a new type of roughing vacuum pump named turbo-viscous pump has been developed. A feature of the pump is that a ceramic rotor assembly and an oil-free driving unit are adopting to prevent the influence of strong magnetic fields or tritium radiation. The rotor assembly, which is made of silicon nitride (Si_3N_4), has eleven parallel disks, between which project stator disks from the outer casing with roter-stator clearances less than 100μm, and a shaft with two gas turbine blades. Spiral grooves are cut on either side of the rotor or stator disk of each stage, each of them starting near the center (or at the periphery) and ending at the periphery (or near the center). The pump shaft is supported by gas bearings and is driven by impulse gas turbines at approximately 25,000rpm. This pump is completely oil-free.

The major specifications of the pump are listed in Table V.1.4-1. This pump and the previously-developed ceramic turbomolecular pump[1.4-1] [1.4-2] can be utilized for a pumping system of the fusion reactors. Figure V.1.4-1 shows the ceramic turbo-viscous pump (this side) connecting to the ceramic turbomolecular pump in series.

Table V.1.4-1 Major specifications of the ceramic turbo-viscous pump.

Diameter of rotor disks	150mm
Number of rotor disks	11
Rotation speed	25,000rpm
Operation pressure range	10^{-5} - 760Torr
Pumping speed	280 $l \cdot min^{-1}$
Ultimate pressure	7 x 10^{-6}Torr

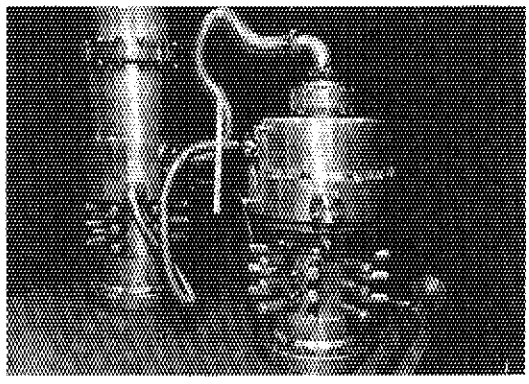

Fig.V.1.4-1
Ceramic turbo-visccous pump (this side) connecting to the ceramic turbomolecular pump in series.

References

[1.4-1] Annual Report 1989 of the Naka Fusion Research Establishment, JAERI-M 89-100.
[1.4-2] T. Abe, et al, Vacuum, to be published.

1.5 Fabrication and test of 3-phase induction motor and dc servomotor for in-vessel manipulators

It is necessary to develop various types of remote manipulators which can be used inside the vacuum vessel of fusion devices since the majority of maintenance operations are to occur due to plasma-wall interactions. In order to provide the driving units for the in-vessel manipulators, we carried out the fabrication and test of two types of electric motors, namely a 3-phase induction motor and a dc servomotor, in 1989 fiscal year. Major technical problems are how to prevent the deterioration of insulators and lubri-cating materials and to mitigate the out-gassing rate of all structural materials at high temperatures and in high vacuum.

The major specifications of the coil insulators and bearings of the prototype motors are listed in Table V.1.5-1. These materials of the motor also have robustness against radiation. The test of these motors have been successfully performed.

Table V.1.5-1 Major specifications of the prototype motors.

Type of motors	3-phase induction motor	dc servomotor
Usage	Carrying motor	Positioning
Working environment	up to 350°C, 10^{-8}Torr	up to 150°C, 10^{-8}Torr
Materials		
Coil insulators	SiO_2 composite	SiO_2 electrolytically coated
Ball bearing	(Retainer) Self-lubricating sintered alloy (Ball) Pb ion-plated	Special greased

1.6 Development of new QMS head movable in vacuum vessel

A quadrupole mass spectrometer (QMS) with a specially-designed analyzing head was fabricated and tested[1.6-1]. The main features of the new QMS are that the head can be moved inside a large vacuum vessel and that it can be operated at elevated temperatures up to 150°C.

Figure V.1.6-1 shows the drawing of the head. The electronic circuit which consists of an rf tuning and a detection sub-circuits is packed in an airtight stainless steel casing which is directly connected to the head. The circuit is tuned by supplying variable frequency of rf voltage since the resonance frequency depends weakly on environmental temperature. With this QMS, normal mass spectra could be obtained for the mass range 1-50 a.m.u. even when the environmental temperature was 150°C.

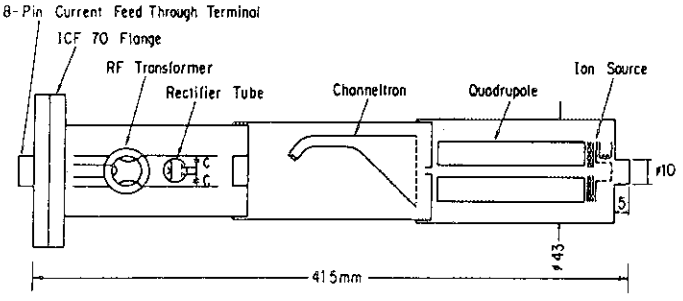

Fig.V.1.6-1 Schematic drawing of the new QMS analyzing head.

References

[1.6-1] S. Hiroki, et al, J. Vac. Sci. Technol., to be published.

1.7 Development of fast pressure monitoring system

In order to measure fast pressure changes in the JT-60 torus vacuum vessel, a modified Penning-type vacuum gauge was developed[1.7-1]. The discharge in the Penning cell is sustained by using the magnetic field which confines the fusion plasma. The response time of the monitoring system involving the gauge is very fast (≦10ms) since the gauge is placed near the vacuum vessel. In 1989 fiscal year the new gauge was installed in JT-60 to measure pressures during and after plasma shots. The abrupt gas release from the wall due to plasma disruption and subsequent adsorption of the gas on the wall were successfully analyzed with the monitoring system.

References

[1.7-1] N. Ogiwara, M. Maeno and M. Matsukawa, to be published in Proc. 13th Symp. on Fusion Technol., Knoxville, (1990).

2. Superconducting Magnet Development

2.1 Introduction

The superconducting magnet development work is being carried out for the purpose of engineering establishment on the magnet system in the Fusion Experimental Reactor (FER). The objectives of the four major developments are as follows:

1) Toroidal Coil	DC Coil	Max. Field 12T	Height 12m
2) Outer Poloidal Coil	Pulsed Coil	Max. Field 7T	Diameter 5-20m
3) Central Solenoid Coil	Pulsed Coil	Max. Field 13T	Diameter 3- 4m
4) Refrigerator System	Refrigeration	Power 30 x 4 kW at 4K	

For toroidal coils, a large coil technology up to the coil height of 5m (Maximum field 8-9T) has been achieved by the IEA Large Coil Task and a high field coil technology up to the maximum field of 12 T (Coil height 1.6m) has been achieved by the Cluster Test Program. Based on these experiences, Prototype Toroidal Coil Program is now under way and three kinds of 12-T, 30-kA prototype toroidal conductors were fabricated in 1989.

Figure V.1.6-1 shows the drawing of the head. The electronic circuit which consists of an rf tuning and a detection sub-circuits is packed in an airtight stainless steel casing which is directly connected to the head. The circuit is tuned by supplying variable frequency of rf voltage since the resonance frequency depends weakly on environmental temperature. With this QMS, normal mass spectra could be obtained for the mass range 1-50 a.m.u. even when the environmental temperature was 150°C.

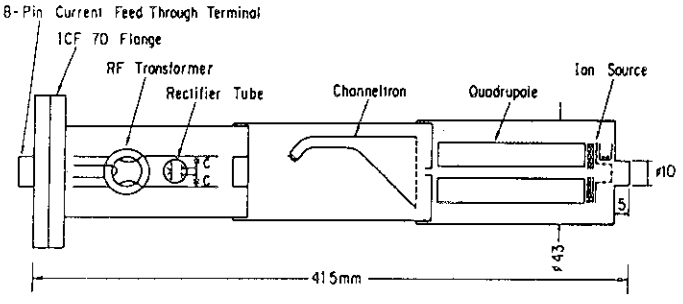

Fig.V.1.6-1 Schematic drawing of the new QMS analyzing head.

References
[1.6-1] S. Hiroki, et al, J. Vac. Sci. Technol., to be published.

1.7 Development of fast pressure monitoring system

In order to measure fast pressure changes in the JT-60 torus vacuum vessel, a modified Penning-type vacuum gauge was developed[1.7-1]. The discharge in the Penning cell is sustained by using the magnetic field which confines the fusion plasma. The response time of the monitoring system involving the gauge is very fast (≦10ms) since the gauge is placed near the vacuum vessel. In 1989 fiscal year the new gauge was installed in JT-60 to measure pressures during and after plasma shots. The abrupt gas release from the wall due to plasma disruption and subsequent adsorption of the gas on the wall were successfully analyzed with the monitoring system.

References
[1.7-1] N. Ogiwara, M. Maeno and M. Matsukawa, to be published in Proc. 13th Symp. on Fusion Technol., Knoxville, (1990).

2. Superconducting Magnet Development

2.1 Introduction

The superconducting magnet development work is being carried out for the purpose of engineering establishment on the magnet system in the Fusion Experimental Reactor (FER). The objectives of the four major developments are as follows:

1) Toroidal Coil	DC Coil	Max. Field 12T	Height 12m
2) Outer Poloidal Coil	Pulsed Coil	Max. Field 7T	Diameter 5-20m
3) Central Solenoid Coil	Pulsed Coil	Max. Field 13T	Diameter 3- 4m
4) Refrigerator System	Refrigeration	Power 30 x 4 kW at 4K	

For toroidal coils, a large coil technology up to the coil height of 5m (Maximum field 8-9T) has been achieved by the IEA Large Coil Task and a high field coil technology up to the maximum field of 12 T (Coil height 1.6m) has been achieved by the Cluster Test Program. Based on these experiences, Prototype Toroidal Coil Program is now under way and three kinds of 12-T, 30-kA prototype toroidal conductors were fabricated in 1989.

For poloidal coils, Demo. Poloidal Coil Program has been carried out to develop a large pulsed coil technology firstly at the level of 7T. In 1989, fabrication of a Nb_3Sn pulsed coil (DPC-EX) was completed and it was charged successfully up to 17kA, 7T in 1s and has demonstrated a significant advance towards poloidal coils of FER.

The cryogenic system technology has proved its reliable capability in the operation for testing of DPC-EX for more than 800 hours and some advanced cryogenic components has been developed in 1989.

2.2 The Demo Poloidal Coil program

2.2.1 Program status

To develop superconducting poloidal coils required in a future tokamak reactor, the Demo Poloidal Coil (DPC) program has been initiated at JAERI in 1985. The goals of DPC are to obtain experimental data, to demonstrate reliable operation, and to prove design principles and fabrication techniques for poloidal coils. The DPC program includes the fabrication and testing of two 30-kA Nb-Ti pulsed coils (DPC-U1 and -U2), and one 10-kA Nb_3Sn pulsed coil (DPC-EX). The coils have circular shape and are cooled by forced-flow helium. Their winding inner diameters are 1 m, which is about one-half size of center solenoid coils to be used in a fusion reactor. The fabrication of DPC-U1 and U2 have been completed in 1988 and their experiment was performed early in 1989 [2.2-1]. Following this, the fabrication of DPC-EX has been completed in September, 1989, and the experiment of DPC-EX being installed between DPC-U1 and U2 was conducted through November to December [2.2-2]. In this experiment DPC-EX achieved the designed pulsed field of 7 T/s and demonstrated the applicability of Nb_3Sn conductor to a pulsed coil. As an international collaboration, the United States Department of Energy (US-DOE) participates in the DPC program, and MIT provide a test coil which has 30-kA Nb_3Sn conductor [2.2-3]. The testing of US-DPC is expected to be taken place in this autumn.

2.2.2 Experiment of the DPC-U1 and U2

DPC-U1, U2, and EX were stacked in a co-axial configuration and were tightened together by stainless steel rods. The entire setup was installed in a vacuum tank (Fig.V.2.2-1). It took 131 hours to cool the three coils and structures to cryogenic temperature. No leak was encountered during the cooldown and subsequent experiment.

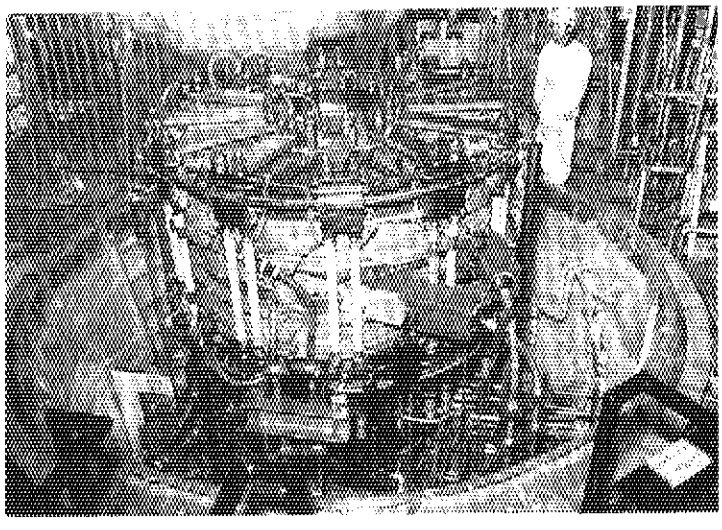

Fig.V.2.2-1 Demo Poloidal Coils installed in vacuum tank. (from top, DPC-U1, EX, and U2)

(1)DC and pulsed operation

In a DC operation, DPC-U1 and U2 reached the design current of 30 kA

and generated a magnetic field of 6.4 T. The stored energy at this point was 30 MJ. For DPC-EX experiment, DPC-U1 and U2 provided the background field and also obtained the maximum field of 6.8 T. Pulsed operations were performed in series connection of DPC-U1 and U2 using the JT-60 power supply. Designed pulsed field of 6.4 T/s was obtained by charging both the coils to 30 kA in one second with a flattop of half second. Unfortunately the flattop was shortened to half second from planned 3 second due to an instability observed in the coils.

(2)AC loss and mechanical performances

In order to reduce AC losses of the coils, many improvements were performed on the conductors and coil structures [2.2-4]. To verify these, AC loss measurements were performed during the pulsed operations. The measured AC losses of DPC-U2 are shown in Fig.V.2.2-2. As we had expected from their design, ac losses were quite small, and in the 30-kA pulsed operation the total losses was 6.8 kJ, which corresponds to only 0.06% of the stored energy (11 MJ). To eliminate AC losses in the coil structures, we adopted an aggressive design concept that the coils had no cases to support windings. Therefore, it was of another interest to us how the winding behave during a charge. From this point of view, 12 extensometers were attached on DPC-U2 and radial displacements at the outer circumference were measured (Fig. V.2.2-3). Measured displacements are in proportion to coil current squared in every case. This indicates that the winding behaves elastically and is mechanically stable. In addition, winding rigidity, which can be estimated from this figure, is much higher than that expected in pool-cooled coils. Thus the coil structure we had adopted was demonstrated to be successful.

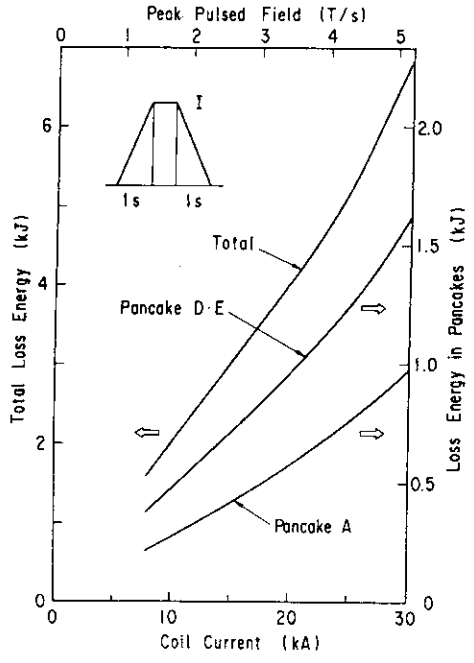

Fig.V.2.2-2 Ac losses of DPC-U2 during the pulsed operation.

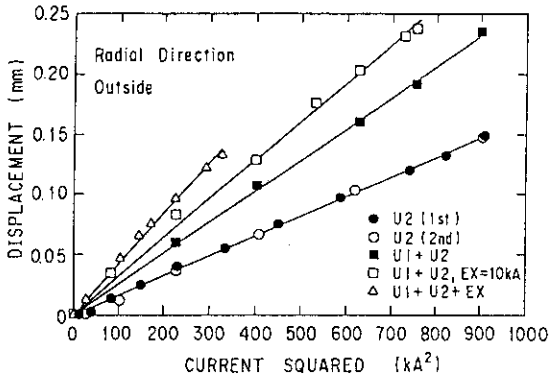

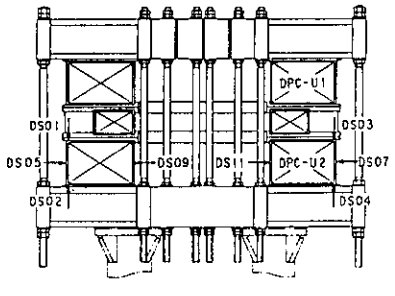

Fig.V.2.2-3 Measured displacements of DPC-U2 and the location of extension-meters

2.2.3 Experiment of the DPC-EX

In order to demonstrate the applicability of Nb_3Sn conductor to pulse poloidal coils for tokamak fusion machines, Nb_3Sn Demo Poloidal Coil (DPC-EX) has been fabricated and tested. An inner and an outer diameter of the DPC-EX are 1 m and 1.6 m, respectively. The nominal current is 10 kA. The DPC-EX consists of two double pancakes, fabricated by a react-and-wind technique. The conductor is a flat cable-in-conduit conductor with 153 Nb_3Sn strands around a stainless steel sheet and separated cooling channels. The strands are formed with a single island which includes 5754 filaments in the copper matrix. Tantalum material is used as diffusion barrier of the tin in the copper matrix in order to reduce hysteresis loss and coupling loss between the filaments. A chrome layer of thickness 5 μm is plated on the surface of strand in order to reduce the coupling loss between the strands. As the conduit material, JK-1 was used, which has excellent mechanical properties for heat treatment in temperature of 700 C. Figure V.2.2-4 shows the DPC-EX being installed between U1 and U2. The characteristics of the DPC-EX is listed in Table V.2.2-1. Experiment of the DPC-EX have been carried out, installing between DPC-U1 and U2. For the operation mode connected with DPC-U1, U2 in series, the DPC-EX has been ramped up to 17 kA in 1 s and ramped down to zero in 1 s after a flat top time for 1 s, without normal transition. The maximum magnetic field is 6.7 T and the changing magnetic field is 6.7 T/s, respectively. For the single operation mode with DPC-EX only, 8.3 T/s has been achieved by ramping up to 17 kA in 0.5 s and then by ramping down to zero in 0.5 s after a flat top time of 5 s. Figure V.2.2-5 shows the trace of the current and the terminal voltage of the DPC-EX on the cyclic operation.

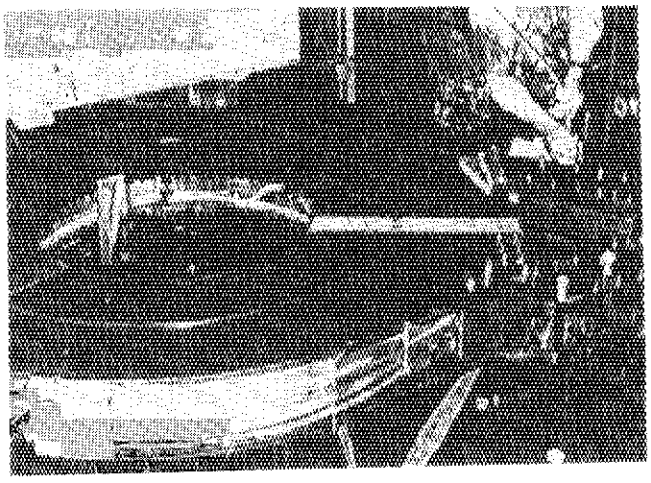

Fig.V.2.2-4 DPC-EC being installed between U1 and U2.

Table V.2.2-1 DPC-EX characteristics

Superconductor	$Nb_3(InSn)$
Rated current	10,000 A
Number of turns	120
Winding method	React and wind, Two double pancakes
Conductor length	508 m
Winding current density	20.6 A/mm2
Self inductance	23.7 mH
Self store energy	1.2 MJ
Magnetomotive force	1.2 MA
Weight	1,360 kg
Cooling method	Forced cooling
Operating temperature	4.1 K
Operating pressure	0.55 MPa
Number of cooling paths	4
One cooling path length	127 m
Operating mass flow rate	8.9 x 4 g/s
Design dump voltage	6.6 KV
Test voltage	19.8 KV

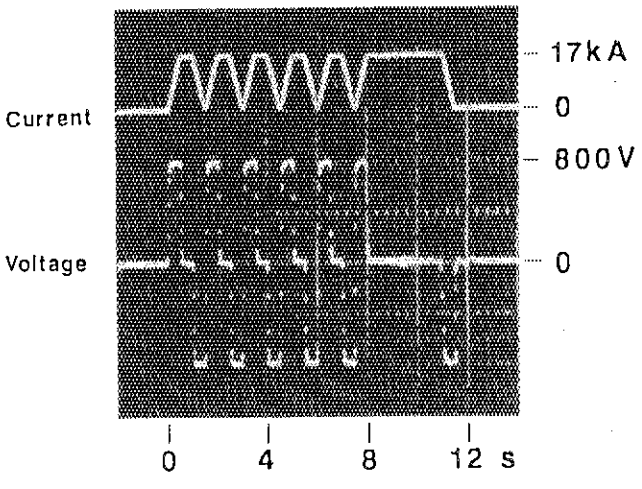

Fig.V.2.2-5 The trace of the current and terminal voltage of the DPC-EXon the cyclic operation.

The ac losses could be evaluated by a difference in enthalpy of the helium between at the inlet and the outlet. Figure V.2.2-6 shows the measured ac losses of the DPC-EX during the pulse operation whose rising time was 1 s. the coupling time constant of the conductor could be estimated to be about 4 ms by the experimental results. The coupling time constant was eight times that of the strand. The ratio of AC loss to stored energy is about 0.24 %. In these tests, the inlet temperature of the coolant helium gas is 4.1 K, the inlet pressure is 5.5 bar and the flow rate is 8.9 g/s. The DPC-EX was operated to 10 kA near 100 times without any trouble. In addition, the margin of the DPC-EX was defined as 1.7 times of the nominal current by the extended test and the possibility of the high current density pulse coil has been realized.

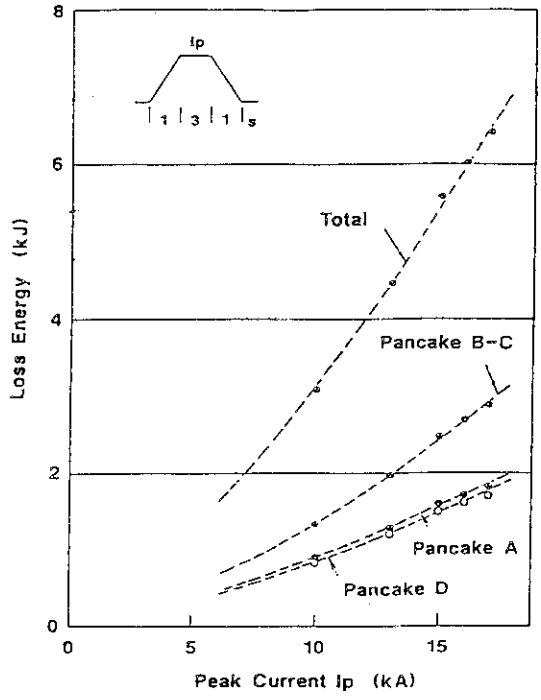

Fig.V.2.2-6 Ac losses of the DPC-EX during the pulse operation whose rising time was 1 s.

References
[2.2-1] Okuno, K. et al., Proc. 13th Symp. on Fusion Engineering, (1989) 776.
[2.2-2] Shimamoto, S. et al., Proc of ICEC-13 (1990).
[2.2-3] Steeves, M. M. et al., IEEE Trans. Magn., MAG-24 No.2 (1988) 1307.
[2.2-4] Tsuji, H. et al., IEEE Trans. Magn., MAG-25 No.2 (1989) 1484.

2.3 The Proto Toroidal Coil project

The Proto Toroidal Coil (PROTO) is planned for development of the TF coil for the FER. Therefore its candidate conductors were designed in 1988. Their trial manufacturings were carried out in 1989. PROTO conductors have three types which are TMC-FF type, Preformed armor type and Advanced disk type. The verification tests of their PROTO conductors were carried out as following items.

(1) Critical current: The strand of 2 mm diameter without copper stabilizer was manufactured. The critical current and the stability margin test samples of the straight real size conductor and the winding were manufactured.

(2) Stability margin: The small model sample which consists of one strand and a copper tube was manufactured for the TMC-FF type conductor.

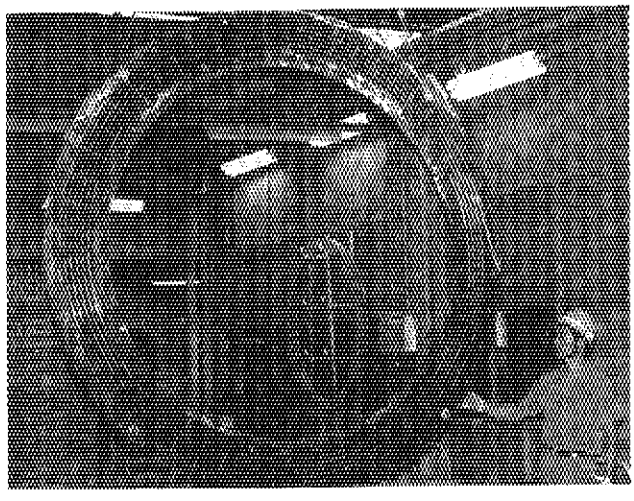

Fig.V.2.3-1 Mechanical test sample of the advanced disk conductor.

(3) AC loss: The copper stabilizer with insulation barrier for the TMC-FF type conductor was manufactured and measured.
(4) Mechanical properties: The mechanical test samples of the straight conductor and the winding were manufactured. The sample for the advanced disk type conductor are shown in Fig.VI. 2.3-1.

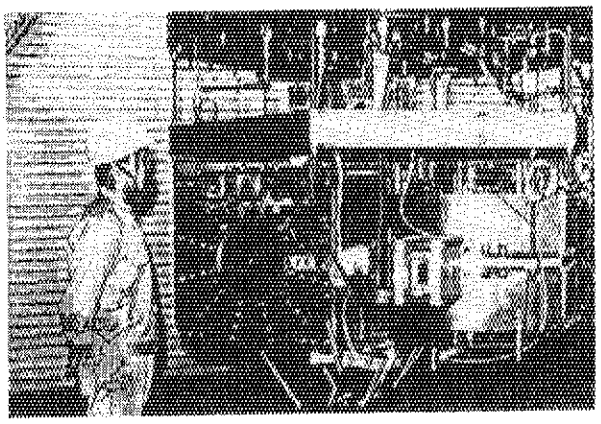

Fig.V.2.3-2 Verification test stand for Ic and the stability margin of the real size conductor.

The verification test stand for the critical current and stability margin of the real size conductors was designed and manufactured. This test stand consists of the superconducting transformer and the backup coils, and can supply 12T and 100kA. This test stand is shown in Fig. VI.2.3-2.

The mechanical and electrical property of the PROTO coil and its test stand were analyzed by the finite element method (NASTRAN) and so on. The experimental condition of the PROTO coil shall be similar to that of the TF coil of the FER. Especially, magnetic field and stress level of each material will be equal between the PROTO and the TF coil of the FER.

2.4 High field coil development

A Nb_3Al coil and two high-performance $(NbTi)_3Sn$ coils were developed in this period.Practical Nb_3Al superconductor is expected to be developed for its better latent capacity than Nb_3Sn. A coil wound with practical-type, that is, copper-stabilized multi-filamentary Nb_3Al superconductor was developed (Fig.V.2.4-1) and the magnetic field of 13.1-T was obtained in the background-field of 12.8-T as was designed. This result shows that the Nb_3Al superconductor used in this coil is homogeneous along its whole length of 200-m, which is very important for practical-use. The transverese-stress-effect of the Nb_3Al superconductor on the critical current was investigated and was confirmed to be much better than that of Nb_3Sn. The critical current density of the practical-type Nb3Al superconductor has been improved and it reached 300-A/mm^2 in 12-T at the end of this period.

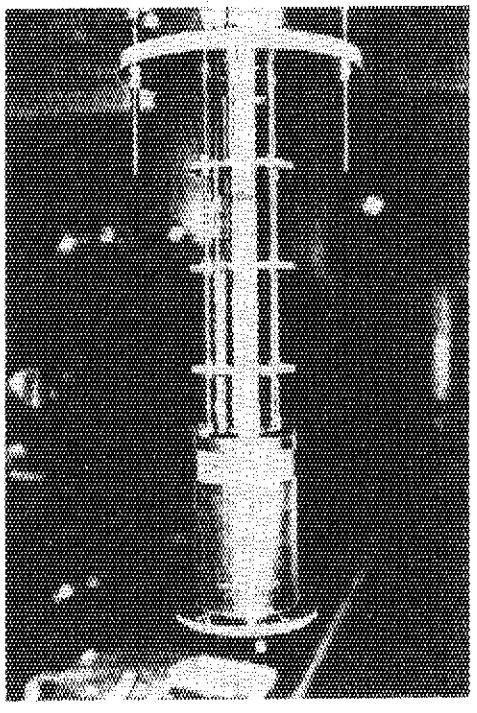

Fig.V.2.4-1 The coil wound with 200-m-long copper-stabilized multi-filamentary Nb_3Al superconductor which generate the magnetic field of 13.1T in the background-field of 12.8T. Dimensions of the winding part are 40-mm inner diameter, 84-mm outer diameter and 100-mm axial length.

A 13-T 140-mm-bore $(NbTi)_3Sn$ coil was developed. A 82-mm-bore $(NbTi)_3Sn$ coil, developed last period, became to generate 15-T by this 13-T coil. These coils are used for high-field superconductor development. A 32-mm-bore $(NbTi)_3Sn$ high-field test coil, which was designed to generate 18-T in the 13-T coil, was completed and is waiting for being tested.

2.5 Cryogenic system development

A large helium cryogenic system, required capacity is around 100 kW at 4 K regime, is indispensable for the Fusion Experimental Reactor (FER). JAERI is performing R&D work for the cryogenic system to realize such a large cryogenic system.

2.5.1 DPC cryogenic system

Through the DPC coil experiment, the DPC cryogenic system had operated to maintain the DPC coil system at 4 K regime for around 800 hours without any troubles. It was demonstrated that the DPC cryogenic system functioned as it was designed and was a world largest, proven forced-flow cooled superconducting magnet test facility. The verified performance results are follows;

(1) Supercritical helium of 350g/s, 4.0K and 6bar(design point) could be supplied to the coil system.

(2) The cryogenic system has demonstrated the wide operation range:
Pressure : 2 - 10 bar (Subcooled liquid helium was available)
Temperature : 3.9 - 4.5 K
Mass flow rate : 100 -350 g/s

(3) Adiabatic efficiency for the circulation pump and the cold compressor were measured to be around 60 %.

2.5.2 Cryogenic component development

A double acting bellow pump was adopted as a supercritical helium circulation pump in the DPC cryogenic system. However, a larger pump should be required for FER, required capacity is a mass flow rate of 2000 - 4000 g/s and a pump head of around 2.5 bar. A centrifugal pump will be used for such pump due to an advantage of large flow capacity. A centrifugal pump, show in Fig. VI.2.5-1, was developed at JAERI, which has the same design point as the DPC pump. Using the DPC cryogenic system, the pump was tested and the performance was measured as follows;

1) Mass flow rate : 100 - 630 g/s

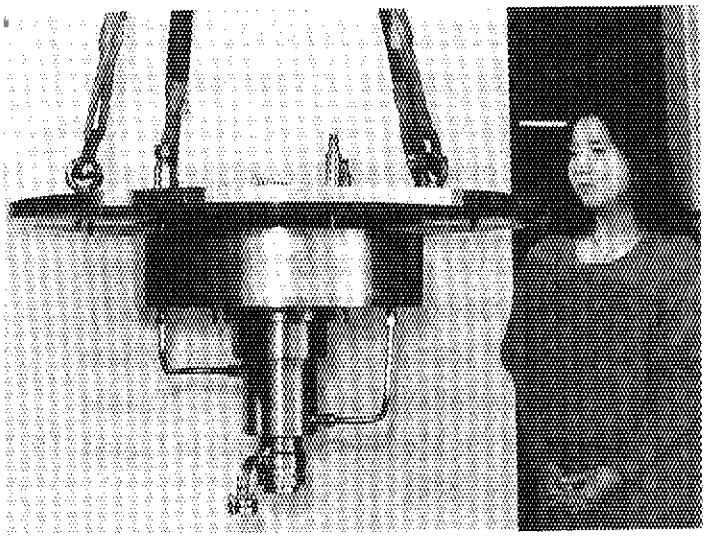

Fig.V.2.5-1 The centrifugal supercritical helium circulation pump

2) Pump head : 0.6 -2.0 bar
3) Adiabatic efficiency : 60 - 80 %

The performance as a function of mass flow rate are shown in Fig.VI.2.5-2 the pump has demonstrated very high efficiency of 80 % at the design point, corresponding to the world highest values. And this development has achieved an advance for the cryogenic system development of FER.

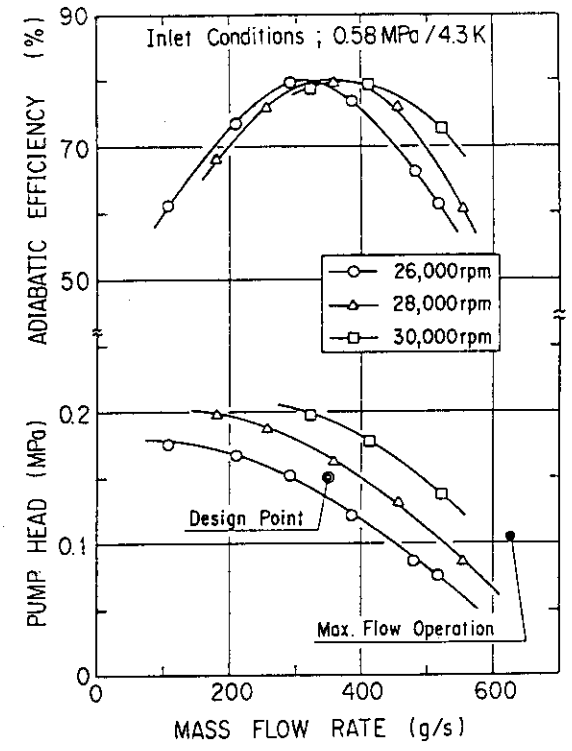

Fig.V.2.5-2 The performance results as a function of mass flow rate

2.6 Development of cryogenic structural materials

The new alloys named "Japanese Cryogenic Steels" (JSC) for the superconducting magnets of the Fusion Experimental Reactor (FER) were successfully developed in collaboration with four steel companies[2.6-1]. These alloys supplied from industrial heats (5 - 50 tons) were passed the requirement(σy>1,200 MPa, K_{Ic}>200MPa$\sqrt{m}$, called JAERI box) that was beyond the capabilities of the existing austenitic stainless steels for cryogenic use. In addition, favorable mechanical properties on the weldments of the JCS were obtained as shown in Fig.VI.2.6-1. The collaboration work of the development was finished on the end of March, 1990 because the purpose of them was almost achieved.

On the other hand, the second round robin tests under US-Japan collaboration were conducted in order to establish the standard methods of cryogenic material testing[2.6-2]. The standard of tension test at liquid helium temperature is established as JIS Z2277 "Tensile Testing Method for Metallic Materials in Liquid Helium" on June, 1990.

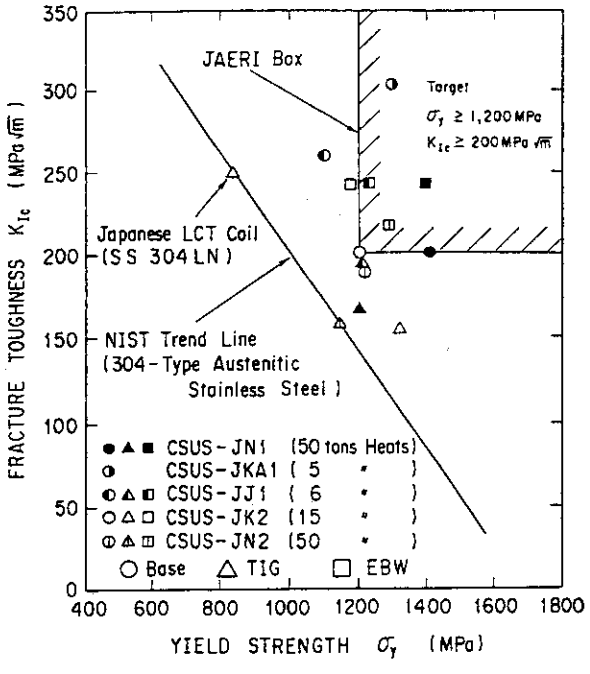

Fig.V.2.6-1 The 4 K mechanical properties of the JCS which are specially developed for the superconducting magnets of the FER.

References

[2.6-1] H. Nakajima, et al., To be published in ISIJ International, Vol 30, No.8, (1990), 567
[2.6-2] H. Nakajima, et al., To be published in Adv. Cryog. Eng. Mater., Vol. 36, Plenum Press, New York, (1990), 1069

3. Beam Technology

3.1 Negative ion beam technology

3.1.1 A multi-ampere negative ion source [3.1-1,2,3,4]

To realize an efficient Neutral Beam Injection (NBI) system such as the ITER and FER, we have developed the negative ion sources since 1984. In 1988, a 3.4 A, 75 keV H^- ion beam have already been produced using the JAERI Multi-Ampere Negative Ion Source which is a pure volume source. To produce negative ions more efficiently, the ion source was operated with cesium. The plasma generator of the source is a magnetically filtered multicusp source, whose dimensions are 24 cm wide, 48 cm long, and 15 cm deep as shown in Fig.V.3.1-1. A small amount of cesium vapor (100mg) was injected from the cesium oven into the generator before the source operation. Once the cesium was injected, the source could be operated for more than one week (3000 shots of 0.2 sec). The H^- ions produced in the generator are extracted by four grids. Each of them has 434 apertures of 9 mm diameter within the area of 15 cm x 40 cm.

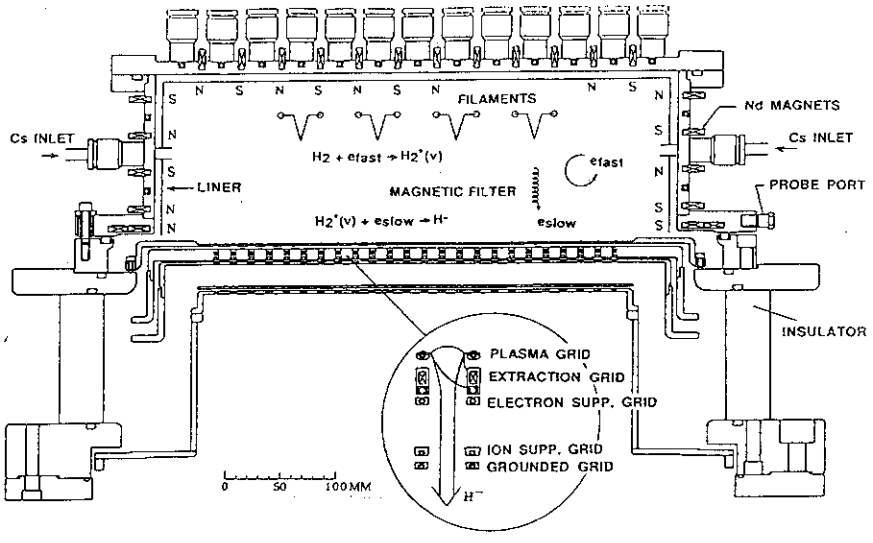

Fig.V.3.1-1 A cross-sectional view of the JAERI negative ion source

Dependence of the H^- ion current on the arc discharge current with and without the cesium vapor is shown in Fig.V.3.1-2. By seeding the cesium, the H^- ion current increases remarkably and reaches 10 A at the arc discharge current of 800 A. The ion current density defined as the ion current divided by the total aperture area is 36 mA/cm^2, which already satisfies the design value of the ITER/FER NBI system.

Besides the enhancement of the H^- ion production efficiency, the electrons extracted with the negative ions decreases to a almost zero in the cesium seeded source. In addition, the operating pressure with cesium is lower than the pressure with cesium. These effects can make the ITER/FER NBI system compact.

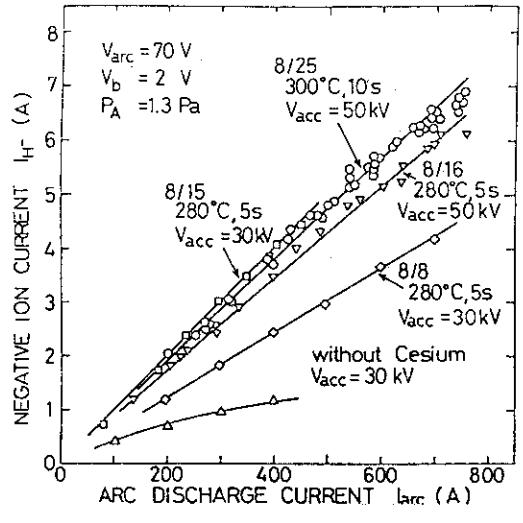

Fig.V.3.1-2 Dependence of the negative ion current on the arc discharge currents with and without cesium

3.1.2 Beam optics of negative ion [3.1-5]

Since the ion source will be placed at about 40 meters from the injecting port in the ITER/FER, the beam divergence angle as low as 5 mrad is required beam. Using a small negative ion source, the beam divergence angle up to the beam energy of 50 keV, which is the pre-acceleration voltage of 1MeV class accelerator for the ITER/FER, was measured. By optimizing the configuration of the accelerator, we have successfully produced a convergent beam of 4.7 mrad (e-folding half-width divergence) from a single aperture of 5 mm diameter.

3.1.3 Isotope effect on negative ion production [3.1-6]

In order to investigate the isotope effect on the negative ion production of deuterium and hydrogen, experimental studies were conducted using the JAERI One-Ampere Negative Ion Source at Lawrence Berkeley Laboratory as a US-Japan cooperative program on negative ion source.

After optimizing a filter strength and arc discharge conditions such as the operating pressure,we obtained experimental results as listed below;

(1) The negative ion current density obtained in deuterium operation was 8.4 mA/cm2 , while the value in hydrogen operation was 10.4 mA/cm^2 at the same arc discharge power of 40 kW.

This result indicates that the D- density in the plasma is same or higher than the H- density.

(2) The optimum filter strength in deuterium operation is stronger than that required in the hydrogen operation

(3) It was demonstrated that electron extraction , which was a serious problem in deuterium operation, can be suppressed by biasing a plasma grid at higher potential

These results offer an important data base for the design of the future NBI systems.

3.1.4 RF ion source for the negative ion production and plasma neutralizer [3.1-7]

The RF ion source has attractive features that (1) the operating gas pressure is low, (2) a hot cathode, whose life time is short, is not required for the discharge. Making use of these features, we have tried to apply the ECR plasma generator to the negative ion source and a plasma neutralizer. The ion source consists of a pair of magnetic coils and a cylindrical vacuum chamber as shown in Fig V.3.1-3. A microwave of 2.45 GHz, 5 kW generated by a magnetron is introduced through a quartz window to the chamber.

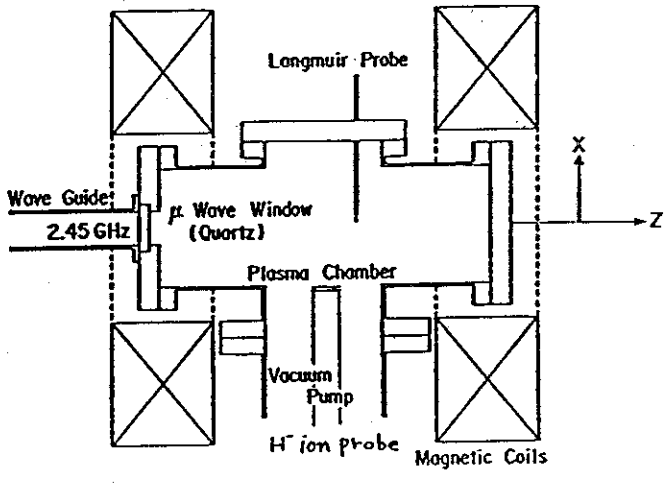

Fig.V.3.1-3 Schematic diagram of the high density ECR plasma generator

Hydrogen plasma and xenon plasma were produced by 5 kW RF power. The plasma densities were higher than 10^{12} cm^{-3}. In the xenon plasma, it was confirmed that the

ionization rate was higher than 30 %.

The Langmuire probe measurement showed the existence of the region in which the negative ions is rich. Further, the measurement by a probe with a low energy extractor showed that the H^- ion current was quantitatively measured to be 7mA/cm^2 at the injection power of 1 kW.

3.1.5 Construction of 350 keV test stand

In order to investigate beam optics, beam acceleration and voltage holding in the accelerator, the test stand which can produce 350 keV ,100mA negative ion beams has been constructed. The test stand consists of a motor-generator, source plasma power supplies, a beam acceleration power supply ,a high voltage feed through into a X-ray shield room and their control system. A negative ion source is mounted on a beamline in the X-ray shield room. The beam acceleration test will be started in April 1990.

3.1.6 Li^- ion source for plasma diagnostics

For plasma diagnostics, a high current negative lithium ion source are being investigated. The Li^- source is basically same as the volume source. However, the inner wall of the source is covered with liners made of molybdenum and tungsten to prevent Li condensation Li vapor, which was supplied from molybdenum boat installing Li metal.

In a preliminary experiment, the maximum Li^- beam current density of 1.1 υA/cm^2 has been obtained, which is still 3 orders of magnitude smaller than that required for the diagnostic system

References

[3.1-1] Y.Okumura, Kakuyuugou Kenkyu 60, 1988, 329.
[3.1-2] M.Hanada, T.Inoue, H.Kojima, et al., Rev. Sci.Instru. 61/1 (1990) 499
[3.1-3] Y. Okumura, M.hanada, T.Inoue, et al., Proc.5th International Symp.on the Production and neutralization of Negative Ions and Beams, BNL, 1989, 149
[3.1-4] H.Kojima, M.Hanada, T.Inoue, et al, Proc.13th Symp.on Ion Sources and Ion-Assisted Technology, Tokyo, 1990, 145.
[3.1-5] K.Watanabe, M.Hanada, T.Inoue, et al., Proc.2nd Symp.on Advanced Nuclear Research, Mito, 1990, 447.
[3.1-6] T.Inoue, G.D.Ackerman, W.S.Cooper, et al., Rev. Sci.Instru. 61/1 (1990) 496
[3.1-7] Y.Matsuda, M.Hanada, T.Inoue, et al., Proc.12th Symp.on Ion Sources and Ion-Assisted Technology, Tokyo, 1989, 107.

3.2 Design study of negative-ion-based NBI[3.2-1,2]

To clarify the goal of the R&D works for the next NBI system, two NBI systems have been designed. One is a 500 keV system for JT-60U and the other is an 1MeV system for the ITER/FER. These designs adopt the cesium mixing negative ion source which can efficiently produce the negative ion beam at the low operating pressure described in Table V.3.2-1.

Table V.3.2-1 Specifications of the ITER NBI

Injection power	50-75MW
Beam energy	0.5-1.3MeV
Pulse length	steady
Beam species	deuterium
Number of NBI ports	3
Number of beam lines per a port	3
Number of ion sources per a beam line	3
EFFICIENCIES	
Acceleration efficiency	82%
Neutralization efficiency	60%
Re-ionization efficiency	95%
Total efficiency	40%

The JT-60U NBI system will inject 0.5 MeV, 10 MW deuterium beams tangentially with

two beamlines. The system is composed of two negative ion sources. It is shown in Fig.IV.4.4-1 and 2. The ITER system designed by Japan is shown in Fig. V.3.2-1. The specifications of the system are shown in Table V.3.2-1. The system injects 1.3MeV, 75MW deuterium beams with nine beamlines each of which has one ion source.

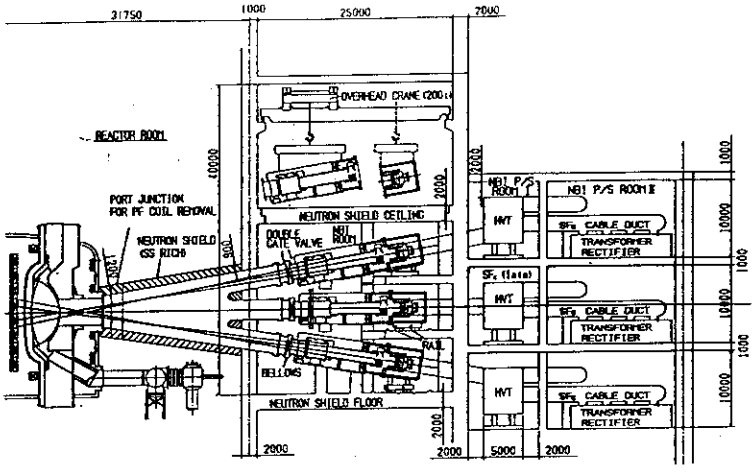

Fig.V.3.2-1 Elevation view of the ITER NBI

References

[3.2-1] Y.Ohara, Proc.13th Symp.on Fusion Engineering, Knoxville,1989,p284
[3.2-2] Y.Ohara, M.Akiba, M.hanada, et al., Proc.5th Int. Symp.on the Production and neutralization of Negative Ions and Beams, BNL,1989, p149

3.3 Positive ion beam technology

3.3.1 Production of large helium beam

To simulate the behavior of helium ashes produced by D-T reaction in the future reactors, the helium gas beam has been injected into JT-60. Before the experiment at JT-60NBI, a high current helium has been produced to confirm the beam properties using the ion source developed for JT-60 NBI at the proto-type unit. By accelerating at single stage to increase the beam power, the high current helium beam of 35 keV, 20A was produced. It offered a date base for the helium beam test at JT-60.

3.3.2 Energy recovery system [3.3-1]

As a collaborative study between Japan and EC, the experiment on the energy recovery system which can improve the power efficiency of the NBI system has been conducted using the JAERI High Proton Ion Source at Cadarache Laboratory in France. An experiment using a 100 keV, 14 A D^+ beam results showed that more than 90 % of the full energy ions of 100 keV were recovered and the power efficiency was improved by 25 %. This indicates that the energy recovery system is useful for the future NBI system.

3.3.3 Large scale cryo-sorption pump [3.3-2]

In long pulse helium beam injection, a high speed helium pumping system is required. For this purpose, we have developed a cryo-sorption pump which uses SF6 layer condensed on the cryopanel. The performance of the cryo-sorption pump was investigated at the proto-type JT-60 NBI unit. It was confirmed that the helium gas can be evacuated stably up to 2000 Pa m^3 keeping the pumping speed of 800 m^3/s. This result was reflected on the helium beam injection at the JT-60 NBI.

References

[3.3-1] M.Araki, Y.Ohara, and Y.Okumura, Fusion Technology, 17 (1990)
[3.3-2] K.Kikuchi, N.Akino, K.Iida, et al., Japan Atomic Energy Research Institute Report JAERI-M 90-056, 1990

4. RF Technology

4.1 Development of high power RF components for LHRF

A 1MW, 2GHz klystron was developed in cooperation with Toshiba and NEC. This klystron was applied to the LHRF system of JT-60 and contributed to the current drive and the heating experiments in JT-60. However, the operation time of these klystrons already exceeds 3000 hours, so that the operations at the output power of more than 0.7 MW of each klystron are sometimes limited by the breakdown at electron guns. To attain the more reliable operation of the klystron, the withstanding voltage of the electron gun must be increased. On the other hand, the high power klystron of more than 1MW is needed for JT-60U, and of higher frequency of 5 GHz for FER and ITER projects. Therefore, the improvement of the klystron which aims the increase in the output power and reliability was carried out.

The main items of the improvement are: (1) the suppression of the evaporation of Ba from the cathode surface using the Ir coated cathode, (2) the improvement of the shape of electron gun to decrease the electric field at the non-cathode surface and to elongate the dimension of ceramic insulators. After these improvements, the withstanding voltage of the electron gun is increased from about 84 kV (previous voltage) to more than 94 kV, which can produce the output power of more than 1.4MW. The output power of 1.4MW was obtained for 10 seconds at 2.17 GHz. Furthermore, the maximum power of 1.47MW for 2 seconds was obtained. Any breakdown do not occurred around output windows, and temperature rise of coolant water at a cavity is less than 10 degrees, which well satisfied the design value. Relations of the efficiency and the output power as a function of the beam voltage are shown in Fig.V.4.1-1. These result will present the perspective of the LHRF system for the next tokamak FER/ITER.

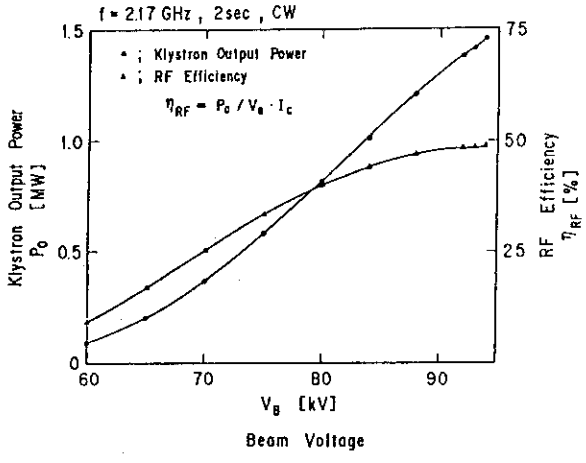

Fig.V.4.1-1 Beam voltage dependences of the output power and RF efficiency.

4.2 Investigation of high power gyrotron and ECH components

The development of 500kW gyrotron at a frequency of 120GHz was started in 1987. The gyrotron was designed for the oscillation of whispering gallery mode ($TE_{12,2}$, $TE_{9,3}$). The design parameters are listed in Table V.4.2-1. Figure V.4.2-1 shows the dependence of the output power and the efficiency on the collector current for $TE_{12,2}$ mode. The open and closed circles denote the output power and the efficiency,

Table V.4.2-1 The design parameters of 120 GHz, 500 kW gyrotron.

Mode	TE 12.2(-)
Power	500kW
Frequency	120.4 GHz
External Q	579
Efficiency	36%
Beam Voltage/Current	80 kV/17.4A
Pitch factor	1.5
Cavity radius	7.45mm
Beam radius/thickness	4.70mm/0.375mm
Beam divergence	5%
Cavity field	4.74T
Cavity wall loss	2.3 kW/cm^2

respectively. In the case of $TE_{12,2}$ mode, the output power (P_{out}) of 517kW was obtained. The efficiency increases gradually as the collector current increases and the maximum efficiency of 27.2% is obtained. On the other hand, $TE_{9,3}$ mode is obtained with a high power and a high efficiency. The maximum power is 610kW at V_b=75 kV, I_c=29.5A. The maximum efficiency is 36.1% at V_b=73 kV, I_c=20.5 A, then the output power is 540kW.

The study of a modified Vlasov converter from a whispering gallery mode to a Gaussian beam mode was developed in cooperation with Kyoto University because the oscillation mode of gyrotron has a high attenuation constant. The radiated beam profile of the modified Vlasov converter with a visor is shown in Fig.V.4.2-2. The main robe can be recognized as an almost Gaussian profile. The gyrotron which has a modified Vlasov converter in itself will be developed in the next stage.

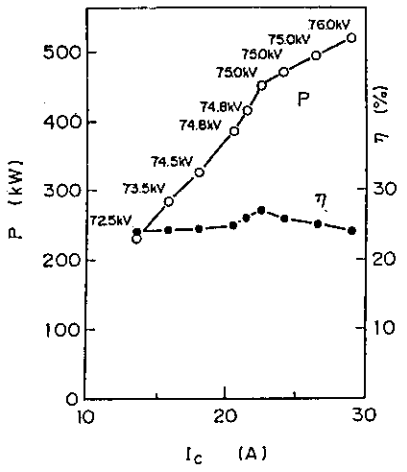

Fig.V.4.2-1 Experimental results of P_{out} and the efficiency η v.s. I_c (collector current) in the case of $TE_{12,2}$ mode.

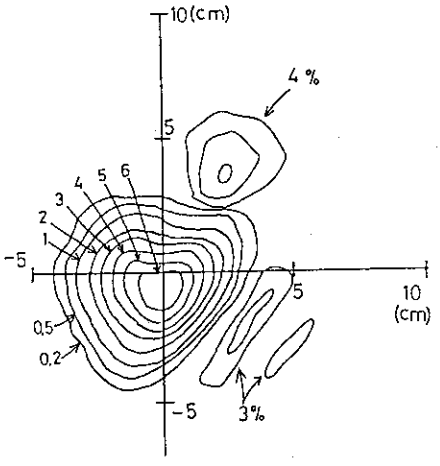

Fig.V.4.2-2 The contour of radiation power from the modified Vlasov convertor. (linear scale).

4.3 FEL research

For a FEL research, an induction linac was constructed in 1989. The operating parameters are a beam energy of 1MeV, a beam current of 3kA, a pulse width of 100 ns and a pulse repetition rate of 1Hz. Using the linac, a millimeter wave FEL was constructed. The wiggler parameters are a wiggler pitch of 4~5cm, a number of pitch of 30 and a total length of 1.5m. The surface of each wiggler magnet piece is curved so that it satisfies so called the focusing wiggler condition[4.3-1]. Figure V.4.3-1 shows the schematic view of the focusing wiggler.

At present, super radiant mode experiments are being done. Figure V.4.3-2 shows the typical waveform of the super radiation from the FEL The wavelength of the super radiation varies by changing the magnetic field strength of the wiggler.

The amplification mode experiment at 60 GHz will start in the mid-summer of this year.

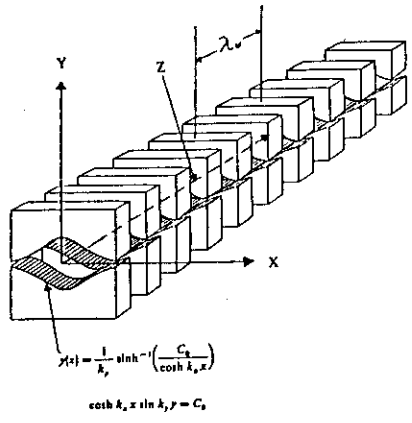

Fig.V.4.3-1 Focusing wiggler.

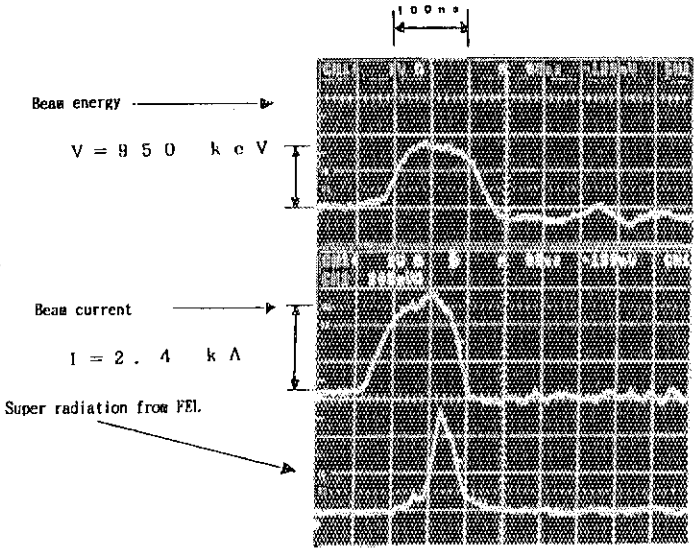

Fig.V.4.3-2 Waveform of the super radiation from the FEL.

References

[4.3-1] Shiho M. et al. :Proc. of 2nd Int. Symp. on Advanced Nucl. Energ. Res. Jan. 1990, Mito, Japan, p.476-481.

5. Tritium Technology

5.1 Development of tritium processing technology in TPL

5.1.1 Fuel cleanup

The gram-level tritium experiments of the fuel cleanup system (FCU) were carried out. One was performed in July to examine the improvement of the system stability after the modification of cold traps and flow/pressure controller. As shown in Fig.V.5.1-1, the system stability improved so that good performance in the palladium diffuser was observed in spite of the large fluctuation of the inlet hydrogen isotopes concentration. More than 99 % of hydrogen isotopes in the inlet flow permeated through the palladium membrane tubes in this diffuser. Thus, the hydrogen isotopes was separated successfully from the simulated plasma exhaust including nitrogen and methane as the impurity.

The other was also performed successfully in December. In this run, the conversion performance of tritiated water vapor in the electrolysis cell was investigated changing the oxygen concentration in its inlet flow that was the cold trap regeneration carrier gas. The use of oxygen-free nitrogen from outside cylinder much improved in the above performance in comparison with the use of system exhaust that included 1-2 % of oxygen, though total tritium-free exhaust from the system increased. In this run, a few percent of moisture as the plasma exhaust impurity was continuously supplied to the system but the total performance of this system did not change comparing to that of the last run.

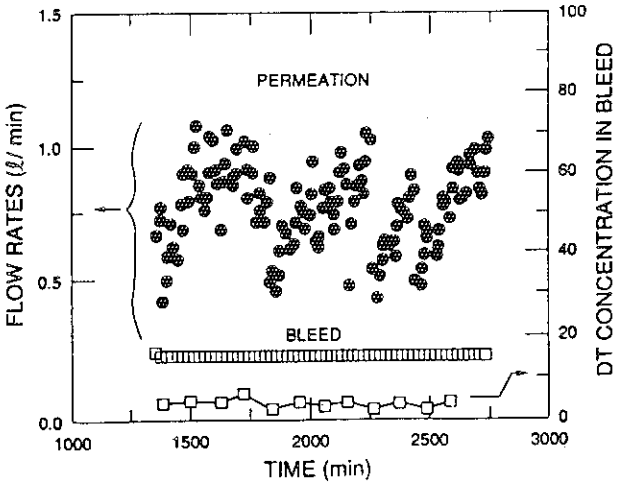

Fig.V.5.1-1 Flow rates of pure DT permeated through the membrane, bleed and the DT concentration in the bleed stream

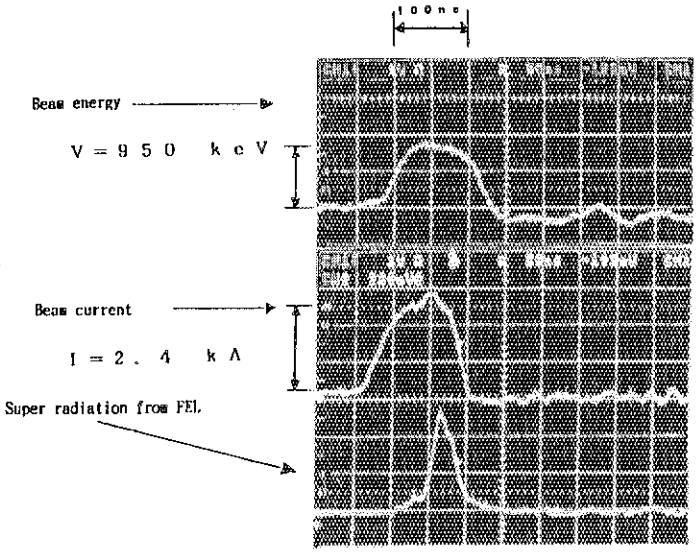

Fig.V.4.3-2 Waveform of the super radiation from the FEL.

References

[4.3-1] Shiho M. et al. :Proc. of 2nd Int. Symp. on Advanced Nucl. Energ. Res. Jan. 1990, Mito, Japan, p.476~481.

5. Tritium Technology

5.1 Development of tritium processing technology in TPL

5.1.1 Fuel cleanup

The gram-level tritium experiments of the fuel cleanup system (FCU) were carried out. One was performed in July to examine the improvement of the system stability after the modification of cold traps and flow/pressure controller. As shown in Fig.V.5.1-1, the system stability improved so that good performance in the palladium diffuser was observed in spite of the large fluctuation of the inlet hydrogen isotopes concentration. More than 99 % of hydrogen isotopes in the inlet flow permeated through the palladium membrane tubes in this diffuser. Thus, the hydrogen isotopes was separated successfully from the simulated plasma exhaust including nitrogen and methane as the impurity.

The other was also performed successfully in December. In this run, the conversion performance of tritiated water vapor in the electrolysis cell was investigated changing the oxygen concentration in its inlet flow that was the cold trap regeneration carrier gas. The use of oxygen-free nitrogen from outside cylinder much improved in the above performance in comparison with the use of system exhaust that included 1-2 % of oxygen, though total tritium-free exhaust from the system increased. In this run, a few percent of moisture as the plasma exhaust impurity was continuously supplied to the system but the total performance of this system did not change comparing to that of the last run.

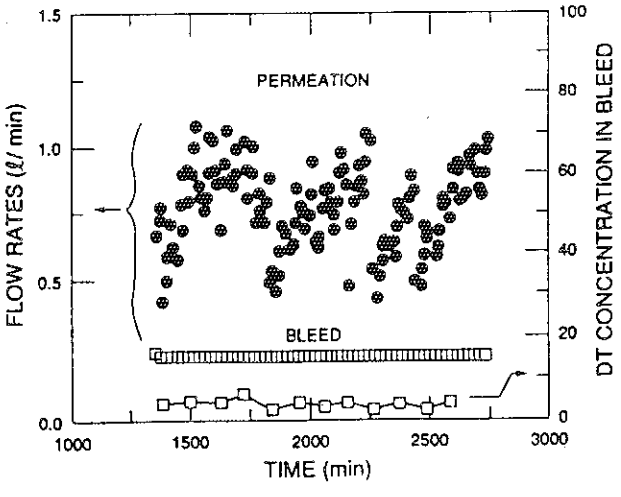

Fig.V.5.1-1 Flow rates of pure DT permeated through the membrane, bleed and the DT concentration in the bleed stream

5.1.2 Hydrogen isotope separation

The first experiment using tritium for hydrogen isotope separation by cryogenic distillation was successfully performed after a series of H-D experiments. For the cryogenic distillation columns which are used in the fusion fuel cycle system, the HETP (Height Equivalent to a Theoretical Plate) is one of the significant design parameters. Factors which are expected to have influence on the HETP are as follows; vapor and liquid velocities within the columns, feed flow rates, packing materials, sizes of packings, and dimensions of the columns. In the present study, the HETP values were measured with H-D-T system (1.5 g of tritium) as function of the vapor velocities, reflux ratios, and feed rates.

Figure V.5.1-2 shows a flow diagram of the experimental apparatus. The apparatus consists of two distillation columns differing in dimensions, adsorption beds removing impurities, equilibrators, circulation pumps, tritium supply and recovery metal beds, a helium refrigerator, and an analysis system composed of gas chromatographes. For both the columns, packed height are 50 cm. The inner diameter and the packing material for one of the columns are 2 cm and 3 mm Dixon Ring, respectively. The other column with 1 cm diameter is packed with 1.5 mm Dixon Ring. The distillation experiments were performed under total reflux and total recycle modes. The HETP was evaluated by comparing compositions of products streams experimentally observed with those for calculated results. An example of the above-mentioned comparison is shown in Table V.5.1-1. The experimental observations were in close agreement with calculation results for trace components(HT,DT and T_2) as well as dominant components(H_2, HD, D_2): The HETP was

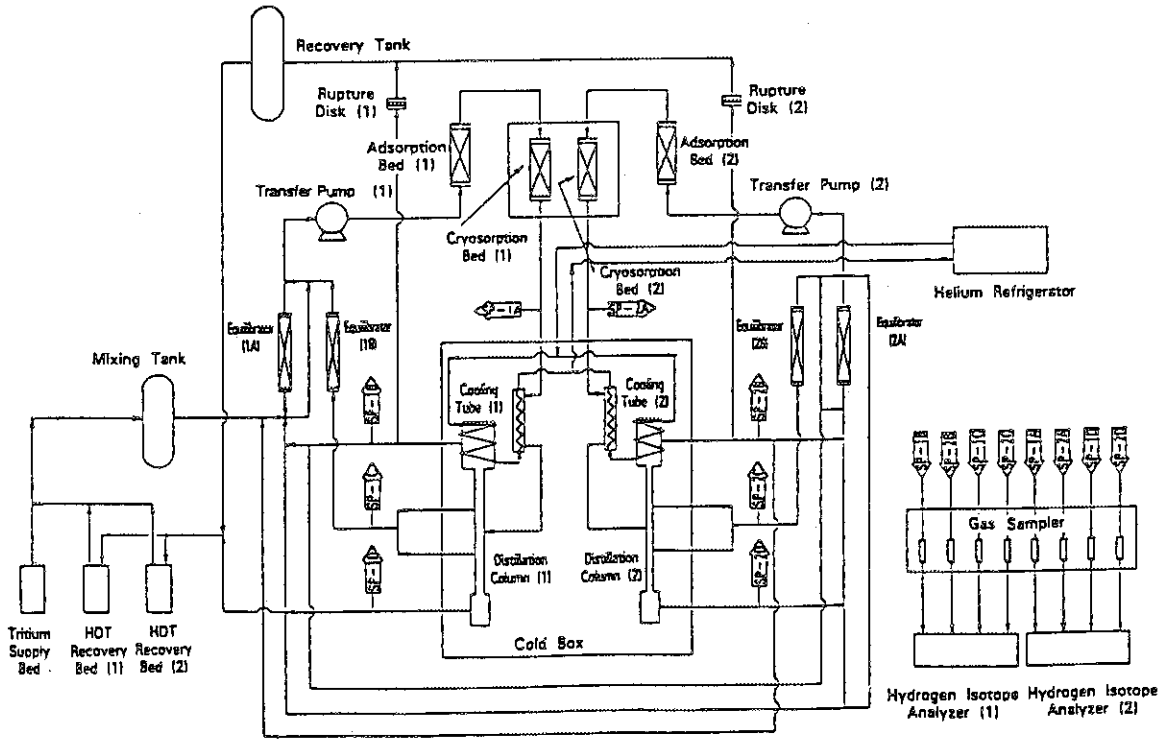

Fig.V.5.1-2 Flow diagram of experimental apparatus

Table V.5.1-1 Comparison between calculated and experimentally observed value

	Experiment	Calculation	Experiment	Calculation
	Top composition (mol fraction)		Bottom composition (mol fraction)	
H_2	7.43E-1	7.43E-1	5.80E-3	6.01E-3
HD	2.56E-1	2.55E-1	6.45E-1	6.52E-1
HT	9.00E-4	8.08E-4	2.58E-2	2.64E-2
D_2	---------	1.23E-3	3.15E-1	3.07E-1
DT	---------	5.47E-6	7.80E-3	7.77E-3
T_2	---------	5.97E-8	5.00E-4	5.00E-4

Flow rate of top stream = 22.5 mol/h
Flow rate of bottom stream = 3.45 mol/h
Vapor flow rate within column = 70.6 mol/h
Number of total theoretical stages = 15
Feed stage number = 7
Pressure = 577 torr
Inner diameter of column = 2 cm
Packed height = 50 cm
Packing species = Dixon Ring (3 mm)
HETP = 3.8 cm

constant regardless of molecular species or their concentrations. The effect of the vapor velocity on the HETP was examined under the total reflux mode. The measured values were 4-5 cm for both the columns, and no apparent dependence on the vapor velocity was observed. Figure V.5.1-3 shows the HETP values measured under a variety of reflux ratios. As common results for the two columns, the HETP values, which were 3-5 cm, decreased with increasing the reflux ratios. The feed flow rate also had influence on the HETP. Especially for the smaller column, the HETP defined for the upper half of the column appreciably differed from that for lower half because of existence of the feed stream. Thus, the major factors affecting the HETP were the phase flow rates (the vapor and liquid velocities within the columns) and the feed flow rates. Consequently, we could correlate the HETP with the feed flow rates and phase flow rates.

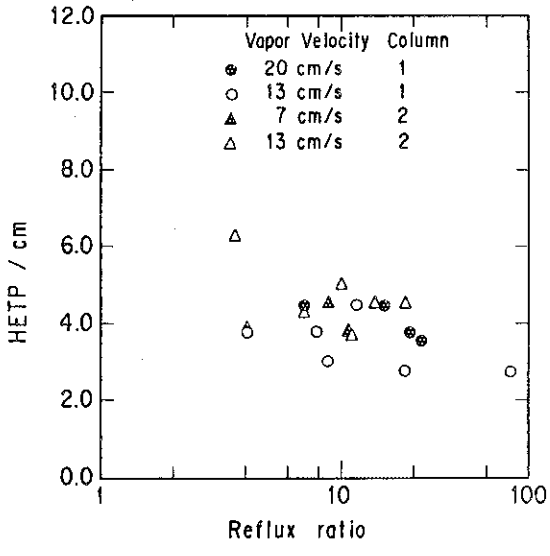

Fig.V.5.1-3 Effect of reflux ratio on HETP

5.1.3 Tritium analysis and measurement

To study capability of ionization chambers for in-line tritium gas measurements in fusion fuel gas processing systems, three ionization chambers with small volumes (0.16, 21.6, and 100 cm^3) were tested using high concentration tritium gas. Optimum electric fields for various back-filled gases in each ionization chamber such as H_2, D_2, He, N_2, and Ne were determined to be in ranging from 100 to 200 V/cm from a plateau region in the curve of applied voltage vs ionization current. The detection efficiencies were observed to be dependent on the ionization abilities of the back-filled gases, and moreover on their stopping powers which are closely correlated with the Z-values. Because, when the range of beta-ray was shortened by its collision with higher Z-value atom,possibility of energy loss decreased. Although loss of ions by recombination is expected to increase in extremely high tritium concentration, it was prevented using a small ionization chamber. For example, linearity between ionization current and concentration of tritium up to 40% was

observed in the ionization chamber with 0.16 cm^3. As shown in Fig.V.5.1-4, memory effect was observed after measurements of high concentrated tritium gases. Less memory effect was observed in smaller ionization chamber, but the 100 cm^3 chamber could not be used anymore due to the memory effect.

Development of in-line analysis by Raman spectroscopy for fusion fuel processing systems has been continued. To accumulate basic data for analysis of various gases expected in plasma exhaust gas, Raman spectra of various deuterided methanes were measured.

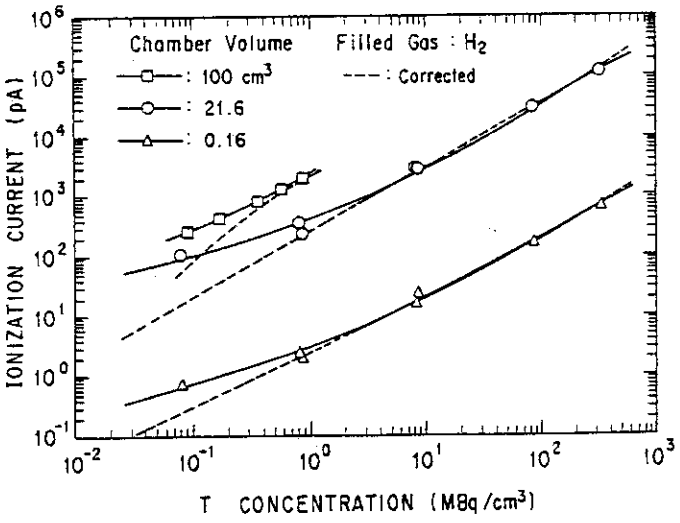

Fig.V.5.1-4 Relation of tritium concentration vs ionization current. Dashed lines express those of subtracting the memory current from the actually measured current.

5.1.4 Tritium-material interaction

Implantation-driven permeation of tritium into first wall coolants could be a serious problem from a viewpoint of tritium safety in D-T fusion reactors. To estimate tritium permeation fluxes through candidates of constructional materials of first walls, we have accumulated experimental data using an apparatus to produce hydrogen isotope ion beams in the energy range from 100 eV to about 2 keV. In this fiscal year, we paid our attention to investigation of permeation behavior of deuterium implanted with low energy into 304SS. We measured dependencies of incident ion energy, incident ion fluxes, and sample temperatures on the permeation fluxes of deuterium implanted into 304 SS (diameter: 25 mm, thickness: 0.1 mm). Figure V.5.1-5 shows the incident energy dependency of the deuterium permeation fluxes. It can be seen from the figure that the permeation fluxes depended significantly on the D^+ ion energy in the range from 100 through 1000 eV, While those above 1000 eV little depended on the energy. The permeation rates decreased with increasing the ion energy up to 1000 eV. In the conditions of the sample temperature of 780 K and the incident ion flux on 2.5 x 10^{14} D^+/cm^2s, the permeation rate at 100 eV (1.4 x 10^{13} D/cm^2s) was about 30 times bigger than that at 1000 eV (5 x 10^{11} D/cm^2s). The temperature dependency of the permeation fluxes were also measured in the tempera-

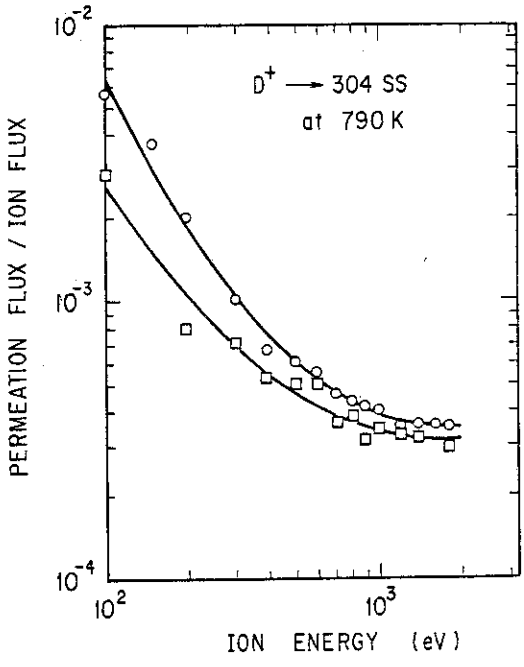

Fig.V.5.1-5 Energy dependency of permeation flux of deuterium implanted into 304SS

ture range from 600 to 870 K. The activation energy for permeation process seemed to have tendency to decrease with increasing the incident ion energy. Those experimental results suggest that energy distribution of tritium implanted in the first wall should be considered as one of important factors in estimation of the tritium permeation into the first wall coolants.

5.2 Development of fuel processing technology under JAERI-LANL(DOE) collaboration

The research program under "Annex III to the Implementing Arrangement between JAERI and United States Department of Energy on Cooperation in Fusion Research and Development for the DOE-JAERI Collaborative Program in Development of Improved Components for the Fuel Cleanup System of the Tritium Systems Test Assembly (TSTA)" that had been extended for one year was concluded in November 1989. The experimental program on the "process ready components" under this program was completed and all of the objectives were achieved experimentally in the tests performed for these three years.

It is concluded that the palladium diffuser is applicable to the processing of plasma exhaust to produce pure hydrogen isotopes for as long as 3 years without any maintenance. The ceramic electrolysis cell was verified as an attractive component for the decomposition of tritiated water in various process. Carbon dioxide affected it little. Both components were proved to be suitable for fusion fuel processing application for years of services.

Based on the results, an integrated process loop, "JAERI Fuel Cleanup System (JFCU)" that utilizes both components was developed and designed by JAERI for full scale demonstration of the plasma exhaust reprocessing.

Joint operation of TSTA at Los Alamos National Laboratory (LANL) under Annex IV has been continued in the third year of the collaboration. The operation of the integrated loop including the Fuel Cleanup, Impurity Simulation and Isotope Separation for a continuous period of 19 days was performed in April-May 1989. This is a major accomplishment of the demonstration of the operation of DT fuel process. Approximately 120 g of tritium was used. Impurities, 0.9% nitrogen and 0.09% methane plus varying concentration of hydrogen and helium were continuously added to the loop and removed. The ISS experiment was performed to verify the separation of helium ash from the plasma exhaust using the cryogenic distillation columns.

Intensive investigation of the tritium accountability and inventory control in the loop has been performed in order to understand the deviation on the measured amount of tritium in the loop uncovered in this fiscal year and identified as important in fusion fuel technology. Considerable progress has been made towards resolving this problem.

The JAERI Fuel Cleanup System (JFCU) is a full-scale plasma exhaust processing device developed and designed by JAERI. Major components such as palladium diffuser, ceramic electrolysis cell and Zirconium-cobalt beds have been tested with tritium at TSTA under previous cooperative programs. The fabrication and check-out finished in September 1989 in Japan and the apparatus was shipped to Los Alamos. Installation was conducted from January to March 1990 and an initial test for acceptance followed. Mixture of D_2, He, CH_4 and NH_3 was continuously

supplied to the system and the function to produce pure deuterium stream and recover hydrogen isotopes from the impurity was tested successfully. This is a major accomplishment of this year.

Some off-loop experiments were carried out with tritium in this period. Studies of the $LaNi_3Mn_2$-H,D and T systems, test of the hydrogenating-dehydrogenating cycles and measurement of ZrCo-T equilibrium pressure were performed. Experimental apparatus for the Raman spectroscopy for fusion fuel application was installed.

5.3 Development of tritium safe handling technology

5.3.1 Backing vacuum pump and compressor

A large oil-free reciprocating vacuum pump have been developed for high level tritium service. The pump is composed of 4-stage tandem type pistons with piston rings made of carbon-polyimide composite and vertical cylinders. Metallic dynamic bellows are used for shaft seal. In process gas side, no oil and elastomer are used so that possible problem by radiation damage and contamination is minimized. Performance tests have been conducted with H_2, D_2, He, and N_2 at discharge pressure ranging from 500 to 875 Torr. Figure V.5.3-1 shows pumping characteristics for these gases. As shown in this figure, pumping speeds for these gases were almost constant at the suction pressures higher than 10 torr, while they drop drastically in lower pressure region. The compressor which has a similar structure to the large oil-free reciprocating vacuum pump was installed in the Effluent tritium Removal System. Performance and tritium test have been conducted.

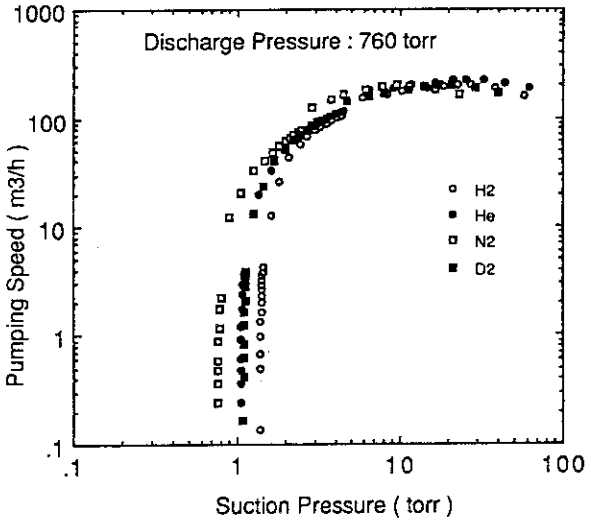

Fig.V.5.3-1 Pumping speed of oil-free reciprocating vacuum pump

5.3.2 Operation of tritium safety systems

The safety system which composed of Glovebox gas Purification System(GPS), Effluent tritium Removal System(ERS), Air Cleanup System(ACS), Dryer Regeneration System(DRS) etc., for sake of tritium safe handling in TPL were fully in tritium service in this period. Table V.5.3-1 shows operational results of main safety systems. The safety system has treated about 400 Ci of tritium and the tritium release to environment through the stack was controlled less than 0.26 Ci in this period.

Table V.5.3-1 Operation of main safety systems (in FY1989)

System		GPS		ERS	ACS
Operation Mode		Tritium Removal (m^3) / (h)	Pressure Control (h)	Tritium Removal (m^3)	Tritium Removal (m^3)
1989.	4	$3.6x10^4$/ 466	712	140	2,300
	5	$6.4x10^4$/ 736	743	270	310
	6	$6.2x10^4$/ 701	720	180	1,200
	7	$7.3x10^4$/ 735	744	320	1,660
	8	$6.5x10^4$/ 682	716	330	5,500
	9	$6.4x10^4$/ 664	670	150	11,000
	10	$6.5x10^4$/ 704	712	170	1,290
	11	$6.8x10^4$/ 690	720	160	1,800
	12	$6.8x10^4$/ 735	743	120	540
1990.	1	$7.6x10^4$/ 738	744	100	170
	2	$7.8x10^4$/ 668	672	90	610
	3	$9.8x10^4$/ 739	741	61	150
Total		$8.2x10^5$/8,255	8,637	2,091	26,530

5.4 Development of blanket technology

5.4.1 Design works

For the purpose of the development of the blanket technology, conceptual design works were carried out on both of Blanket In-pile Testing facility and Blanket Out-pile Testing facility.

The in-pile facility is intended to be constructed in the Japan Material Testing Reactor (JMTR). The main purpose of the facility is the in-situ test of tritium recovery and heat transfer in kilogram scale solid breeder blanket. Thus, the conceptual design work has been performed under the collaboration with the Department of Japan Material Testing Reactor Project.

The out-pile facility is intended to include the mock-up testing apparatus, the beryllium (which is the indispensable neutron multiplier) safe handling system and the basic engineering unit testing apparatus. The conceptual design work for the out-pile facility has been performed with the aids of the Department of Fuels and Materials Research, the Department of Reactor Engineering and the Department of Chemistry.

5.4.2 Experimental works

Experimental works for the development of the blanket technology included the compatibility among breeder materials, neutron multiplier and structural materials. Also, research and development were initiated to confirm the mass-producing technology of spherical particles of lithium ceramics and beryllium.

As for the first step of the R & D for the alternative blanket technology, reference review was carried out about the aqueous lithium solution blanket and the liquid lithium-lead blanket. According to the discussion on the R & D item of the alternative blanket technology, a LiPb Test Loop was designed, constructed and installed for the purpose of the experimental study on the recovery of hydrogen isotopes from the liquid metal breeder (LiPb) and the compatibility of the structural materials. The overview of the loop is shown in Fig.V.5.4-1. The basic operation characteristics will be tested next year.

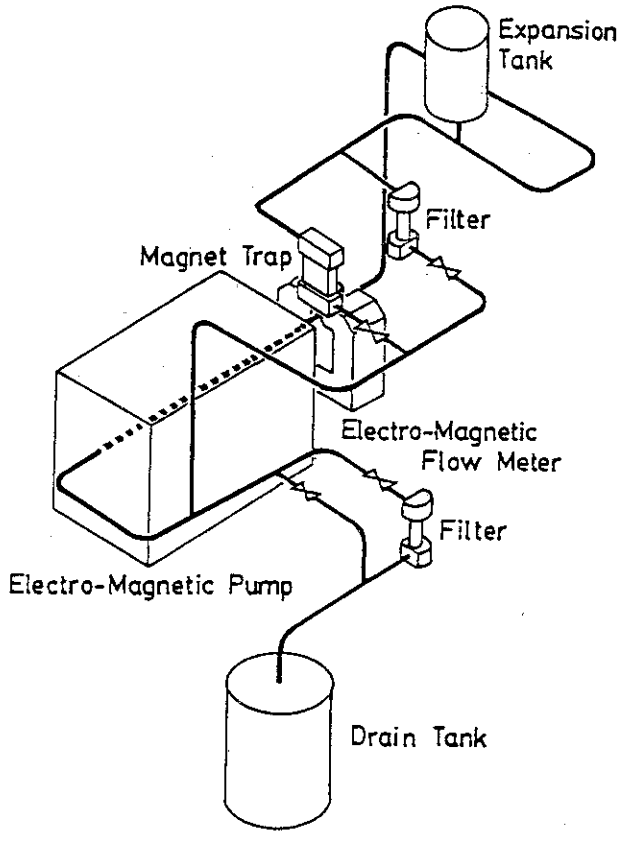

Fig.V.5.4-1 Illustrated overview of LiPb test loop at TPL (JAERI)

5.5 System analysis

5.5.1 Design works for fusion experimental reactors

Conceptual design works of tritium handling facilities for the Fusion Experimental Reactor (FER) and the International Thermonuclear Experimental Reactor(ITER) were carried out incorporated in the Fusion Experimental Reactor Design Team. The tritium handling facilities included the main vacuum system, the fuel circulation system, the plasma heating system, the building and safety system and the solid and liquid waste treatment systems, as well as the tritium recovery system for the driver blanket and the test module of the breeding blanket for ITER. The conceptual design works concerned the specification, the operation manuals, the maintenance and the accident scenario of each facility. Also, Japanese proposal and the status of the R&D of the fuel supply system and the exhaust gas pumping system for the ITER were presented in the specialist meetings of the ITER in Garching, West Germany. The Japanese proposal of the fuel circulation system included a new ISS scheme which was designed to produce 60% T_2 + 40% D_2, 70% T_2 + 30% D_2, 80% T_2 + 20% D_2 and 90% T_2 + 10% D_2.

5.5.2 Development of components for the FER

The research and discussion on the waste treatment method was carried out for graphite of the first wall armour material. And the SF_6 condensation panel cryo-compound pump and the large scale (25000 l/s) magnetic bearing type turbo molecular pump were picked up to be developed for the use of the main vacuum system.

The SF_6 condensation panel cryo compound pump was installed at the Plasma Heating Laboratory I in Naka site under the collaboration and has been operated to perform preliminary helium pumping experiments which will be followed by the pumping experiments with helium and hydrogen isotopes (H_2 and D_2). Also, SF_6 is expected to be used as the gaseous isolation material in the FER, however, its decomposability under irradiation condition was unknown characteristics. Thus, we carried out the decomposition experiments of SF_6 with gamma ray of ^{60}Co and certified the stability and decomposition products under 10^7 - 10^8 R of gamma ray irradiation.

As for the development of the turbo-molecular pump, the test rotor with the magnetic bearing and the touch-down bearing was manufactured and tested to demonstrate its mechanical performance.

6. High Heat Flux Technology

6.1 Introduction

The development of the plasma facing components is essential to realize the FER and ITER. Therefore, we have been performing the experimental and analytical studies on plasma facing components. Two test facilities are available for high heat flux experiments at JAERI. One is a hydrogen ion beam irradiation test stand called PBEF (Particle Beam Engineering Facility) and the other is an electron beam irradiation test stand called JEBIS (JAERI Electron Beam Irradiation Stand). The JEBIS has enabled us to carry out experiments that simulate disruption conditions for

the first time in the world. Figure V.6.1-1 shows schematic views of JEBIS and PBEF. The major performances of JEBIS and PBEF are shown in Table V.6.1-1.

6.2 The electron beam characteristics of JEBIS

The JEBIS was constructed as a high heat flux test facility to promote R&D's on plasma facing components and materials. The JEBIS has a plasma electron gun as a heat source, and can deliver high heat fluxes of more than 2500 MW/m^2 with a duration ranging from 1 ms to CW. Therefore, the JEBIS can be used not only for steady - state heat load experiments but also for thermal shock experiments simulating plasma disruption conditions. To determine the electron beam characteristics of the JEBIS, electron beam profiles were measured using a calorimeter made of copper. Figure V.6.2-1 shows an example of the beam profiles at a beam current of 2 A with an acceleration voltage of 50 kV. The peak heat flux of the stationary beam reaches 360 MW/m^2 with a full width at half maximum (FWHM) of about 12 mm. A flat distribution of the heat flux is obtained by beam sweeping at a frequency of 1 kHz. The beam shape can be easily altered from a pencil beam to a sheet beam by changing the acceleration grid.

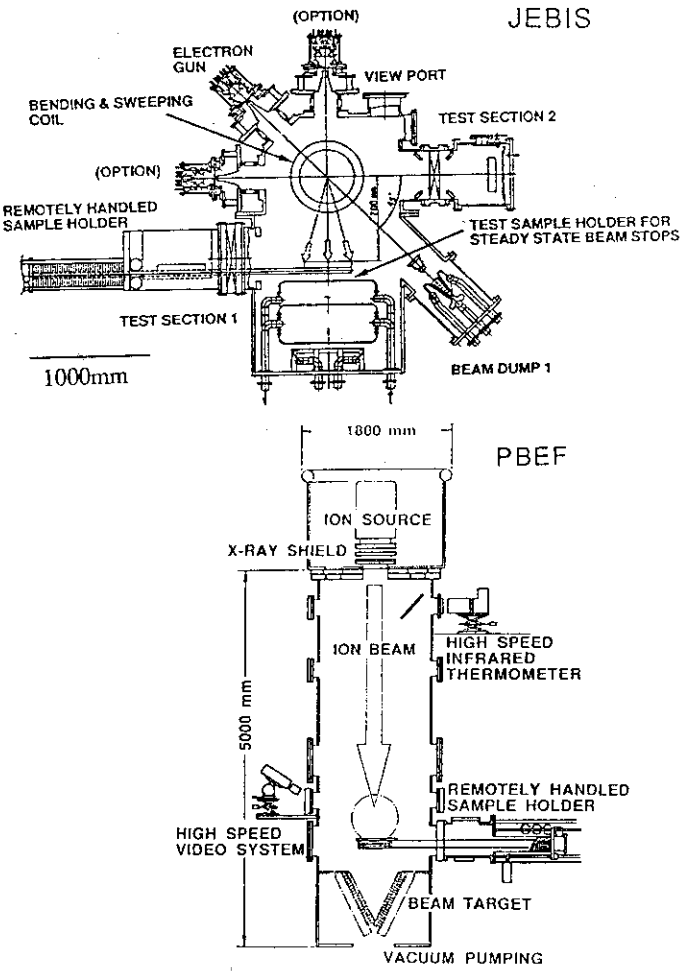

Fig.V.6.1-1 Scematic views of the JEBIS and PBEF

Table V.6.1-1 Major performances of the JEBIS and PBEF

	JEBIS	PBEF
Acceleration Voltage	20 - 100 kV	30 - 100 kV
Acceleration Current	up to 4 A	up to 50 A
Pulse Duration	0.001 - CW	0.01 - 10 s
Working Gas	H_2	H_2
Beam Species	Electron	Hydrogen
Type of Ion/Electron Source	Magnetic Multi-pole Ion Source	
Sweeping Coil	0.01- 1 kHz in one dim.	None
Maximum Heat Flux (MW/m2)	> 2000	> 260
Maximum Heating Area	30cm x 60 cm	10cm x 20cm
Water Cooling System	40m^3/hr with 4 MPa	60m^3/hr with 2 MPa
Pressure in the Test Bed	0.05 Pa	< 0.053 Pa

6.3 R&D's on plasma facing materials and components

6.3.1 Thermal shock tests of CFC composites and graphite materials

Carbon fiber reinforced carbon (CFC) composites and graphite materials have been selected as primary candidates for the armor material of plasma facing components in FER/ITER because of their low atomic number, high evaporation temperature and high thermal conductivity. To evaluate their characteristics under intense thermal shocks during a plasma disruption, we have performed tests under disruption-simulation conditions on various CFC composites and graphite materials in

the JEBIS and PBEF. Specimens made of CX-2002U (felt type CFC), MCI-1 (felt type CFC), pyrolytic graphite (anisotropic graphite) and IG-430U(ultra fine grain graphite) are used in this experiment.

Major dimensions of the specimens are 30 mm x 30 mm and the heated area is about 60 mm^2. A maximum heat flux of 1800 MW/m^2 is imposed on the test surface in the JEBIS. Figure V.6.3-1 shows the weight loss of IG-430U as a function of absorbed energy. The weight loss reaches 25 mg at a heat flux of 1800 MW/m^2 with a duration of 5 ms. As results of this experiment, the weight loss strongly depends on the absorbed energy. Furthermore, at a constant energy density, the higher the heat flux, the more the weight loss. The comparison of the erosion depth for IG-430U and CX-2002U (CFC) is shown in Fig.V.6.3-2. After the test, the heated surface of CX-2002U became rough because carbon fibers were selectively eroded from the surface.

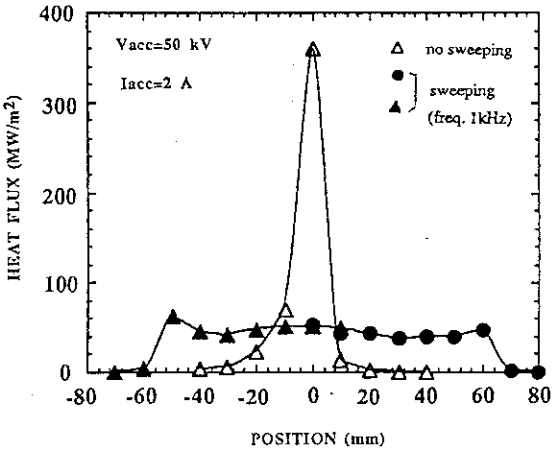

Fig.V.6.2-1 Beam profiles of the JEBIS

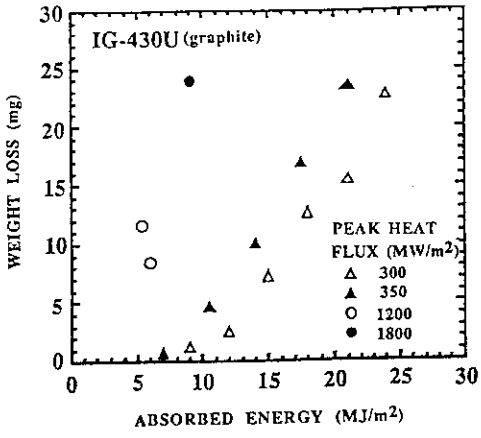

Fig.V.6.3-1 Absorbed energy dependence of weight loss of IG-430U

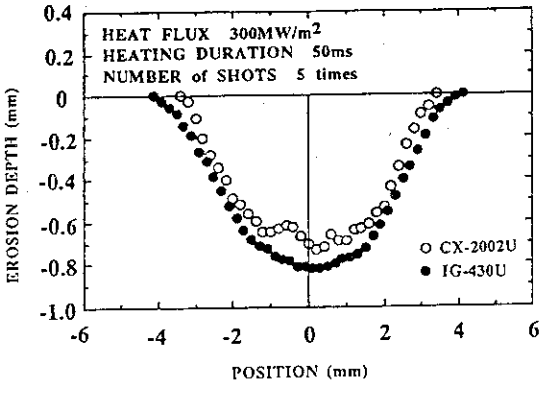

Fig.V.6.3-2 Comparison of erosion depth of CX-2002U and IG-430U

6.3.2 Thermal cycling tests of a simulated divertor plate

The plasma facing materials and components are exposed to high heat load from the plasma. Tungsten is one of the most promising materials for plasma facing components, since it has a high melting temperature and low sputtering yield. Therefore, we have performed thermal cycling tests on simulated divertor plates composed of tungsten-copper bonds (W/Cu bonds), and have evaluated the durability against thermal cycling. The specimen is composed of a tungsten plates of 25 mm(l) x 25 mm(w) x 5.5 mm(t) that are brazed on a copper heat sink with a cooling tube. The copper heat sink is cooled by water with a total flow rate of 35 l/min at an inlet pressure around 1 MPa. The array of specimens was repeatedly irradiated by hydrogen ion beam in the PBEF. A test condition with a peak heat flux of 30 MW/m^2 and duration of 1 s was selected so that the temperature of the bonding interface was heated to about 250 C at the end of the beam pulse. This temperature is equivalent to the value that is

expected at the steady state operation with a heat flux of 10 MW/m^2. Figure V.6.3-3 shows a typical bonding interface after 360 thermal cycles. Several cracks are observed in a tungsten side of the interface. The maximum temperature in the copper close to the interface gradually decreased with thermal cycles. This indicates that the thermal conductance at the interface decreased by crack initiation and propagation. Furthermore, some of the tungsten armor pieces were detached from the copper and melted. The result clearly shows that further improvement of bonding technology is required.

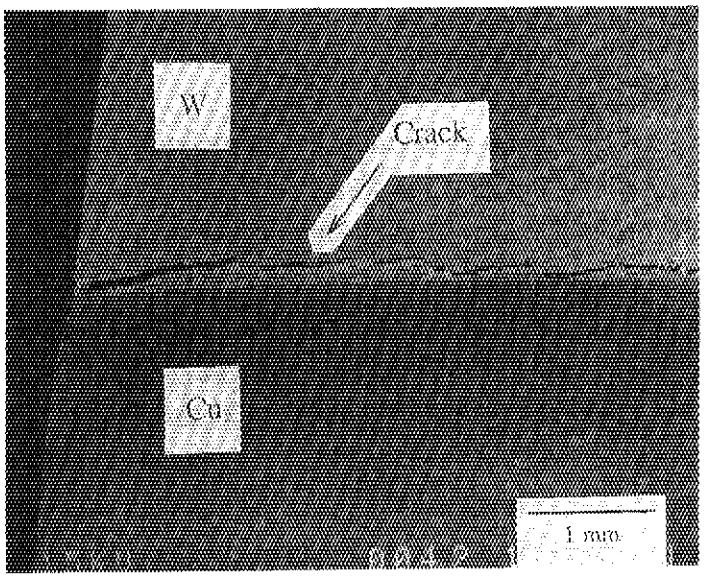

Fig.V.6.3-3 SEM photographs of W/Cu bonds near the interface

VI. NEXT STEP FOR JAERI TOKAMAK PROGRAM

1. Fusion Experimental Reactor (FER)

1.1 FER design

The Fusion Council of Japan recommended in the National Research and Development Program that the next step fusion device should have a mission of achieving a long ignited and controlled DT burn. In 1987, the design study of FER (Fusion Experimental Reactor) with the above mission was conducted. Since the joint work of the ITER began on May 1988, a new organization (Fusion Experimental Reactor Team) was established to support the ITER activities and also to design the FER. The FER, which is more compact than the ITER, had been defined as the engineering-oriented machine for demonstrating the engineering feasibility of a fusion reactor. The design guideline of the FER has been established in 1988. The next step tokamaks will provide sufficient physics information and technological experience to proceed to a DEMO fusion reactor which will demonstrate electric power generation by the fusion reactions:

1) The FER is to be the minimum-sized domestic machine which includes the highest technical reliability in its construction.

2) The ITER is to be the maximum-sized international tokamak machine with the maximum jump in the technology from the present level of achievement.

Particular efforts in selecting the plasma parameters have been made to realize the above mentioned mission with minimum device size. The plasma parameters listed in Table VI.1.1-1 enable us to obtain the following plasma performances. The fusion multiplication factor Q=5-10 is a basic plasma performance with the enhancement factor of 1.5-2.0 for both Shimomura-Odajima(SO) and Goldston(G) L-mode energy confinement scaling laws. The burn time more than 1000 sec is to be achieved by introducing a hybrid operation mode in which some fraction of the plasma current is driven inductively with significant assistance of non-inductive and bootstrap current. Demonstration of a steady state operation is one of the key issues for the DEMO reactor. A 0.5-1.0 MeV negative-ion-based injection system is used for both heating and current drive.

Table VI.1.1-1 FER major parameters

Plasma current	(MA)	15	-	20
Major radius	(m)	4.5	-	4.7
Manor radius	(m)	1.6	-	1.8
Elongation		1.6	-	2.0
Plasma volume	(m^3)	400	-	600
Field on axis	(T)	5.2	-	5.4
OH coil flux	(Vs)	160	-	170
Fusion power	(MW)	200	-	500
Burn time	(s)	100	-	1000
Heating/CD power	(MW)	80	-	1000

Through the conceptual design activity of the reactor structure, two major critical issues were identified as follows and some feasible solutions have been found.

1) Process & procedure of initial assembling

2) Supporting structure of in-vessel components

Two kinds of in-vessel maintenance systems for the replacement of the divertor plate have been designed. One is an articulated "boom" type and the other is a rail-mounted vehicle type. The boom type has fifteen joints with the total length of 28 m. When the divertor plate of 1000 kg is suspended at the tip of the boom, The maximum deflection is up to 58 mm. On the other hand, the

"vehicle" type consists of six rail modules of a circular arc, a rail deploying device, a vehicle with a manipulator and a rail supporting device.

Concerning the TF coil design, it was made clear that the stresses in the structural material satisfy the design criteria. As for the center solenoid coil design, the structural grading is required in order to satisfy the volt-seconds requirements. In order to verify the appropriateness of the design, it is indispensable to accumulate the fatigue test data of the stainless steel in conduits.

In the neutronics field, a new nuclear group constant set "FUSION-J3" has been developed on the basis of an evaluated nuclear data file "JENDL-3".

Preliminary design study for the plant system was conducted. The required capacities for electric power, cryogenic and heat removal were evaluated. Based on those evaluations, the outlines of the cooling system, cryogenic system, power plant, baking system and fueling system have been presented. The concept of the reactor building was constructed in consideration of each system designs. A heat ventilation system and an air conditioning system were also designed. Those works brought us to draw the plant layout shown in Fig.VI.1.1-1.

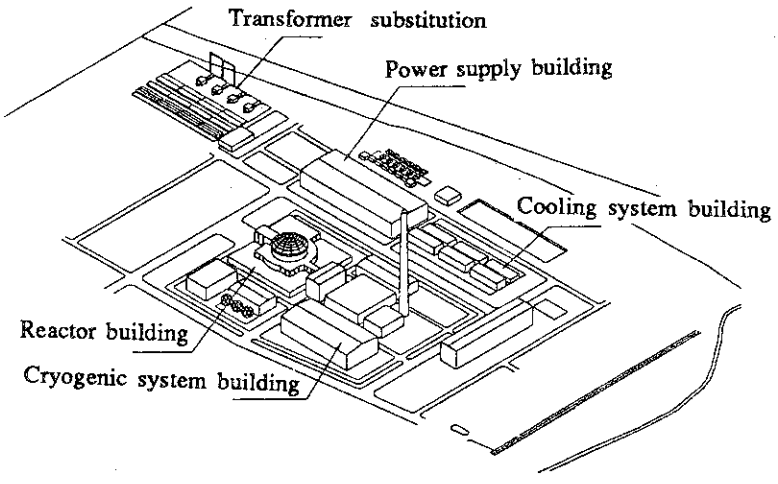

Fig.VI.1.1-1 FER plant layout

1.2 Technology R&D

A wide range of Research and Development(R&D) is inevitably required to bridge from the present technology to the realization of FER construction. Up to now, necessary items to be developed in various technology area and the R&D program have been discussed and well established to focus on the technological feasibility of the FER prior to the DEMO reactor. This program involves key technology development such as reactor structure, remote maintenance, superconducting magnet, plasma facing component, heating and current drive, fuel cycle, breeding blanket, diagnostics and plant systems. Based on this program, key component technologies are being developed by accumulating activities of hardware developing laboratories in JAERI under a good collaboration with industries. The recent progress obtained in the reactor structure and remote maintenance is described below.

In the reactor structure area, locking structure of in-vessel components is one of critical issues, since the locking structure has to be designed to have sufficient mechanical rigidity for supporting the large electromagnetic forces due to plasma disruption under high nuclear heating condition. In addition, easy assembling/reassembling feature is required from the remote maintenance point of view. In order to meet these requirements, a special locking structure with

movable part such as thin flexible tubes or bellows driven by hydraulic pressure is proposed. The trial fabrication of key elements and the basic performance tests are being conducted.

In the remote maintenance area, there are two basic scheme which are in-vessel maintenance and ex-vessel maintenance. The in-vessel maintenance provides quick repair or replacement of plasma facing components such as armor tiles and divertor plates by using remote handling equipment from inside the plasma vacuum vessel. On the other hand, the ex-vessel maintenance is remotely performed from the outside of cryostat as a backup of the in-vessel maintenance. Two kinds of in-vessel maintenance systems, which are articulated boom type and rail-mounted vehicle type, are being considered. As the first step, a 1/5-scaled vehicle system was fabricated and the basic tests of rail mounting and divertor plate replacement are being conducted.

2. International Thermonuclear Experimental Reactor (ITER)

The primary purpose of the International Thermonuclear Experimental Reactor(ITER) is to develop an experimental fusion reactor through the united efforts of many technologically advanced countries. With its origins in the "summit" level discussions, the ITER is now proceeding under the auspices of the International Atomic Energy Agency according to the terms of a quadripartite agreement reached among the European Community, Japan, the United States and the Soviet Union. The ITER will demonstrate plasma ignition and extended burn, with steady-state operation as an ultimate goal. In so doing, it will provide the physics data base needed for a demonstration tokamak power reactor, demonstrate many of the reactor technologies needed for fusion power, and act as a test bed for high heat flux and nuclear components.

The present "Conceptual Design Phase" of the ITER extends until the end of 1990. The global expenditure on the ITER at present is estimated to be equivalent to about 200 million dollars for the design and ITER-related R&D.

2.1 ITER conceptual design

The basic concept of the ITER is "robust" in the sense that it is based upon a reasonably conservative assessment of our present knowledge of plasma physics and because it allows for appreciable operational and experimental flexibility.

Although the final design is the result of many complex technical compromises and adjustments, many of the main machine characteristics and parameters are rather easily traced to the technical objectives of the program. The goal of achieving extended burn (ultimately steady-state) dictates the use of superconducting coil systems. The requirement for ignition sets the plasma current. The design targets for both the first wall flux and fluence dictate approximately the same minimum shield thickness in the device. When these are combined with considerations of plasma stability, impurity control and current drive, the general features and approximate size of the reactor are determined. Nevertheless, within the freedom allowed by the objectives, the design philosophy has been to control size and minimize cost.

The overall layout of the ITER and its parameters are given in Fig. VI.2.1-1 and Table VI.2.1-1. The nominal fusion power generated in the reactor is approximately one giga watt. The

movable part such as thin flexible tubes or bellows driven by hydraulic pressure is proposed. The trial fabrication of key elements and the basic performance tests are being conducted.

In the remote maintenance area, there are two basic scheme which are in-vessel maintenance and ex-vessel maintenance. The in-vessel maintenance provides quick repair or replacement of plasma facing components such as armor tiles and divertor plates by using remote handling equipment from inside the plasma vacuum vessel. On the other hand, the ex-vessel maintenance is remotely performed from the outside of cryostat as a backup of the in-vessel maintenance. Two kinds of in-vessel maintenance systems, which are articulated boom type and rail-mounted vehicle type, are being considered. As the first step, a 1/5-scaled vehicle system was fabricated and the basic tests of rail mounting and divertor plate replacement are being conducted.

2. International Thermonuclear Experimental Reactor (ITER)

The primary purpose of the International Thermonuclear Experimental Reactor(ITER) is to develop an experimental fusion reactor through the united efforts of many technologically advanced countries. With its origins in the "summit" level discussions, the ITER is now proceeding under the auspices of the International Atomic Energy Agency according to the terms of a quadripartite agreement reached among the European Community, Japan, the United States and the Soviet Union. The ITER will demonstrate plasma ignition and extended burn, with steady-state operation as an ultimate goal. In so doing, it will provide the physics data base needed for a demonstration tokamak power reactor, demonstrate many of the reactor technologies needed for fusion power, and act as a test bed for high heat flux and nuclear components.

The present "Conceptual Design Phase" of the ITER extends until the end of 1990. The global expenditure on the ITER at present is estimated to be equivalent to about 200 million dollars for the design and ITER-related R&D.

2.1 ITER conceptual design

The basic concept of the ITER is "robust" in the sense that it is based upon a reasonably conservative assessment of our present knowledge of plasma physics and because it allows for appreciable operational and experimental flexibility.

Although the final design is the result of many complex technical compromises and adjustments, many of the main machine characteristics and parameters are rather easily traced to the technical objectives of the program. The goal of achieving extended burn (ultimately steady-state) dictates the use of superconducting coil systems. The requirement for ignition sets the plasma current. The design targets for both the first wall flux and fluence dictate approximately the same minimum shield thickness in the device. When these are combined with considerations of plasma stability, impurity control and current drive, the general features and approximate size of the reactor are determined. Nevertheless, within the freedom allowed by the objectives, the design philosophy has been to control size and minimize cost.

The overall layout of the ITER and its parameters are given in Fig. VI.2.1-1 and Table VI.2.1-1. The nominal fusion power generated in the reactor is approximately one giga watt. The

exact amount of fusion power produced will depend on the particular mode of operation, as described later in this summary. A non-circular cross-section plasma with an elongation of approximately two is employed. Helium ash exhaust and impurity control are accomplished through the use of a "double-null" divertor. The required super-conducting poloidal field coil system is located outside of the toroidal coils in order to facilitate assembly and maintenance.

Table VI.2.1-1 ITER parameters and performances

Nominal fusion power	(GW)	1
Pulse length	(s)	>200 to continuous
Energy multiplication	(Q)	>5 to infinity
Plasma major radius	(m)	6.0
Plasma half-width at mid-plane	(m)	2.15
Nominal maximum plasma current	(MA)	22
Toroidal field on-axis	(T)	4.85
Toroidal coil outer radius	(m)	11.5

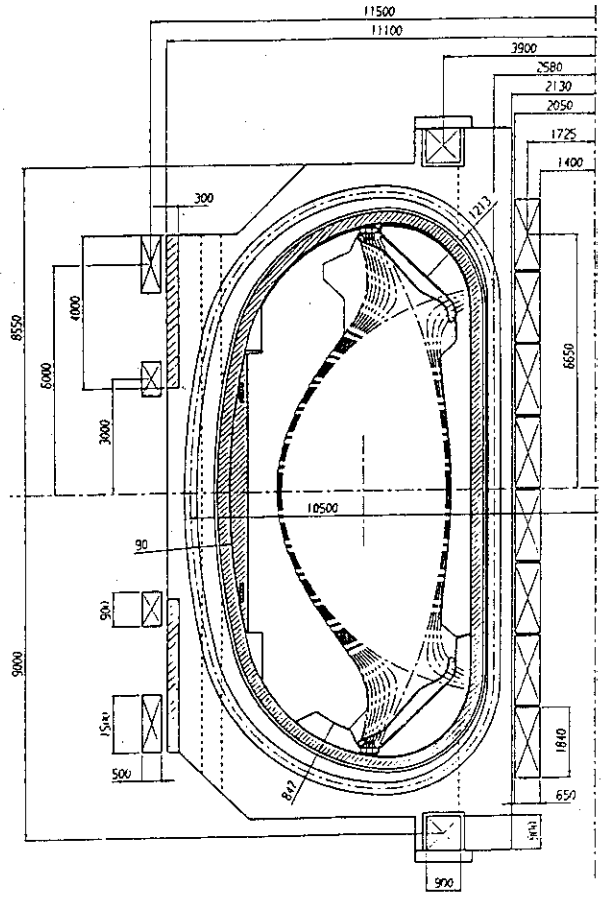

Fig.VI.2.1-1 Cross Sectional view of ITER

Breeding blankets, located just inside the vacuum vessel, are expected to supply most of the required tritium fuel. In addition, access is provided to insert and remove large modules intended to test advanced schemes for tritium breeding and power conversion. The arrangement and ordering of components and maintenance access ports have been chosen to allow the replacement or repair of plasma-facing components and of the tritium breeding and shielding system without the need to disassemble the tokamak.

The nominal plasma current of the ITER is 22 MA. The machine is capable of sustaining this current for at least 200 seconds utilizing inductive drive alone. This is accomplished with a poloidal field coil system capable of delivering about 325 V-sec. The toroidal field on axis is 4.85 T and the safety factor, q_ψ, on the 95% flux surface is 3.0. The major radius of the plasma is 6.0 meters and the minor radius is 2.15 meters. This is slightly larger major radius and smaller minor radius (slightly higher aspect ratio) than was considered in the first year of the design. Slight size and shape changes were made to accommodate more volt-seconds, provide more room for a divertor, and provide thicker shielding. The outer dimensions of the reactor did not change.

Heating of the plasma and non-inductive current drive of the plasma current are achieved with a multi-function heating and current drive system. The first option for this system is based on 1.3 MeV negative-ion neutral beams working in conjunction with lower hybrid and electron cyclotron wave sources. This system will be used to study very long pulses and steady-state discharges.

2.2 System analyses

In safety and environment area, normal effluent evaluation, accident scenario analysis based on FMEA, analyses of major accidents and estimation of radioactive waste amount were done. As major accidents, those which could release tritium and volatile radioactive materials (especially oxidized tungsten) are identified. Possible hydrogen production during LOCA and/or LOVA accidents are pointed out and implementation of inert gas atmosphere around torus was proposed to limit the hydrogen production and eliminate possible consequent hydrogen explosion. Japanese contributions are made mainly on the evaluation of-normal effluent, radioactive waste estimation and some of accident analyses (tritium system accident and LOCA/LOVA in the torus).

In the plant design area, each party except US conducted reactor building design. Japan also contributed by conducting extensive reactor building design and engineered safety systems (detritiation system, etc.) based on the developed building design. As an agreement , for reactor hall which is located on the upper part of the building, linear configuration concepts proposed by EC and USSR will be employed but for lower part which requires complex consistency with torus and its auxiliary equipment configuration and their maintenance scheme, Japanese concept will be employed as a reference approach. Basic idea for engineered safety system was established based on Japanese proposal which require further adjustment to the future revised building design.

ITER construction and operational costs are estimated to be B$4.9 and B$4.9, respectively. Construction cost includes those of tokamak and its auxiliary, buildings, plant auxiliaries, contingency and assembly and does not include those of test blankets,ultimate radioactive disposal, central project team, taxes and insurance. Main items for operation cost are manpower for operation, energy and spares.

In the area of parametric analysis, design point analysis in Ip-A space is readdressed using unified scaling law for ITER and other revised physics guideline. Technology phase operation scenario is also investigated looking at non-inductive current drive options and hybrid operation. Based on the ITER physics guideline, implications for commercial fusion reactor are studied.

2.3 Long-term R&D program

2.3.1 Physics R&D

The approach to the preparation of an ITER-related Physics R&D program for the period of the ITER Engineering Design Activity, assumed from 1991 to 1995, and the framework program for the ITER-related Physics R&D were developed and they were discussed at the Specialist Meeting, held on 15-16 February 1990, in which representatives of the fusion programs of the ITER partners participated. The overall objectives of the ITER-related Physics R&D program are to provide support to the design optimization and eventually to complete the data base necessary for taking the decision to start construction. To reach these objectives dedicated aim-oriented R&D work is necessary, and at the same time the program has to maintain the sufficient breadth to include basic research and innovative approach for the concept improvement. It is of greatest importance to arrive at an overall optimization of tokamak discharge conditions which can be extrapolated to the ITER. The main specific areas to be covered: 1) power and particle exhaust

physics (i.e. the combined fields of the physics of the plasma edge and plasma wall interaction as well as impurity control), 2) disruption control and operational limits, 3) enhanced confinement, 4) heating and fuelling physics, 5) long-pulse operation and of discharge start-up and shutdown (including non-inductive current drive), 6) physics of burning plasma. From the framework program the draft of the detailed R&D tasks was developed. The resulting program is binding for the years 1991 and 1992, it also contains actions providing results in the period 1993-1995. The most crucial areas, from the point of view of the research needs to complete the physics data base required for starting the ITER construction, in practical terms, are: 1) the demonstration in experiments proto-typical to the ITER, that operation with a cold divertor plasma is possible, keeping the divertor heat load below 10 MW/m^2, 2) the characterization of disruptions, 3) the demonstration that steady-state operation in a regime with enhanced confinement and satisfactory plasma purity is possible, 4) ensure that the presence of an appreciable population of fast ions does not jeopardize plasma performance in the ITER.

2.3.2 Technology R&D

The ITER is an international experimental reactor with the maximum jump from the present technology achievement, but the requirements in technology R&D area are basically same as that in the FER. In the conceptual design phase, basic R&D items and procedure including technical specifications and rough cost estimation have been discussed by specialists from the four parties. It was agreed that the R&D should be shared by four parties in plural approach and categorized into a scalable model test (SMT) requesting a large test facility and a component development. Furthermore, it was recommended that the resources of around 750M$ should be at least prepared by four parties for 5 years beyond 1991. Detailed specifications of each items proposed will be decided in further discussion before the task sharing commitment.

3. Fusion Reactor Design

3.1 Steady State Tokamak Reactor(SSTR) design

The Steady State Tokamak Reactor (SSTR) concept has been proposed [3.1-1] as a fusion power reactor to be built after the ITER or FER. The SSTR design is based on the extension of the present day physics and technologies. An observation of a high bootstrap fraction up to 80% of the total plasma current by the recent JT-60 experiments allows us to adopt high bootstrap fraction for the reactor design. The major feature of the SSTR is focussed on the maximum utilization of the bootstrap current in order to reduce the power required for the steady-state operation. A significant fraction (70 %) of the total plasma current is sustained by the bootstrap current resulting in the Q-value of ~35. This requirement leads to the choice of low current, and high β_p for the device, which were achieved by selecting high aspect ratio and high toroidal magnetic

Table VI.3.1-1 Main parameters of SSTR

Plasma major radius	7.0 m
Plasma minor radius	1.75 m
Aspect ratio	4
Plasma current	12 MA
Plasma elongation	1.8
Magnetic field on axis	9 T
Maximum on coil	16 T
Plasma volume	780 m^3
NBCD	80 MW
Fusion power	3000 MW
Net electric power	900 MW
Max. neutron wall load	5 MW/m^2
Q-value	~35
Tritium breeding ratio	>1.0
Divertor	Single null

physics (i.e. the combined fields of the physics of the plasma edge and plasma wall interaction as well as impurity control), 2) disruption control and operational limits, 3) enhanced confinement, 4) heating and fuelling physics, 5) long-pulse operation and of discharge start-up and shutdown (including non-inductive current drive), 6) physics of burning plasma. From the framework program the draft of the detailed R&D tasks was developed. The resulting program is binding for the years 1991 and 1992, it also contains actions providing results in the period 1993-1995. The most crucial areas, from the point of view of the research needs to complete the physics data base required for starting the ITER construction, in practical terms, are: 1) the demonstration in experiments proto-typical to the ITER, that operation with a cold divertor plasma is possible, keeping the divertor heat load below 10 MW/m^2, 2) the characterization of disruptions, 3) the demonstration that steady-state operation in a regime with enhanced confinement and satisfactory plasma purity is possible, 4) ensure that the presence of an appreciable population of fast ions does not jeopardize plasma performance in the ITER.

2.3.2 Technology R&D

The ITER is an international experimental reactor with the maximum jump from the present technology achievement, but the requirements in technology R&D area are basically same as that in the FER. In the conceptual design phase, basic R&D items and procedure including technical specifications and rough cost estimation have been discussed by specialists from the four parties. It was agreed that the R&D should be shared by four parties in plural approach and categorized into a scalable model test (SMT) requesting a large test facility and a component development. Furthermore, it was recommended that the resources of around 750M$ should be at least prepared by four parties for 5 years beyond 1991. Detailed specifications of each items proposed will be decided in further discussion before the task sharing commitment.

3. Fusion Reactor Design

3.1 Steady State Tokamak Reactor(SSTR) design

The Steady State Tokamak Reactor (SSTR) concept has been proposed [3.1-1] as a fusion power reactor to be built after the ITER or FER. The SSTR design is based on the extension of the present day physics and technologies. An observation of a high bootstrap fraction up to 80% of the total plasma current by the recent JT-60 experiments allows us to adopt high bootstrap fraction for the reactor design. The major feature of the SSTR is focussed on the maximum utilization of the bootstrap current in order to reduce the power required for the steady-state operation. A significant fraction (70 %) of the total plasma current is sustained by the bootstrap current resulting in the Q-value of ~35. This requirement leads to the choice of low current, and high β_p for the device, which were achieved by selecting high aspect ratio and high toroidal magnetic

Table VI.3.1-1 Main parameters of SSTR

Plasma major radius	7.0 m
Plasma minor radius	1.75 m
Aspect ratio	4
Plasma current	12 MA
Plasma elongation	1.8
Magnetic field on axis	9 T
Maximum on coil	16 T
Plasma volume	780 m^3
NBCD	80 MW
Fusion power	3000 MW
Net electric power	900 MW
Max. neutron wall load	5 MW/m^2
Q-value	~35
Tritium breeding ratio	>1.0
Divertor	Single null

field. Negative-ion-based neutral beam injection (NNBI) is adopted for both heating and current drive. This NNBI system also enables to control current profile and heating profile.

Main parameters of the SSTR are given in Table VI.3.1-1. The schematic cross section view of the SSTR is shown in Fig. VI.3.1-1 together with the ITER, FER and JT-60 Upgrade for comparison. It can be seen that although the major radius of the SSTR is only slightly larger than that of the ITER, the plasma volume is actually smaller than the ITER because of the smaller plasma radius. This figure shows that a tokamak machine comparable to the ITER in size can become a steady-state power reactor which is capable of generating about 1GW of electricity with a plant efficiency of ~30%.

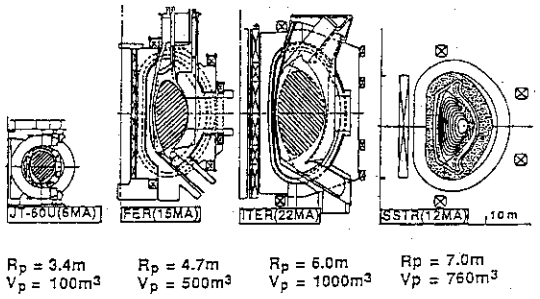

Fig.VI.3.1-1 Cross section of JT-60, FER, ITER and SSTR

3.2 Safety analyses

The development of a methodology for a comprehensive safety evaluation of a fusion reactor has been continued. The model of a fusion reactor system to be used in the evaluation is shown in Fig.VI.3.2-1. Using the model, the radioactive inventory and the radioactive release pathway under normal and accidental conditions have been evaluated.

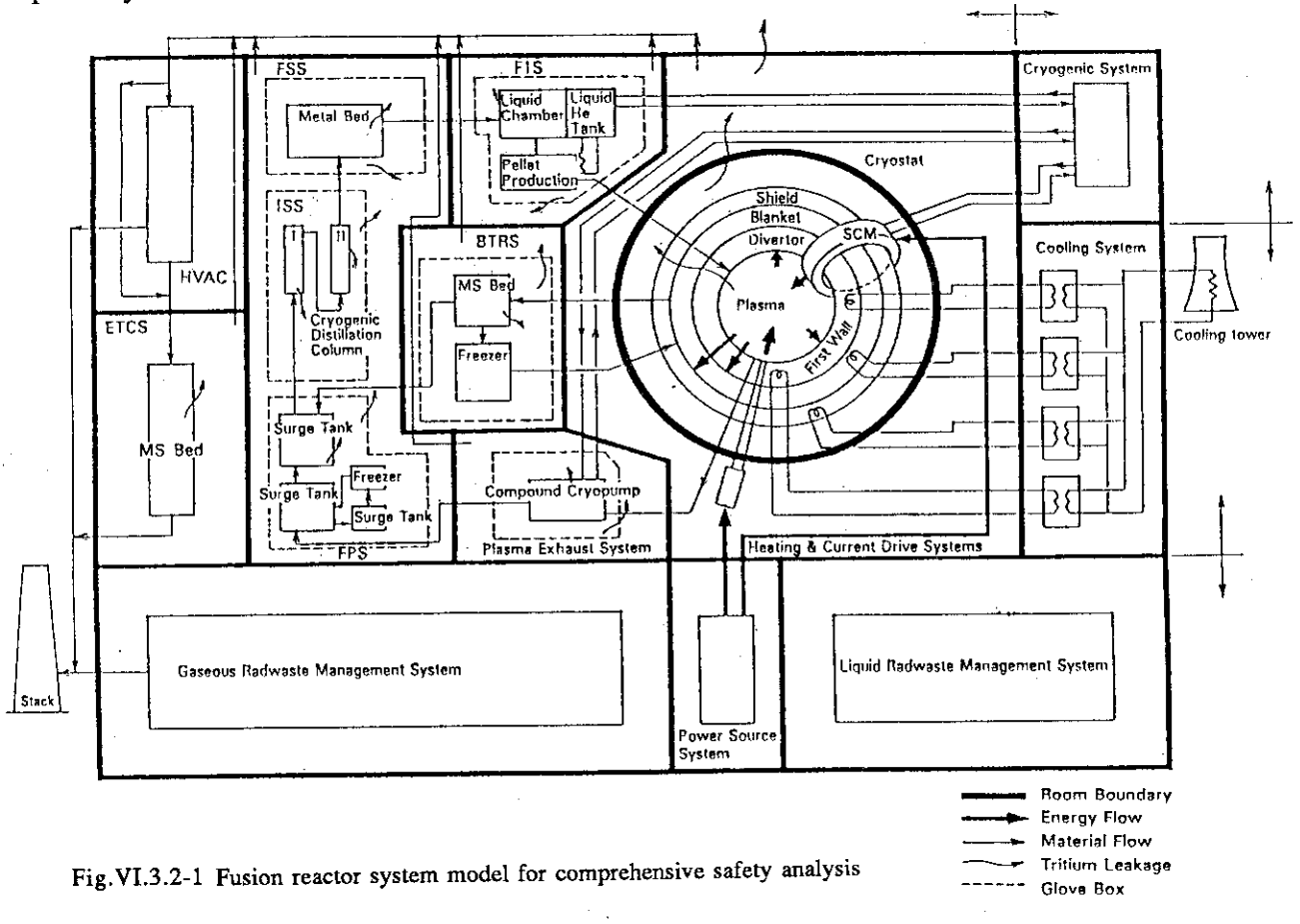

Fig.VI.3.2-1 Fusion reactor system model for comprehensive safety analysis

The evaluation methodology has been development for the radioactive inventory in the reactor system and its release probability The final objective is in the evaluation of the public and worker risk as the product of equivalent dose and the probability.

References

[1] Kikuchi, M., Nuclear Fusion 30 (1990) 265

APPENDICES

A.1 Publication List(April 1989 - March 1990)

A.1.1 List of JAERI-M reports

1) Miura Y., Okano F., Matsuzaki Y., "Low Energy Neutral Particle Energy Analyzer by Time of Flight Method", JAERI-M 89-018 (in Japanese).
2) Matsumoto H., Goldston R.J.(*37), Funahashi A., et al., "Characteristics of Edge Localized Mode in JFT-2M", JAERI-M 89-020.
3) Shinya K. , Sugihara M. , Nishio S. , "Study on Poloidal Field Coil Optimization and Equilibrium Control of ITER" JAERI-M89-028
4) Tamai H., Ogawa T., Matsumoto H., et al., "Experimental Observation of Ion Bernstein Wave Heating on JFT-2M", JAERI-M 89-036.
5) Hoshino K., Yamamoto T., Kawashima H., et al., "Observation of H-mode by Edge Heating Solely by Electron Cyclotron Heating in a Divertor Configuration of JFT-2M Tokamak", JAERI-M 89-038.
6) Kamada Y., Yoshino R., Nagami M., et al., "Confinement Properties of Pellet Injected JT-60 Plasmas", JAERI-M 89-050.
7) Tsunematsu, T., Hogan, J.(*19), Borrass, K.(*74), et al., Operational limits and disruptions in tokamaks," JAERI-M 89-056.
8) Kishimoto, Y., Oda, H.(*68), "One-dimensional single-mode nonlinear FEL amplification code --User's mannual--," JAERI-M 89-061 (in Japanese).
9) Hiratsuka H., Kawasaki K., Miyo Y., et al., "Upgrade of JT-60 Pellet Injector for Higher Velocity", JAERI-M 89-081 (in Japanese).
10) Tachikawa K. , Horie T. , Seki Y. , et al "Quick Installation / Removal Technology for First Wall Tile." JAERI-M89-084(in Japanese)
11) Tani, K., Takizuka, T., Azumi, M., "Ripple loss of alpha particles in ITER," JAERI-M 89-086.
12) Ozeki T., Tokuda S., Tsunematsu T., et al., "ERATO-code Analysis of Vacuum Magnetic Field Oscillations in JT-60 Divertor Configuration", JAERI-M 89-087 (in Japanese).
13) Kishimoto, Y., Oda, H.(*68), Shiho, M., et al., "Energy conversion efficiency in high current Raman regime free electron laser(FEL) --I. Single mode analysis--," JAERI-M 89-088.
14) Y.Okumura, M.Hanada, and H.Kojima et.al., " Measurement of Impurities in a Volume Produced H^- Ion Beam", JAERI-M 89-090.
15) Fracto-fusion --Mechanism of cold fusion --," JAERI-M 89-093.
16) Neuffeld C. R.(*4), Yoshino R., Yamamoto T., et al., "Numerical Simulation of Non-inductive Current Drive for Tokamak Plasmas with Time-Varying Electron Temperature", JAERI-M 89-103.
17) Saigusa M., Kimura H., Fujii T., et al., "Design of ICRF Antenna for JT-60U" JAERI-M 89-105
18) Yoshino R., "The Current Profile Modification in JT-60 Pellet Injection Experiments", JAERI-M 89-115.
19) Yoshino R., Ushigusa K., Imai T., "Numerical Investigation of Current Profile Flattening During Lower Hybrid Current Drive in JT-60", JAERI-M 89-116.
20) Matsuoka M., Kamata H., Kikuchi M., "Study on Negative-Ion-Based Nuetral Beam Injecton System for JT-60 Upgrade", JAERI-M 89-117 (in Japanese).
21) Kurihara K., Honda M., Nakamura Y., et al., "Program Package for Control System Design and Analysis (DPACS/J)", JAERI-M89-126(in Japanese)
22) Hoshino K., "A Study on the Heating and Diagnostic of a Tokamak Plasma by Electromagnetic Waves of Electron Cyclotron Range of Frequencies", JAERI-M 89-133 (in Japanese).
23) Yoshino R and Kamada Y., "Sawtooth Activity and Density Profile in Pellet Injection Plasmas on JT-60", JAERI-M 89-134.
24) Nishitani T., "Monte Carlo Simulation for the Calibration of Neutron Source Strength Measurement of JT-60 Upgrade", JAERI-M 89-138.
25) Shimizu K., Hirayama T., Shirai H., et al., "New Program Organization System (NEWORG)", JAERI-M 89-146 (in Japanese).
26) Okuno K. , Hatayama M., Sugihara M. , "Lower Hybrid Wave Spectrum Broadness and Driven Current Profile Controls by Non-Uniform Phasing of Grill Launchers" JAERI-M89-148
27) Kikuchi M and Azumi M, "Transport Modelling by a Heat Pinch Theory in the JT-60 Tokamak", JAERI-M 89-149.
28) Kurita, G., Azumi, M., Takizuka, T., et al., "Numerical code AEOLUS-E1 for analysing free boundary resistive MHD mode," JAERI-M 89-157(in Japanese).
29) Kikuchi M., "High b_p Bootstrap Tokamak Reactor", JAERI-M 89-164.
30) Tani K., Kihara K.(*67), Haginoya H.(*68), "Interpretation and Handling Manual of Fusion Experimental Data Monitor System DAISY Version I", JAERI-M 89-166 (in Japanese).
31) Kikuchi M., Azumi M., Tani K., et al., "Current Drive and Sustain Experiments with the Bootstrap Current in JT-60", JAERI-M 89-169.
32) Fukuyama A.(*10), Hamamatsu K., Itoh S-I.(*22), et al., "Analysis of ICRF Heating and Current Drive in ITER", JAERI-M 89-193 (in Japanese).
33) Nishitani T. and Ishida S., "Study of Marfe Phenomena on JT-60", JAERI-M 89-209.
34) Aikawa H., "A Model of L-H Transition", JAERI-M 89-217.
35) Kurihara K., Kimura T., Takahashi M., et al., "Tokamak Plasma Shape Identification with a Legendre-Fourier Expansion of the Vacuum Poloidal Flux Function in the Toroidal Coordinates", JAERI-M90-001(in Japanese)
36) Kawamata Y., Kurihara K., Kimura T., et al., "Test on Fast Data Transfer between a VME-bus System and a CAMAC system", JAERI-M90-005(in Japanese)

37) Zeritis D., "The transverse stress effect on the critical current of jelly-roll multifilamentary Nb_3Sn wire", JAERI-M 90-014
38) Okuno K., Enoeda M., Ide T., et al., "Joint operation of TSTA under the collaboration between JAERI and DOE-LANL - an integrated loop operation with 100-g tritium in July 1988 -", JAERI-M 90-028.

A.1.2 List of papers published in Journals

1) Tokuda, S., Takeda, T., Okamoto, M.(*9), "Neoclassical MHD equilibria with ohmic current," J. Phys. Soc. Japan **58** (1989) 871.
2) Takeda, T., Takizuka, T., "Fractofusion mechanism," J. Phys. Soc. Japan **58** (1989) 3073.
3) Yamagiwa, M., Kimura, H., Takizuka, T., "Simulation of high Q plasma by ICRF heating of alpha particles," Nucl. Fusion **29** (1989) 1799.
4) Itoh, S.-I.(*75), Fukuyama, A.(*10), Takizuka, T., et al., "Steady-state operation regime of tokamak reactor plasma: consistency analysis," Fusion Technol. **16** (1989) 346.
5) Kishimoto, Y., Oda, H.(*68), Shiho, M., et al., "Effect of electrostatic field on energy conversion efficiency in high current Raman regime free electron laser," J. Phys. Soc. Japan **59** (1990) 118.
6) Hasegawa M.(*15), Shoji T., Ohtsuka H., et al., "Observation of Divertor Plasma during H- and L-mode Operation in JFT-2M Tokamak", Fusion Technology (1988) 835.
7) Yamauchi T. and JFT-2M Experimental Group, "Measurement of Visible Emission Profile of JFT-2M Tokamak H-mode Plasmas with Thomson Scattering Apparatus", Jpn. J. Appl.Phys.**28** (1989) L707.
8) Hoshino K., Yamamoto T., Kawashima., et al., "Edge Pedestal during the H-mode of a Tokamak Plasmas measured by the Electron Cyclotron Emission", J. Phys. Soc. Jpn. **58** (1989) 1248.
9) Hoshino K., Yamamoto T., Kawashima H., et al., "H-mode Observed in JFT-2M Tokamak with Edge Heating by Electron Cyclotron Waves", Phys. Rev. Letters **63** (1989)770.
10) Yamamoto T., Uesugi Y.(*9), Kawashima H., et al., "Observation of Direct Electron Heating by the Fast Waves in the Lower-Hybrid Range of Frequencies in the JFT-2M Tokamak", Phys. Rev. Letters **63** (1989) 1148.
11) Abe M.(*15), Kameari A.(*23), Kishimoto A., et al., "Energy Confinement Characteristics of Neutral Beam Heated Plasmas with a Divertor Configuration in Doublet III: Experiments and Analysis by the JAERI Team", Nucl. Fusion **29** (1989) 1659.
12) Sengoku S., Aikawa H., Hoshino K., et al., "Pump Limiter Experiment on the JFT-2M Tokamak", J. Nucl. Materials **162**(1989) 667.
13) Odajima K., "Application of Free Electron Laser for Plasma Heating and Current Drive", J. Atomic Energy Soc. Jpn. **31** (1989) 1093 (in Japanese).
14) Kasai S., "Solid Hydrogen-isotope Pellet Injector", Cryogenic Engineering **24** (1989) 318 (in Japanese).
15) Tada E., Takahashi Y., Tsuji H., et al., "Down stream effect on stability in cable-in-conduit superconductor", Cryogenics **29**, (1989) p830
16) Shimada M.,Konoshima S., "Status of DIII-D Experiments", Kakuyugo Kenkyu **62**(1989)5.
17) Abe M.(*2),Kameari A.(*7),Kitsunezaki A.,et al.,"Energy Confinement Characteristics of Neutral Beam Heated Plasmas with a Divertor Configuration in Doublet III : Experiments and analysis by the JAERI team", Nucl. Fusion **29**(1989) 162.
18) Burrell K.(*1),Matsumoto H.,Neyatani Y.,et al.,"Confinement physics of H-mode discharges in DIII-D",Plasma Physics and Controlled Fusion Research **31**(1989)1649.
19) Schissel D.(*1),Shimada M.,et al.,"Energy confinement properties of H-mode discharges in the DIII-D tokamak", Nucl. Fusion **29**(1989)185.
20) Madarame H.(*8), Terai T.(*8), Kamada Y., et al., "A Conceptual Design of RFP fusion Power Core -REPUTER - 1", Fusion engineering and Design **7** (1989) 389.
21) Taylor P. L.(*1), LaHaye R. J.(*1), Kamada Y., et al., "Characteristics of Ultra-low q Plasmas in the OHTE Device", Nucl. Fusion **29**(1989) 92.
22) Usigusa K., Imai T., Ikeda Y., et al., "Simultaneous Heating by High Power Lower Hybrid Waves and Neutral Beams in the JT-60 Tokamak", ibid **29** (1989) 265.
23) Kamada Y., Fujita T.(*8), Murakami Y.(*8) , et al., "Recent Results of Ultra Low q Experiments in TORIUT-6 and REPUTE-1", ibid **29**(1989) 713.
24) Ushigusa K., Imai T., Ikeda Y., et al., "Lower Hybrid Current Drive Efficiency in the JT-60 Tokamak", ibid **29** (1989) 1052.
25) Tsuji S. and Azumi M., "Sawtooth Oscillations in Tokamaks", Kakuyugo Kenkyu **61** (1989) 287 (in Japanese).
26) Hosogane and JT-60 Team, "Characteristics of the JT-60 Divertor and Limiter Plasmas with High Power Auxiliary Heating", J. Nucl. Mater. **162** (1989) 93.
27) Jackson G. L.(*1) , Taylor T. S.(*1), Nakamura H., et al., "Reduction of Recycling in DIII-D by Degassing and Conditioning of the Graphite Tiles", ibid **162** (1989) 489.
28) Yoshino R., Neyatani Y., Ninomiya H., et al., "Density Control for Gutting Stable Discharges in JT-60 Graphite Wall Experiment", ibid **162**(1989) 527.
29) Nagami M., and JT-60 Team, "Recent Results in JT-60 Experiment", Plasma Phys. and Controll. Fusion **31** (1989) 1597.
30) Morimoto H.(*8), Kamada Y., Fujita T.(*8), et al., "Bolometer Measurements of Ultra-Low-q and Reversed Field Pinch Plasmas in REPUTE-1", Nucl. Fusion **29** (1989) 1171.
31) Kamada Y., Yoshino R., Nagami M., et al., "Improved Confinement Characteristics of Pellet Fuelled Discharges on JT-60", ibid **29** (1989) 1785.
32) Yoshino R., "Current Profile Modification in JT-60 Pellet Injection Experiments", ibid **29** (1989) 2231.
33) Itoh K.(*9)and Shimada M., "Impurity Control", ibid **29** (1989) 2239.

34) Imai T., Ushigusa K., Ikeda Y., et al., "Enhancement of Energy Confinement by Acceleration of Fast Ions in Combined Lower Hybrid and Neutral Beam Heating on JT-60", ibid **30** (1990) 161.
35) Naito O., Hosogane N., Tsuji S., et al., "Global Energy Confinement in JT-60 Neutral Beam Heated L-mode Discharges", ibid **30** (1990) 195.
36) Nakamura H., Tsuji S., Nagami M., et al., "H-mode Experiments with Outer and Lower Divertor in JT-60", ibid **30** (1990) 235.
37) Kikuchi M., "Steady State Tokamak Reactor based on the Boot-strap Current", ibid **30** (1990) 265.
38) Kikuchi M., Azumi M., Tsuji S., et al., "Bootstrap Current during Perpendicular Neutral Injection in JT-60", ibid **30** (1990) 343.
39) Ushigusa K., Imai T., Naito O., et al., "Energy Confinement in JT-60 Lower Hybrid Current Drive Plasmas", ibid **30** (1990) 541.
40) Tsuji S., Ushigusa K., Ikeda Y., et al., "Observation of the Limiter H-mode in the JT-60 Tokamak with Lower Hybrid Current Drive", Phys. Rev. Lett. **64** (1990) 1023.
41) Shirai H., Hirayama T., Shimizu K., et al., "Transport Analysis of JT-60 Plasma with the Drift Wave Turbulence Model", Nucl. Fusion **29** (1989) 805.
42) Shimizu K., Hirayama T., Shirai H., et al., "Numerical Simulation of L/H Transitions in Divertor Discharges", J. Nucl. Matter. **162** (1989) 612.
43) Hamamatsu K., Saigusa M., Kimura H., et al., "Comparison between Theoretical Analysis and Experimental Results of an ICRF loading in JT-60", Jpn. J. Appl. Phys. **28** (1989) 1708.
44) Tani K. and Yamamoto S., "Report of The IAEA Technical Committee Meeting for Alpha Particles in Fusion Research", Kakuyugo Kenkyu **63** (1989) 62 (in Japanese).
45) Ozeki T., Azumi M., "Access to the Second Stability Regime near the Plasma Surface in a High-q, Low-Shear Tokamak Plasma", J. Phys. Soc. Japan, **59** (1990) 927.
46) Kubo H., Sugie T., Sakasai A., et al., "Spectroscopic Study of Impurities in Neutral Beam Heated and Ohmically Heated JT-60 Discharges", Nucl. Fusion **29** (1989) 571.
47) Fukuda T. and JT-60 Team, "Interferomentric Density Measurements in the Divertor and Endge Plasma Regions for the Additionally Heated JT-60 Plasmas", J. Nucl. Mater. **162** (1989) 258.
48) Nishino N. and JT-60 Team, "Behavior of Light Impurities in Beam-heated JT-60 plasmas with Hot Graphite Walls", J. Nucl. Mater. **162** (1989) 386.
49) Fukuda T. and Nagashima A., "Frequency-stabilized Single-mode CW 118.8 mm CH_3OH Waveguide Laser for Large Tokamak Diagnostics", Rev. Sci. Instrum. **60** (1989) 1080-1085.
50) Kubo H., Sakasai A. Nishino N., et al., "Absolute Calibration of a Normal Incidence Vacuum Spectrometer Using Synchrotron Radiation", Jpn. J. Appl. Phys. **28** (1989) 2610-2614.
51) Tamura S., "Present Status of Nuclear Fusion Research ", Kagaku-Asahi July (1989) 112-114.
52) Oikawa A., "Nuclear Fusion Research Proceeding to Technology Development", Energy, Jan. (1990) 39-45.
53) Miya N., Nakamura H., Tsuji S., et al., "Neutral Pressures in JT-60 Divertor Discharges", J. Nucl. Mater. **162** (1989) 618.
54) Tobita K., Kusama Y.,Itoh T. et al.: "A Parasitic Effect of Neutral Particle Diagnostic Using a Helium Probing Beam",Jpn.J.Appl.Phys **29**(1990) 760.
55) Nishitani T. and Strachan, J. D.: "Neutral Spectroscopy with a ^3He Ionization Chamber on TFTR",Jpn.J.Appl.Phys **29** (1990) 591.
56) Matsuzaki Y and the JFT-2M Team, "Probe Measurement of Hydrogen Fluxes during Discharge Cleaning in JFT-2M", J. Nuclear Materials **162-164** (1989) 752
57) Kimura T., Kurihara K., Takahashi M., et al., "VME Multiprocessor System for Plasma Control at the JT-60 Upgrade", IEEE trans. on Nuclear Science **36** (1980) 1554
58) Kurihara K., Kimura T., Yonekawa I., et al., "JT-60 Plasma Control System", Fusion Engineering and Design **11** (1990) 441
59) Ogiwara N., Maeno M., "Partial Pressure Measurement by Analizing the Light from a Penning Discharge", J. Vac. Soc. Jpn. **32** (1989) 292 (in Japanese).
60) Ogiwara N., Maeno M., "Hydrogen Pressure Measurement Using the Intensity of the Light Emitted from a Penning Discharge", J. Vac. Sci. Technol. **A7** (1989) 2804.
61) Seki M.,Saigusa,M.,Nemoto M.,et al.,. ,"Observation of Ion Cyclotron Wave Instability caused by Perpendicular Neutral Beam Injection in the JT-60 Tokamak",Phys.Rev. Lett. **62** (1989) 1989.
62) Uehara K.,Nemoto M.,Nagashima T.,"Parameter for Lower Hybrid Current Driven Tokamaks", Nucl.Fusion **29** (1989) 735
63) Ikeda Y.,Imai T.,Ushikusa K.,and ,JT-60 Team, "Efficient Lower Hybrid Current Drive Using a Multi-junction Launcher on JT-60",Nucl.Fusion **29** (1989) 1815
64) Uehara K.,Naito O.,Seki M., et al.,,"Deterioration and Improvement of Hot Plasma Confinement of Magnetic Fusion Devices",Phys.Rev.Lett. **64** (1990) 757
65) Uehara K.,Watanabe Y(*27).,Loring M(*71).et al.,,"Status of Solid State Amplifier Application to Plasma Heating and Klystrode Development",Kakuyugo-Kenkyu **62** (1990) 196 (in Japanese)
66) Kuriyama M., Araki M., Horiike H., et al., "Beam Stops of JT-60 Neutral Beam Injector", Fusion Engineering Design, **9** (1989) 237-243.
67) Araki M., Dairaku M., Inoue T., et al., "Burnout Experiments on the Externally-Finned Swirl Tube for Steady State and High Heat Flux Beam Stops", Fusion Engineering Design, **9** (1989) 231-236.
68) Imai T., Ushigusa K., Ikeda Y., et al., "Enhancement of Energy Confinement by Acceleration of Fast Ions in Combined Lower Hybrid and Neutral Beam Heating on JT-60", Nuclear Fusion **30**, No.1 (1990) 161.

69) Sakamoto K., Ikeda Y., Imai T. et al., "Numerical Study of RF Discharge Caused by Secondary Electron Emission.", J.Phys. D Appl. Phys. **22**(1989) 1840-1847.
70) Shibanuma K. , Okuno, Shibata T. , "Development of gas density calculation code by Monte Carlo Method" Shinkuu, **32**, No.3 (1989)284 in Japanese
71) Shibanuma K. , Shibata T. , "Development of Large Sealed Cryopump for Negative Ion Beam Extraction" Shinkuu, **32**, No.3 (1989)296 in Japanese
72) Shibanuma K. , Araki M. , Dairaku M. , et al "Natural Circulation two phase helium flow characteristics in cryopump for JT-60 Neutral beam injector", Nihon Genshiryoku Gakkaishi, **31**, No. 3(1989)83 in Japanese
73) Seki M. , Yamazaki S. , Kobayashi T. , "Development of Disruption Thermal Analysis Code DREAM." FAPIG, No. 122 (1989)44
74) Okuno K. , Yamamoto S. , Sugihara M. , et al "Potential of Neutral Beam Current Drive for Steady-State and Quasi-Steady-State Tokamak Reactors" Fusion Technology **16** (1989)p.73
75) Yamagiwa M., Kimura H. , Takitsuka T. , "Simulation of High b Plasma by ICRF Heating of Alpha Particles" Nucl. Fusion **29**, No.10 (1989)
76) Mori M. , Kimura H. , Tanaka S. , "Non-inductive Current Drive in Toroidal System. 5. Prospect for Nuclear Fusion Reactor" Kakuyuugou Kenkyuushi, Vol. in Japanese
77) Seki Y. , Iida H. , Kobayashi S. , et al "Safety Analysis of the FER Fuel Circulating System" Fusion Engineering and Design **10** (1989) 373
78) Nakahara K. , Seki Y. , Kobayashi S. , "Thermal Effect of Periodical Bakeout on Tritium Inventory in First wall and Permeation to Coolant in Reactor Life" ibid. p385
79) Kosako T. , Seki Y. , "Radiation Protection in a Large Fusion Experiments." Nihon Genshiryoku Gakkaishi, Vol.32, No. 1(1990)33 in Japanese
80) O'hira S., Hayashi T., Okuno K., et al., "Tritium dissolution in and release from Li_2O", Fusion Engineering & design **8** (1989) 335.
81) Okuno K., Kudo H., "Tritium Diffusivity in lithium-based ceramic breeders irradiated with neutrons", ibid. **8** (1989) 355.
82) Naruse Y., Matsuda Y., Tanaka., et al., "Commissioning of the Tritium Process Laboratory at the JAERI", ibid. **10** (1989) 197.
83) Sze D. K.(*64), Naruse Y., Yoshida H., et al., "The role of a blanket tritium system on the fusion fuel cycle", ibid. **10**(1989) 203.
84) Enoeda M., Yamanishi T., Yoshida H., et al., "Hydrogen isotope characteristics of cryogenic distillation column", ibid. **10**(1989) 319.
85) Konishi S., Nagasaki T., Yokogawa N.(*29), et al., "Development of zirconium-cobalts beds for recovery, storage and supply of tritium", ibid. **10** (1989) 355.
86) Hayashi T., Konishi S., Okuno K., "Tritium release behavior from neutron-irradiated Li_8PbO_6", J. Nucl. Mater. **170** (1990) 60.
87) Saidoh M., Yamada R., "Study of Modification Process in Sputtering during Oxygen Exposure", Nucl. Instrm. Methods **B39** (1989) 599.
88) Yamada R., Saidoh M., "Hydrocarbon Release from Graphite and Titanium Carbide", J. Nucl. Mater **162-164** (1989) 1040.
89) Obara K., Nakamura K., Murakami Y., et al, "Design and Test of a Multi-joint Remote Manipulator for Use in High Vacuum", Fusion Engineering & Design **10** (1989) 495.
90) Ioki K.(*7), Kameari A.(*7), Ueda N.(*7), Hikita K.(*23), Hata S.(*23), Abe T., Iida H. Murakami Y., "Ceramic Turbomolecular Pumping System in Reactor Structure of FER", ibid 223.
91) Murakami Y., "Application of Vacuum to Atomic Energy Research", J. Jpn. Soc. Mech. Eng. **92** (1989) 637. (in Japanese)
92) Hiroki S., Maebara N., Abe T., et al, "Secondary Electron Emisson Coefficient of Aluminum Nitride" Trans. Inst. Electr. Engi. Jpn. **109-A**(1989) 372. (in Japanese)
93) Abe T., "Development of Ceramic High Vacuum Pump", J. At. Energy Soc. Jpn. **31** (1989) 1106. (in Japanese)
94) Tanaka S., Akiba M., and Araki M.,et.al., "Production of High Current Ion Beams of Various Gas Species from a Magnetic Multipole Ion Source", Nucl. Instrum and Methods in Phys. Res. **B37/38**, (1989)128.
95) Tanaka S., "Industrial Application of High Power Ion Source", Energy Forum, **413**(1989)120 (in Japanese)
96) Inoue T., Araki M. and Hanada M. et.al.,"Multi-Ampere Negative Hydrogen Ion Source for Fusion Application", Nucl. Instrum and Methods in Phys. Research **B37/38**, (1989)111.
97) Inoue T., Ackerman G.D.(*3) and Cooper V.(*3), et.al., "Comparison of H^- and D^- Production in a Magnetically Filtered Multicusp Source", Rev. Sci.Instrum., **61** (1990)496.
98) Hanada M., Inoue T. and Kojima H., "A 14 cm x 36 cm Volume Negative Ion Source Producing Multi-Ampere H^- Ion Beams", Rev. Sci.Instrum., **61** (1990)499.
99) Okumura Y., " A Large Scale Ion Source", Mukizairyou, July (1989)42

A.1.3 List of papers published in conference proceedings

1) Yamauchi T. and JFT-2M Group, "Rotational Raman Scattering of Molecular Nitrogen Gas for Calibrating a Thomson Scattering Device", Sym. on Gaseous Molecular Luminescence (Los Angels, 1989).
2) Tamai H., Ogawa T., Odajima K., et al., "Edge Plasma Characteristics during ICRF Heating on JFT-2M Tokamak", IAEA Technical Committee Meeting on ICRH/Edge Physics, (Garching1989).
3) Hoshino K., Yamamoto T., Kawashima H., et al., "H-mode by Edge ECH in JFT-2M", 8th Topical Conf. on Radio-Frequency Power in Plasmas (Irvine, 1989), AIP Conference Proc. **190** (1989) 52.

4) Kawashima H. and JFT-2M, "Electron Behavior during FWCD Experiment on JFT-2M", ibid 142.
5) Maebara S., Ikeda Y., Sakamoto K. et al., "High Power Test of Lower Hybrid Vacuum Window.", ibid 154.
6) Saigusa M., Kimura H., Fujii T. et al., "Observation of Parametric Decay Wave During Second Harmonic ICRF Heating Experiment in JT-60.", ibid 326.
7) Shiho M., Kishimoto Y., Odajima K., "Recent Status of Millimeter Wave FEL Development for Plasma Heating at JAERI", 2nd Int. Sym. on Advanced Nuclear Energy Research (Mito, January 1990).
8) Maebara S., Nagashima T., Miyake S., "Development of 2 GHz High Power Klystron for Fusion Application.", 2nd Int. Sym. on Advanced Nucl.Energy Res. Paper C7 (1990).
9) Sakamoto K., Nagashima T., Okazaki Y. et al., "Development of 500 kW Whispering Gallery Mode Gyrotron.", ibid.
10) Shiho M., Hoshino K., Kishimoto Y. et al., "Recent results and Future Plan of the JFT-2M Tokamak ECRH Experiment.", IAEA 7th Tech. Committee Meeting on ECE and ECH Hofei, China (1989).
11) Shiho M., Kishimoto Y., Sakamoto K. et al., "Present Status of Millimeter Wave FEL Development for Plasma Heating at JAERI.", 2nd Int. Sym. on Advanced Nucl.Energy Res. Paper C7 (1990).
12) Saigusa M., Matsuda K., James R.A., et al., "Design Study for ECCD using Outside Launched Ordinary Mode." 31th APS Annual Meeting, Anaheim CA., USA. (1989).
13) Murakami Y., Abe T., "Ceramic Turbomolecular Pumping System", Proc. Japan-US Workshop P-118 on Vacuum Technology for Fusion Devices (Nagoya) IPPJ-T38 (1989) 145.
14) Abe T., Murakami Y., "Performance Test of Ceramic Rotor Turbomolecular Pumps", ibid 153.
15) Nakamura K., Obara K., "Calculation of Pipe Conductance for Energetic Gases by Monte Carlo Method", ibid 240.
16) Obara K., Nakaumra K., Murakami Y., "Design and Testing of a Mainipulator Arm Used in High Vacuum", ibid 227.
17) Tsuji H., Tada E., Okuno K., et al., "Evolutions of the demo poloidal coil program", 11th Inter. Conference on Magnet Technology (Tsukuda)
18) Okuno K., Tsuji H., Takahashi Y., et al., "The first experiment of the 30-kA, Nb-Ti demo poloidal coils (DPC-U1 and -U2)", ibid.
19) Ando T., Nishi M., Nakajima H., et al., "Compression stress effect on the critical current of Nb_3Sn cable-in-conduit conductors", ibid.
20) Nakajima H., Okuno K., Tsuji H., et al., "Fabrication and mechanical characteristics in experiment of Nb-Ti demo poloidal coils (DPC-U1, U2)", ibad.
21) Tada E.,Kawano K., Ando T., et al., "Thermal performance results of the Nb-Ti demo poloidal coils (U1, U2)", ibid.
22) Nishi M., Tsuji H., Takahashi Y., et al., "Results of verification tests and coil test of DPC-TJ", ibid.
23) Takahashi Y., Ando T., Tsuji H., et al., "Verification tests of the Nb_3Sn demo poloidal coil (DPC-EX)", ibid.
24) Kato T., Yoshida J., Tada E., et al., "Operation performance of DPCF in the test of the NbTi DEMO Poloidal coils (DPC-U1&U2)", ibid.
25) Yoshida K., Nishi M., Takahashi Y., et al., "Development of the Prot-type conductor and design of the test coil for the fusion experimental reactor", ibid.
26) Yoshida K., Koizumi K., Sugimoto M., et al., "Design study of FER superconducting magnet system", ibid.
27) Ando T., Nishi M., Kato T., et al., "Propagation velocity of the normal zone in a cable-in-conductor", Cryogenic Engineering Conference 1989 (los Angels)
28) Nakajima H., Yoshida K., Shimamoto S., et al., "Round robin testing and fracture toughness test results for CSUS-JN-1 (Fe-25Cr-15Ni-0.35N) austic stainless steel at 4K", ibid.
29) Kato T., Yamamua H., Kawano K., et al., "A large scale turboexpander development and its performance test results", ibid.
30) Konishi S., Ohno H., Hayashi T., et al., "Diffusion of lithium and tritium in Li_8PbO_6", Second International Symposium on the Fabrication and Properties of lithium ceramics, Indianapolis, (April 1989).
31) Clemmer R. G.(*64), Anderson J. L.(*47), Naruse Y., et al., "The breeding blanket interface (BBI) : Recent results for the solid breeder and the aqueous salt solution concepts", Proceedings of the 13th Symposium on Fusion Engineering, Knoxville, Vol.1 p.78 (1989).
32) Ide T.(*29), Okuno K., Konishi S., et al., "$LaNi_3Mn_2$ alloy as a tritium storage material", ibid. Vol.1 p.616 (1989).
33) Konishi S., O'hira S., Sakai F.(*29), et al., "Experiments on the fusion fuel processing in the Tritium Process Laboratory", ibid. Vol.1 p.626 (1989).
34) Enoeda M., Fukui H.(*23), Ide T.(*29), et al., "Separation of helium and hydrogen isotopes by cryogenic distillation at the Tritium Systems Test Assembly", ibid. Vol.1 p.630 (1989).
35) Willms R. S.(*47), Naruse Y., Okuno K., "Fusion fuel purification during the Tritium Systems Test Assembly 3-weeks loop experiment", ibid. Vol.1 p.795 (1989).
36) Anderson J. L.(*47), Okuno K., Fukui H.*23, "Dispersion and removal of tritium released into the main cell of TSTA", ibid. Vol.1 p.798 (1989).
37) Anderson J. L.(*47), Sze D. K.(*64), Naruse Y., et al., "The breeding blanket interface (BBI) and the Tritium Systems Test Assembly (TSTA)", ibid. Vol.1 p.804 (1989).
38) Naruse Y., Matsuda Y., Tanaka K., et al., "Operation of the Tritium Process Laboratory in the Japan Atomic Energy Research Institute", ibid. Vol.1 p.808 (1989).
39) Lohr J.(*1),Okazaki T.(*2),et al.,"Recent Electron Cyclotron Heating Experiments with Low Field Launch of the Ordinary Mode on the DIII-D Tokamak", IAEA Tech. Meeting on ECE and ECRH(Hefei)(May 1989).
40) Matsumoto H.,et al.,"Edge Fluctuation on DIII-D", Review meeting for Transport Initiative in Tokamak Fusion Plasmas(Maryland)(July 1989)
41) Matsumoto H.,et al.,"Edge Fluctuation Studies in DIII-D",TTF Workshop(San Diego)(Aug.1989)
42) Matsumoto H.,Lehecka T.(*69),et al.,"Fluctuation Studies of the L-H Transition in DIII-D",APS meeting(Anaheim) (Nov.1989).

43) Saigusa M.,Matsuda K.(*1),et al.,"Design Study for ECCD Using Outside Launched Ordinary Mode",APS meeting (Anaheim) (Nov.1989).
44) Kikuchi M., Ando T., Araki M., et al., "JT-60 Upgrade Program", Proc. 15th Symp. on Fusion Technol., Utrecht, 1988 (Pergamon Press, 1989) Vol. 1, pp. 287.
45) Ninomiya H., Yoshino R., Akiba M., et al., "MHD Activities and Related Impurity Behaviour in JT-60 Discharges", Proc. 12th Internal. Conf. on Plasma Phys. and Controll. Nucl. Fusion Research, Nice, 1988 (IAEA, Vienna,1989) Vol. 1, pp. 111.
46) Burrell K. H.(*4), Fukumoto H.(*5), Hosogane N., et al., "Energy Confinement in Auxiliary-Heated Divertor and Limiter Discharges in the DIII-D Tokamak", ibid Vol. 1, pp. 193.
47) Tsuji S., Akiba M., Ando T., et al., "Energy Confinement with Auxiliary Heating in JT-60", ibid Vol. 1, pp. 265.
48) Kikuchi M., Hirayama T., Kubo H., et al., "Characteristics of Banana Regime Conductivity in JT-60", ibid Vol. 1, 505.
49) Ushigusa K., Imai T., Nakamura H., et al., "Lower Hybrid Experiments in JT-60", ibid Vol. 1, pp. 621.
50) Shimomura Y., "ITER: Operation Scenario", ibid Vol.3, pp. 273.
51) Fukuda T., Kikuchi M., Ushikusa K., et al., "Evaluation of the Plasma Internal Inductance via Polarimetry on JT-60", The 4th International Symposium on Laser-aided plasma diagnostics.
52) Fukuda T., Konoshima S. and Matoba T., "Reflectometric measurements on the JT-60 tokamak", ibid.
53) Sato M., Ishida S., Isei N., et al., "Development of a Grating Polychromater System on JT-60", The 14th International Conference on Infrared and Millimeter waves.
54) Fukuda T. and Matoba T., "Broadband Millimeter-wave Reflectometry on the JT-60 Tokamak", ibid.
55) Kusama Y. and JT-60 Team: "Proposal of Confined Fast Alpha-particle Measurement Using 2 MeV Li-Beam on JT-60", IAEA Technical Committee Meeting on Alpha Particle Confinement and Heating Kiev, USSR.
56) Tada E. , Hasegawa M. , Honda C. , et al "The Fusion Experimental Reactor-Design Concepts" 13th Symp. on Fusion Eng. Knoxville, USA, October 1989
57) Koizumi K. , Yoshida K. , Hasegawa M. , et al "Design Study of the FER superconducting Magnet System" ibid
58) Fujii ., Saegusa ., Kimura ., et al "Interaction Between RF and Edge Plasma During ICRF Heating in JT-60" IAEA TCM on ICRH / Edge Physics October 1989
59) Seki Y. , Takeyasu Y. , "Long-Term Radioactive Waste for the Fusion Experimental Reactor (FER)" IAEA TCM on Fusion Reactor Safety, Jackson Hole, USA April 1989
60) Seki Y. , "Low Activation Considerations for Fusion Experimental Reactor (FER) and Power Reactors" 4th International Conference on Fusion Reactor Materials, Kyoto (1989) December 1989
61) Nakamura H., Tobita K., Koide Y., "Initial Results of Helium Ash Experiment in JT-60 Lower Divertor" IAEA TCM on 'Alpha Particle in Fusion Research'"
62) Kuroda T., "Engineering Issues for Plasma Facing Components of ITER" IAEA TCM on Impurity Control, Nakamachi, Ibaraki-ken Japan, February (1990)
63) Sugihara M., "Power and Particle Control for ITER" ibid.
64) Matsuzaki Y., Omori K., Shimada R.(*62). et al., "High Switching Frequency Amplifier of IGBT for Disruption Feedback Control Systems", 13th Symp. on Fusion Engineering (Knoxville) (October, 1989)
65) Shimizu M. and JT-60 Team, "Present Status and Future Plan of JT-60 Engineering", ibid.
66) Arakawa K. and JT-60 Team, "JT-60 Operational Experience and Trouble Analysis", ibid.
67) Ogiwara N., Maeno M., "The fast Pressure Monitoring System on JT-60", ibid.
68) Hiratsuka H., Kawasaki K., Takatsu H., et al., "Development of Upgrade Pellet Injector for JT-60", ibid.
69) Ando T., Takatsu H., Nakamura H., et al., "Performance of JT-60 Divertor Plates", 4th Int. Conf. on Fusion Technol. Reactor Mater., Kyoto.3.
70) Uehara K.,Kimura H., JT-60 Team, "RF Current Drive and Heating in JT-60",Proceeding of 8th Topical Conference on RF Power in Plasmas,Irvine Ca.,USA AIP 190,p.106
71) Ikeda Y.,Imai T.,Ushikusa K.,and .,JT-60 Team, "First Operation of Multi-junction Launcher on JT-60" ibid.p.138
72) Seki M.,Ikeda Y.,Imai T.,et al.,.,"Design of New LHRF Launcher on JT-60 upgrade" ,ibid.p.170
73) Uehara K.,Naito O.,Seki M., et al.,.,"On the deterioration and improvement of plasma confinement during additional heating in magnetic fusion traps" ibid.p.478
74) Konishi K.(*29),Ikeda Y.,Seki M.,et al.,.,Proc of 13th Symposium on Fusion Engineering(Knoxville)
75) Moriyama S.,Ogawa Y.(*4).,Fujii T.,et al.,,"First JT-60 system high power 11 0 to 130 MHz test results with an X-2242 tetrode.",ibid.
76) Tsuneoka M.,Takeuchi M.(*72),Takahashi I.(*72),"Design of RF Power Supply using DC-DC Convertor", ibid.
77) Fujii T.,Saigusa M.,Kimura H.,and.,JT-60 Team, IAEA technical Committee Meeting on ICRF Edge Physics,Garching West-germany 1989
78) Ohara Y., Akiba M., Araki., et al., "Recent Activities on Negative Ion Beams at JAERI", Proc. of 13th Symp. on Fusion Engineering, Knoxville (1989) 284.
79) Mizuno M., Dairaku M., Ohara Y., et al., "Inverter Type High Voltage DC Power Supply for Negative-Ion-Based Neutral Beam Injectors", ibid 574.
80) Kuriyama M., Akiba M., Akino N., et al., "Operation of JT-60NBI and NBI system for JT-60 Upgrade", ibid 996.
81) Porter G. D.(*1), Matsuoka M., et al., "Neutral Beam Current Drive Scaling in DIII-D", 16th Europ. Conf. on Controlled Fusion & Plasma Phys., Venice (1989).
82) Takeda, T., Takizuka, T., "Fracto-fusion as a mechanism of cold fusion," Riken Symposium on Muon Catalyzed Fusion (Wako, November 1989).
83) Takeda T., "On application of muon catalyzed fusion," ibid.
84) Kishimoto, Y., Oda, H.(*68), Shiho, M., et al., "Effect of electrostatic field on energy conversion efficiency and side-band excitation in high current Raman regime free electron laser," International Conference on Plasma Physics, New Delhi, November 1989, Vol.II p.465.

85) Tokuda, S., Yamagiwa, M., Tsunematsu, T., et al., "MHD stability analysis of tokamak plasmas with non-ohmic currents," ibid Vol.III p.925.
86) Tsunematsu, T., Tokuda, S., Azumi, M., et al., "Pressure profile effects on ideal MHD stability," ibid Vol.III p.929.
87) Kishimoto, Y., "Parasitic wave excitation in Raman FEL," International Symposium on Free Electron Laser (Tokyo, January 1990).
88) Tani, K., Tsunematsu, T., Takeda, T., et al., "Multi-element tokamak-oriented integrated simulator METIS," First International Conference on Supercomputing in Nuclear Applications (Mito, March 1990).
89) Takeda, T., Tokuda, S., Todoroki, J.(*75), "MHD simulation for magnetic confinement in Japan," ibid.
90) Tachikawa K. , Adachi J. , Iida H. , et al "Maintenance Approach and Remote Equipment Design for FER." IAEA-TECDOC-495 Proc. of Technical Committee Mtg. on Robotics and Remote Maintenance Concepts for Fusion Machines Karlsruhe, FRG pp. 51-62
91) Shinohara Y. , Tachikawa K. , "Highlights of the Technical Status of Nuclear Robots in Japan." ibid. pp.103-111
92) Tanaka S., "Possibility of an Intence 14 MeV Neutron Source Using High Current Ion Sources for The Neutral Beam Injector", 2th Int. Sympo. on Adv. Nucl. Energy. Research, Mito, 1990, p249.
93) Ohara Y., "Fusion Reactor Development Using High Power Particle Beams", 2th Int. Sympo. on Adv. Nucl. Energy. Research, Mito, 1990, p120.
94) Okumura Y., "Review of The High Current ion Sources for Fusion from a Viewpoint of Accelerator Application", ibid p441.
95) Watanabe K., Hanada M.and Inoue T. et.al., "Development of a Large H^- Ion Source", ibid p447.
96) Okumura Y., Hanada M. and Inoue T. et.al., "Cesium Mixing in the Multi-Ampere Volume H^- Ion Source", 5th International Symp. on the Production and Neutralization of Negative Ions and Beams, Brookhaven, 1989, p149.
97) Ogasahara M.(*77), Yamakawa T.(*77), Sato F.(*77) and Okumura Y., "Transport Processes through Magnetic Filter of Negative Ion Source", ibid
98) Ohara Y., " Negative Ion Beam Programs at JAERI", ibid
99) Hanada M., Inoue T. and Kojima H. et.al., "Multi-Ampere Negative Ion Source", 12th Symp. on Ion Sources and Ion-Assisted Technology, Tokyo, 1989, p17.
100) Matsuda Y., Hanada M. and Inoue T. et.al., Proc.12th Symp.on Ion Sources and Ion-Assisted Technology, Tokyo, 1989, p107.
101) Ohara Y., Matsuda Y. and Okumura Y. et.al., "Beam Optics of a Multi-Single Type Negative Ion Beam Accelerator", ibid p143.

A.1.4 List of other reports

1) Yamada R., "The Status and Data Needs of Sputtering for Fusion", IPPJ-AM-64 (1989)
2) Mayberry M.(*1),Uesugi Y.,et al.,"Coupling Fast Waves in the ICRF to H-Mode Plasmas in DIII-D",GA-A19565(May 1989).
3) Neyatani Y.,Carlstrom T.(*1),Matsumoto H.,et al.,"Edge magnetic fluctuations in DIII-D",GA-A19698(May 1989).
4) Ozeki T.,Chu M.(*1),Kinoshita S.(*2),et al.,"Plasma shaping,edge ballooning stability, and ELM behavior in DIII-D",GA-A19495(June 1989)
5) Kinoshita S.(*2),Fukumoto H.(*2),Kellman A.(*1),et al.,"Independent Control of Gaps in Single-Null Divertor Discharges on the DIII-D Tokamak",GA-A19584(Dec. 1989).
6) Wooton A.(*70),Carreras B.(*19),Matsumoto H.,et al.,"Fluctuations and anomalous transport in tokamaks",Fusion Research Center Report FRCR#340(Jul. 1989).
7) Burrell K.(*1),Carlstrom T.(*1),Matsumoto H.,et al.,"Physics of the L to H transition in the DIII-D tokamak",GA-A19918(Feb. 1990).
8) Porter G.D.(*1), Matsuoka M., et al., "Neutral Beam Current Drive Scaling in DIII-D", UCRL-99938 (March 1989).
9) ITER.TEAM, "ITER Concept Definition, Vol.1" IAEA / ITER / Document Series(DS) / 3
10) Yamane M., Coccorese R., Kameari A ., et al "Passive Control of Vertical Instabilities in ITER" IAEA / ITER /DS / 4
11) Spears W. , Mizoguchi T. , Perkins J. , et al "Design Point Selection for an Ignited ITER" IAEA / ITER / DS / 5
12) ITER.TEAM, "ITER Concept Definition, Vol.2" IAEA / ITER / DS / 3
13) ITER.TEAM, "ITER Conceptual Design : Interim Report" IAEA / ITER / DS / 7
14) Araki M., Watanabe K., and Yokoyama K. et.al., "JAERI-CEA Collaboration on Energy Recovery in Neutral Beam Injector", Cadarache Lab. Note TS81-8902.

A.2 Personnel of the Establishment

A.2.1 Scientific Staffs and Officers during FY 1989

Naka Fusion Research Establishment

TANAKA Masatoshi(Director General)

TOMABECHI Ken (Scientific Advisor)
MIYAMOTO Goro(*8) (Scientific Advisor)
SEKIGUCHI Tadashi (Scientific Advisor)

Department of Thermonuclear Fusion Research

TANAKA Masatoshi(Director) SHIMAMOTO Susumu(Deputy Director)

Administration Office

KOMAKI Akira(General Manager)

ANDOH Yoko	OHNAWA Yasuko	SATOH Takashi
FURUHASHI Yumiko	OHUCHI Keiko	SHIINA Kimio
KATOH Yuko	OKABE Isamu	TERUNUMA Akiko
KIMURA Syoko		

Plasma Theory Laboratory

TAKEDA Tatsuoki(Head)

KISHIMOTO Yasuaki	TAKIZUKA Tomonori	TUDA Takashi
KURITA Gen-Ichi	TOKUDA Shinji	YAMAGIWA Mitsuru
NAKAMURA Masatoshi(*68)	TSUNEMATSU Toshihide	YAMAGUCHI Yuji(*49)
NAKAMURA Yukiharu	TSUTSUI Hiroaki(*8)	

Experimental Plasma Physics Laboratory

MAEDA Hikosuke (Head)

AIKAWA Hiroshi	MATSUMOTO Hiroshi	SENGOKU Seio
FUJITA Takashi (*8)	MIURA Yukitoshi	SHOJI Teruaki
HOSHINO Katsumichi	MORI Masahiro	SUZUKI Norio
KASAI Satoshi	ODAJIMA Kazuo	TAMAI Hiroshi
KAWAKAMI Tomohide	OGAWA Hiroaki	YAMAMOTO Takumi
KAWASHIMA Hisato	OGAWA Toshihide	YAMAUCHI Toshihiko
MATSUDA Toshiaki	OHOASA Kazumi	

Facility Operational and Engineering Division

SUZUKI Kihachiro (Head)

HAMANO Takashi	KAZAWA Minoru	SHIINA Tomio
HASEGAWA Koichi	KIKUCHI Kazuo	SUZUKI Sadaaki
HONDA Atsushi	OKANO Fuminori	TOKUTAKE Toshikuni
ISHIBORI Ikuo	SHIBATA Takatoshi	UNO Sadanori
KASHIWA Yoshitoshi		

Plasma Heating Laboratory I

SEKI Masahiro (Head)

AKIBA Masat	INOUE Takashi	OKUMURA Yoshikazu
ARAKI Masanori	ISE Hideo(*16)	TANAKA Shigeru
DAIRAKU Masayuki	KOJJIMA Hiroaki(*2)	WATANABE Kazuhiro
HANADA Masaya	MAZUDA Yasuhiro(*59)	YOKOYAMA Kenji
IIDA Kazuhiro	OHARA Yoshihiro	

Plasma Heating Laboratory II

NAGASHIMA Takashi (Head)

FUJITA Hideo (*25)	SAKAMOTO Keishi	SHIHO Makoto
MAEBARA Sunao	SEKI Norikazu (*25)	WATANABE Akihiko(*40)
SAIGUSA Mikio		

Plasma Engineering Laboratory

MURAKAMI Yoshio(Head)

ABE Tetsuya	HIROKI Seiji	YAMADA Reiji
HAMAZAKI Masanori(*30)	OBARA Kenjiro	

Superconducting Magnet Laboratory

SIMAMOTO Susumu (Head)
ANDO Toshinari
ISONO Takaaki
ITOH Noboru(*56)
HIYAMA Tadao
KAMIYAUCHI Youichi(*18)
KATO Takashi
KAWAGOE Eiji (*16)
KAWANO Katsumi
KOIZUMI Koichi
KONNO Masayuki(*58)
NAKAJIMA Hideo
NISHI Masataka
NISUGI Hikaru(*30)
OKUNO Kiyoshi
SUGIMOTO Makoto
TADA Eisaku
TAKAHASHI Yoshikazu
TSUJI Hiroshi
YOSHIDA Jun(*2)
YOSHIDA Kiyoshi
ZERITIS Dimites(*6)

Tritium Engineering Laboratory

NARUSE Yuji (Head)
AMANO Junzo (*23)
ENOEDA Mikio
FUKUI Hiroshi (*23)
HAYASHI Takumi
HONMA Takashi
IDE Masahiko (*29)
INOUE Masahiko (*23)
ITO Hideki (*16)
KAWAMURA Hiroshi
KONISHI Satoshi
KURASAWA Toshimasa
MATSUDA Yuji
MISUMI Masahiro (*16)
NAKAMURA Takuya (*29)
OKUNO Kenji
OHARA Atsushi (*4)
O'HIRA Shigeru
SAKAI Fumio (*29)
SUZUKI Takumi
UDA Tatsuhiko (*2)
WATANABE Tetsurou (*16)
YAMADA Masayuki
YAMANAKA Keiichi (*16)
YAMANISHI Toshihiko
YOSHIDA Hiroshi

Department of Large Tokamak Research

TAMURA Sanae(Director)

Administration Office

HINO Shuhji (General Manager)
HARA Sachiko
HARUYAMA Kyoko
ISOZAKI Youko
KIKUCHI Isao
SATOH Tamami
SATOH Yuh
SUZUKI Masataka

Large Tokamak Program Division

KISHIMOTO Hiroshi(Head)
KONOSHIMA Shigeru
MATSUMOTO Hiroshi
MIYA Naoyuki
NIMOMIYA Hiromasa
OIKAWA Akira
OKAZAKI Takashi(*2)
TOYOSHIMA Noboru

Large Tokamak Experimental Division I

SHIMOMURA Yasuo (Head)
HOSOGANE Nobuyuki
IMAI Tsuyoshi
KAMADA Yutaka
KIKUCHI Mitsuru
NAGAMI Masayuki
NAKAMURAHiroo
NAITO Osamu
SHIMADA Michiya
TSUJI Shunji
USHIGUSA Kenkichi
YOSHINO Ryuji

Large Tokamak Experimental Division II

AZUMI Masafumi (Head)
HAMAMATSU Kiyotaka
HIRAYAMA Toshio
OZEKI Takahisa
SHIRAI Hiroshi
SHIMIZU Katsuhiro
TANI Keiji

Diagnostic Division

FUNAHASHI Akimasa (Head)
AKAOKA Noboru
AOYAGI Tetsuo
CHIBA Shinichi
FUKUDA Takeshi
GUNJI Hideo
HARA Makoto
HARAGUCHI Kazumi
ISEI Noriaki
ISHIDA Shinichi
ITAMI Kiyoshi
ITOH Takao
KAKIZAKI Sadayuki
KANEKO Takashi
KAWANO Yasunori
MATOBA Tohru (Duputy Head)
KOIDE Yoshihiko
KONOSHIMA Shigeru
KONDOH Takashi
KUBO Hirotaka
KUSAMA Yoshinori
MIURA Yoshikazu
NAGASHIMA Akira
NAGASHIMA Keisuke
NAKAJIMA Toshiyuki(*69)
NEMOTO Masahiro
NEYATANI Yuzuru
NISHINO Nobuhiro(*2)
NISHITANI Takeo
OHSHIMA Takayuki
SAITO Naoyuki
SAKASAI Akira
SAKUMA Takeshi
SATO Masayasu
SHITOMI Morimasa
SUGIE Tatsuo
TAKAHASHI Toranosuke
TAKEUCHI Hiroshi
TOBITA Kenji
TSUKAHARA Yoshimitu
TSUGITA Tomonori
YAMASHITA Osamu
YOSHIDA Hidetoshi
URAMOTO Yasuyuki

Fusion Reactor System Laboratory

FUJISAWA Noboru (General Manager)
SEKI Yasushi　　TACHIKAWA Katsuhiro

Fusion Experimental Reactor Team

MATSUDA Shinzaburo (Team Leader)

HASEGAWA Mitsuru	KURODA Toshimasa	SHIBANUMA Kiyoshi
HONDA Tsutomu	MAKI Koichi	SHINYA Kichiro
HORIE Tomoyoshi	MATSUOKA Fusiki	SUGIHARA Masayoshi
HOSOBUCHI Hideo	MIZOGUCHI Tadanori	TAKATSU Hideyuki
IIDA Hiromasa	NISHIO Satoshi	YAMAMOTO Shin
KASHIHARA Shin-ichirou	SATO Keisuke	
KIMURA Haruyuki	SEKI Shogo	

Department of JT-60 Facility

IIJIMA Tsutomu(Director)　　TANAKA Yuji (Deputy Director)

JT-60 Administation Division

HINO Shuhji (General Manager)	MIZUNUMA You(Deputy Manager)	
AKAOSUGI Shouji	MORI Tomoko	YANAGISAWA Akemi
FUJISAKU Kuniko	NUISHIBA Miho	

JT-60 Facility Division I

SHIRAKATA Hirofumi(Head)	SHIMIZU Masatsugu(Deputy Head)	
AKASAKA Hiromi	MATSUKAWA Makoto	TAKAHASHI Minoru
ARAKAWA Kiyotsugu	MATSUZAKI Yoshimi	TAKAHASHI Shunji
FURUKAWA Hiroshi(*30)	MUTOH Mitsugu	TAKESHITA Akira(*15)
HONDA Mitsuteru(*38)	NAGAYA Susumu	TANI Takashi
ICHIGE Hisashi	NOBUSAKA Hiromichi(*28)	TERAKADO Tsunehisa
IKEDA Yukiharu	OMORI Kenichirou	TOTSUKA Toshiyuki
ISAJI Nobuaki(*39)	OMORI Shunzo	YAGYUU Junichi
ISAKA Masayoshi	OMORI Yoshikazu	YAMAZAKI Takeshi(*28)
KAWAMATA Youichi	SAKATA Shinya	YASUDA Taizou(*28)
KIMURA Toyoaki	SEIMIYA Munetaka	YONEKAWA Izuru
KURIHARA Kenichi	SEKIGUCHI Shuichi(*30)	

JT-60 Facility Division II

KONDO Ikuo (Head)		
ANDO Toshiro	KUSHIMA Takanori	SASAJIMA Tadayuki
ARAI Takashi	MAENO Masaki	SUNAOSHI Hidenori
HIRATSUKA Hajime	MIYACHI Kengo	TACHIBANA Hidetoshi
HONDA Masao	MIYAKE Kazuyuki	TAKASAKI Manabu
HORIIKE Hiroshi	MIYO Yasuhiko	TANAKA Takejiro
KAMINAGA Atsushi	NAGAYAMA Kiyoshi	TSURUMI Satoshi
KAWABE Masaru	NAKAFUJI Takashi	YAMAMOTO Masahiro
KODAMA Kozo	OGIWARA Norio	YOSHIOKA Yuji
KOIKE Tsuneyuki	OHTA Kazuya	

JT-60 Facility Division III

OHTA Mitsuru (Head)		
AOKI Isao	KOGURE Shigeyuki(*73)	TAKAHASHI Shunji
FUJII Tsuneyuki	OGAWA YOSHIRO(*4)	TERAKADO Masayuki
FUJISHIRO Kenji(*27)	SATOH Minoru	TSUNEOKA Masaki
IKEDA Yoshitaka	SATO Kazuya(*30)	UEHARA Kazuya
KUSAKA Makoto(*28)	SAWAHATA Masayuki	YAMAGISHI Kohjirou
KITAI Tatsuya(*28)	SEKI Masami	YONEDA Tsuyoshi(*27)
KIYONO Kimihiro	SHINOZAKI Shinichi	YOKOKURA Kenji
KONISHI Kazumasa(*29)	SUGANUMA Kazuaki	

JT-60 Facility Division IV

KUNIEDA Shunsuke (Head)	HIRUTA Kazuharu (Deputy Head)	
AKINO Noboru	KURIYAMA Masaaki	OHUCHI Shouji (*32)
EBISAWA Noboru	MATSUOKA Mamoru	OHUCHI Yutaka
KAWAI Mikito	MIZUNO Makoto	OOHARA Hiroshi
KASHIMURA Takanori (*30)	MOGAKI Kazuhiko	SUGAWARA Tadayoshi (*2)
KIKUCHI Katumi (*30)	NEMOTO Hironori (*28)	SHIMIZU Kazuhiko (*30)
KITAMURA Sigeru	NOMOTO Hiroki (*31)	USAMI Hiroji (*2)
KOMATA Masao	OHGA Tokumichi	USUI Katsutomi

A.2.2 Number of the Staffs during FY 1989

Department	Regular staff1)	Staff on loan 2)
Thermonuclear fusion research	103	13
Large tokamak research	69	10
JT-60 facility	83	26
Administrative service	47	0
Fusion experimental reactor team	11	10
Total	313	59

1) Including scientists, technicians and secretaries. 2) From industries.

*1 General Atomics, USA
*2 Hitachi Ltd.
*3 Lawrence Livermore National Laboratory, USA
*4 Toshiba Corpl
*5 Max-Planck Institut für Plasmaphysik, FRG
*6 Massachusetts Institute of Technology, USA
*7 Mitsubishi Atomic Power Industry Inc.
*8 The University of Tokyo
*9 Nagoya University
*10 Okayama University
*11 Kyoto University
*12 Hiroshima University
*13 Institut für Reaktorbauelements, KfK, FRG
*14 Ishikawajima-Harima Heavy Industries
*15 Mitsubishi Electric Co., Ltd.
*16 Kawasaki Heavy Industry Ltd.
*17 Hazama-gumi Ltd.
*18 Kobe Steel Ltd.
*19 Oak Ridge National Laboratory, USA
*20 Century Research Center Corp.
*21 Northwestern Laboratory
*22 Institute of Plasma Physics, Nagoya University
*23 Mitsubishi Heavy Industry Ltd.
*24 NAIG Nuclear Research Laboratory
*25 Japan Atomic Industrial Forum
*26 Central Research Institute for Electric Power
*27 Nippon Electric Co., Ltd.
*28 Kaihatsu Denki Co.
*29 Sumitomo Heavy Industry Co.
*30 Nuclear Engineering Co., Ltd.
*31 Tomoe Shokai
*32 Ibaraki Kohsan
*33 Tokyo Nuclear Service Co., Ltd.
*34 ULVAC Co.
*35 Kyushu University
*36 Contract Researcher
*37 Princeton Plasma Physics Laboratory, USA
*38 I.B.S. Data Center Co., Ltd.
*39 Japan Expert Clone Corp.
*40 Nissei Sangyo Co., Ltd.
*41 JET Joint Undertaking, UK
*42 Hodaka Seiki Ltd.
*43 Sumitomo Electric Industry Co.
*44 Nikon Corp.
*45 National Laboratory for High Energy Physics
*46 Tsukuba University
*47 Los Alamos National Laboratory, USA
*48 Japan Radiation Engineering Co.
*49 MEITEC Co., Ltd.
*50 Osaka University
*51 Imperial College, UK
*52 Institute of Research Hydro-Quebec, Varenns, Canada
*53 KFA-IPP, FRG
*54 Ewic Engineering Co., Ltd.
*55 ORC Manufacturing Co., Ltd.
*56 Koike Sanso Kogyo Co., Ltd.
*57 Hitachi Oxygen Co., Ltd.
*58 Fuji Electric Co., Ltd.
*59 Nissin Electric Co., Ltd.
*60 Sandia National Laboratories, USA
*61 JGC Corporation
*62 Tokyo Institute of Technology
*63 Nuclear Research Center Karlsruhe, FRG
*64 Argonne National Laboratory, USA
*65 ITER Team
*66 Yokohama National University
*67 Nihon Software Kaihatsu, Inc.
*68 Kanazawa Computer Service Corp.
*69 University of California at Los Angeles
*70 University of Texas
*71 Varian Company Co.Ltd.
*72 Nagaoka University of Technology
*73 Denki Kogyo Co. Ltd.
*74 The NET Team
*75 National Institute for Fusion Science
*76 I.V. Kurchatov Institute of Atomic Energy
*77 Keio University

A.3 Budget of the Establishment

Item	FY1987	FY1988	FY1989
JT60 Construction	22,630	17,078	16,429
Research & Development	3,827	3,885	3,628
Japan-US Cooperation	837	1,107	1,440
Site Construction	829	73	78

(Unit: Million yen)